Author:
Papatheodorou, Marianthi

Title:
Dynamic finite element modelling, measurement and updating of cable stayed bridges

UNIVERSITY OF BRISTOL

DEPARTMENTS OF AEROSPACE AND CIVIL ENGINEERING

DYNAMIC FINITE ELEMENT MODELLING, MEASUREMENT AND UPDATING OF CABLE-STAYED BRIDGES

Marianthi Papatheodorou

A thesis submitted to the University of Bristol for the degree of Doctor of Philosophy in the Faculty of Engineering

September 2001

ABSTRACT

This thesis is concerned with the application of model updating techniques to a civil structure and in particular a cable-stayed bridge cantilever. For many years, model validation techniques have been applied to aerospace structures with some success, but never to a civil engineering structure. This is mainly due to the fact that civil structures are complicated systems and do not possess the simplicity required by the optimisation techniques.

An extensive literature review is presented concerning various types of analyses and modelling techniques applied to cable-stayed bridges, including an account on cable dynamics and cable-structure interaction. Literature reviews on sensor placement techniques, model updating methods and on the variability of results are also covered.

A description of the various components that compose a cable-stayed bridge and some of its aerodynamic characteristics are presented.

Some sensor placement techniques are introduced and are applied to an aluminium plate tested in the laboratory under free-free conditions. These techniques use the dynamic characteristics of an analytical model and place sensors on the model so as to obtain the most information about the dynamics of the structure using as few sensors as possible. The techniques are successful in identifying the principal modes of the plate.

An extensive account of the various methodologies that exist to compare and correlate modeshapes and frequencies are presented, together with methods for model reduction and.

An analytical and experimental model of the cable-stayed bridge cantilever was built based on various assumptions and made as simple as possible. The sensor placement techniques were applied to locate transducers on the experimental model. The experimental modeshapes and frequencies were used to optimise the mass and stiffness matrices of the analytical model in order to replicate the experimental data.

The eigensensitivity method used was successful in optimising the analytical model. However, some limitations were identified and presented together with some recommendations for future work.

ACKNOWLEDGEMENTS

Thanks are first and foremost due to my advisors, Drs Nicholas Lieven and Colin Taylor, for their encouragement and invaluable advice during the course of this project.

I would especially like to thank Mr David Ward for his extensive technical assistance.

Thanks due to the University of Bristol for the scholarship that supported me throughout the Ph.D.

DECLARATION

I declare that the work in this presentation was carried out in accordance with the Regulations of the University of Bristol. The work is original except where indicated by special reference in the text and no part of the dissertation has been submitted for any other degree.

Any views expressed in the dissertation are those of the author and in no way represent those of the University of Bristol.

The dissertation has not been presented to any other University for examination either in the United Kingdom or overseas.

Marianthi Papatheodorou

Marianthi Papatheodorou

PERMISSION TO COPY

Marianthi Papatheodorou

Advisers: Dr N.A.J. Lieven

Dr C.A. Taylor

Department of Civil Engineering

University of Bristol

I, the undersigned, am willing that this thesis should be made available for consultation in Bristol University Library, for inter-library lending, for use in another library or for photocopy in part or in full – at the discretion of the librarian – on the understanding that users are made aware of their obligations under copyright.

Marianthi Papatheodorou.

Marianthi Papatheodorou

NOMENCLATURE

Wherever possible notation has been defined in the text of this thesis. The definitions that follow are only a list of the most frequently used notation.

ABBREVIATIONS

COMAC	Co-ordinate Modal Assurance Criterion
FE	Finite Element
FRF	Frequency Response Function
MAC	Modal Assurance Criterion

SYMBOLS

$\| \|$	magnitude
$\| \|_2$	Euclidean norm
$[\ ]$	matrix
$\{\ \}$	vector
$\{\ \}^*$	complex conjugate
$[\ ]^T$	transpose of matrix
$[\ ]^+$	pseudo -inverse of a matrix
x	displacement
$\dot{x}$	velocity
$\ddot{x}$	acceleration
i, j, k	indices
x, y, z	co-ordinates
p	updating parameter
$n_{\text{mod es}}$	number of modes
n_{freq}	number of frequencies
n_{dofs}, N	number of degrees of freedom

n_p	number of updating parameters
n_e	number of elements
f	frequency, Hz

GREEK LETTERS

$[\alpha]$	receptance matrix
$[\Psi]$	modeshape matrix
$[\Phi]$	mass-normalised modeshape matrix
$\{\phi\}$	mass-normalised modeshape vector
ω	radial frequency, rads/sec

CONTENTS

LIST OF FIGURES

LIST OF TABLES

CHAPTER 1

INTRODUCTION

1.1 Introduction

The importance of finite element model updating has been emphasised, in the last few years, by the need for improved performance of the engineering products. It started as a useful tool in the aerospace industry, but since the 1990s it has become important to the design, construction and maintenance of mechanical and civil engineering systems. As designs become more and more complicated, the requirements for valid numerical models have increased and attention to detail has emerged to be very important. Developments in the computer modelling and hardware industries have enabled the engineers to use sophisticated analysis techniques, such as the finite element method, to build large models that represent real structures, and to process large matrix problems with high speed.

Since the 1960s, the finite element method has become the most accepted method of analysis in structural design, and is best described in Zienkiewicz et al (1986). It is used widely in all sectors of engineering, aerospace, mechanical and civil, where analytical simulations are a necessity. The method leads to a description of the system by means of its mass and stiffness matrices. These matrices are an assembly of the individual matrices of the finite elements that form the model. The elements are assigned material and section properties and boundary conditions are defined at the nodes between those elements. Usually the engineer has to make assumptions about the properties of the elements or the boundary conditions of the analytical model, which should replicate the real structure. However, errors and misjudgement are usually present in those assumptions, and this is where the importance of finite element model updating becomes significant. The updated model will be a more accurate representation of the real structure and could be used with confidence for further analyses, such as, to predict forced response arising from wind, traffic and seismic motions.

Model updating is a reconciliation process, where an analytical model is corrected in order to replicate the real or the test structure with which it is compared. Therefore. real data or data from a model structure in the laboratory are needed. These data can either be natural frequencies and modeshapes or Frequency Response Functions. The success of the reconciliation process depends on the quality of the data collected, since the engineer assumes that the experimental data is correct and the analytical model has inaccuracies. However, it is common knowledge that the measurements will be both imprecise and incomplete. Imprecise because of the presence of noise from the instruments, which can be eliminated largely by the use of filters and good quality transducers, and of the presence of systematic errors such as a failure to replicate correctly the boundary conditions. The data will also be incomplete, since the measurement frequency range is smaller than that of the analytical model. Also, the engineer cannot measure all the degrees-of-freedom present in the analytical data, and it is not always possible to detect all the modes since the number of sensors one can use and their positioning on the model are limited. However, various methods have been devised to overcome the problem of incompleteness, which either expand the experimental model to the analytical coordinates or reduce the analytical model to the test degrees-of-freedom.

Moreover, methods for sensor placement on a model have been developed in order to improve the quality of the data obtained from the modal tests. These methods have been developed for the aerospace industry, which requires precision measurements, and have been very successful. The methods use the analytically derived modeshapes to select a set of sensors that will give the most dynamic information of the test structure. The application of those methods to other sectors of engineering is very challenging.

Civil engineering has always been a progressive industry, with a long history of achievements, which are accompanied by a vast amount of structural examples, such as, bridges, railways and buildings. Most of them still in use, despite the years that have passed, a fact largely attributed to the engineer's insight and advanced knowledge of structural design. Nowadays, the modern designs are more complex, lightweight and large. Bridges are built with ever increasing spans, cable-stays are used more frequently, which makes the structure quicker to construct and look more pleasing to the eye than existing designs. The severity of the surrounding

environment, traffic, wind, earthquakes influence the behaviour of the bridge and certainly the design of the structure. The performance requirements and the aesthetics have become very important and a significant factor in the choice of design. Therefore, the engineers recognise more and more the need for accurate analytical models, to use for advanced structural analyses, and for paying attention to detail. This is where model updating becomes very important.

It was thought to be interesting to apply these methods to a complex civil engineering structure, a cable-stayed bridge cantilever. The reason for choosing a cable-stayed cantilever is because data from one of the Second Severn Crossing cantilevers is available to the University of Bristol, since the monitoring of the bridge was undertaken by the Department of Civil Engineering. These data will be used to prepare the analytical model, which is described in Chapter 6. Moreover, during the construction phase, a bridge is at its most sensitive to wind and earthquake excitation, since not all of its supports are in place and the cables are not fully stressed Therefore, a cantilever is thought to present a challenge for modal analysis and for the application of sensor placement techniques and model updating methods, which will be used to locate sensors on a test structure and correct the finite element model of the cantilever, respectively. The limitations of the use of those methods will be identified and discussed.

1.2 Sensor locations

The problem of predicting reliably the response of a structure to a type of loading is closely related to the validity of the model used to represent the structure. The proper knowledge of various parameter values is very important in establishing the usefulness of such model. These parameter values can be obtained from the response data collected from the sensors located at various positions on the structure. However, only a limited number of sensors can be used because of practical and economic considerations. This is not really a problem when dealing with small-scale models in the laboratory. For example, with mechanical and aeronautical models, the sensors can be moved and distributed at different positions along the structure, allowing many readings to be taken so that one can obtain the appropriate information needed for subsequent applications. On the other hand, re-locating arrays of sensors becomes a problem when dealing with large civil engineering

structures where one has to take measurements in-situ. Only a limited number of transducers can be used, and moving the sensors around the structure is usually very inconvenient. Therefore, the problem of positioning the sensors in the best possible locations within the structure becomes important.

The benefits from optimally position sensors in a structure are many and can be summarised as follows:

1. minimise the cost of instrumentation, data processing and data handling by using fewer sensors, data channels;
2. obtain better estimates of the model parameters from noisy data;
3. improve structural control by using better structural models;
4. determine efficiently structural properties and their change in order to improve the assessment of structural integrity; and
5. improve the early fault-detection capability for large, flexible systems, Udwadia (1994).

Many researchers have developed techniques for optimum transducer placement. The most commonly used techniques, namely the Effective Independence Method (EfI), Kammer (1991), the Energy Matrix Rank Optimisation technique (EMRO), Hemez et al (1994) and the Energy Optimisation Technique (EOT) Heo et al (1997), are presented in Chapter 4.

1.3 Model Updating

Model updating is a reconciliation process, applied to an analytical model in order to replicate the measured or un-measured characteristics of the experimental model, assuming that the experimental data are correct. The various strategies adopted for model reconciliation fall into three categories, which are: Comparison, Location, and Correlation.

The methods falling into the first group, Comparison, are used to assess the compatibility of the analytical and experimental models. They give an indication of which modes correspond to each other. This is usually achieved in the modal domain and the most commonly method used is the Modal Assurance Criterion

(MAC), Ewins (1998). However, there will always be an incompatibility in the size of the finite element and test models. The problem of coordinate incompleteness has to be resolved before any comparison is performed. This can be done either by reducing the finite element model or by expanding the experimental model. For the former, it is necessary to reduce the size of the stiffness and mass matrices and the most widely deployed method is Guyan reduction, Guyan (1965), which eliminates coordinates at which no forces are applied. For model expansion, several techniques have been developed, such as the Kidder's method (1984), which is derived from an inverse Guyan reduction.

The second group is Location. The methods falling into this group detect the location of differences between the analytical and experimental models. The most commonly used technique is the Coordinate Modal Assurance Criterion (COMAC), Lieven et al (1988), which provides information as to where two sets of modes differ.

The third category is Correlation. The methods falling into this group apply localised perturbations to mass and/or stiffness properties or to elemental parameters of the analytical model in order to obtain a model that represents accurately the physical characteristics of the real structure. There are three groups of optimisation methods: Least squares updating, Direct optimisation and Neural Networks.

The methods belonging to the first group are modal and FRF sensitivity methods, where, the sensitivity of the dynamic response or modes of vibration to parameter variation is evaluated. The methods belonging to the second group are Simulated Annealing and Genetic Algorithms, which are probabilistic search algorithms, derived from analogies with the thermodynamic cooling process and natural evolution, respectively. Finally, Neural Networks consist of a number of simple processing units linked to each other, which have multiple inputs and a single output. Neural Networks need to be trained before they can be used using a training algorithm and training data.

Model Updating, although has been used in aerospace industry for many years, is not considered to be a standard tool. It is still on-going research, and not many examples either of successful or unsuccessful updating are available. The reason for this is because there are many problems associated with the data used for updating, such as

not enough measured data points, poor choice of sensor locations, approximation of boundary conditions and noisy experimental data, just to mention a few.

1.4 Variability

One of the problems that engineers have to overcome when testing experimental or real models is the fact that structures vary in time. If different tests are performed in the same structure, the results obtained can be very different. Balmes (1998) identifies the sources of variability, which affect the response of structures. These sources are:

1. the structure changes in time because of ageing, temperature effects, loading conditions, etc.;
2. the same model can be used to represent a number of structures that should be identical but they are not. For example, manufacturing tolerances, residual stresses, changes in welding point positions, etc.;
3. material and geometrical properties are not measurable at all points and one has to assume values for these properties; and
4. complex parts of structures are represented by simple assemblies of beams, plate/shell elements with equivalent properties leading to the same global behaviour as the real structure.

The author describes the variability in the results obtained using the GARTEUR SM-AG-19 testbed. The sources of variability in this exercise are: value of additional masses, value of sensor masses, stiffness of suspension, shaker position. In Model Updating we assume that the test results are the correct ones and we use these results to update our analytical model. However, since we use our updated model to support design decisions, it is important to minimise the variability in the test procedure. This variability can depend on many factors, including the test set-up, data acquisition, effects of non-linearities. Cafeo et al (1998) address some issues in order to minimise test variability, which include shaker attachment, transducer calibration, accelerometer placement, measurement method and signal processing. However, one can face variability in real in-situ testing of structures. Farrar et al (1997) deal with the study of modal parameter variability of a bridge caused by environmental effects, service conditions and data reduction methods. The authors

suggest that a thorough study of the variability must be conducted before modal-based identification algorithms can be applied with confidence. Hasselman et al (1997) deal with the existence of product and experimental variability, which are ignored in the model verification process. Experimental variability is affected by the boundary conditions of the structure, actuators, sensors, data acquisition and processing equipment and procedures. Product variability refers to the variability among like products as they come off the assembly line. The authors compare the relative degrees of product and experimental variability and evaluate their combined effects on the predictive accuracy of a physically representative analytical model of a test structure.

1.5 Objectives of the work

One of the objectives of this research work is to apply the sensor placement techniques to a civil structure and in particular to the cable-stayed bridge cantilever. The aim is to use those methods to identify the best positions to place the transducers on the experimental model of the cantilever and identify any limitations that may exist in their application.

The second objective is to update the analytical model of the cantilever using the experimental data obtained using the sensor locations identified. The updating method, which will be used, is the eigenvalue sensitivity technique, which updates the natural frequencies of the analytical model so that they match better the corresponding frequencies of the experimental model. Any limitations of applying this method will be identified.

In more detail, the aim of Chapter 2 is to present a study into cable-stayed bridges in general, introducing the various components that compose such as structure and a review of the research work that has been undertaken up to now for this type of structure. More importantly, one of the most important characteristics of cable-stayed bridges, their nonlinearities, is explained.

The objective of Chapter 3 is to explain with more detail the nonlinearities of cable-stayed bridges, called *geometric nonlinearities*, involving stress stiffening and large deformation effects. These nonlinearities are explained using as an example a

simply-supported beam, which has distributed parameter values. The influence on the natural frequencies and modeshapes of the application of an axial force to the beam is described.

Chapter 4 aims to present a description of the pre-test planning steps that can be taken in order to carry out a successful vibration test. The various techniques that can be used to find the best possible positions to mount a structure, to place the excitation source and to locate the transducers are presented. The optimal sensor location techniques are described in detail and an example of their application to a plate tested in free-free conditions is presented.

The objective of Chapter 5 is to provide a description of the various techniques that can be used to reduce an analytical or expand an experimental model, to compare data and update a model. The model updating techniques, presented in detail, are the modal and FRF sensitivity methods. A comparison of the experimental and analytical data of the plate presented in Chapter 4 is included together with an example of the modal sensitivity updating of a 2-dimentional beam.

Chapter 6 aims to present all the experimental results of the cable-stayed bridge cantilever. A description of the finite element model, which is built using the commercial program ANSYS, is firstly presented. The pre-test planning procedure, which is followed for the experimental testing, and in particular the sensor location techniques are applied to the model in order to obtain the sensor configurations. The experimental and analytical results are compared and correlated and finally the eigenvalue updating process is presented.

Finally, Chapter 7 contains the conclusions drawn, the contributions made by this work and some recommendations for future work.

CHAPTER 2

CABLE-STAYED BRIDGES

2.1 Introduction

The use of cables to support bridges is not a new method of construction. Cable-stayed bridges can be traced back to 1600's, when a Venetian carpenter called Verantius built a timber bridge supported by several chain stays. In 1784 another carpenter from Switzerland called Löscher built a 32m span bridge made wholly of timber, even the stays. However, only in the recent years cable-stayed bridges have been constructed widely in many parts of the world. The reasons for this are, firstly, that the engineers of that time could not fully understandt the static and dynamic behaviour of such structures, and secondly, the available materials were unsuitable. Timber sections, bars and chains were the low strength materials used as cables, which could not be fully tensioned allowing the deck to undergo large deformations before they could take the tensile loads for which they were intended. The recent improvements and understanding of the construction materials such as high strength steels, the development of orthotropic-type decks where the deck plates are stiffened along their span length by longitudinal stiffeners, the new and improved construction and erection methods and the more sophisticated analysis techniques have rendered it possible to analyse such complicated systems with great accuracy, and led to the successful development of cable-stayed bridges.

Modern cable-stayed bridges consist of the stiffening girder with the bridge deck, the cable system supporting the stiffening girder, the pylons and the anchor blocks, which support the cable system. A description of the various components follows at the next sections. The information was taken from Gimsing (1982), Ito et al (1991), Walther (1988) and Troitsky (1988).

2.2 Cable system

2.2.1 Cable types

A cable may be composed of a number of structural strands. The simplest strand is the *seven-wire strand* which consists of a single straight wire core surrounded by a single layer of six wires, all having the same pitch and direction of helix. As the pitch is quite large, the inclination of the wire axis from the strand axis is small and, therefore, the stiffness of such a strand is close to that of straight wires.

The *multi-wire helical strand* is fabricated by successive spinning of layers with opposite direction of helix, starting out with a straight core.

The *locked-coil strand* is formed by a number of different shapes of wires. The core consists of a normal helical strand and around this core are one to several layers of wedge-shaped wires. The outer layers consist of special z-shaped wires. This is a very dense material and the specially shaped wires of the outer layers make the strand less sensitive to side pressures at saddles and anchorages as the wires have surface contact.

Finally, the *parallel-wire strand* consists of straight wires that remain straight from one end to the other. Figure 2.2.1-1 shows some types of cross sections of a cable.

2.2.2 Layout of the cable stays

The layout of the cable stays influences the structural behaviour of the bridge and also the erection method and the economics. It is, therefore, one of the most important aspects of bridge design. In the transverse direction, perpendicular to the longitudinal bridge axis, the bridge could possess a single, double or multiple plane of cables. In the longitudinal direction, the arrangement of the cables can fall into four basic systems, namely, suspension, fan, harp and semi-harp systems.

2.2.3 Number of cable planes

The two basic arrangements of the planes of the cable system are a single-plane and a two-plane configuration where the planes can either be vertical or inclined.

In the case of a *vertical two-plane* system, there are two layouts that a designer can adopt, Figure 2.2.3-1a. The cable anchorages can either situated outside the deck structure or inside the main girder. The first layout prevents the deck area from being obstructed by the presence of cables and pylons. However, the transverse distance of the anchorage points from the webs of the main girders requires substantial cantilevers to be constructed so that the shears and bending moments are transferred into the deck. The second layout makes a part of the deck area to be obstructed by the cable system. However, such an area can be used as a sidewalk.

An *inclined two-plane system* can be used for very long spans where high A-shaped pylons are used, Figure 2.2.3-1b. The cables are attached at the edges of the deck and converge at the top of the A-shaped pylons. This system provides both vertical and torsional support to the stiffening girder, since it behaves like a rigid triangular section in bending.

In the case of the *single-plane* configuration, the stiffening girder is supported by one vertical cable system, Figure 2.2.3-1c. Such a system requires a deck of considerable torsional rigidity in order to limit the cross-sectional deformations caused by the eccentric live loads. This configuration is aesthetically very pleasant since there is no visual crossing of cables and it provides a lane separation.

Finally, the *multiple-plane* arrangement is best suited to bridges with a very wide roadway. The deck of such a bridge is subjected to transverse bending forces that are greater than the longitudinal bending. The cost of constructing such a deck is reduced by the use of a multiple-plane cable system.

2.2.4 Arrangement of cable stays

The different types of cable-supported bridges are characterised by the longitudinal arrangement of the cables and are separated into suspension and the cable-stayed bridges.

In a *suspension* bridge, the main cable is supported at four points: at the two anchor blocks and on the two pylons. Vertical or slightly inclined hanger cables connect the stiffening girder to the main cable. Such a suspension method has a low bending stiffness and in order to avoid excessive deformation of the structure under wind or eccentric loading a suitable deck is required.

There are three main configurations for the cable system of a cable-stayed bridge: the fan, the harp and the semi-harp systems.

In the *harp* system, the cables are parallel and cross each other at a constant angle and such appearance is very attractive, Figure 2.2.4-1b. The use of a high pylon increases the stiffness of the cable system against deflections, since the greater component of the load applied is the vertical component taken by the tower, whereas, the horizontal load, which would cause the tower to deflect, decreases with a high pylon.

The *fan* system brings the cables together at the top of the pylons, Figure 2.2.4-1a. Such a pattern may appear less attractive than the harp pattern because of the visual crossing of the cables, but such a disadvantage becomes less apparent in large span bridges.

The *semi-harp* configuration is an intermediate solution between the fan and harp systems, which combines the advantages of both patterns but avoids their disadvantages. The cables are spread sufficiently at the top part of the pylon to separate each cable anchorage, Figure 2.2.4-1c. Combined suspension and cable-stayed systems have also been applied, Figure 2.2.4-1d.

2.3 Stiffening girder

As already mentioned, the successful development of modern cable-stayed bridges is contributed to the development of the orthotropic steel deck, Figure 2.3-1. It constitutes the top chord of the main girders or trusses. However, a reinforced concrete deck acting monolithically with the main reinforced or prestressed concrete girders is an alternative solution. The work presented here does not intend to discuss the types of deck in more detail since they are treated extensively in the literature, Gimsing (1982), Ito et al (1991), Walther (1988) and Troitsky (1988) just to name a few.

The stiffening girder is the element that is subjected to the major part of the external load. It must be able to transfer the load locally and it will be assisted by the cable system in the global transmission of the load to the supports at the main piers. There are three types of main girders used in cable-stayed bridges: steel girders, trusses and reinforced or prestressed concrete girders.

The *steel girders* may either be of an I-section or a box-section, Figure 2.3-2. Plated I-girders, with their bottom flange made of a number of plates, possess the required inertia to fit the moment envelope exactly. Therefore, the minimum amount of steel is used. Since the section of the girder is open its torsional stiffness is insignificant and, therefore, the cable system will have to provide the torsional support. The box-shaped girders need to have a minimum plate thickness to prevent local buckling and to be protected from corrosion. They may be rectangular or trapezoidal, having their webs vertical or sloping, respectively. They possess high torsional stiffness, which is an advantage since unsymmetrical live loading and wind forces induce large torsional moments on the deck. They reduce the torsional rotations in the deck.

Girder elements constructed from *trusses* have not been used very much during the recent years probably because they require extensive maintenance and protection against corrosion, as shown in Figure 2.3-3. However, they may be used instead of steel girders for aerodynamic reasons, since they provide the required bending and torsional support, or in the case of combined highway and railway traffic.

Reinforced or prestressed concrete girders and decks possess high stiffness and have high internal damping, thereby assisting the structure to exhibit only small deflections, see Figure 2.3-4.

2.4 Pylons

The pylon is a tower structure. The type of tower, used in a particular bridge, is influenced by the number of bays erected, the soil conditions in the area and the configuration of the cable system. It could be of the form of twin towers, portal frame, A-frames and single towers, Figure 2.4-1.

The *twin* towers are used for the lateral or two-plane configuration of the stays described previously. They consist of two freestanding columns, which can either be rigidly connected to the stiffening girder or to the piers. In the second case, the axis of the tower must coincide with the cable plane so that the cables are anchored outside the stiffening girder. This type of pylon is usually used in moderate span bridges.

Portal frame towers consist of two pylon legs connected by a single strut at the top. They are usually used in suspension bridges in order to raise the stiffness sufficiently to react against the wind load transferred by the cables to the top of the towers.

The *A-shaped* tower and the *single* tower are used in single-plane cable arrangements. However, the A-shaped pylon can also be used in bridges with two inclined cable systems joined at the top.

The pylons can either be made of steel or concrete. A steel tower has the advantages of faster fabrication and erection. However, the towers of large cable-stayed bridges can be built more economically from reinforced or prestressed concrete.

2.5 Anchorage

The way the cable system is anchored at the ends characterises the cable- supported bridges. The cables can either be *earth-anchored* or *self-anchored*. In the first case,

the vertical and horizontal components of the cable force are transferred to the anchor block, whereas, in the second case, the vertical component is transferred to the anchor pier and the horizontal component is taken by the stiffening girder, Figure 2.5-1. The earth-anchored system is more preferred in suspension bridges, whereas, the self-anchored system is mostly used in cable-stayed bridges, since it leads to symmetric loading about the pylons and there is no moment on the tower.

2.6 Structural characteristics of cable-stayed bridges

One of the most important characteristics of cable-stayed bridges is the integral action of the stiffening girder and the cable system. The girder takes the horizontal forces due to cable action and, therefore, the size of the cable anchorages required at the stiffening girder is reduced. This characteristic makes the structure more economical.

The introduction of orthotropic decks added another advantage to the cable-stayed bridges. The structure can carry the horizontal thrust of the cables without any additional material. The stiffened plate acts not only as the upper chord of the main girders but also as the horizontal plate girder against wind forces which gives the structure more lateral stiffness than the bracing system used in older structures. This leads to shallower girders and a reduction in steel usage. Moreover, the orthotropic deck provides continuity of the deck at the towers and at centre span, which is a major advantage of this type of structure. The cables in a cable-stayed bridge are always in a state of tension independently of the position of the load on the deck.

2.7 Aerodynamic characteristics of cable-stayed bridges

The turning point into the study of the aerodynamic stability of cable-stayed bridges came after the collapse of the Tacoma Narrows Bridge in 1940. Before that time the engineers were designing bridges taking into account only the static loads produced by lateral winds. However, after the collapse they realised the importance of taking into account the dynamic effects of the wind and include in the design the rigidity, the damping characteristics and the aerodynamic shape of the bridge.

A cable-stayed bridge under the effect of the wind can oscillate and this motion can be reduced or even eliminated by designing an aerodynamic deck shape and taking into account in the design the factors that influence the frequencies of oscillation of the bridge. It is possible to design such a structure to resist aerodynamic forces by finding the natural frequencies and associated modes of vibration and carrying out wind tunnel tests. The results of these tests allow designers to determine the factors governing the dynamic behaviour thereby allowing these factors to be applied to the prototype by suitable analysis. If the analysis does not suggest a stable aerodynamic behaviour, a modified design should be used.

2.7.1 The effect of the wind

Three different aerodynamic mechanisms can be distinguished considering the effect of the wind on cable-stayed bridges: Vortex shedding, Flutter and Turbulence.

Vortex shedding

If one considers the flow of air around a cylinder at rest, eddies are shed periodically from the cylinder forming the von Karman vortex trail, Figure 2.7-1. In the case of cable-stayed bridges, and especially those with I-shaped girders, the formation of vortices alternately from the upper and lower surfaces of the deck produce aerodynamic forces on the structure that vary periodically. The vortex shedding is proportional to the wind speed and if the frequency of the vortices matches closely one of the natural frequencies of the bridge, the structure will vibrate with increasing amplitude. The amplitude of vibration can be decreased by increasing the damping of the structure. The strength of vortex excitation varies with the deck configuration, the number of girders, the inclination of the webs and the edge details of the deck.

Flutter

Under wind forces the deck can oscillate both transversely and torsionally. This motion is called flutter. Larsen (1998). After the collapse of the Tacoma Narrows bridge, the effect of flutter has been analysed extensively and it was concluded that the bending and torsional frequencies must be different from each other in order to eliminate flutter. The wind speed that causes flutter depends on the mass of the

structure and ratio of its first torsional and vertical bending natural frequencies. A structure should be designed for a critical wind speed that is greater than the maximum wind speed of the area that it is destined for.

Turbulence

The wind is not steady but turbulent in nature and this causes random velocity fluctuations in the vertical and horizontal directions. Therefore, the wind pressures along the length and height of the bridge are non-uniform. Turbulence affects vortex shedding and can cause dynamic excitation through fluctuation of the local wind speed. Turbulence can produce a narrow oscillation called buffeting. The bridge then will respond to one or more of its natural modes.

Cable-stayed bridges with an aerodynamic deck are superior to suspension bridges for the following reasons:

1. Since such structures are highly redundant they possess high structural damping, which prevents flutter from becoming dangerous. This is not the case with suspension bridges since they can easily be excited in the region of resonance with large amplitudes.

2. In suspension bridges, the most dangerous mode of oscillation, the antisymmetric torsional mode, is easy to develop. The two cables move against each other, one going down in half of the span, the other going up and therefore they give no resistance against the torsional movement of the deck. This is the reason why suspension bridges need high torsional rigidity of the stiffening girder systems, whereas, in a cable-stayed bridge the cables provide resistance against torsional movement.

Many researchers have undertaken studies on the aerodynamic behaviour of cable-stayed bridges in order to understand better how the aerodynamic characteristics of the various components influence the overall behaviour of the structure. The cables, deck and pylons are coupled both structurally and aerodynamically. Some of these interactions have a stabilising effect on the aerodynamic performance of the bridge, whereas, others have a de-stabilising effect. Disregarding these effects will lead to an over-estimation or under-estimation of the aerodynamic behaviour of the bridge. For example, when the tower oscillates together with the cables, it may cause the deck to vibrate, which will provide an additional mass component and will damp the motion

of the bridge. A study of these aerodynamic and structural interactions of the different components of a cable-stayed bridge is presented in Ogawa et al (1992), whereas, Yoshimura (1992) studies the aerodynamic stability of three medium-span cable-stayed bridges. The author examines the stability of the girders, the galloping of the towers and the cable rain-wind induced vibrations and wake galloping.

2.8 Modelling of cable-stayed bridges

One important property of cable-stayed bridges that characterises them is that they are non-linear structures. The non-linearities are due to the non-linear behaviour of the cable stays, caused by the variation in sag with tensile force, and of the towers and girders when they are subjected to combined bending and axial loads. The latter interaction is particularly significant and should be considered in this type of bridge due to large displacements that can occur, Fleming (1979), Fleming et al (1980).

There are three factors that should be taken into consideration when dealing with this type of bridge. The first consideration is the non-linear axial force-deformation relationship for the cable stays due to the change in sag with tensile force. When a cable is supported at its ends and subjected to its own weight and an axial tensile force, it will deflect into the shape of a catenary. The axial stiffness of the cable will change with changing sag, which, in turn, varies with the displacement at the ends of the cable. An increase in axial load elongates the cable and leads to a decrease in sag. The changes in the displacement of the ends influence the cable in three ways. Firstly, the strain in the material of the cable changes. This change is usually considered to be linear and is governed by the material's Young's Modulus. Secondly, there is a rearrangement of the wires in the cable under loading. Part of this rearrangement is permanent. The non-permanent deformation leads to the reduction of the Young's Modulus of the material. Finally, the sag of the cable changes, which depends on the length, weight and the tensile force of the cable. The sag does not vary linearly with the tensile force and this relationship causes the cable to behave non-linearly.

The second non-linear consideration is the behaviour of the towers and girders when they are subjected to combined bending and axial loads. As the member deflects laterally, additional bending moments are created when an axial force is applied

simultaneously, thus changing the flexural stiffness of the member. Also, the bending moments cause shortening of the member, which affects its axial stiffness. Usually, the combined effect of bending and axial loads is ignored in the analyses.

The third consideration is the large displacements that can occur in the structure under normal design loads. It is common practice to design a structure assuming that the geometric changes in the structure under design loads are small. However, a cable-stayed bridge can undergo large displacements, and the effect of geometry changes should be considered in the structural analysis.

The non-linear behaviour of a cable-stayed bridge is taken into account in its static and dynamic analyses in Fleming (1979), Fleming et al (1980) and Kanok-Nukulchai et al (1992). In all three papers, the deck and pylons are modelled as standard beam elements and the cables are represented as straight chord members with an *equivalent modulus of elasticity*, which takes into account the change of sag. In Kanok-Nukulchai et al (1992), the authors conclude that this method of cable modelling does not take into account the change of geometry at cable ends and, therefore, this approach is only suitable for preliminary design. The authors develop the cable modelling technique further by using the *multiple straight links method*, which considers the cables as mass-less, pin-jointed, straight links with an axial stiffness taking into account the gravity stiffness, the cable self-weight and any additional loads lumped at the nodes. A nonlinear analysis ensures that equilibrium and compatibility are satisfied at the nodes. Another method used in the same paper, is the *Curved finite element method*, which models the cable as with one or more curved elements. The element stiffness matrices are developed using polynomial or Lagrangian interpolation functions with continuity of cable displacement and possibly slopes at the common nodes.

2.9 Testing of cable-stayed bridges

There is quite a large amount of literature dealing with the testing of cable-stayed bridges. Some papers concentrate on small scale modelling and dynamic testing in the laboratory, whereas, others involve full scale testing under ambient conditions. Independently of which type of testing is used, all papers include an analytical model of the bridge under testing, which is used to compare the results obtained from the

model testing. Garevski et al (1991) concentrate on small scale modelling and laboratory testing of the Jindo bridge. Two and three-dimensional analyses are carried out to calculate the dynamic characteristics which were compared with the laboratory observations. It is concluded that the analytical model can be used to calculate the linear response of the real structure. Wilson et al (1991) present a description of a three-dimensional model of the Quincy Bayview bridge, whereas in Wilson et al (1990, 1991) the dynamic properties of the Quincy Bayview cable-stayed bridge are determined by using wind and traffic vibrations. Gentile et al (1997) deal with the dynamic testing of a cable-stayed bridge after major repairing. Full-scale tests are conducted and a two and three-dimensional models are used. The experimental and analytical results are found to compare well. Casas (1995) measures the accelerations and displacements on the deck and towers of the Alamillo cable-stayed bridge. The dynamic excitation is caused by traffic. The agreement between the dynamic parameters of the analytical, scaled and real bridge is satisfactory. Gupta et al (1988) present a two and three-dimensional analyses of a cable-stayed bridge including the foundation interaction. Including the substructure in the analysis increases the flexibility of the bridge. Kawano et al (1988) presents a random seismic response analysis of a soil/cable-stayed bridge interaction. Nazmy et al (1992) describe the dynamic analysis of a concrete and a steel cable-stayed bridge, under synchronous and asynchronous support motions. Kawashima et al (1988) study the damping characteristics of a cable-stayed bridge. Damping in such a structure may be developed by hysteretic damping of materials, energy dissipation at movable supports, radiational damping at foundation, viscous damping with air, sag of cables. The authors assumed that damping occured either at movable supports or foundation and it was found that the damping ratio depends on modeshape.

A considerable amount of literature deals with the seismic response of cable-stayed bridges. Pandley et al investigates the seismic response of a long span cable-stayed bridge subjected to strong ground motion. Azevedo et al present the model of the International Guadiana bridge based on a three diamensional finite element idealisation. Yokoyama et al (1988) analyse the nonlinear response of a cable-stayed bridge with a tall tower considering the degrading of the stiffness under severe earthquake motion. The influence of the cable vibration on the bridge behaviour was also studied. Abdel-Ghaffar et al (1988) study the nonlinear seismic response of a

three-dimensional long span cable-stayed bridge. They consider the cases of multiple support and uniform seismic excitations and took into account the sources of nonlinearity in this type of structure. Parvez et al (1988) study the seismic behaviour of a continuous multi-span cable-stayed bridge across the Jamuna River in Bangladesh. Linear material behaviour is assumed. Finally, Vaz et al (1988) perform a study to assess the earthquake behaviour of a cable-stayed bridge to be built across the Arade River.

One important aspect of the dynamic behaviour of a cable-stayed bridge is the dynamic interaction between the cables and the deck/towers. Caetano et al (1997) present a study, which evidences a clear coupling between cable and deck/tower motions and includes an experimental and numerical investigation of the importance of this aspect in terms of the response to seismic excitations. Abdel-Ghaffar et al (1991) also deal with the dynamic behaviour of cable-stayed bridges when the vibration characteristics of the cables are taken into consideration. Both papers include two discretisation systems, named the One-Element-Cable-System (OECS) and the Multi-Element-Cable-System (MECS).

2.10 Cable vibrations

Cable vibrations has become a major issue in the design of cable-stayed bridges, because their ever increasing span makes them more sensitive to flutter instability as well as to wind and traffic induced vibrations. This is a problem mainly because of the highly non-linear behaviour of the cables with sag, as explained in section 2.8, which has attracted a great deal of interest from various researchers. There is a number of research papers, which examine the vibrations of hanging cables under various end conditions. Irvine (1978) deals with the case of an inclined cable hanging under its self-weight. The author shows that the natural frequencies of the symmetric in-plane modes depend on just one dimensionalised parameter, whereas, the frequencies of the anti-symmetric in-plane modes and the out-of-plane modes are independent of any parameters. The results apply to any chord inclination. Triantafyllou et al (1986) derive simple formulae for inclined cables. The authors consider an elastic, taut, inclined cable and derived equations for the natural frequencies and modeshapes. Darbre (1989) obtains the frequency equation of

parabolic cables fixed at the lower end and free to move in the horizontal direction at the upper end. The solution of the frequency equation is presented in the form of frequency curves and the expressions for the modes of vibration are given. Veletsos et al (1983) present a closed-form expression for the steady-state horizontal stiffness of a viscously damped, uniform, inclined cable supported at the lower end and subjected to a harmonically varying horizontal displacement at the upper end. Special attention is paid to the influence of damping, which is considered to be due to an external viscous source exerting a restraining force in the normal direction only. Ali (1986) considers the forced vibrations of sagged cables with movable supports. The author studies the nonlinear response of a cable, which can deflect in all three dimensions. The equations of motion of the cable are developed for the case when the cable is supported in two different elevations and subjected to static and dynamic loadings between supports. The nonlinear strain-displacement relationship for the cable is used, which accounts for the change in cable tension during motion. Benedettini et al (1987) study the nonlinear dynamics of a suspended cable subjected to planar excitation. Numerical results are presented for the symmetric in-plane vibrations by considering different cable, forcing and damping parameters. Ahmadi-Kashani (1989) evaluates the in-plane and out-of-plane natural frequencies, for the entire range of sag/span ratio, for a hanging cable. The phenomenon of 'cross-over' is observed which is related to the elasticity of the cable. Triantafyllou (1985) treats the problem of a cable translating between ideal end supports, horizontal or inclined. Burgess et al (1988) show that the elastic modes of catenaries present phenomena of coalescence and avoidance, which up to now have been associated only with the low frequency transverse modes of catenaries. Expressions for the natural frequencies of a taut cable are obtained and used to investigate the behaviour of the modes of horizontal and inclined cables at frequencies high enough to excite elastic modes. Iyengar et al (1988) study the vibrations of a laterally loaded cable. A cable under a steady uniform wind experiences dynamic forces due to vortex shedding. The cable deflects away from the vertical plane due to the lateral load and oscillates in a coupled lateral-vertical fashion exhibiting a beat pattern of oscillations. If the loading is uniform along the length of the cable, the oscillations will be in the plane containing the initial static profile. Out-of-plane oscillations occur if the initial static profile is in three dimensions or with a non-uniform lateral load. Luongo et al (1982) consider a two-degree of freedom nonlinear elastic model to analyse the effects of

nonlinearities on the free vibration of a suspended cable in the absence of internal resonance. The conditions under which in-plane and out-of-plane monofrequent oscillations exist and those for which effects arise due to nonlinear coupling are examined. Al-Nouri et al (1985) examine the influence of geometrical nonlinearities on the forced coupled vibrations of cables having small sag-to-span ratios and for which the parabolic profile provides a good approximation for the initial shape of the cable. The equations for the coupled transverse-vertical vibrations of cables are presented, in which the nonlinearities due to geometry, stiffness nonlinearities and cable sag, are included but Hooke's law is assumed to be valid. Takahashi et al (1987) consider the nonlinear vibrations of both horizontal and inclined sagged cables, supported at fixed ends. The study is not limited to small sag-to-span ratios. The nonlinear equations of motion are solved using the Galerkin method in the space coordinate and the Harmonic Balance method in time coordinate. The authors obtain information about the frequency-amplitude relations of the non-linear free vibrations of cables for various geometrical and material parameters. Takahashi et al (1987) analyse the out-of-plane vibrations of cables under in-plane forcing using a multiple degree of freedom approach. The Harmonic Balance method is used to obtain the in-plane non-linear responses and the corresponding unstable out-of-plane vibrations. Benedettini et al (1989), Rega et al (1989) study the planar non-linear response of a suspended elastic cable subjected to super harmonic excitation. The cable vibrates with an assumed deflected shape. The investigation is performed for various sag-to-span ratios.

2.11 Damping

It is common knowledge that one of the common modes of structural failure is due to excessive stresses caused by large amplitude vibrations near resonance. As inherent damping in many structures is quite small, it is necessary to introduce further damping. Dry friction damping is very common and relies on energy dissipation when the contact point slips due to relative motion caused by vibration. Menq et al (1991) analyse the vibratory response of a turbine blade. Although the paper deals with a turbine blade, its concept can be applied to a cable-stayed bridge. The authors take into account the two-dimensional effects arising from the flexural and torsional modes of the blade. The blade is modelled as a single mass and the damper as a

massless spring of finite stiffness. Three cases of joint motion are considered: fully stuck, stick-slip and complete slip. The steady-state forced response of the system is calculated. Shaw (1986) considers the response of a single degree of freedom system with dry friction. It is shown that for positive viscous damping, the non-sticking, steady-state solutions, of the same period as the forcing, are nearly always asymptotically stable. For negative viscous damping, which may arise from aerodynamic forces, such motions become unstable. Anderson et al (1990) study the dynamic behaviour of a single degree of freedom system with amplitude and rate dependent friction forces. A system with amplitude dependent friction is likely to experience intermittent sticking. If the system sticks for a significant amount of time, the energy dissipation capability may be seriously degraded. Different sticking conditions are considered and the equations of motion are obtained. Menq et al (1986) study the response of frictionally damped structures in which the interface is subjected to high normal loads. A new microslip model of friction, which allows partial slipping on the friction interface, is presented. The force-displacement relationships are derived. Beards et al (1977) consider the frictional damping obtained in a joint allowed to slip in rotation but not in translation. As the friction torque capacity of a joint, before slip occurs, increases, the resonant frequencies increase whilst the resonant mobility decreases to a minimum and then increases again, indicating a certain torque for minimum resonant mobility.

2.12 Conclusions

As one can conclude from the literature review in sections 2.8 to 2.10, cable-stayed bridge modelling and testing has drawn a great deal of attention in the last few years mainly because of the non-linear nature of the structure. The static and dynamic behaviour of the bridge cannot be represented accurately by assuming the structure to be linear and the non-linearities, described in section 2.8, should be taken into account in the analytical development of the model. The accurate representation of real structures can be benefited by the use of model updating techniques, since it aims to provide accurate models that match the real structures and can be used with confidence for further forced response analyses. A description of the various model updating techniques will be given later in Chapter 5.

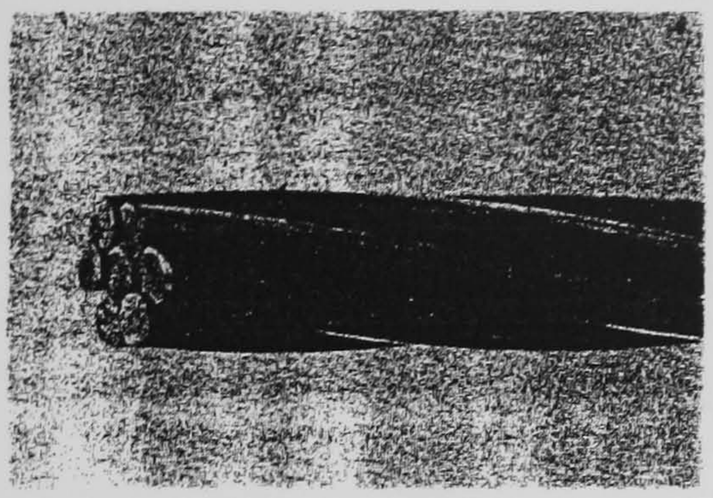

Seven-wire strand

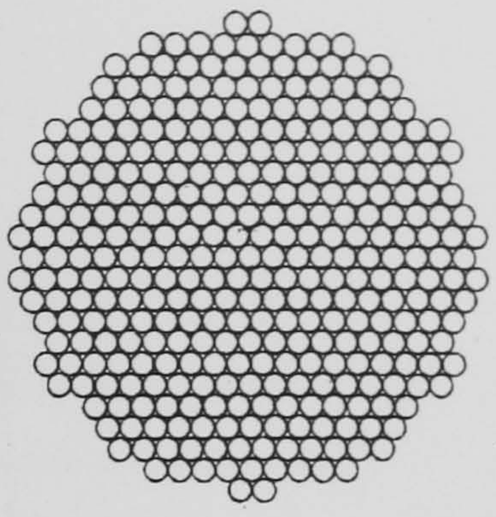

Parallel-wire strand

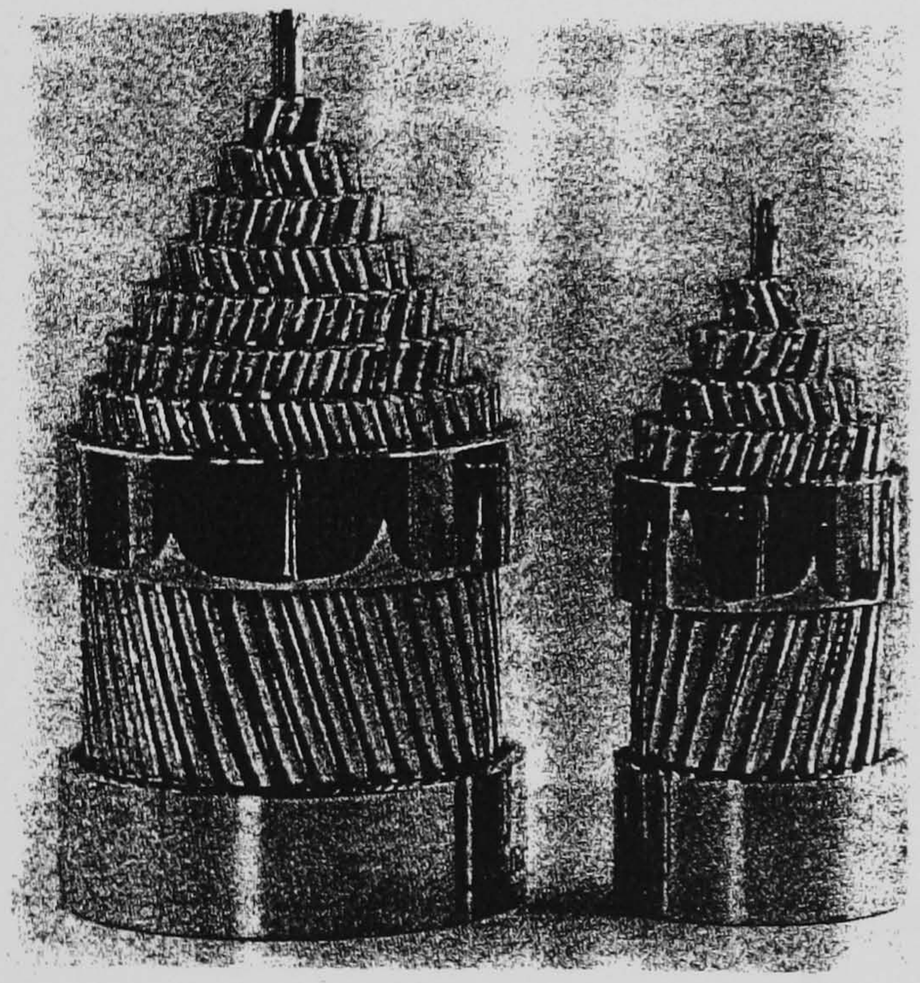

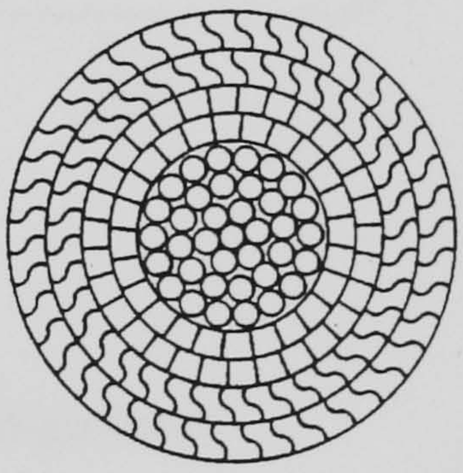

Locked-coil strand

Figure 2.3-1: Cross sections of strands

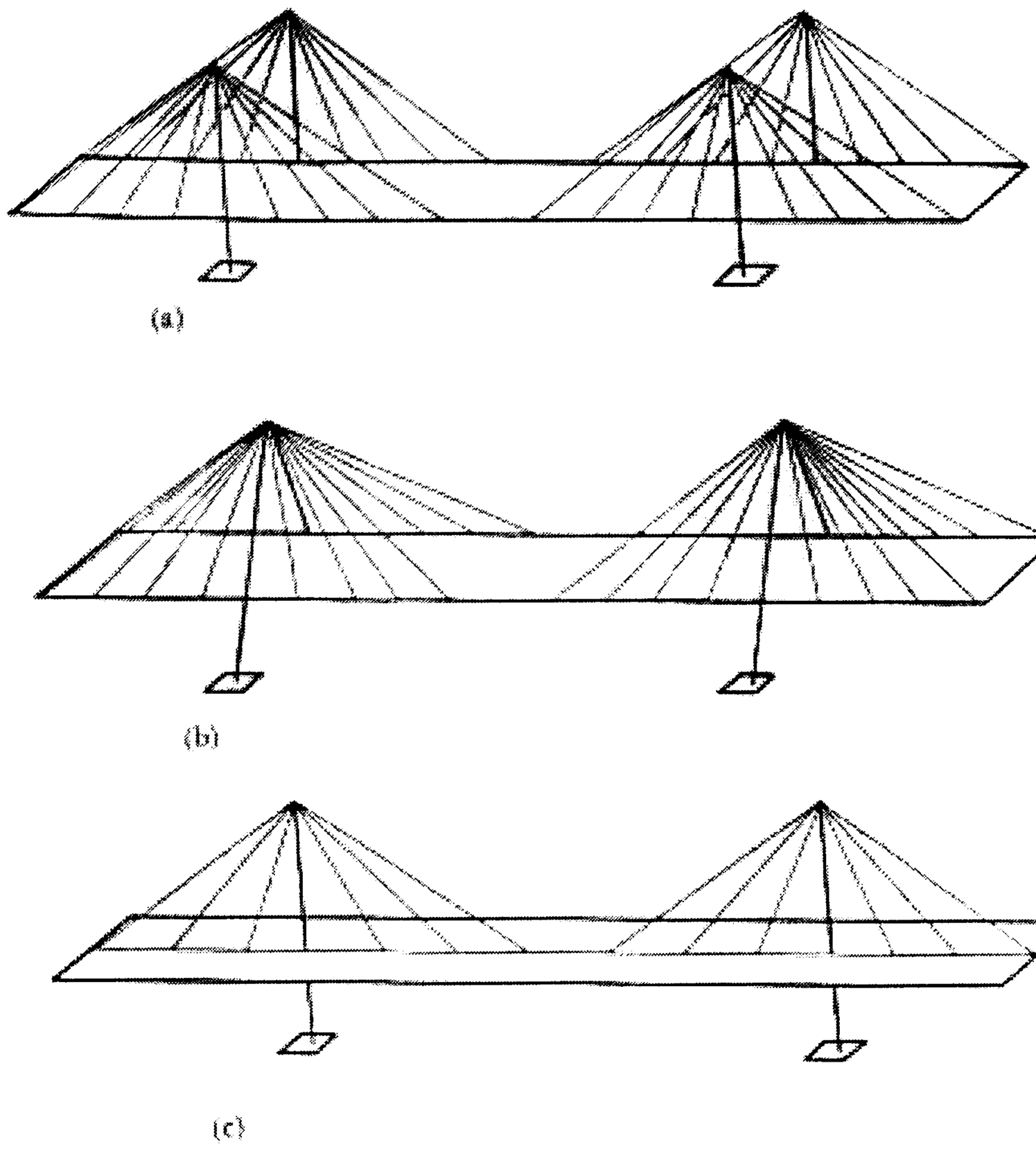

Figure 2.2.3-1: Transverse cable configuration

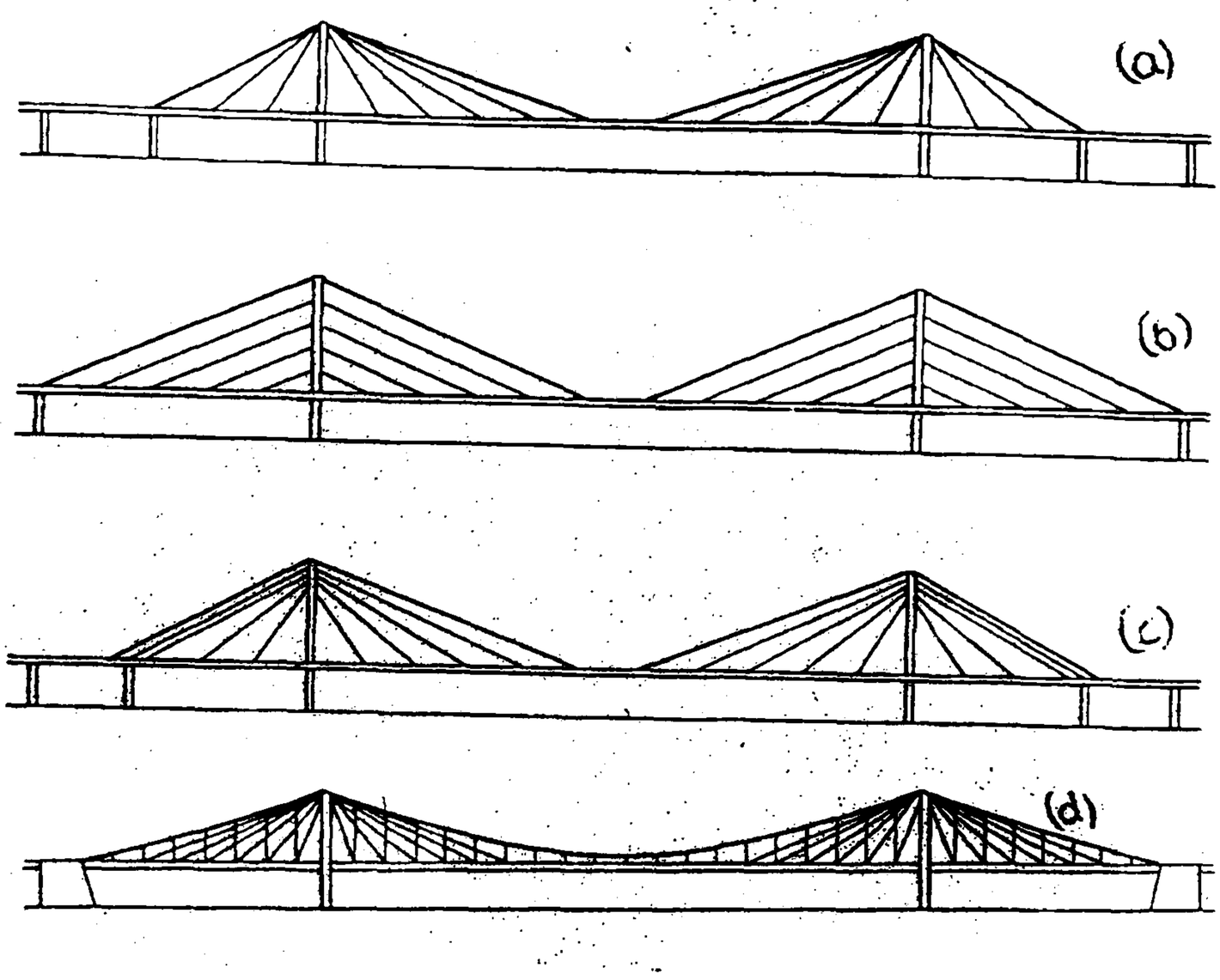

Figure 2.2-4: Longitudinal cable configuration – a) fan, b) harp, c) semi-harp, d) combined

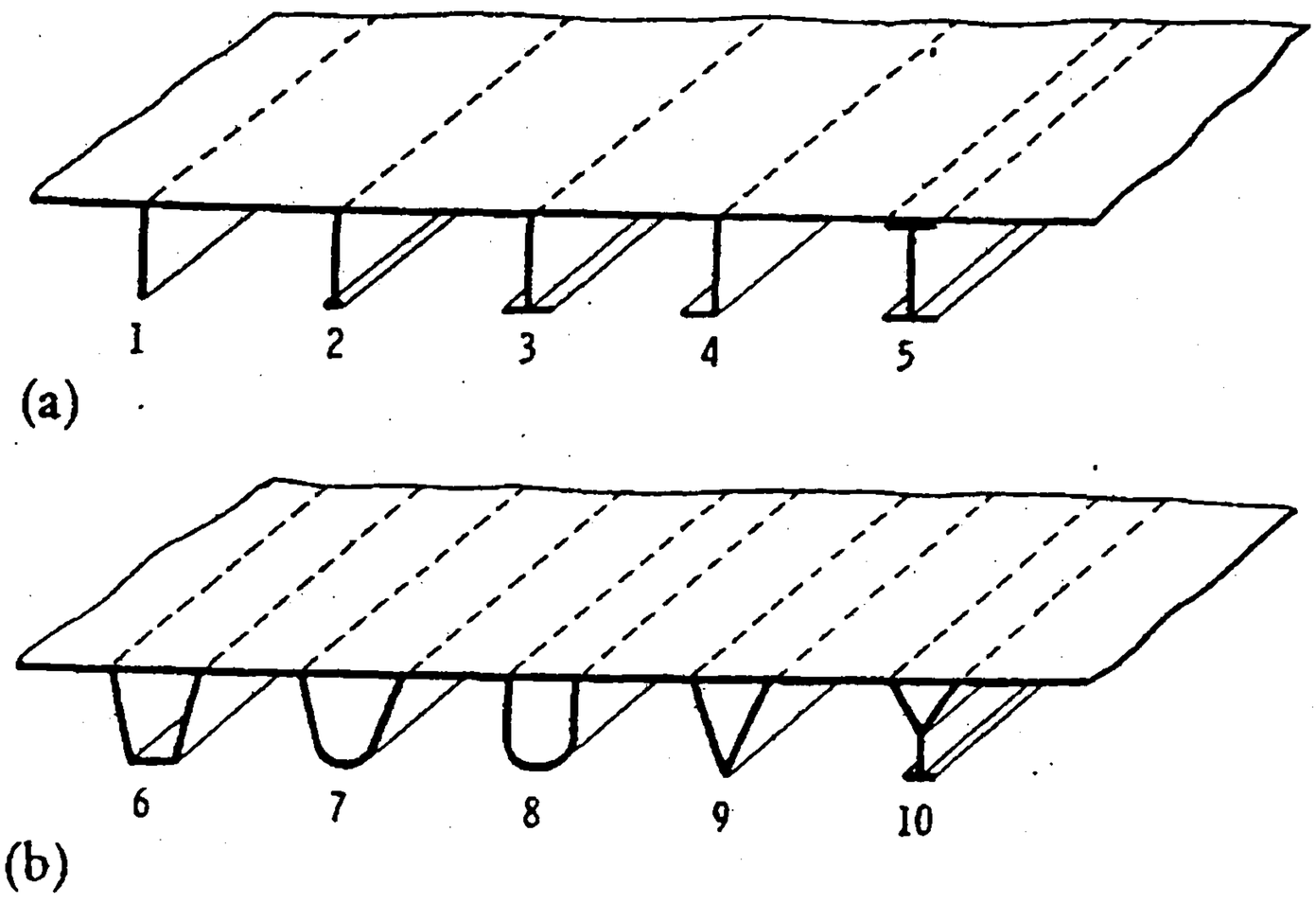

Figure 2.3-1: Orthotropic type deck

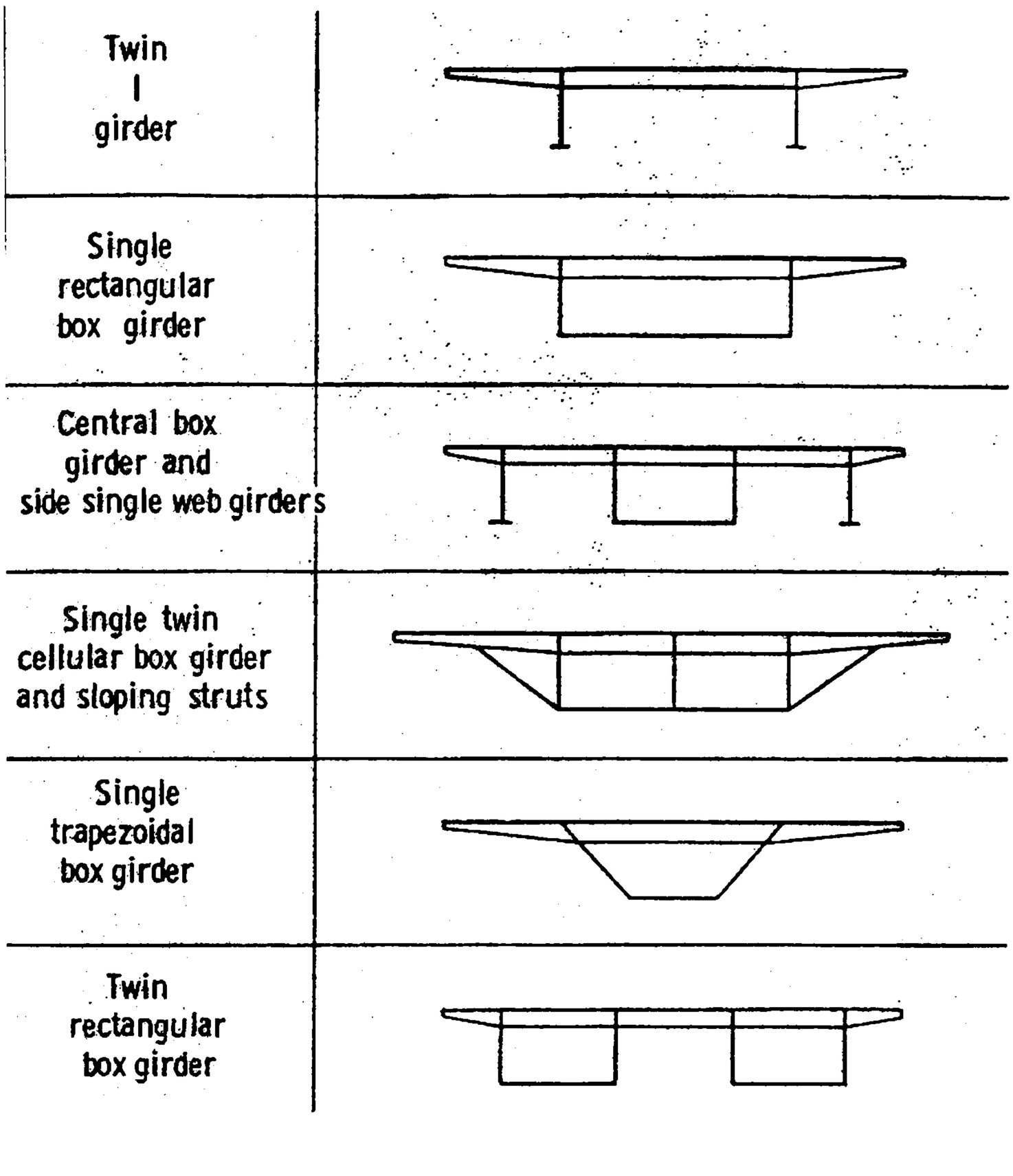

Figure 2.3-2: Types of steel girder

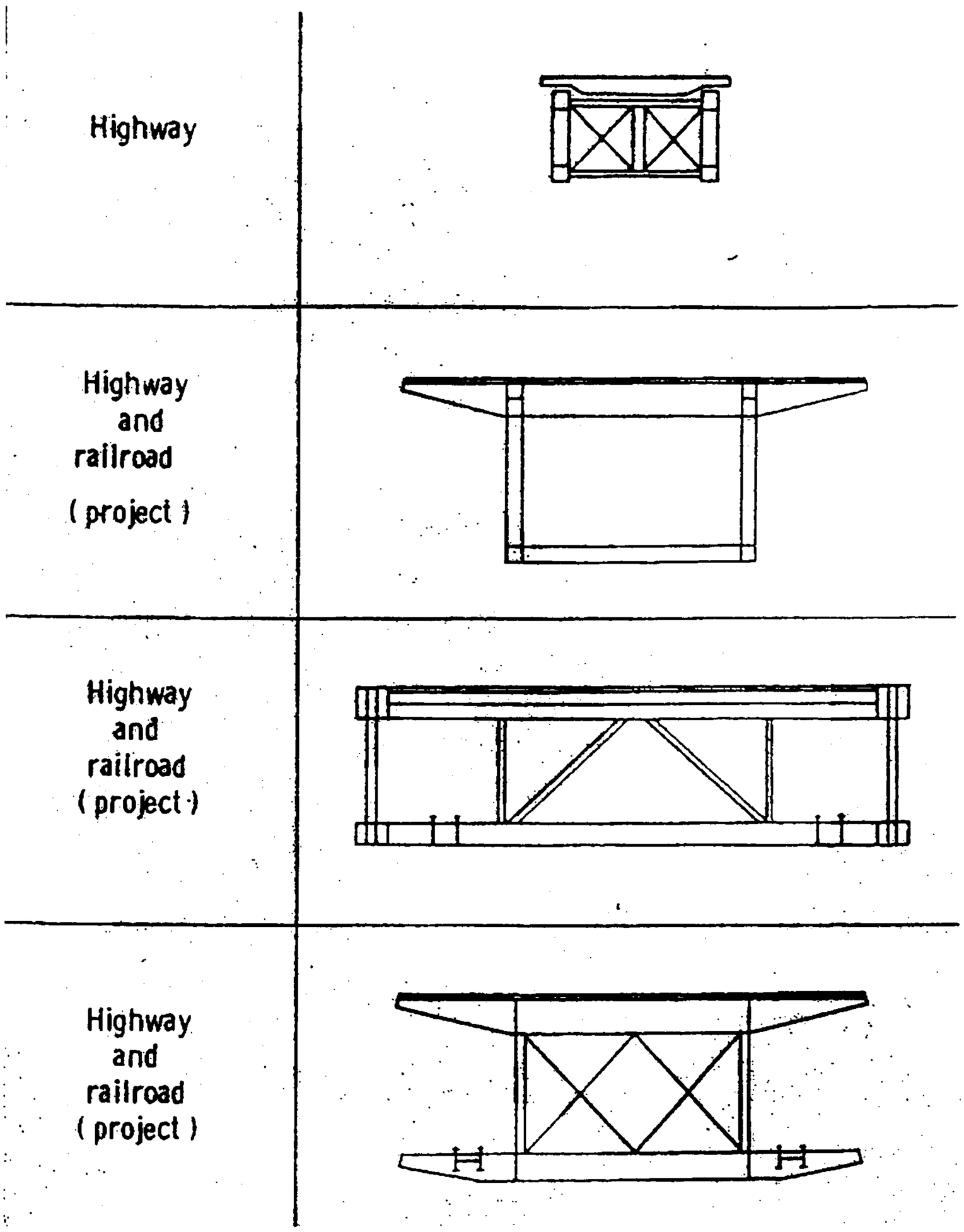

Figure 2.3-3: Types of truss girder

Single box girder (Wadi Kuf Bridge, Libya)	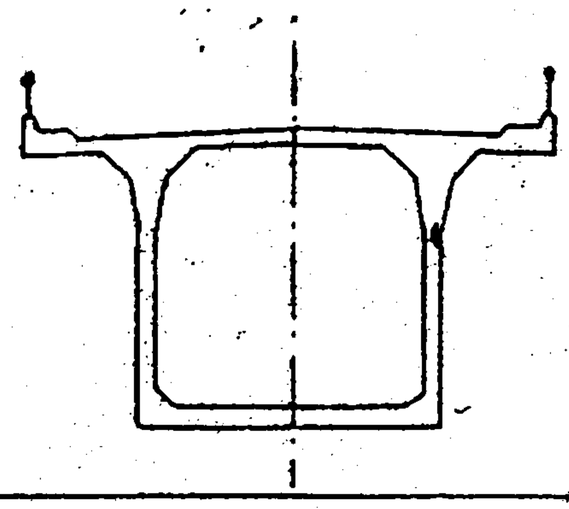
Twin box girders (River Parana Bridge, Argentina)	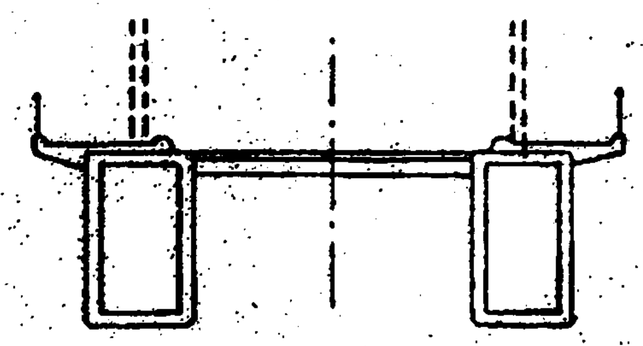
Twin box girders (River Waal Bridge, Holland)	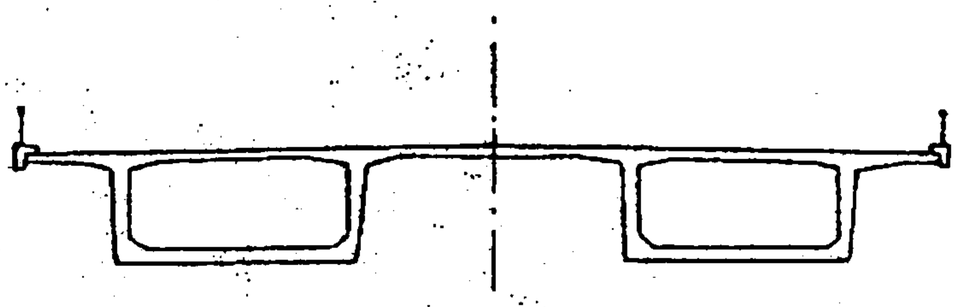
Multiple box girder (Polcevera Viaduct, Italy)	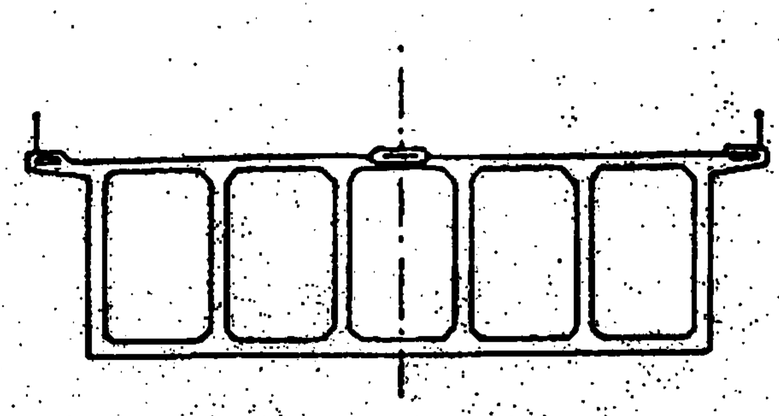

Figure 2.3-4: Types of concrete girder

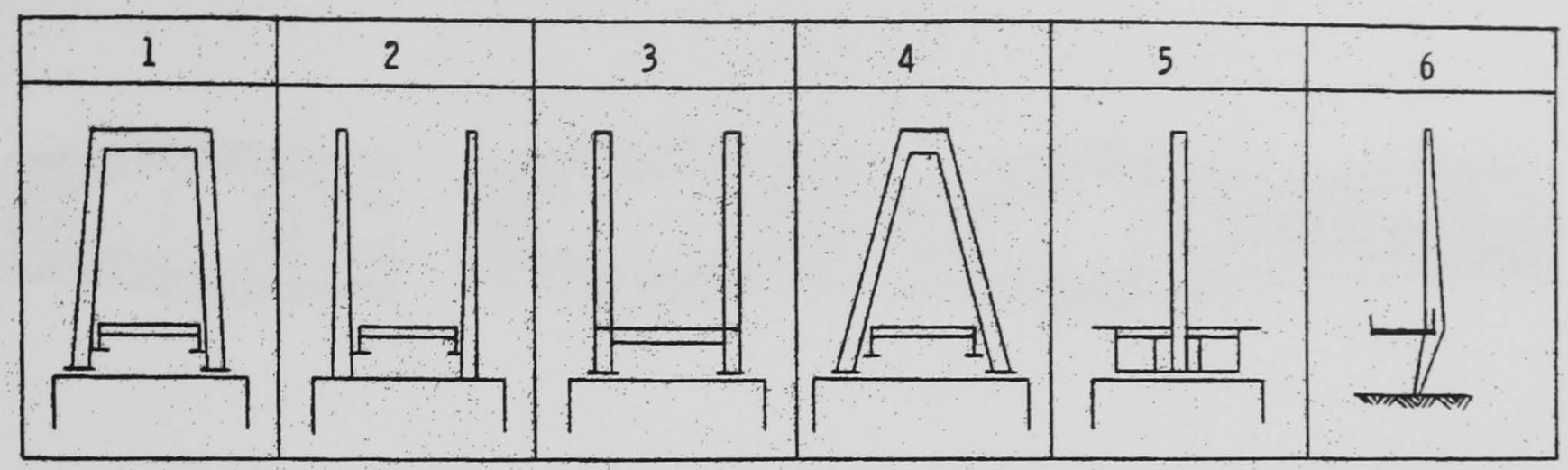

Figure 2.4-1: Types of tower

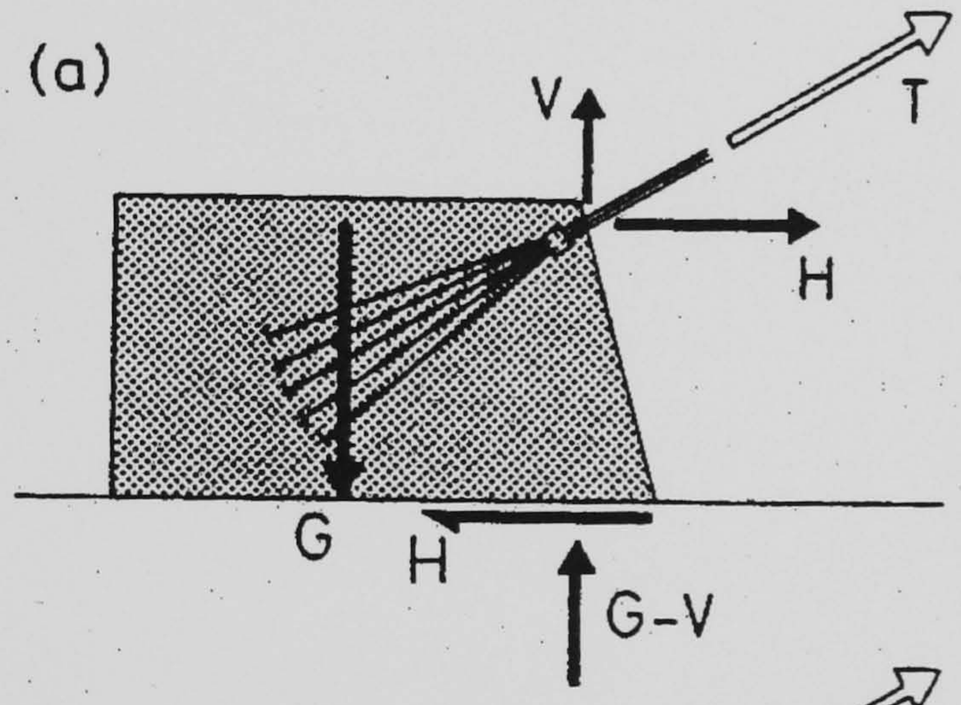

Figure 2.5.1: Types of anchorage – a) earth-anchored, b) self-anchored

Figure 2.7-1: Vortex development

CHAPTER 3

STRUCTURAL NONLINEARITIES

3.1 Introduction

One of the most common types of non-linearity that everybody encounters in everyday life falls into the category of Structural nonlinearities. A very simple example is when a person heavily loads a wooden shelf, the shelf sags more and more as time passes by. If the load-deflection curve for the shelf is plotted, it can be seen that it exhibits the characteristic non-linear behaviour – a changing stiffness –, which can be seen in Figure 3.1-1. The stiffness of the structure is proportional to the force applied to it and inversely proportional to the displacement it undergoes, and since in this case the force remains constant, the deflection of the shelf increases, causing the stiffness to decrease.

The causes of nonlinear structural behaviour fall into three categories: Changing Status, Geometric Nonlinearities and Material Nonlinearities, which are described very well in the ANSYS manual, ANSYS (1997).

The first category concerns non-linear behaviour that is status-dependent. For example, a tension-only cable can be either slack or taut. The stiffness of such an element, changes according to the state of the element, which in turn, depends on the load applied to it. When the cable is slack, it has no stiffness, whereas, when it is taut the cable possesses maximum stiffness.

The second category concerns structures that experience large deformations and the geometric rearrangement of the structure causes it to behave nonlinearly. For example, a fishing rod is extremely flexible. When the load at the tip is increased the rod deflects so much that the moment arm decreases, causing the rod tip to exhibit increasing stiffness at higher loads, Figure 3.1-2.

The last category concerns nonlinear stress-strain relationships. The factors that influence the stress-strain properties of a material are the load history, ambient conditions, such as temperature, and how long a load is applied on the structure (e.g. creep).

Cable-stayed bridges, as any other type of structure, experience a variety of loading conditions during their lifetime. This loading can either be due to traffic or due to ambient conditions such as wind, temperature fluctuations and earthquakes. The loading causes the bridge to deflect, induces internal stresses and both of these phenomena influence the dynamic behaviour of the structure.

As already mentioned in Chapter 2, section 2.8, cable-stayed bridges behave nonlinearly, and therefore, their analysis cannot be based on the assumption that the displacements of the structure are proportional to the applied load, since it has been proven to be approximate and for large spans unsafe. A nonlinear static analysis is required, and the use of finite element packages has made this requirement feasible.

The nonlinearities, present in cable-stayed bridges, fall into the category of *geometric nonlinearities.* In a non-linear structural analysis, they are divided into *stress-stiffening* and *large deformation* effects. Both of these effects influence the dynamic behaviour not only of cable-stayed bridges but also of any structure subjected to axial forces.

This chapter firstly investigates the phenomena of stress-stiffening and large deformations since they are used in the finite element analyses of the cable-stayed bridge cantilever presented in this work. However, the finite element formulation of these stiffness matrices has not been included in this work, but can be found in Fleming (1979), Fleming et al (1980). Secondly, the effect of stress stiffening on the dynamic characteristics of a simply supported beam is investigated. The undamped free vibrations of the beam are derived and the differences in the natural frequencies and modeshapes, between the cases of having an axial force acting on the beam or not, are shown.

3.2 Stress Stiffening and Large Deformations

Two types of non-linearity need to be considered in the design of cable-stayed bridges: Stress-stiffening and Large deformations.

Stress-stiffening

Stress stiffening is the stiffening of a structure caused by the interaction of an axial load with transverse displacements. It should be considered when dealing with thin structures with an axial stiffness significantly larger than their bending stiffness, such as cables, thin beams and shells. In finite element analyses, the stress stiffening effect is accounted for by creating an additional stiffness matrix, called the *stress stiffness matrix*, which is added to the regular stiffness matrix to form the total stiffness of the structure.

The stress stiffness matrix is calculated based on the state of stress of the structure at each equilibrium iteration. The load on the structure is applied in steps and at the end of each step, the stress state of the structure is determined and used to compute the stress stiffness matrix. At the end of the loading the stress stiffness matrix is added to the regular matrix to produce the total stiffness matrix of the structure, which will be used for modal analyses.

Stress stiffening capabilities are present in most commercial packages. However, the application of stress stiffening is not done by default, since at least two loading steps are required to determine the axial load on the structure. The engineer should consider the worst case-loading scenario applied on the structure, and this may involve the application of stress stiffening effects in the finite element analyses. This is necessary especially when dynamic data from a loaded structure is used to update an analytical model. The inclusion of stress stiffening in the analyses will increase the computer's processing time, but it is a requirement when dealing with loaded structures.

Large deflections

Sometimes, when the structure is particularly flexible and the load applied to it is quite large, as is the case with cable-stayed bridges, the structure undergoes

significant changes in its geometry that cannot be accounted for by the inclusion of stress stiffening alone. As the load is applied in steps, the structure deforms and the equilibrium equations should be satisfied in order to account for the new geometry of the structure.

The displacements experienced by any element used in finite element analyses can be decomposed into a rigid body translation coupled with a rotation and a component that causes straining of the element:

$$\{u^{tot}\} = \{u^{rigid}\} + \{u^{strain}\} \tag{3.2-1}$$

where,

$\{u^{rigid}\}$ is for rigid body motion, containing both rotation and translation, and

$\{u^{strain}\}$ is for the displacements that cause straining of the element.

The application of large deformation effects is possible in most commercial packages.

3.3 Eigenvectors and Eigenvalues of a MDOF system

A brief description of the theory behind the natural frequencies and modeshapes of a MDOF system is given herein. Lets consider the system in Figure 3.3-1, which, has a mass $[M]$, damping $[D]$ and stiffness $[K]$, and is subjected to an external force $\{f(t)\}$ which is a function of time.

The equation of motion of this system is given in Equation (3.3-1):

$$[M]\{\ddot{x}\} + [D]\{\dot{x}\} + [K]\{x\} = \{f(t)\} \tag{3.3-1}$$

where,

$\{x\}$ is the displacement of the structure and $\{\dot{x}\}, \{\ddot{x}\}$ are the first and second derivatives of the displacement with respect to time.

The mass and stiffness properties of a structure are usually easily measured or derived, but the modelling of damping is less easily achieved. The damping parameter is the one that dominates the amplitude of the response of the structure in the region of resonance. However, its value is usually quite low and can often be neglected.

The most straightforward case to demonstrate the derivation of natural frequencies and modeshapes is not to consider the damping parameter, and therefore, have an undamped system.

The undamped equation of motion becomes:

$$[M]\{\ddot{x}\}+[K]\{x\}=\{f(t)\} \tag{3.3-2}$$

For free oscillations, the above relationship becomes:

$$[M]\{\ddot{x}\}+[K]\{x\}=0 \tag{3.3-3}$$

A possible solution to the above equation can be the following:

$$\{x\}=\{\Psi\}_j e^{i\omega_j t} \tag{3.3-4}$$

where, ω_j are the natural frequencies.

Substituting equation (3.3-4) into equation (3.3-3) leads to the eigenvalue problem:

$$[K]\{\Psi\}_j=\lambda_j[M]\{\Psi\}_j \tag{3.3-5}$$

where,

$$\lambda_j=\omega_j^2 \tag{3.3-6}$$

and $\{\Psi\}_j$ are the *modeshapes* or *eigenvectors* corresponding to *natural frequencies* or *eigenvalues* $\{\omega\}_j$.

The eigenvectors have two very important properties. One is *orthogonality*:

$$\{\Psi\}_i^T [M]\{\Psi\}_j = 0, \qquad i \neq j \tag{3.3-7}$$

and

$$\{\Psi\}_i^T [K]\{\Psi\}_j = 0, \qquad i \neq j \tag{3.3-8}$$

The other property is *normalisation*. The arbitrarily scaled modeshapes can be normalised with respect to unity or mass. If they are *mass-normalised*, the following expressions are valid:

$$[\Phi]^T [M][\Phi] = [I] \tag{3.3-9}$$

and

$$[\Phi]^T [K][\Phi] = diag(\lambda) \tag{3.3-10}$$

where, $[\Phi]$ are the mass-normalised eigenvectors.

3.4 Modeshapes and Natural Frequencies of a distributed system

Consider the beam shown in Figure 3.4-1. The beam has a flexural stiffness $EI(x)$, mass per unit length $m(x)$ and is of length L. The stiffness and the mass of the beam vary with position x along its length. The beam is loaded with a load $p(x.t)$, which varies with position along the beam and with time. The displacement response of the beam $u(x,t)$ is also a function of these variables. The beam is considered to be simply-supported at both ends.

In order to write the equation of motion of this system, one needs to consider the equilibrium of forces acting on a segment of the beam shown in Figure 3.4-2.

Summing all forces acting vertically:

$$V(x,t)+p(x,t)dx-\left[V(x,t)+\frac{\partial V(x,t)}{\partial x}dx\right]-f_I(x,t)dx=0 \qquad (3.4\text{-}1)$$

where,

$V(x,t)$ is the vertical force acting on the cut section and $f_I(x,t)dx$ is the resultant transverse inertial force equal to the mass of the element multiplied by its transverse acceleration:

$$f_I(x,t)dx=m(x)dx\frac{\partial^2 u(x,t)}{\partial t^2} \qquad (3.4\text{-}2)$$

Substituting equation (3.4-2) into equation (3.4-1) and dividing by dx one gets:

$$\frac{\partial V(x,t)}{\partial x}=p(x,t)-m(x)\frac{\partial^2 u(x,t)}{\partial t^2} \qquad (3.4\text{-}3)$$

The second equilibrium equation is obtained by taking moments about point A. If only first order terms are considered, then one gets:

$$M(x,t)+V(x,t)dx-\left[M(x,t)+\frac{\partial M(x,t)}{\partial x}dx\right]=0 \qquad (3.4\text{-}4)$$

The above equation is simplified into the following expression:

$$\frac{\partial M(x,t)}{\partial x}=V(x,t) \qquad (3.4\text{-}5)$$

Differentiating (3.4-5) with respect to x and substituting into equation (3.4-3):

$$\frac{\partial^2 M(x,t)}{\partial x^2} + m(x)\frac{\partial^2 u(x,t)}{\partial t^2} = p(x,t) \tag{3.4-6}$$

Introducing the moment-curvature equation:

$$M(x,t) = EI(x)\frac{\partial^2 u(x,t)}{\partial x^2} \tag{3.4-7}$$

Equation (3.4-6) becomes:

$$\frac{\partial^2}{\partial x^2}\left[EI(x)\frac{\partial^2 u(x,t)}{\partial x^2}\right] + m(x)\frac{\partial^2 u(x,t)}{\partial t^2} = p(x,t) \tag{3.4-8}$$

This is the equation of motion of a 2-dimensional beam in flexure. The solution to the above equation should satisfy the boundary conditions at $x = 0$ and $x = L$.

3.5 Undamped free vibrations of the distributed system

The equation of motion of a beam subjected to a transverse loading has been derived in the previous section. This section is concerned with the evaluation of the natural frequencies and modeshapes of the system. However, in order to simplify the problem, the beam is considered to have uniform properties along its length. Therefore, $EI(x)$ and $m(x)$ are set as constants EI and m, respectively. Using equation (3.4-8), the free-vibration equation of motion of the beam becomes:

$$EI\frac{\partial^4 u(x,t)}{\partial x^4} + m\frac{\partial^2 u(x,t)}{\partial t^2} = 0 \tag{3.5-1}$$

If equation is divided by EI then one obtains:

$$u^{iv}(x,t) + \frac{m}{EI}\ddot{u}(x,t) = 0 \tag{3.5-2}$$

where, the dot notation indicates derivatives with respect to time, whereas, the prime notations denote derivatives with respect to x.

A solution to the last equation could be the following:

$$u(x,t) = \phi(x)\mathrm{Y}(t) \tag{3.5-3}$$

where, $\phi(x)$ denotes the shape of the vibration of the beam and $\mathrm{Y}(t)$ is the time-dependent amplitude of the vibration.

Substituting equation (3.5-3) into equation (3.5-2) one gets:

$$\phi^{iv}(x)\mathrm{Y}(t) + \frac{m}{EI}\phi(x)\ddot{\mathrm{Y}}(t) = 0 \tag{3.5-4}$$

Dividing equation (3.5-4) by $\phi(x)\mathrm{Y}(t)$

$$\frac{\phi^{iv}(x)}{\phi(x)} + \frac{m}{EI}\frac{\ddot{\mathrm{Y}}(t)}{\mathrm{Y}(t)} = 0 \qquad 5\text{-}5)$$

The above equation is satisfied only if each term is a constant:

$$\frac{\phi^{iv}(x)}{\phi(x)} = -\frac{m}{EI}\frac{\ddot{\mathrm{Y}}(t)}{\mathrm{Y}(t)} = a^4 \tag{3.5-6}$$

This equation leads to two differential equations:

$$\ddot{\mathrm{Y}}(t) + \omega^2\mathrm{Y}(t) = 0 \tag{3.5-7}$$

and

$$\phi^{iv}(x) - a^4\phi(x) = 0 \tag{3.5-8}$$

where,

$$\omega^2 \equiv \frac{a^4 EI}{m} \tag{3.5-9}$$

The solution to equation (3.5-7), which is the equation of motion of an undamped SDOF system with no forcing, is given by:

$$\mathrm{Y}(t) = A\cos\omega t + B\sin\omega t \tag{3.5-10}$$

where the constants A, B can be found using initial conditions.

A solution to equation (3.5-8) can be of the form:

$$\phi(x) = \mathrm{Re}^{sx} \tag{3.5-11}$$

Substituting equation (3.5-11) into (3.5-8) one gets the following expression:

$$\left(s^4 - a^4\right)\mathrm{Re}^{sx} = 0 \tag{3.5-12}$$

where,

$$s_{1,2} = \pm ia \quad \text{and} \quad s_{3,4} = \pm a \tag{3.5-13}$$

The solution can be written in the form:

$$\phi(x) = A_1\cos ax + A_2\sin ax + A_3\cosh ax + A_4\sinh ax \tag{3.5-14}$$

The values of the constants can be found from the boundary conditions.

Since the beam is considered to be simply-supported at both ends, the following boundary conditions apply:

When:

$$x = 0 \qquad \phi(0) = 0, \quad M(0) = EI\phi''(0) = 0 \tag{3.5-15a}$$

$$x = L \qquad \phi(L) = 0, \quad M(L) = EI\phi''(L) = 0 \tag{3.5-15b}$$

By doing all the mathematics, one gets the n natural frequencies of the vibrations and the modeshapes as:

$$\omega_n = \frac{n^2\pi^2}{L^2}\sqrt{\frac{EI}{m}} \tag{3.5-16}$$

and

$$\phi_n(x) = A_2 \sin\frac{n\pi}{L}x \qquad n = 1,2,... \tag{3.5-17}$$

3.6 Equation of motion of a distributed system subjected to an axial force

The beam considered in the previous sections is now subjected to an axial force, Figure 3.6-1, which alters the equilibrium of the forces and produces an extra term in the moment equation, derived in Section 3.4.

Taking moments at A, Figure 3.6-2, the new moment equilibrium equation becomes:

$$M(x,t) + V(x,t)dx + N(x)\frac{\partial u(x,t)}{\partial x}dx - \left[M(x,t) + \frac{\partial M(x,t)}{\partial x}dx\right] = 0 \tag{3.6-1}$$

The vertical force is given by:

$$V(x,t) = -N(x)\frac{\partial u(x,t)}{\partial x} + \frac{\partial M(x,t)}{\partial x} \tag{3.6-2}$$

The new equation of motion including axial force effects becomes:

$$\frac{\partial^2}{\partial x^2}\left[EI(x)\frac{\partial^2 u(x,t)}{\partial x^2}\right]-\frac{\partial}{\partial x}\left[N(x)\frac{\partial u(x,t)}{\partial x}\right]+m(x)\frac{\partial^2 u(x,t)}{\partial t^2}=p(x,t) \qquad (3.6\text{-}3)$$

As one can see, an axial force affects the dynamic behaviour of the beam, which consequently, affects the frequencies and modeshapes of the system. The next section describes the effects of the inclusion of an axial force on the dynamic characteristics of the beam.

3.7 Natural frequencies and modeshapes of the distributed system subjected to an axial force

Assuming that the beam has uniform properties as discussed in Section 3.5 the equation of motion of the beam becomes:

$$EI\frac{\partial^4 u(x,t)}{\partial x^4}-N\frac{\partial^2 u(x,t)}{\partial x^2}+m\frac{\partial^2 u(x,t)}{\partial t^2}=0 \qquad (3.7\text{-}1)$$

Separating the variables as before and using the prime and dot notation for simplicity,

$$\frac{\phi^{iv}(x)}{\phi(x)}-\frac{N}{EI}\frac{\phi''(x)}{\phi(x)}=-\frac{m}{EI}\frac{\ddot{\mathrm{Y}}(t)}{\mathrm{Y}(t)}=a^4 \qquad (3.7\text{-}2)$$

The two equations of motion are given by:

$$\ddot{\mathrm{Y}}(t)+\omega^2\mathrm{Y}(t)=0 \qquad (3.7\text{-}3)$$

and

$$\phi^{iv}(x)-g^2\phi''(x)-a^4\phi(x)=0 \qquad (3.7\text{-}4)$$

where,

$$g^2 \equiv \frac{N}{EI} \tag{3.7-5}$$

By considering that the beam is simply-supported, a solution to equation (3.7-1) could be the following:

$$u(x,t) = B\sin\left(\frac{n\pi x}{L}\right)\sin(\omega_n t + \alpha) \tag{3.7-6}$$

The natural frequencies of the beam are given by:

$$\omega_n = \left(\frac{n\pi}{L}\right)^2 \sqrt{\frac{EI}{m}\left(1 + \frac{NL^2}{n^2\pi^2 EI}\right)} \tag{3.7-7}$$

Substituting the Euler buckling load in the above equation

$$\omega_n = \left(\frac{n\pi}{L}\right)^2 \sqrt{\frac{EI}{m}\left(1 + \frac{N}{N_{Euler}}\right)} \tag{3.7-8}$$

where, the Euler load is given by

$$N_{Euler} = \frac{n^2\pi^2 EI}{L^2} \tag{3.7-9}$$

The expression for the modeshapes is given by:

$$\phi(x) = A_1 \cos gx + A_2 \sin gx + A_3 x + A_4 \tag{3.7-10}$$

The constants can be found by considering the boundary conditions.

As one can see from equations (3.7-7) and (3.5-16), the frequencies of a system, when axial loads are included, are reduced compared with the frequencies of the same system when no axial forces are applied.

3.8 Concluding remarks

This chapter presented the phenomena of stress-stiffening and large deformations, which should be considered when modelling cable-stayed bridges. Also derivations of the undamped free vibrations of a beam, with and without an axial load, are included and the differences in the natural frequencies and modeshapes between the two cases were shown. It was concluded that the frequencies of the beam subjected to an axial load were reduced compared with the corresponding frequencies of the beam before the application of axial loading.

A theoretical description of both of these phenomena was considered to be important since stress-stiffening and large deformations will be taken into account in the theoretical modelling of the cable-stayed bridge cantilever presented in Chapter 6. The model's stiffness matrix will include the stress stiffness matrix together with the regular matrix and will be used to calculate the natural frequencies and modeshapes of the cantilever model. This model will then be used for further studies and in particular for the planning of the experimental testing and for model optimization carried out in Chapter 6.

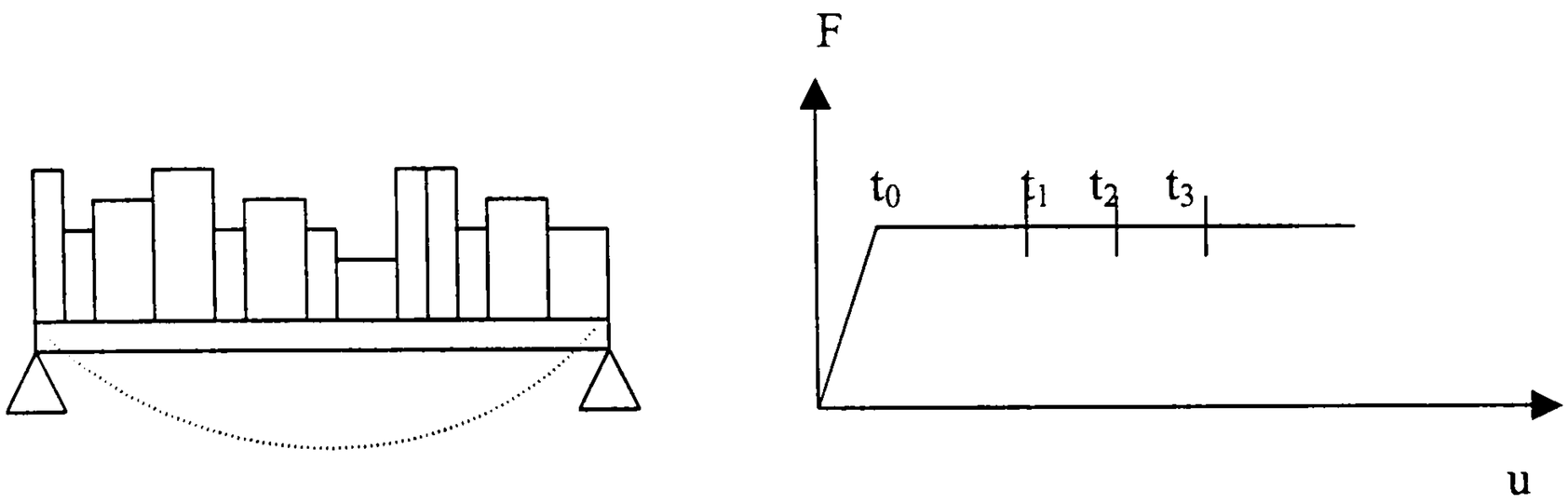

Wooden shelf

Load – deflection curve

Figure 3.1-1: Example of non-linear behaviour

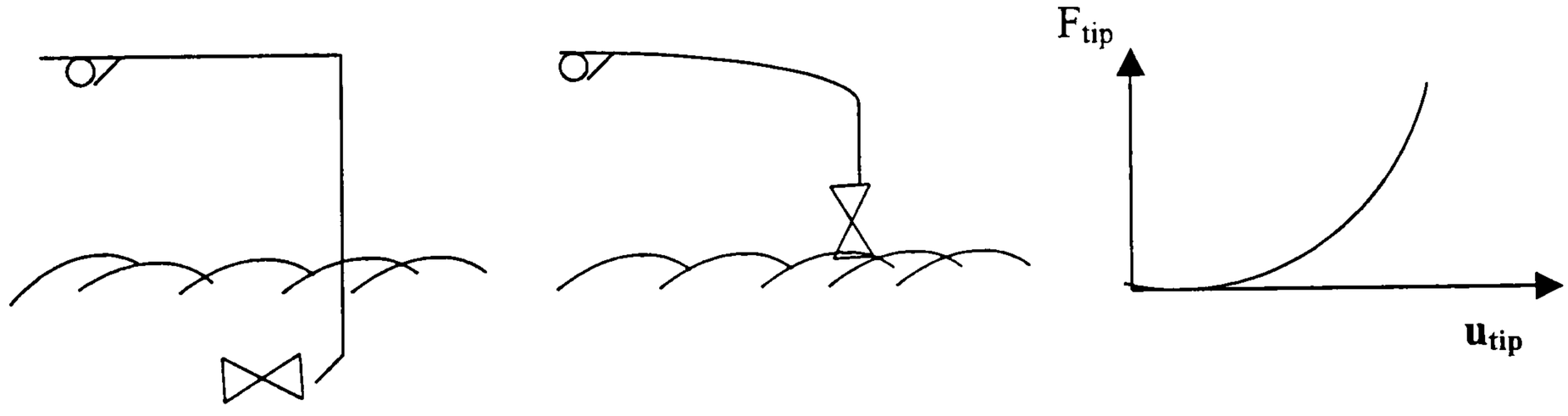

Figure 3.1-2: Fishing rod demonstrating geometric nonlinearity

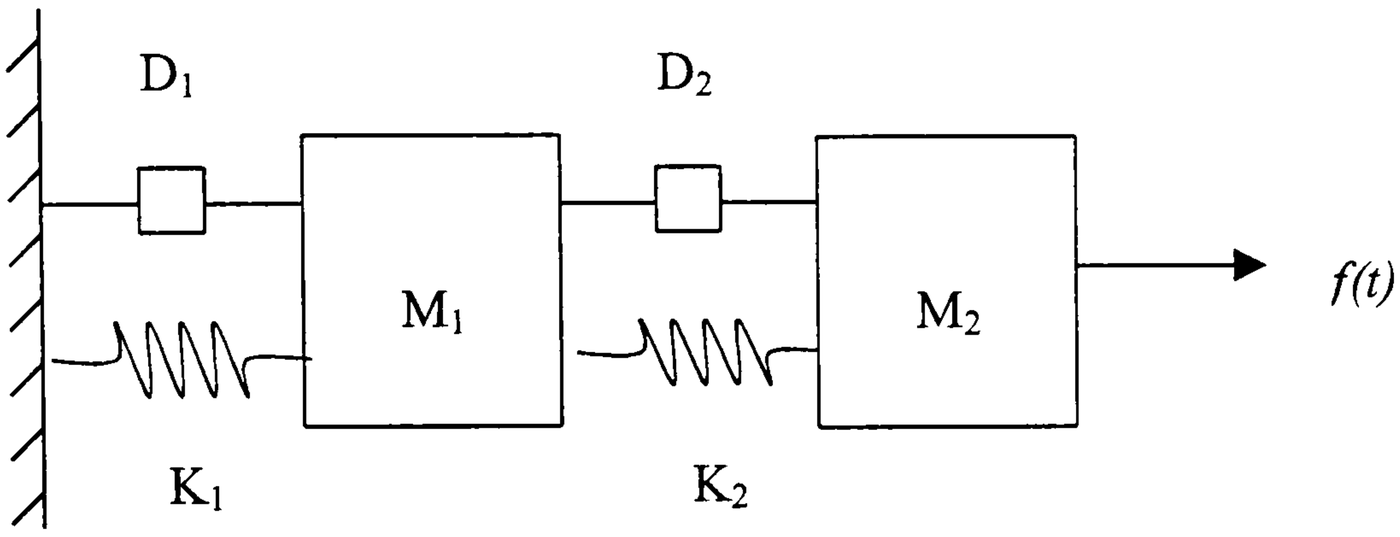

Figure 3.3-1: Multi-degree-of-freedom oscillator

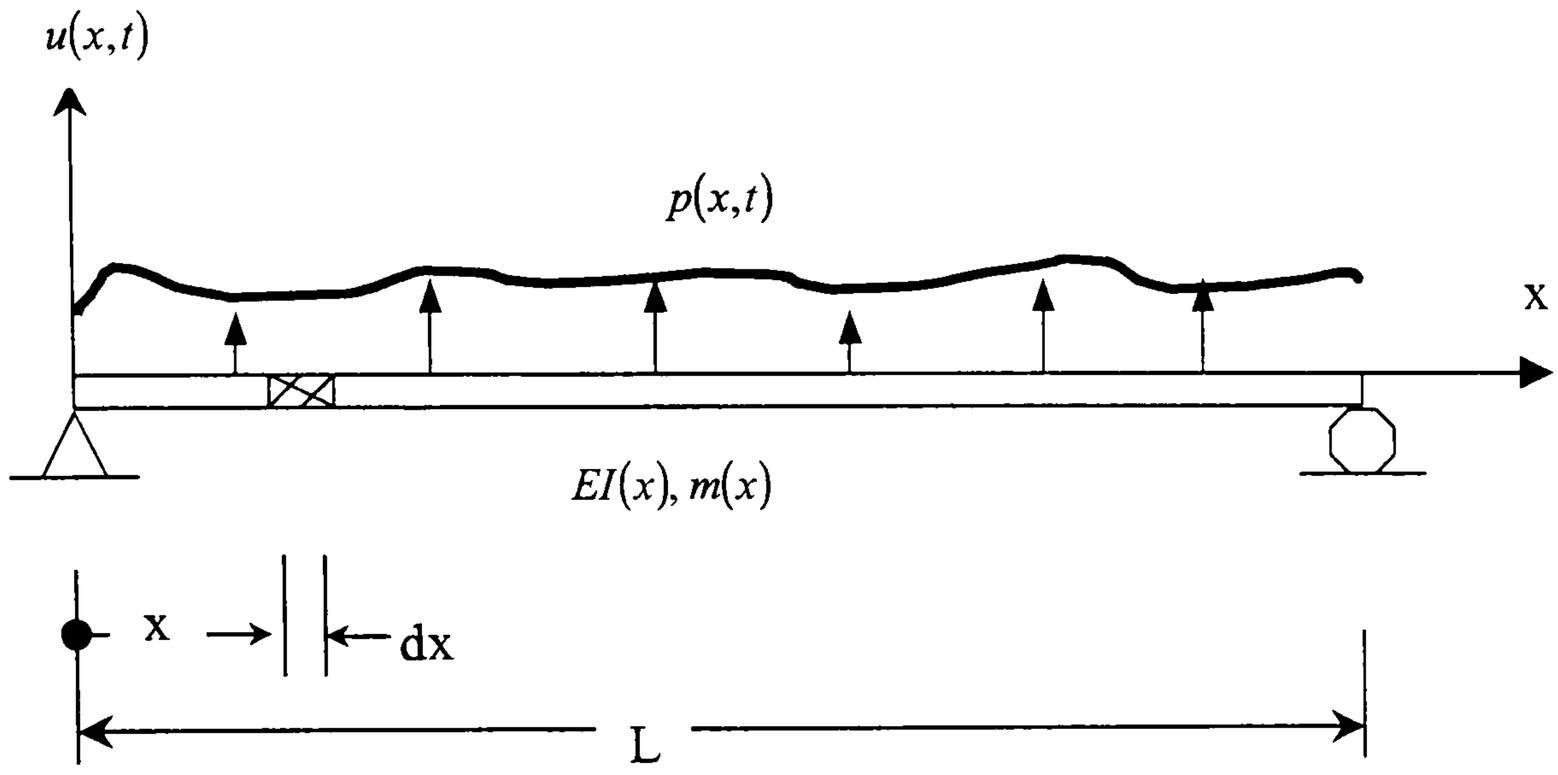

Figure 3.4-1: 2-D beam subjected to dynamic loading

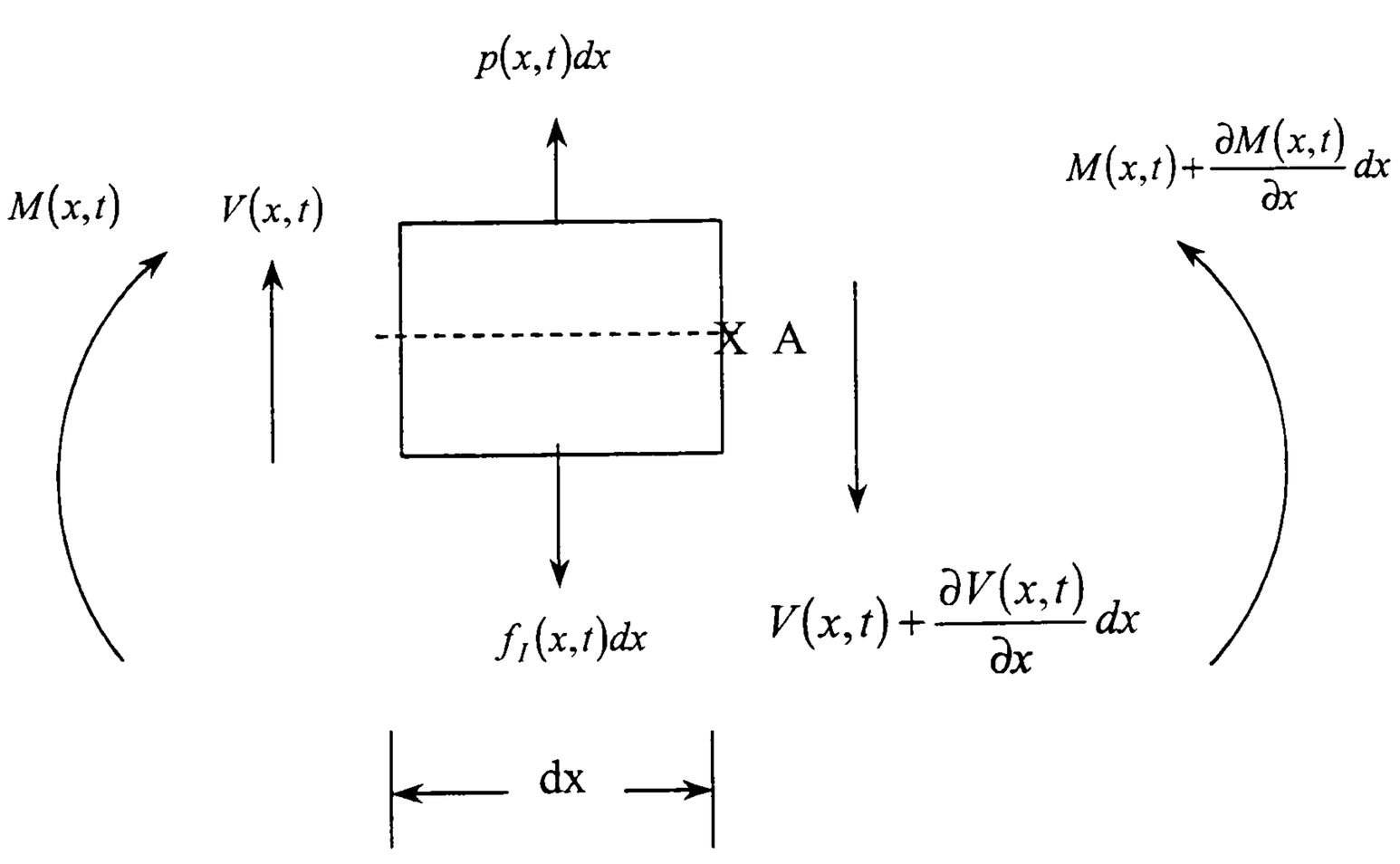

Figure 3.4-2: Forces acting on beam segment

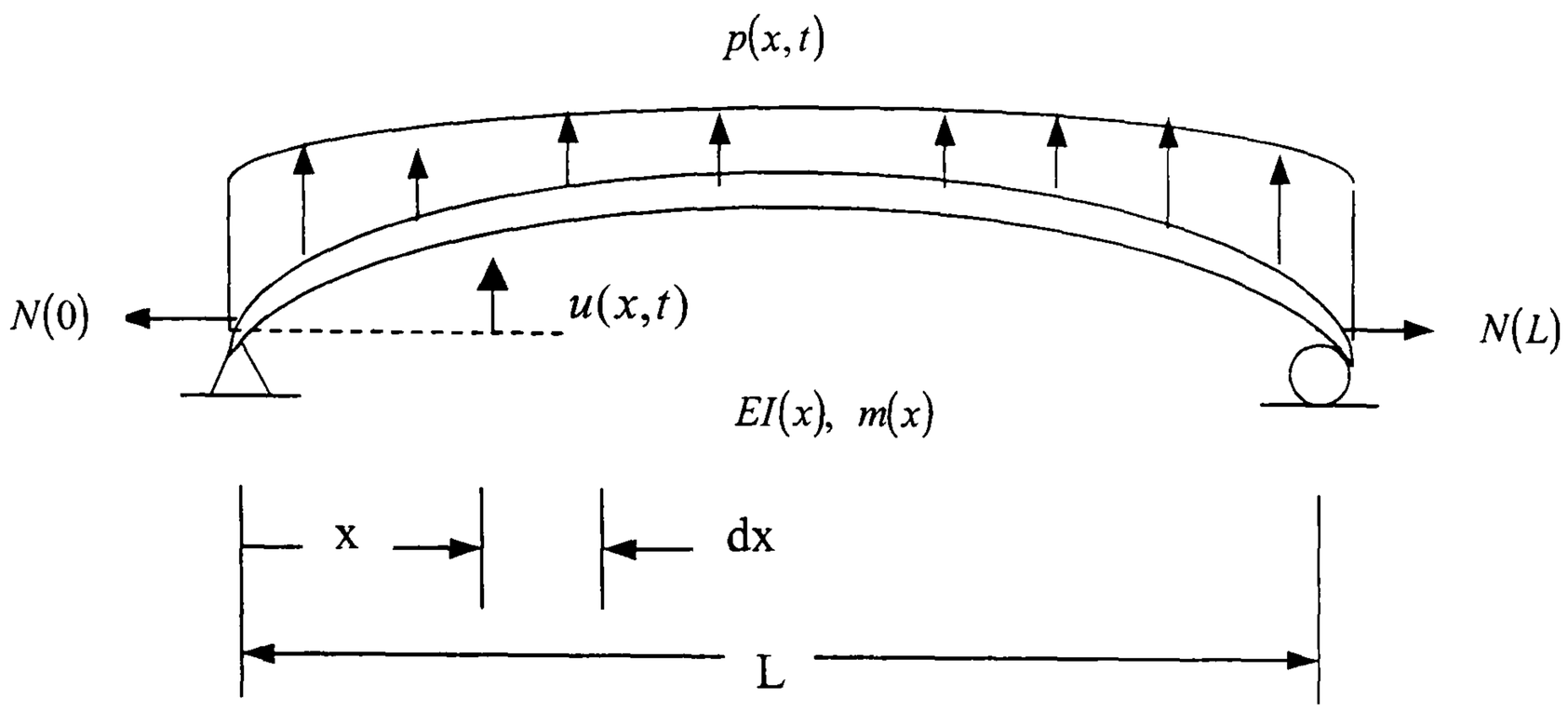

Figure 3.6-1: Beam with lateral and axial loading

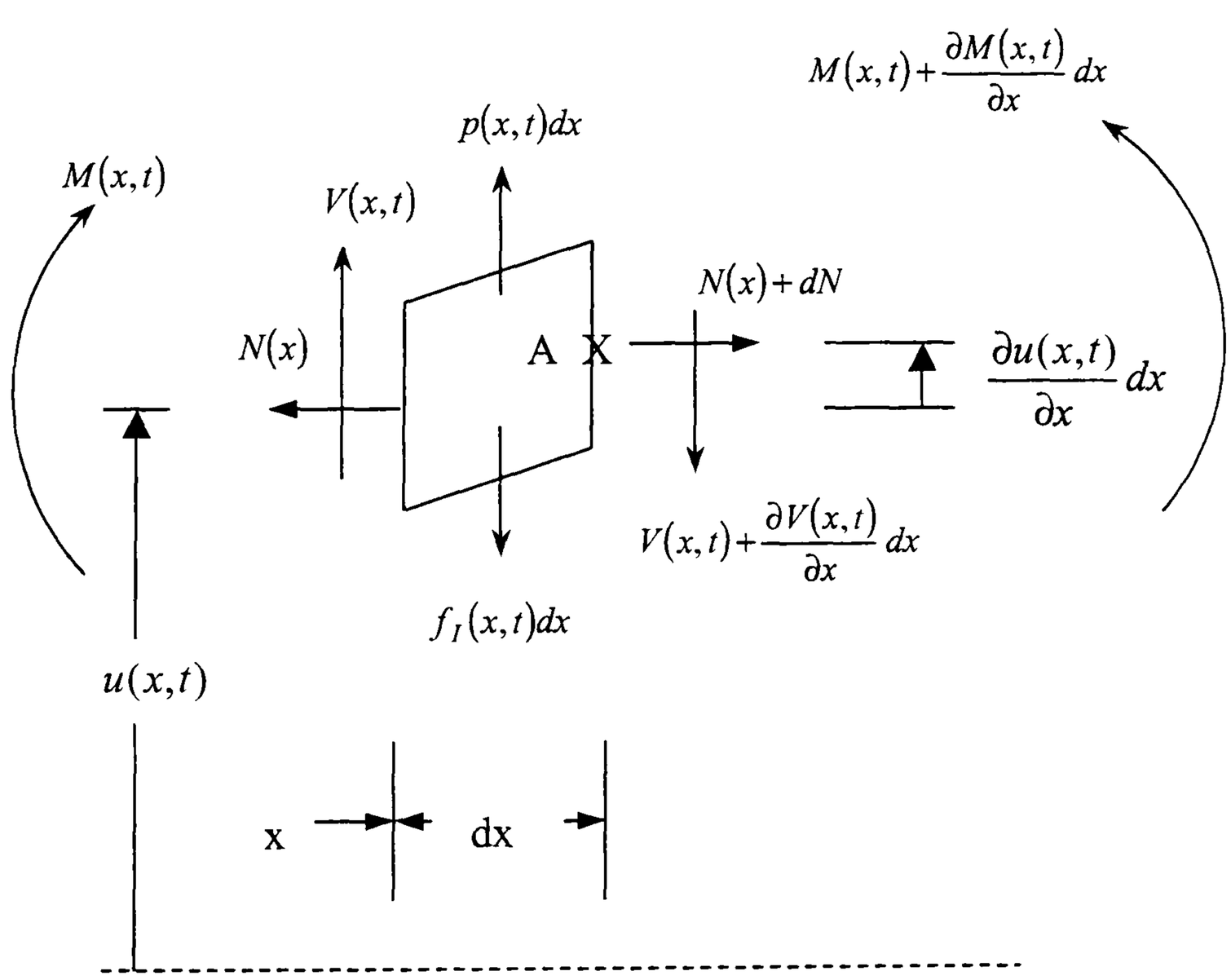

Figure 3.6-2: Forces acting on element with applied axial load and shear force

CHAPTER 4

PLANNING OF EXPERIMENTAL TESTING

4.1 Introduction

Vibration analysis is a useful tool for obtaining information about the dynamic properties of a structure. These properties could either be the mass, stiffness and damping distribution of the structure or its natural frequencies and modeshapes. There are two routes to vibration analysis, named the Analytical and the Experimental route shown in Figures 4.1-1 and 4.1-2.

The three phases of a theoretical route to vibration analysis are shown in the Figure 4.1-1. One usually starts with a description of the structure's spatial characteristics, such as the mass and stiffness of the structure – damping is a rare luxury from an analytical model. By performing analytical modal analysis, one obtains the modal model, which is described by a set of vibration modes. This solution describes the ways in which the structure can vibrate naturally, without external forcing or excitation and these modes of vibration are called the natural modes of the model. The third stage describes how the structure vibrates under excitation conditions. This depends on the structure's inherent properties and on the type and magnitude of the excitation. An analysis of the response of the structure to an external force leads to the Response model of the structure. This model consists of a set of Frequency Response Functions (FRF), which is defined over the applicable frequency range.

However, this process can be undertaken in the reverse direction, which can be seen in Figure 4.1-2. One starts with a set of Frequency Response Functions from an experimental test and, after modal analyses, can obtain the mass, stiffness and damping properties of the structure. Modal testing is the technique used to obtain the Frequency Response Functions of a structure tested in the laboratory.

In order to carry out modal testing in the laboratory and obtain the Frequency Response Functions or the natural frequencies and modeshapes of a model. the support positions, the location of the excitation source and the sensor arrangement should be planned carefully beforehand. Various methods have been developed for defining the support, excitation and sensor locations and these are presented in the following sections. More attention is paid to optimum sensor placement techniques, since, due to limited number of transducers available for any experimental test, the sensors should be placed in the right positions on the model in order to obtain the most relevant dynamic information from the vibration test.

4.2 Pre-test planning

Modal testing is a method of constructing a mathematical model, ie a set of modes of vibration and natural frequencies, of a structure's dynamic behaviour based on data obtained from vibration tests. Therefore, an accurate representation of the structure's dynamics requires results of high quality, which is sensitive to the experimental set-up.

Each time an experimental test on a structure is to be carried out, one has to decide how the structure can be supported and which positions are suitable to place the measurement transducers and excitation source. In order to select the best measurement, excitation and support positions, a theoretical model of the structure's dynamics is required, so that the modeshapes and natural frequencies will be used to select the set of locations. However, one should also keep in mind that only a limited number of positions and modes can be measured in any experimental test, making the test data relatively incomplete in comparison with the theoretical data. However, there are some techniques available to the experimentalist, which either reduce the analytical or expand the experimental model, so that the two models are comparable. These techniques are described in the next chapter, which is dedicated to model updating, for which, the number of measured degrees-of-freedom is generally greater than the number of measured modes.

4.3 Optimum actuator positions

An approach to find the best possible excitation locations for a modal test on a structure is described in Imamovic (1998). A brief description of the mathematical background of this approach is given here. However, the reader can find a detailed derivation of the formulae in the above thesis.

The equation of motion of an oscillator, Figure 3.3-1, of mass [M], damping [D] and stiffness [K], subjected to an number of external harmonic forces:

$$\{f(t)\} = \{F(\omega)\}e^{i\omega t} \tag{4.3-1}$$

is given by:

$$[M]\left\{\ddot{x}(t)\right\} + [D]\left\{\dot{x}(t)\right\} + [K]\{x(t)\} = \{f(t)\} \tag{4.3-2}$$

$$\left(-\omega^2\,[M] + i[D] + [K]\right)\{X(\omega)\}e^{i\omega t} = \{F(\omega)\}e^{i\omega t} \tag{4.3-3}$$

$$\{X(\omega)\} = [\alpha(\omega)]\{F(\omega)\} \tag{4.3-4}$$

where, the receptance matrix of the system is given by:

$$[\alpha(\omega)] = \left(-\omega^2\,[M] + i[D] + [K]\right)^{-1}, \tag{4.3-5}$$

A general term of the receptance can be written as a function of the natural frequencies and modeshapes of the system in the form:

$$\alpha_{jk}(\omega) = \sum_{r=1}^{N} \frac{\phi_{j,r}\phi_{k,r}}{\omega_r^2 - \omega^2 + i\eta_r\omega_r^2} \tag{4.3-6}$$

where,

ω and ω_r are the forcing frequency and the natural frequency of the system, respectively.

$\phi_{j,r}$ and $\phi_{k,r}$ is the modeshape r at j, k coordinates, and

η_r is the damping parameter of the system.

If the system is excited at a frequency that is equal to the natural frequency of mode r, then,

$$\omega \approx \omega_r \tag{4.3-7}$$

and the receptance is given by:

$$\alpha_{jk}(\omega_r) \approx \frac{\phi_{j,r}\phi_{k,r}}{i\eta_r\omega_r^2} \tag{4.3-8}$$

Substituting this expression into equation (4.3-4), which gives the amplitudes of vibration, it can be seen that the term $\frac{\phi_{j,r}\phi_{k,r}}{i\eta_r\omega_r^2}$ can be associated with a displacement quantity because it is directly proportional to the amplitude vector at the frequency ω_r:

$$X(\omega) \propto \frac{\phi_{j,r}\phi_{k,r}}{i\eta_r\omega_r^2} \tag{4.3-9}$$

The displacement, velocity and acceleration can be expressed as:

$$x(t) = X(\omega_r)e^{i\omega_r t} \tag{4.3-10}$$

$$\dot{x}(t) = i\omega_r X(\omega_r)e^{i\omega_r t} \tag{4.3-11}$$

$$\ddot{x}(t) = -\omega_r^2 X(\omega_r)e^{i\omega_r t} \tag{4.3-12}$$

Substituting (4.3-9) into expressions (4.3-10), (4.3-11) and (4.3-12) the amplitudes of vibration of these quantities are given by:

$$Displacement\ Amplitude \propto \frac{\phi_{j,r}\phi_{k,r}}{\omega_r^2} \tag{4.3-13}$$

$$Velocity\ Amplitude \propto \frac{\phi_{j,r}\phi_{k,r}}{\omega_r} \tag{4.3-14}$$

$$Acceleration\ Amplitude \propto \phi_{j,r}\phi_{k,r} \tag{4.3-15}$$

The damping parameter, which appears in expression (4.3-9), is omitted in equations (4.3-13) to (4.3-15) because it is difficult to predict the damping parameters in the preliminary theoretical analysis. In this case, the structure is assumed to undergo undamped vibrations with maximum amplitude. If the inclusion of damping is required, it is usual to specify the same value of damping to all modes, which will give the same weighting to the modes and make the analysis insensitive to damping.

4.3.1 Average Displacement, Velocity and Acceleration Amplitudes

When a structure vibrates at a particular excitation, there is a pattern of amplitudes of vibration, which is determined by the contribution of all modes.

In order to predict the average response at a particular degree-of-freedom, j, for displacement, Imamovic (1998) gives the following expression for the Average Driving DOF Displacement (ADDOFD), which is the average sum of all contributing modes, m:

$$ADDOFD(j) = \sum_{r=1}^{m} \frac{\phi_{jr}^2}{\omega_r^2} \tag{4.3.1-1}$$

Similarly the Average Driving DOF Velocity (ADDOFV) is given by:

$$ADDOFV(j) = \sum_{r=1}^{m} \frac{\phi_{jr}^2}{\omega_r} \tag{4.3.1-2}$$

The Average Driving DOF Acceleration (ADDOFA) is given by:

$$ADDOFA(j) = \sum_{r=1}^{m} \phi_{jr}^2 \qquad (4.3.1\text{-}3)$$

The term 'Average' is assigned to the above definitions because there are several modes that contribute to the response.

Imamovic suggests the use of the above parameters in order to find the best locations to place the excitation source. If the structure is excited using a hammer, regions of high velocity must be avoided, because hitting in the vicinity of these positions could cause double-hit effects. Therefore, the ADDOFV parameter should be used to decide where the structure can be excited using a hammer and regions of high values of ADDOFV should be avoided. However, if the structure is excited using a shaker, then the experimentalist should minimise the interference of the shaker during the testing. The interference will be the least where the acceleration of the structure is minimum. Therefore, the parameter ADDOFA can be used to find the regions where the acceleration has a minimum value.

4.4 Optimum support positions

Before a modal test is undertaken, the experimentalist should determine the support positions of the structure so that the required boundary conditions are achieved. A common case of modal testing is testing for free-free boundary conditions, where in theory, the structure is not attached to the ground at any of its coordinates and is freely suspended in space. However, in practice a truly free support is not feasible and the structure is suspended on soft springs, eg light elastic bands. To ensure that these support conditions will not interfere much with the results, the suspension should be attached as close to nodal points as possible. The optimum suspension positions are, therefore, in locations where the displacement response of the structure is lowest. The parameter ADDOFD can be used to find these regions of minimum displacement. However, one should never forget that there are practical limitations as to where and how a structure can be suspended.

4.5 Optimum measurement positions

As already mentioned in Chapter 1, the requirement for optimal sensor placement stems from the fact that there is always a limited number of transducers that can be used during a modal test and the need for good quality estimates of modal parameters from noisy data.

The problem of optimal sensor placement can be addressed as follows: "given a limited set of sensors, where should they be located on a structure so that the data collected from those locations yields the best information about the structure's dynamics?"

Many researchers have proposed techniques for optimally position sensors on a structure for system identification. This work considers three different methods: the Effective Independence method (EIM), the Energy Matrix Rank Optimisation (EMRO) and the Energy Optimisation Technique (EOT). The methods are described below.

4.5.1 Optimum sensor location techniques

4.5.1.1 Effective Independence method (EfI)

This section presents a methodology for selecting an optimum set of sensor locations for identification and correlation of a given set of target modes, Kammer (1991, 1992). Initially, a candidate set of sensor locations is selected which should be large enough to include all of the important dynamics within the target modes. However, the placement of the sensors in the initial set of locations is impossible and the set must be reduced in an optimal fashion.

For the purpose of test-analysis correlation, the analyst must obtain measurements at such locations on the structure that the modeshapes will be linearly independent or spatially differentiable. This implies that if the sensor output equation is given by

$$\{u\}_s = [\Phi]_s \{q\} \qquad (4.5.1.1\text{-}1)$$

where,

$\{u\}_s$ is the output from the sensors,

$[\Phi]_s$ is the matrix of the target modes partitioned to the sensor locations,

$\{q\}$ is the vector of the target modal coordinates,

an estimate for the target coordinates can be computed from

$$\left\{\hat{q}\right\} = \left[[\Phi]_s^T[\Phi]_s\right]^{-1}[\Phi]_s^T\{u\}_s \qquad (4.5.1.1\text{-}2)$$

The target coordinates must be absolutely identifiable, which means that they must be independent. If the candidate sensor set contains *s* locations but one has to limit the number of sensors down to only *m*, $m<s$, one will have to place the *m* sensors within the *s* locations while maintaining as much independent information as possible and obtaining the best estimates of the target states. The best estimate means that the covariance matrix of the estimate errors will be a minimum. A modification is introduced in equation (4.5.1.1-1)

$$\{u\}_s = \{H(q)\} + \{N\} = [\Phi]_s\{q\} + \{N\} \qquad (4.5.1.1\text{-}3)$$

where,

{H} represents the process measurement,

{N} represents stationary Gaussian white noise of variance $\left[\Psi_o^2\right]$.

For an efficient unbiased estimator, the covariance matrix of the estimate error is given by:

$$[P] = E\left[\left(\{q\} - \left\{\hat{q}\right\}\right)\left(\{q\} - \left\{\hat{q}\right\}\right)^T\right] = \left[\left(\frac{\partial H}{\partial q}\right)^T\left[\Psi_o^2\right]^{-1}\left(\frac{\partial H}{\partial q}\right)\right]^{-1} \qquad (4.5.1.1\text{-}4)$$

where, E denotes the expected value.

The covariance matrix is given by:

$$[P] = \left[[\Phi]_s^T [\Psi_o^2]^{-1} [\Phi]_s \right]^{-1} = [Q]^{-1} \qquad (4.5.1.1\text{-}5)$$

Maximising [Q] leads to the minimisation of the covariance matrix and the best estimate {q}. In order to simplify the analysis, the measurement noise is assumed to be uncorrelated and possess identical statistical properties for each sensor leading to a diagonal noise covariance matrix.

The matrix [Q] can be expressed as

$$[Q] = [\Psi_o^2]^{-1} [\Phi]_s^T [\Phi]_s = [\Psi_o^2]^{-1} [A_o] \qquad (4.5.1.1\text{-}6)$$

Therefore, to minimise $[P]$, a suitable norm $[A_0]$ must be maximised, and therefore, the rank of the modal matrix $[\Phi]_s^T [\Phi]_s$ must be maximised. $[A_0]$ will be referred to as the "Fisher information matrix". One property that this matrix possesses is that its determinant can be related to the definition of information. The larger the determinant, the more information the matrix contains.

The matrix $[A_0]$ can be expressed in terms of the contribution of each degree of freedom as following

$$[A_o] = \sum_{i=1}^{s} \{\Phi\}_s^{iT} \{\Phi\}_s^i = \sum_{i=1}^{s} [A]^i \qquad (4.5.1.1\text{-}7)$$

where, $\{\Phi\}_s^i$ is the ith row of the modal partition $[\Phi]_s$ corresponding to the ith degree of freedom or sensor location.

The number of degrees of freedom in the candidate sensor set can be reduced by eliminating locations that do not contribute significantly to the independent information contained within the target modal partitions.

The fractional contributions of each sensor to the spatial independence is measured by the vector EfI:

$$\{EfI\} = diag\left(\sum [[\Phi]_s [U][\Sigma]^{-1/2}]^2 \right) \qquad (4.5.1.1\text{-}8)$$

The matrices $[U]$ and $[\Sigma]$ denote the eigenvectors and eigenvalues of the reduced Fisher Information matrix, where:

$$[A_o][U] = [U][\Sigma] \quad \text{and} \quad [U]^T[U] = [I] \qquad (4.5.1.1\text{-}9)$$

This vector is referred to as the Effective Independence distribution of the candidate sensor set. The i^{th} term within EfI is the fractional contribution of the i^{th} sensor location to the linear independence of the modal partitions $[\Phi]_s$. Each entry in EfI is a measure of the contribution of each sensor to the measured kinetic energy. The normalisation factor $[\Sigma]^{-1/2}$ prevents the contribution of high frequency modes from dominating those of the low modes.

The vector EfI can be used to rank the sensor locations based on their importance to the identification and correlation of the target modes. A sensor location can have a contribution in the range

$$0.0 \leq \{EfI\} \leq 1.0 \qquad (4.5.1.1\text{-}10)$$

If EfI= 0.0 the sensor location does not contribute and can be eliminated from the target modal partitions, whereas, a value of 1.0 means that the sensor location must be retained in the final sensor configuration. The final sensor configuration is generated in an iterative manner and contains the number of sensors that will give the best chance to identify and correlate the target modes.

There is a number of researchers that used the Effective Independence method to place sensors on experimental models. Larson et al (1994) used the method to place sensors on an 8-bay truss in order to identify the first five modes of vibration. Kammer (1992) presents a study, where the Effective Independence method is used for on-orbit identification of a set of selected modes. whereas, Brillhart et al (1994)

evaluate the validity of the algorithm in identifying sensor locations for modal extraction.

4.5.1.2 Energy Matrix Rank Optimisation (EMRO)

This technique is proposed by Hemez et al (1994). The authors extend the Effective Independence concept into an algorithm where sensor placement is achieved according to the strain energy distribution of the structure. The strain energy distribution in a structure is a direct measure of its load carrying capacity. The modes that contribute the most to storing the energy are indicated by large energy values:

$$[E]_r = [\Phi]_r^T [K] [\Phi]_r \qquad (4.5.1.2\text{-}1)$$

where, r is the mode number.

The basic idea behind this method is to achieve a sensor configuration that maximises the measure of strain energy among the structural members. The researchers' goal is to reduce the number of sensor locations while ensuring the identification of the target modes.

The stiffness matrix is decomposed into upper and lower triangular Cholesky factors:

$$[K] = [C][C]^T \qquad (4.5.1.2\text{-}2)$$

The strain energy matrix $[E]$ is given by:

$$[E] = [[\Psi]^T [\Psi]] \qquad (4.5.1.2\text{-}3)$$

where:

$$[\Psi] = [C]^T [\Phi] \qquad 4.5.1.2\text{-}4)$$

Once the matrix $[\Psi]$ is obtained, the procedure follows the Effective Independence scheme with $[\Psi]$ and $[E]$ replacing the modes $[\Phi]$ and the Fisher Information matrix, respectively. At any iteration, the strain energy measured by a reduced number of sensors is obtained from the initial energy by removing the contribution of the sensors that have been eliminated:

$$[E]_s = [\Psi]_s^T [\Psi]_s \qquad (4.5.1.2\text{-}5)$$

An eigenanalysis of the symmetric positive semi-definite energy matrix is performed:

$$[E]_s[U] = [U][\Sigma] \quad \text{and} \quad [U]^T[U] = [I] \qquad (4.5.1.2\text{-}6)$$

where, $[U]$ is a singular vector matrix and denotes the eigenvectors and $[\Sigma]$ denotes the eigenvalues of the reduced energy matrix.

A positive semi-definite matrix is a matrix whose eigenvalues are zero or positive but never negative, whereas, a singular matrix is a matrix whose determinant is zero and therefore does not possess an inverse, Stewart (1973).

The fractional contributions of each remaining sensor to the strain energy are assembled into the vector EMRO:

$$\{EMRO\} = diag\left(\sum \left[[\Psi] s [U][\Sigma]^{-1/2} \right]^2 \right) \qquad (4.5.1.2\text{-}7)$$

Each entry EMRO is a measure of the contribution of each sensor to the measured strain energy. The normalisation factor $[\Sigma]^{-1/2}$ prevents the contributions of high frequency modes from dominating those of the lower modes.

The parameter in the summation denotes a characteristic that is desirable in order to avoid eliminating sensors, which may result in a rank deficiency of the strain energy

matrix since the column rank of $[E]_s$ is equal to the number of linearly independent measured modeshapes, assuming that the stiffness matrix is non-singular.
The procedure is repeated until the removal of a sensor creates a rank deficiency.

4.5.1.3 Energy Optimisation Technique (EOT)

This technique is proposed by Heo et al (1997). They describe an optimisation technique, which is a modification of the Effective Independence method and maximises the measured kinetic energy of the structure. The distribution of the kinetic energy in the system, for a mode r, is given by:

$$[E]_r = [\Phi]_r^T [M][\Phi]_r \qquad (4.5.1.3\text{-}1)$$

The mass matrix is decomposed into upper and lower Cholesky factors:

$$[M] = [C][C]^T \qquad (4.5.1.3\text{-}2)$$

where:

$$[\Psi] = [C]^T [\Phi] \qquad (4.5.1.3\text{-}3)$$

The energy measured by a reduced number of sensors is obtained by removing the contribution of the sensors that have been eliminated from the initial energy matrix:

$$[E]_s = [\Psi]_s^T [\Psi]_s \qquad (4.5.1.3\text{-}4)$$

An eigenanalysis of the square, symmetric and positive-definite energy matrix is performed:

$$[E]_s[U] = [U][\Sigma] \quad \text{and} \quad [U]^T[U] = [I] \qquad (4.5.1.3\text{-}5)$$

The fractional contributions of each remaining sensor to the kinetic energy are assembled into the vector EOT:

$$\{EOT\} = diag\left(\sum [[\Psi]_s [U][\Sigma]^{-1/2}]^2 \right) \qquad (4.5.1.3\text{-}6)$$

The sensor location with the minimal contribution in the vector EOT is eliminated. The new matrix is checked for rank deficiency. If the removal of a sensor creates a rank deficiency then that sensor should not be removed. Each entry in EOT is a measure of the contribution of each sensor to the measured kinetic energy. The normalisation factor $[\Sigma]^{-1/2}$ prevents the contribution of high frequency modes from dominating those of the low modes.

4.6 Example of a plate tested in free-free conditions

As already mentioned earlier in this chapter, the first stage in any experimental process is to decide where to place the excitation source and the sensors. The methods used to find those locations were described in the previous sections. A simple application of those methods is given here by way of an example, by considering an aluminium plate tested in free-free conditions. The finite element model of the plate has been constructed in the commercial finite element package called ANSYS, version 5.5, using simple four-noded SHELL elements. Each node has six degrees-of-freedom. The plate was 2 m long and 0.42 m wide and was divided into 240 elements. Table 4.6-1 gives the principal material and section properties of the model.

Parameter	Value
Young's Modulus	70×10^{9} Nm^{-2}
Poisson's ratio	0.35
Density	2700 kgm^{-3}

Table 4.6-1: Material and Section properties of plate model

Sixteen modes were calculated. These modes were used to find the excitation positions and the sensor locations. Since the excitation source was a hammer, the ADDOFV parameter was used to find the best positions to place the excitation. Figure 4.6-1 shows the ADDOFV distribution on the plate using all sixteen modes and all the degrees-of-freedom. Figure 4.6-2 shows the ADDOFV distribution on the plate using all modes but only the three translational degrees-of-freedom. As one can see, both figures show that the four-circled corners of the plate have high ADDOFV values, which indicate that these positions should be avoided when using the hammer. Figure 4.6-1 shows that the ADDOFV has the lowest value in the middle of the plate, whereas, Figure 4.6-2 shows that the ADDOFV parameter has its lowest value at two positions, at the outmost two thirds of the plate. These lowest values of the ADDOFV parameter, enclosed in rectangular boxes, indicate that the experimentalist should use these positions to hit the structure with a hammer so that to avoid double hit effects.

Once the excitation positions are found, the engineer then needs to determine the optimal sensor locations for the accelerometers. Three methods were described in section 4.5, named the Effective Independence method, the Energy Matrix Rank Optimisation and the Energy Optimisation technique. Using the mode information obtained from the finite element model, the sensor location methods were applied to find the best positions to place the transducers. However, only the Effective Independence method and the Energy Optimisation technique were applicable, since both of them use the kinetic energy of the system to place sensors and the mass matrix is non-singular. The Energy Matrix Rank Optimisation could not be applied because the stiffness matrix of the plate was singular and could not be decomposed into Cholesky factors. One explanation for this could be because the plate was modelled as free-free. This may have been avoided if weak springs were put in the system to be grounded.

Both methods gave an arrangement of 19 sensors, but of course, in different positions. Figure 4.6-3 shows the EFI sensor configuration, whereas, Figure 4.6-4 shows the EOT sensor configuration.

After the sensor configurations have been obtained, the engineer should check whether these arrangements can actually identify the modes of the structure. A way

of checking independence is described in Chapter 5 and the modes of the plate are checked in the same chapter, Section 5.3.2.

After the sensor and excitation locations are obtained, the engineer will have to decide whether it is feasible to have as many accelerometers on a structure as sensor locations. Usually, for economic reasons in civil engineering applications, it is possible to have one or two accelerometers and, therefore, 19 sensors would normally be considered unnecessarily expensive. It was decided to use only one accelerometer placed at a key position on the structure and move the hammer around the model using the principle of dynamic reciprocity. The accelerometer should be placed at a position of maximum response. Therefore, looking at the ADDOFV plots, one can see that the best positions to place the sensors are at the corners of the structure, which are circled for clarity, where the ADDOFV parameter has its highest value. Then the hammer could hit all the positions given by the two sensor configurations. Figure 4.6-7 shows the ADDOFV distribution for all degrees-of-freedom with the Effective Independence method sensor configuration, whereas, Figure 4.6-8 shows the ADDOFV distribution with the Energy Optimisation technique sensor arrangement. Similarly, Figures 4.6-9 and 4.6-10 show the ADDOFV distribution for the three-translational degrees-of-freedom with the Effective Independence and Energy Optimisation technique sensor arrangements, respectively. As one can observe from Figures 4.6-7 to 4.6-10 the Effective Independence method places sensors around the edges of the plate including the corners where the ADDOFV parameter has a high value, whereas, the Energy Optimisation Technique places sensors mainly at the inside of the plate where the ADDOFV parameter has lower values. As already mentioned, the experimentalist should hit a structure with a hammer at positions of low ADDOFV values in order to avoid double-hit effects. Since in this example a hammer is used to excite the structure at the predetermined sensor locations, it is possible that the Energy Optimisation Technique may yield in better modal identification. A comparison of the results will be made in the next chapter.

4.7 Concluding remarks

Many researchers have undertaken studies on optimal sensor placement, using not only the three methods presented in the previous sections but also other optimisation procedures as in Baruh et al (1990) and Shah et al (1978). Worden et al (1995) use Neural Networks to locate faults in a structure and Genetic algorithms to determine the optimal sensor distribution. All methods aim to give an optimal sensor configuration so that the experimentalist will obtain the most information about the structure's dynamics. The requirement for best sensor locations is mainly due to the limited number of sensors that can be used in any modal test. The problem becomes particularly important when testing real large civil engineering structures, where, given their physical scale, the number of available transducers is always limited and therefore it is essential to place the sensors in the right positions.

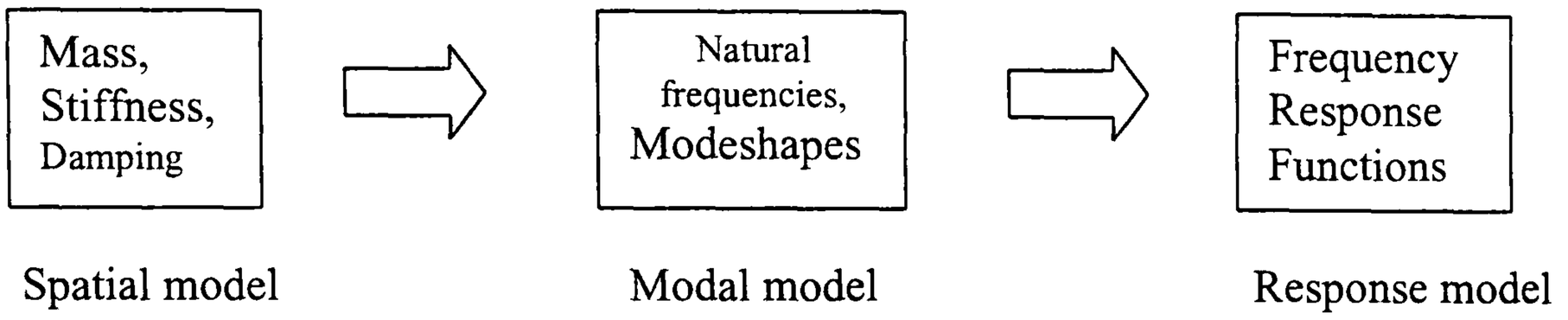

Figure 4.1-1: Theoretical route to vibration analysis

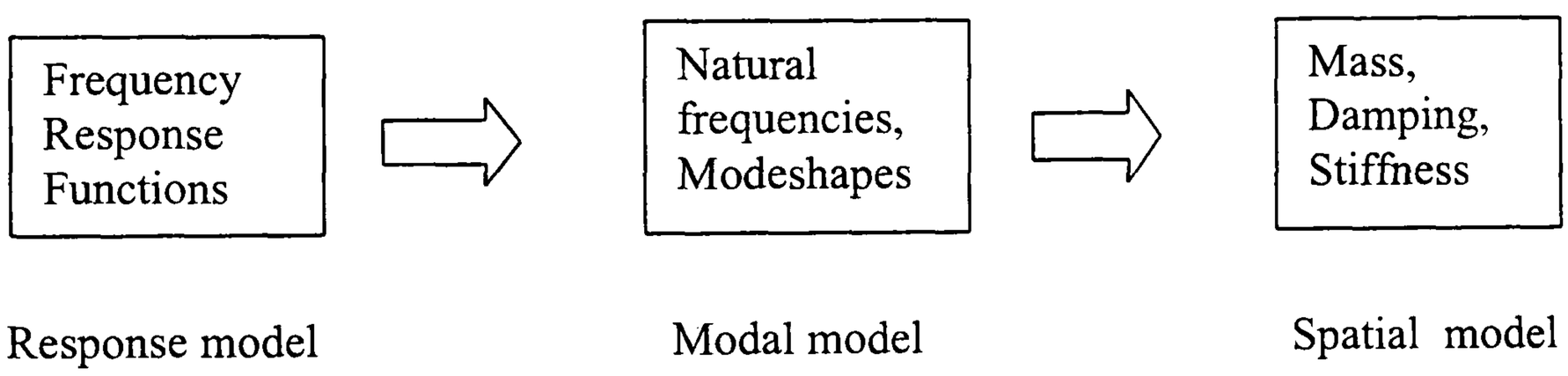

Figure 4.1-2: Experimental route to vibration analysis

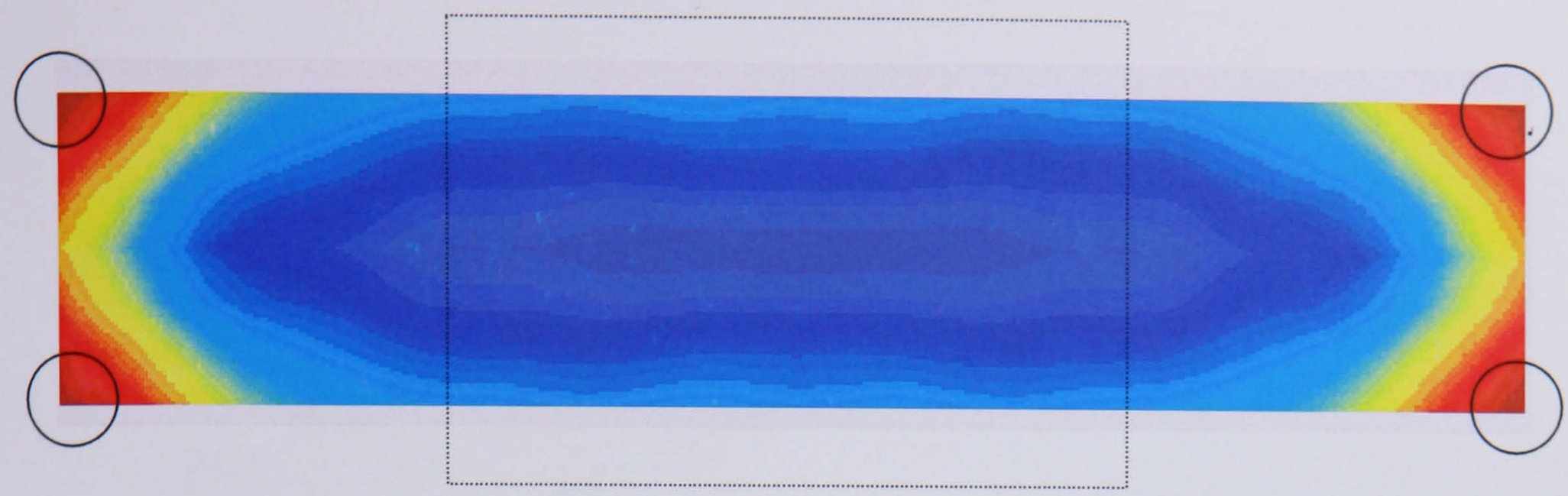

Key: max; min

Figure 4.6-1: ADDOFV distribution for 16 modes and all degrees-of-freedom

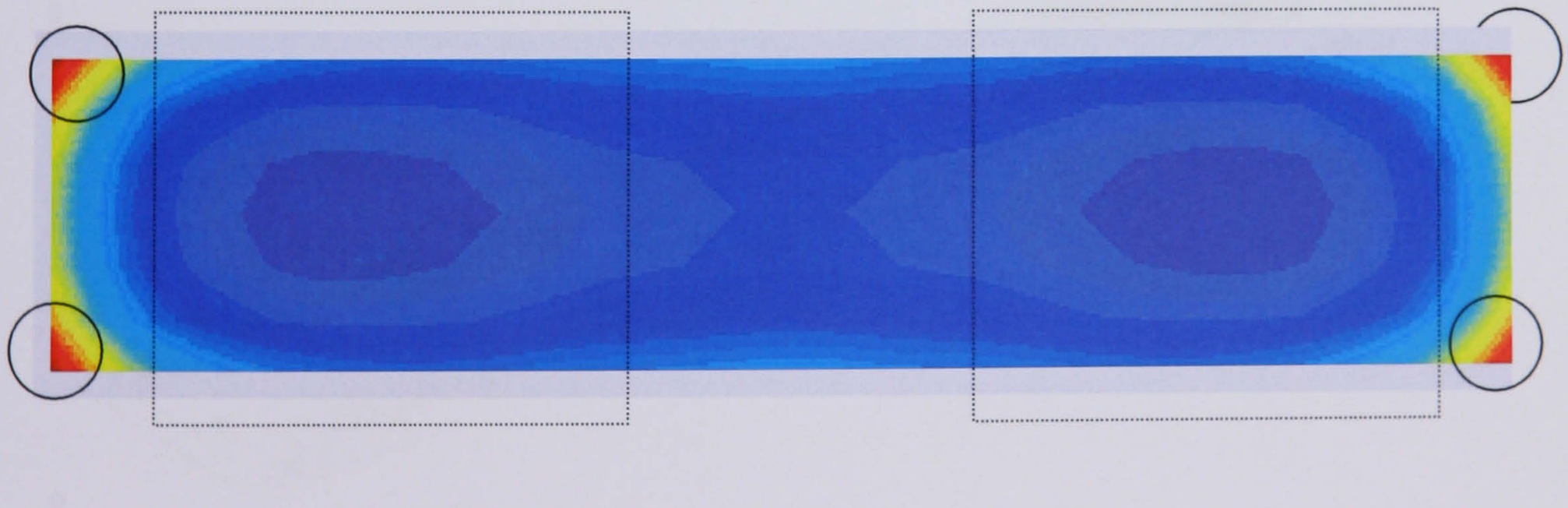

Key: max; min

Figure 4.6-2: ADDOFV distribution for 16 modes and the three translational degrees-of-freedom

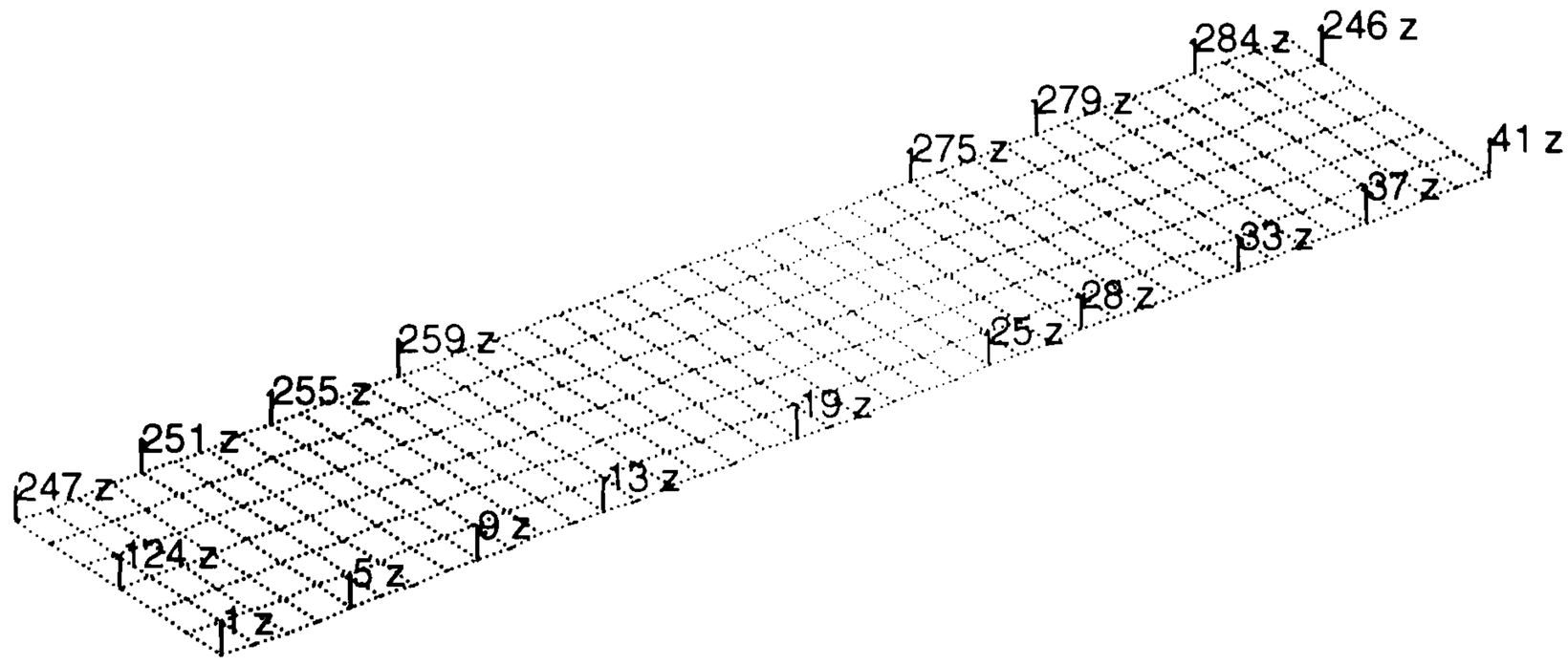

Figure 4.6-3: Effective Independence sensor configuration for 16 modes

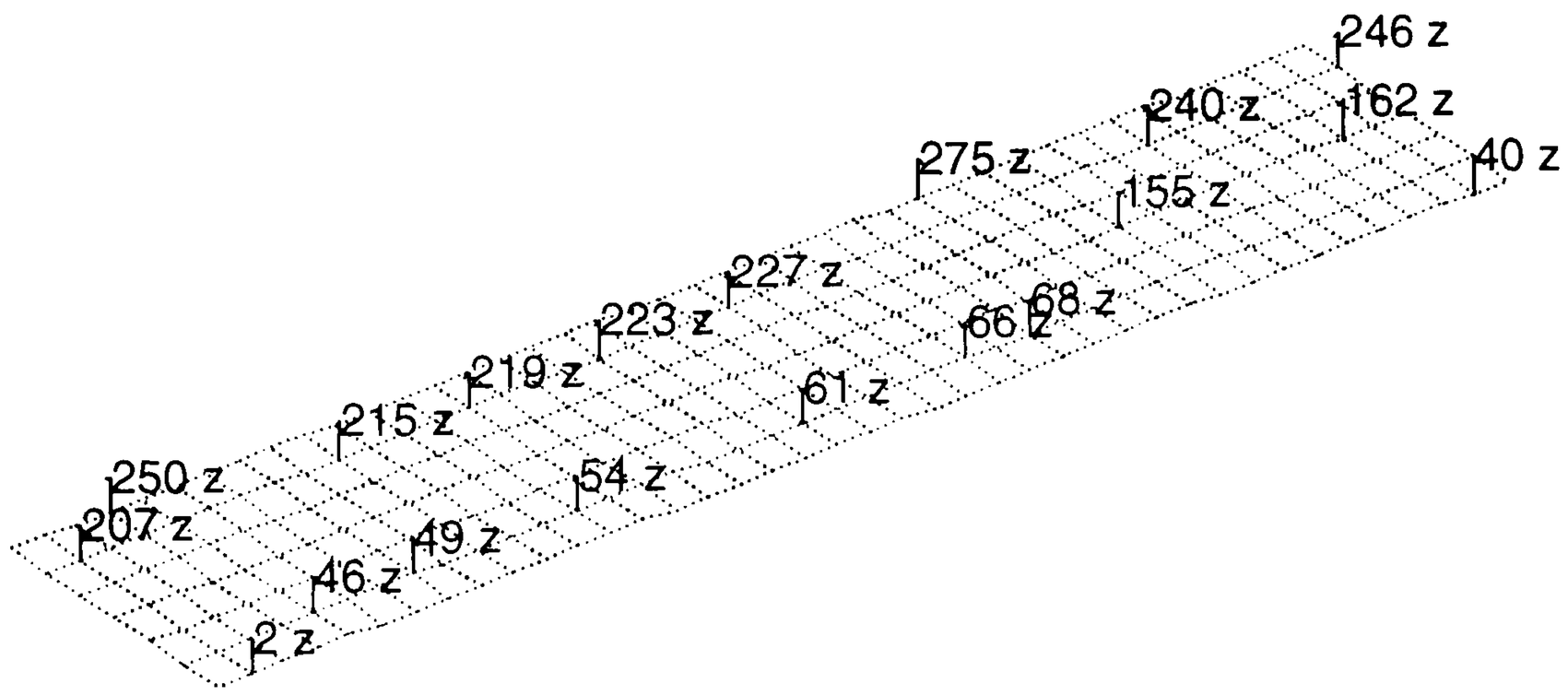

Figure 4.6-4: Energy Optimisation Technique sensor configuration for 16 modes

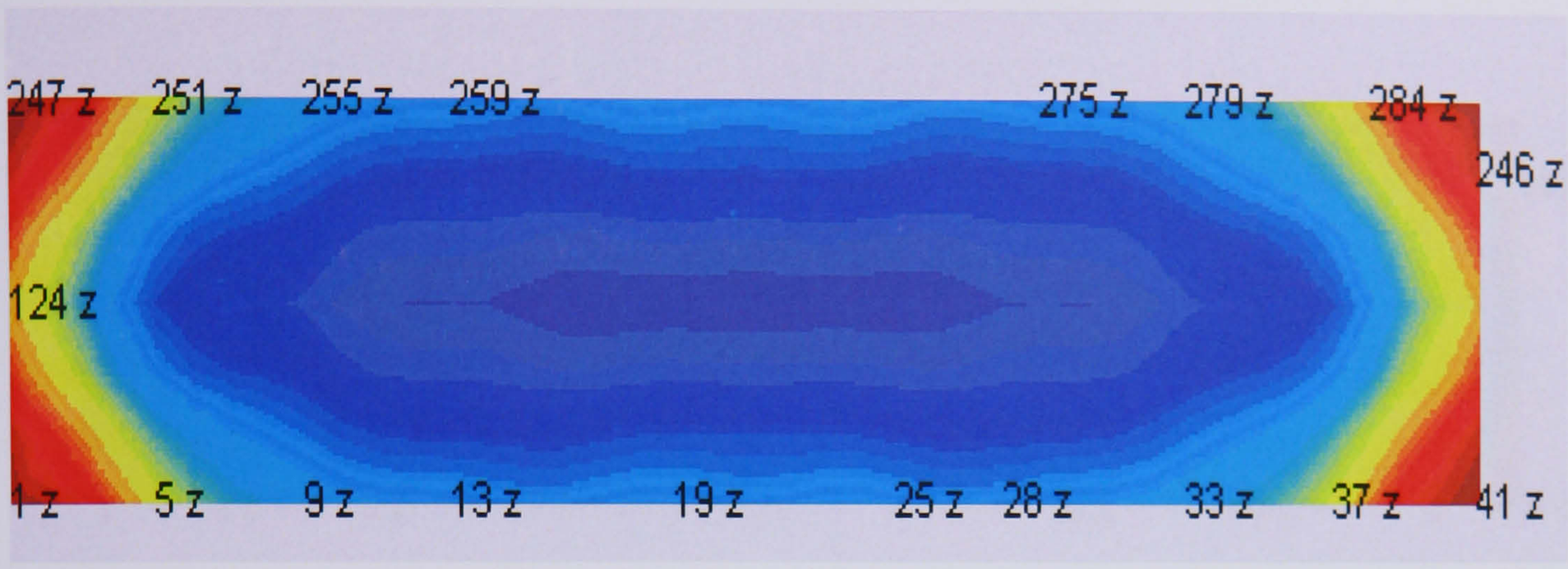

Figure 4.6-5: ADDOFV distribution for all DOFs with EFI sensor arrangement

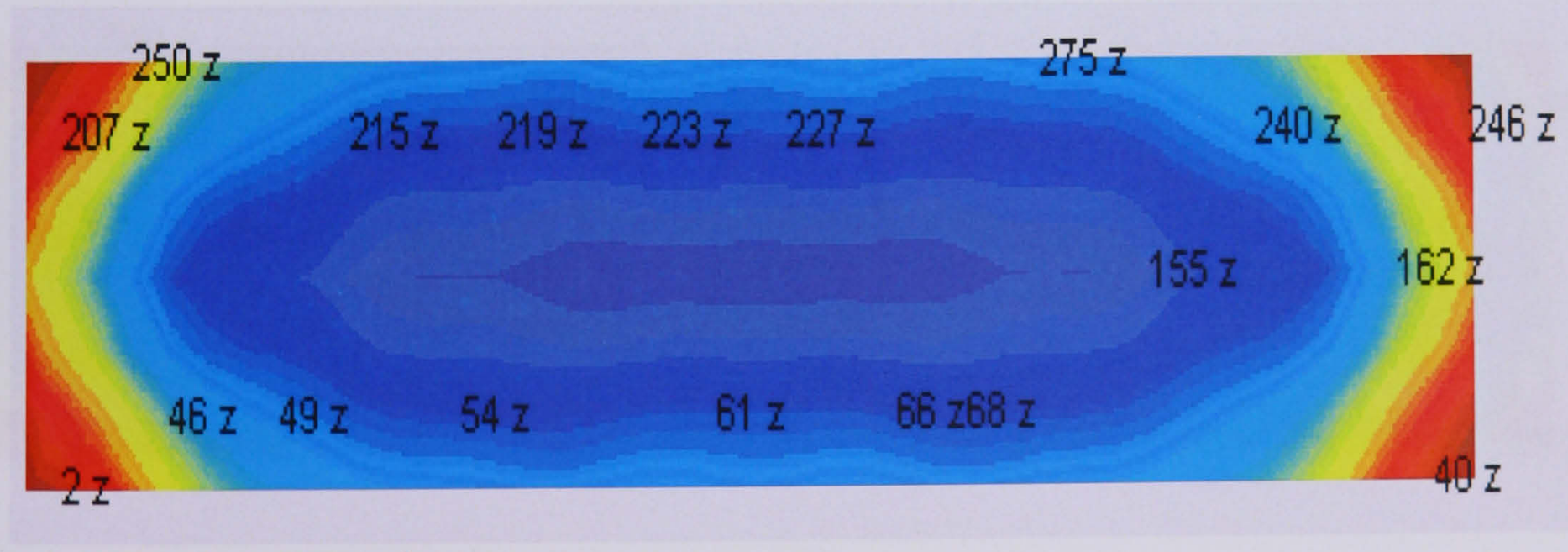

Figure 4.6-6: ADDOFV distribution for all DOFs with EOT sensor arrangement

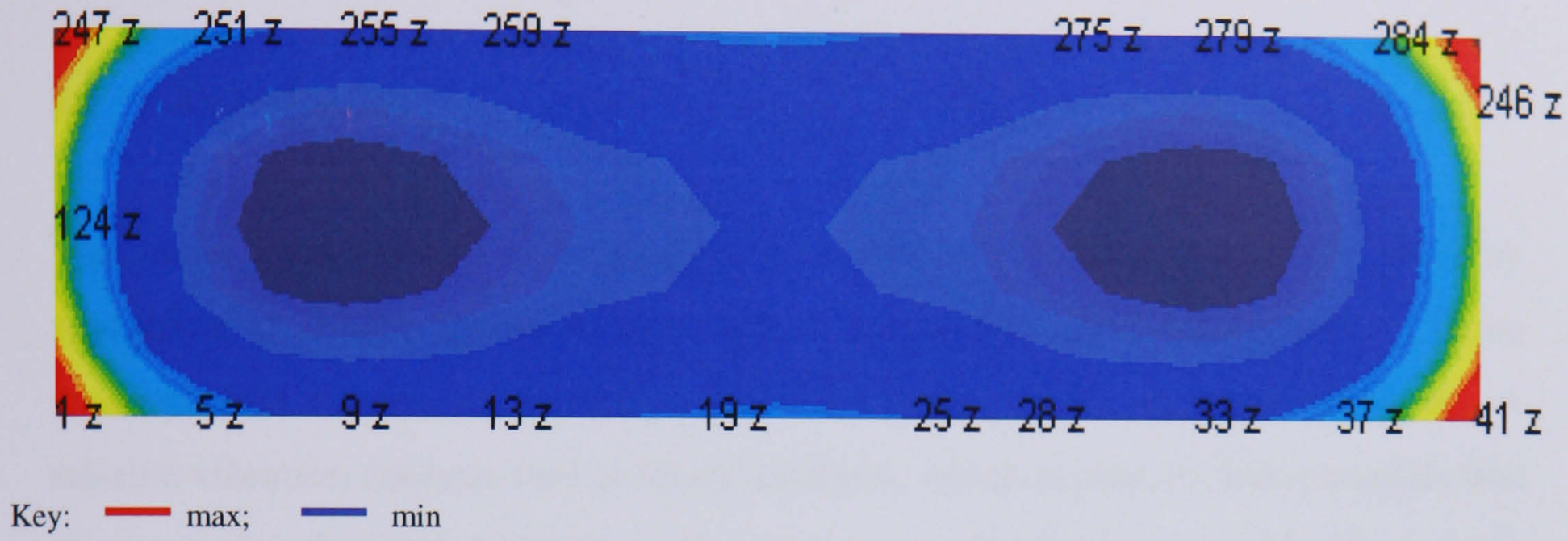

Figure 4.6-7: ADDOFV distribution for translational DOFs with EFI sensor arrangement

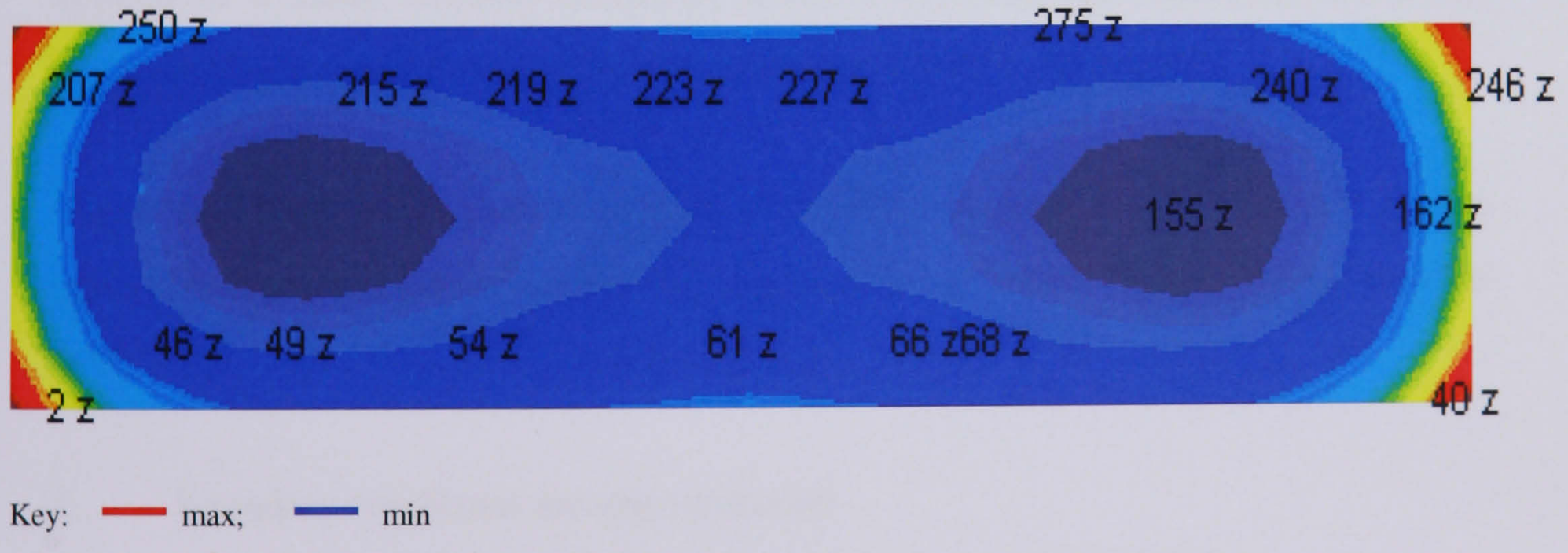

Figure 4.6-8: ADDOFV distribution for translational DOFs with EOT sensor arrangement

CHAPTER 5

DYNAMIC MODEL UPDATING

5.1 Introduction

The recent developments in technology, the use of new improved materials and more sophisticated design methods have led to larger and lighter structures. These developments created an increasing need for more reliable dynamic analyses. A reliable vibration analysis tool is Modal analysis, which is used to derive models that represent the dynamic behaviour of a structure. Applications of Modal analysis include the validation, correction and updating of finite element models.

Model updating has drawn a lot of attention in the last few years and many papers have been published in this field. Nowadays, engineers recognise the need for reliable analytical models, which can be used with confidence for further analyses.

A definition of model updating could be: "Model updating is a reconciliation process applied to a finite element model in order to replicate the characteristics of an experimental model, assuming that the experimental data are correct".

There are many problems associated with finite element models mainly due to approximations or estimations that the engineer has to make. A list of these is given here:

1. boundary conditions are approximated;
2. estimation of the physical properties of the structural material;
3. approximation or even omission of damping or the engineer assumes proportional damping;
4. inadequate modelling of joints;
5. discretisation of distributed parameter systems.

The approximations or modelling errors in the finite element model are not the only source of difficulties that the engineer has to deal with during the updating process. Problems can arise from the quality of the experimental data, which can be summarised as follows:

1. the experimentalist can only measure a limited number of degrees-of-freedom which can be different from the analytical ones;
2. it is difficult to measure rotational degrees-of-freedom;
3. only a limited number of modes can be identified with their corresponding modeshapes;
4. complex modes can be obtained which must be realised to correspond with an undamped finite element model;
5. un-modelled errors, such as noise or non-linearity, can be present in the measurements;
6. some modes may not be excited or if excited not be identified; and
7. poor modal analysis of the experimental data.

There are three stages in any updating exercise, named Comparison, Location and Correlation. In the first stage, *Comparison*, the engineer compares the analytical and the experimental model and checks their compatibility. The methods used to compare the two sets of data provide the engineer with information as to which modes of one set correspond to the modes of the second set but do not explain why they differ. The methods used in the second stage, *Location*, provide information as to where the two models differ without indicating whether the differences are caused by mass or stiffness irregularities. Finally, in the third stage, *Correlation*, the engineer changes the mass and/or stiffness properties or elemental parameters of the analytical model to achieve a better match with the experimental model. The updated analytical model represents accurately the test or real structure. These stages are followed in this order every time model updating is undertaken.

The next sections describe some of the methods most commonly used for each of the three stages in an updating exercise.

5.2 Finite element model reduction

Before proceeding to describe model updating techniques, it is important to mention the problem of incompatibility between the analytical and the experimental data. The size of the finite element model is larger than the size of the test model mainly because the experimentalist cannot measure all the degrees-of-freedom and obtain all the modes present in the test structure. The latter problem arises from the fact that the data acquisition has a limited bandwidth and the modal density increases at higher frequencies making modal extraction very difficult beyond the lower order modes. The former problem can be dealt with by finding the optimum sensor and excitation locations in order to obtain a good modal description of the structure as described in Chapter 4.

In order to overcome the problem of incompatibility, two strategies can be followed:

1. reduce the larger model (FE model) to the test degrees-of-freedom; or
2. expand the smaller model (experimental model) to match the analytical one.

This problem should be resolved before any methods of model updating are used. When finite element model reduction is used, the engineer should keep in mind that spatial information will be lost and this could compromise the effectiveness of the updating process. However, sufficient information is retained to allow comparison between the analytical and experimental data. On the other hand, when experimental model expansion is unavoidable, the engineer should be aware that the experimental information can be too diluted, if the number of the analytical degrees-of-freedom is too large in comparison with the experimental ones, and it cannot provide sufficient localised information for updating.

The most common techniques for model reduction and expansion are described in the following sections.

5.2.1 Finite element model reduction methods

The most preferred reduction technique for model updating is *Guyan reduction*. Guyan (1965), since it preserves the low order modal properties.

Starting from the equation:

$$\{F\} = [M]\{\ddot{x}\} + [K]\{x\} \tag{5.2.1-1}$$

and after partitioning in the form:

$$\begin{Bmatrix} F_1 \\ F_2 \end{Bmatrix} = \begin{bmatrix} M_{mm} & M_{ms} \\ M_{sm} & M_{ss} \end{bmatrix} \begin{Bmatrix} \ddot{x}_1 \\ \ddot{x}_2 \end{Bmatrix} + \begin{bmatrix} K_{mm} & K_{ms} \\ K_{sm} & K_{ss} \end{bmatrix} \begin{Bmatrix} x_1 \\ x_2 \end{Bmatrix} \tag{5.2.1-2}$$

where, m is for master and s is for slave degree-of-freedom, the forces F_2 are to be zero. Neglecting the inertia terms, the forces F_1 are given by:

$$F_1 = \left(K_{mm} - K_{ms} K_{ss}^{-1} K_{sm}\right) x_1 \tag{5.2.1-3}$$

The reduced stiffness matrix is given by:

$$K_1 = K_{mm} - K_{ms} K_{ss}^{-1} K_{sm} \tag{5.2.1-4}$$

The coordinate transformation equations are:

$$x = T x_1 \quad \text{or} \quad \begin{Bmatrix} x_1 \\ x_2 \end{Bmatrix} = \begin{bmatrix} I \\ -K_{ss}^{-1} K_{sm} \end{bmatrix} \{x_1\} \tag{5.2.1-5}$$

Similarly, the reduced mass matrix is given by:

$$M_1 = M_{mm} - M_{ms}\left(K_{ss}^{-1}K_{sm}\right) - \left(K_{ss}^{-1}K_{sm}\right)^T\left(M_{sm} - M_{ss}\left(K_{ss}^{-1}K_{sm}\right)\right) \qquad (5.2.1\text{-}6)$$

If the structure's kinetic and strain energies are written as:

$$E = \frac{1}{2}\dot{x}^T M\dot{x} \quad \text{and} \quad V = \frac{1}{2}x^T Kx \qquad (5.2.1\text{-}7)$$

and the transformation is employed, then the energies become:

$$E = \frac{1}{2}\dot{x}_1^T T^T MT\dot{x}_1 \quad \text{and} \quad V = \frac{1}{2}x_1^T T^T KTx_1 \qquad (5.2.1\text{-}8)$$

The reduced mass and stiffness matrices are given, respectively, by:

$$M_1 = T^T MT \quad \text{and} \quad K_1 = T^T KT \qquad (5.2.1\text{-}9)$$

In the case of the reduced stiffness matrix, all elements of the original stiffness matrix contribute, so none of the structural complexity is lost. In the reduced mass matrix combinations of mass and stiffness elements appear. Therefore, the eigenvalue-eigenvector problem is closely but not exactly preserved.

Two other methods, which are very frequently mentioned in the literature, and are only included here for completeness, are the *System Equivalent Reduction Expansion Process* (SEREP), O'Callahan et al (1989), and the *Improved Reduction System* (IRS), O'Callahan (1989).

The first method (SEREP) was originally formulated as a technique that was used to develop rotational degrees-of-freedom for modal test data. It has been used for checking correlation and orthogonality between analytical and experimental modal vectors. The technique maps the complete finite element eigenvectors onto the experimental slave degrees-of-freedom using the transformation matrix:

$$[T] = \left[\frac{[\phi_{am}]}{[\phi_{as}]}\right]\left[[\phi_{am}]^T[\phi_{am}]\right]^{-1}[\phi_{am}]^T \qquad (5.2.1\text{-}10)$$

where,

a is for analytical model,

m is for master degrees-of-freedom and

s is for slave degrees-of-freedom.

The second method (IRS) develops the Guyan technique to include the contribution from the slave inertias. The result is an improved modal matrix that represents better the physical properties of the system. The transformation matrix that can be used to expand the master to the full degrees-of-freedom becomes:

$$[T] = \begin{bmatrix} I \\ -[K_{ss}]^{-1}[K_{sm}] \end{bmatrix} + \begin{bmatrix} 0 & 0 \\ 0 & [K_{ss}]^{-1} \end{bmatrix}[M]\begin{bmatrix} 0 & 0 \\ 0 & [K_{ss}]^{-1} \end{bmatrix}\left[M^R\right]^{-1}\left[K^R\right] \qquad (5.2.1\text{-}11)$$

The advantage of the SEREP method is that it reproduces the lower order eigenvalues exactly and, for this reason, it is usually recommended for model reduction.

5.2.2 Experimental model expansion

The most commonly used method for model expansion is the *Kidder's method*, Kidder (1984). The method is derived from an inverse Guyan reduction.
Starting from the partitioned eigenvalue problem:

$$\left(\begin{bmatrix} K_{mm} & K_{ms} \\ K_{sm} & K_{ss} \end{bmatrix} - \omega_r^2 \begin{bmatrix} M_{mm} & M_{ms} \\ M_{sm} & M_{ss} \end{bmatrix}\right)\begin{Bmatrix} \phi_m \\ \phi_s \end{Bmatrix}_r = \{0\} \qquad (5.2.2\text{-}1)$$

where,

r is the r^{th} mode

m is for master degrees-of-freedom and

s is for slave degrees-of-freedom.

Substitution of the measured eigenvalues and eigenvectors in the above equation, leads to the expanded slave degrees-of-freedom which are given by:

$$\{{}_x\phi_s^*\}_r = -([K_{ss}] - \omega_r^2[M_{ss}])^{-1}([K_{sm}] - \omega_r^2[M_{sm}])\{{}_x\phi_m\}_r \qquad (5.2.2\text{-}2)$$

The advantage of this method is that by using the partitioned unreduced analytical system matrices, the physical connectivity properties are consistent with the structure of the final model.

5.3 Comparison methods

The first stage in a reconciliation process is the comparison of the analytical and the experimental data, carried out usually in the modal domain. The engineer determines how closely the two models correspond by comparing and correlating their natural frequencies and modeshapes.

5.3.1 Comparison of natural frequencies - Graphical

This is probably the most obvious and easiest comparison to make. By simply tabulating the analytical and experimental natural frequencies the engineer can compare their corresponding values. However, a more useful way of comparison is to plot the experimental against the analytical values of each of the corresponding modes. The points on the plot should lie on or be close to a straight line of slope 1. If they lie close to a line of different slope, then a wrong material property was used in the predictions. If there is a great scatter of points about the 45° line, then there is a serious problem with the experimental model and a re-evaluation is necessary.

A frequency comparison using the tabulating and the plotting techniques can be seen in Tables 5.3.1-1 and 5.3.1-2 and Figures 5.3.1-1 and 5.3.1-2, respectively. These plots are for the free-free plate described in Chapter 4 using the analytical and experimental results obtained from the two methods of sensor placement used. As

can be seen from the plots, the Energy Optimisation Technique places sensors on positions, which give a better correlation of the frequencies. They lie very closely to the straight line, which indicates that the values are almost identical. On the other hand, the Effective Independence method does not give such good results since some frequency points are away from the straight line, indicating that these frequencies do not exhibit a close match. This is a very interesting result since it leads to the conclusion that the quality of the experimental data depends on the selection of the set of nodes where sensors are placed. The Effective Independence method gave a set of nodes that do not seem to result in the best identification of the structure's frequencies. As already mentioned at Chapter 4, section 4.6, the Effective Independence method placed sensors at the edges of the plate where the ADDOFV parameter has high values, Figures 4.6-5 and 4.6-7, whereas, the Energy Optimisation Technique placed sensors at positions on the structure where the ADDOFV parameter has low values, Figures 4.6-6 and 4.5-8. Since a hammer was used to excite the structure at those positions, one can assume that double-hit effects were minimized for the Energy Optimisation Technique leading to better modal identification, which was not the case for the Effective Independence method.

5.3.2 Comparison of modeshapes - Graphical

Another type of comparison involves the use of the modeshapes. This comparison can be graphical or by making a similar graph to the case of the frequency comparison. In the graphical comparison, the engineer plots the deformed shapes – in each mode - of the two models and overlays one plot to the other. However, differences may be present and they may be difficult to explain why they exist. The second means of comparison is a more convenient way. As with the natural frequencies, the engineer can make a x-y plot in which each element in the analytical modeshape vector is plotted against each corresponding element in the experimental vector. The individual points on the plot correspond to degrees-of-freedom on the model.

Mode	Analytical Freq. (Hz)	EFI experimental Freq. (Hz)
1	5.25	5.3226
2	14.57	-
3	14.91	15.4467
4	28.77	29.5688
5	30.71	29.7763
6	47.82	-
7	48.21	48.2864
8	68.12	68.2272
9	71.7	74.0568
10	91.07	91.4939
11	100.14	103.5599
12	117.6	118.1532
13	124.48	128.4997
14	129.43	132.0503
15	133.8	132.1955
16	143.04	-

Table 5.3.1-1: Comparison of natural frequencies of free-free plate using the Effective Independence sensor location method

If the modeshapes are mass-normalised, then all points should lie on a straight line of slope 1. If the points lie close to a line of different slope, then one of the modeshapes is not mass-normalised. If there is a great scatter of points about the 45° line then the two modeshapes compared do not relate to the same mode. Figures 5.3.2-1 to 5.3.2-4 show four plots of modeshapes obtained from the plate tested in free-free conditions described in Chapter 4 using the two sets of sensor locations. The first two figures are obtained using the Effective Independence method. Figure 5.3.2-1 presents the comparison of two correlated modeshapes, since all points lie on the 45° line, whereas, Figure 5.3.2-2 presents the comparison of two uncorrelated modeshapes. As one can observe the plotted points are scattered around the 45° line.

Figures 5.3.2-3 and 5.3.2-4 present the comparison of correlated and uncorrelated modeshapes, respectively, obtained using the Energy Optimisation Technique.

Mode	Analytical Freq. (Hz)	EOT experimental Freq. (Hz)
1	5.25	5.3906
2	14.57	-
3	14.91	15.4671
4	28.77	29.6219
5	30.71	30.7858
6	47.82	-
7	48.21	48.2841
8	68.12	68.1912
9	71.7	74.0636
10	91.07	91.532
11	100.14	103.5928
12	117.6	118.1452
13	124.48	-
14	129.43	128.5389
15	133.8	132.1534
16	143.04	-

Table 5.3.1-2: Comparison of natural frequencies of free-free plate using the Energy Optimisation Technique for sensor location

5.3.3 Comparison methods - Formulations

Many methods have been developed to quantify the comparison between two sets of modal data. These techniques can be used to compare analytical with experimental data, analytical with analytical or experimental with experimental. These techniques are based on the orthogonality conditions:

$$[\phi]^T[M][\phi]=[I] \quad \text{and} \quad [\phi]^T[K][\phi]=[\omega^2] \tag{5.3.3-1}$$

where,

$[\phi]$ are the mass-normalised eigenvectors (analytical or measured) and

$[\omega^2]$ is the diagonal eigenvalue matrix.

If the measured eigenvector matrix is substituted in the above equations, the orthogonality conditions will not be true and off-diagonal terms will appear in the identity and eigenvalue matrices.

The most common technique used to compare analytical and measured modeshapes is the *Modal Assurance Criterion* (MAC), which provides a measure of the scatter of points from the straight line correlation, Ewins (1998). The MAC is given by the formula:

$$MAC\left(\{\phi_x\}_i,\{\phi_a\}_j\right)=\frac{\left|\{\phi_x\}_i^T\{\phi_a\}_j^*\right|^2}{\{\phi_x\}_i^T\{\phi_x\}_i^*\{\phi_a\}_j^T\{\phi_a\}_j^*} \tag{5.3.3-2}$$

where,

x stands for experimental,

a stands for analytical,

i,j are mode numbers of the models.

^{T} stands for transpose and * stands for complex conjugate.

The MAC is a scalar quantity even if the modeshapes are complex. It is based on the orthogonality properties of the modeshapes. It can take values between 0 and 1. A MAC value of 0 means that the modeshapes compared do not relate with each other, whereas, a MAC value of 1 means that the two eigenvectors are perfectly correlated.

In practice, it is difficult to obtain exact values of 1 or 0 and it is found that a value of more than 0.9 denotes well-correlated modes, whereas, a value of less than 0.1

denotes un-correlated modes. Values of the MAC of less than unity can be caused by:

1. incorrect modelling;
2. presence of noise in the measurements;
3. presence of non-linearities in the experimental model;
4. poor modal analysis of the experimental data; and
5. poor choice of degrees-of-freedom used in the correlation.

The advantage of using the Modal Assurance Criterion, instead of other methods, which are based on the orthogonality properties of the modes, is that it is not affected by co-ordinate incompleteness. It is sufficient to partition the analytical model to the experimental co-ordinates. However, care should be taken if the experimental degrees-of-freedom are just a very small subset of the full set of co-ordinates, since the MAC is not very reliable in correlating localised modes described by only a few degrees-of-freedom. The MAC plots, which correlate the analytical with the experimental modes of the plate, tested in free-free conditions, obtained by the two methods, are given in Figures 5.3.3-1 and 5.3.3-2. The Effective Independence method not only identifies more modes but also seems to give better results than the Energy Optimisation technique. In Figure 5.3.3-1 most of the diagonal terms of the plot have MAC values of more that 0.9 which suggests that there is almost a perfect correlation between the corresponding modes. Also, there are only few off-diagonal terms appearing, suggesting that only a few modes correlate with other non-corresponding ones. However, in Figure 5.3.3-2 only five of the diagonal terms have MAC values of more than 0.9, which means that this arrangement of sensors does not provide the best correlated results. Also, there are more off-diagonal terms in this plot in than Figure 5.3.3-1.

A special case of the MAC is the so-called *AUTOMAC*, in which the eigenvectors are correlated with each other. The AUTOMAC can be used to check whether the selected set of degrees-of-freedom, from the sensor location techniques, is sufficient or not. Figure 5.3.3-3 shows the AUTOMAC plot of the analytical modeshapes of the free-free plate using all 1716 degrees-of-freedom, whereas, in Figures 5.3.3-4 and 5.3.3-5 the AUTOMAC is plotted for the same modeshapes partitioned to the 19

sensor locations given by the EOT and EFI methods. From these plots one can observe that all the diagonal values are 1 and this is what one should expect since each modeshape must correlate perfectly with itself.

Also the AUTOMAC matrix is symmetric. In Figure 5.3.3-4 there are some non-zero off-diagonal terms appearing, which means that some modeshapes seem to exhibit a degree of correlation with others. This is not usually expected since the modes are supposed to be orthogonal. However, a perfectly diagonal AUTOMAC is valid only when all the degrees-of-freedom are used in the calculations. In this case, only a limited number of co-ordinates is used, corresponding to the sensor locations obtained by applying the EOT and EFI methods. Another reason for the presence of the off-diagonal terms is that the orthogonality properties are only valid when the mass matrix is used in the calculations and in this case, the mass matrix is not used in the formulation of the AUTOMAC. Observing these two figures, one can see that the Effective Independence method gives slightly better results since there are fewer off-diagonal terms than in the Energy Optimisation technique, which seems to give more off-diagonal terms but of lower value. These off-diagonal terms suggest that there is a degree of correlation between the modes compared, however, this degree of correlation is quite small and it should not impose a problem in the identification of the modes. The diagonal terms have all AUTOMAC values of one, and this is expected since all modes correlate perfectly with each other.

Another version of the MAC is the Normalised MAC or *Normalised Cross Orthogonality* (NCO), which includes the mass or stiffness matrix in the calculation of the correlation, Ewins (1998).

The NCO is given by the formula:

$$NCO\left(\{\phi_x\}_i, \{\phi_a\}_j\right) = \frac{\left|\{\phi_x\}_i^T [W_a] \{\phi_a\}_j\right|^2}{\{\phi_x\}_i^T [W_a] \{\phi_x\}_i \; \{\phi_a\}_j^T [W_a] \{\phi_a\}_j} \qquad (5.3.3\text{-}3)$$

where, the matrix $[W_a]$ can either be the mass or stiffness matrix of the analytical model. The difficulty that must be overcome in this case is that of reducing the mass

or stiffness matrix to the experimental degrees-of-freedom. Guyan reduction described in Section 5.2.1 is usually used. The NCO takes values between 0 and 1.

Apart from the above established methods of correlation, some researchers have developed other techniques, such as Blaschke et al (1997), which presents a technique that does not require normalisation and mode pairing and is based on an iteration of the MAC coefficient. Pascual et al (1997) present two correlation techniques, in the frequency domain, the Frequency Response Scale Factor (FRSF) and the Frequency Domain Assurance Criterion (FDAC). These two methods quantify the level of correlation between two sets of modes, determine the frequency shift at all measured frequencies and establish a set of frequencies to use during the updating.

5.4 Location techniques

Once the comparison of the two sets of data is complete, the engineer proceeds to the second stage of the reconciliation process, which deals with locating the regions of difference between the two models. The commonly used technique for identifying the coordinates at which the two sets of data do not agree is the *Co-ordinate Modal Assurance Criterion* (COMAC), Lieven et al (1988), Ewins (1998). The COMAC for a degree-of-freedom *i* is given by:

$$COMAC(i) = \frac{\left(\sum_{j=1}^{n} \left| \phi_a(i,j)\, \phi_x(i,j)^* \right| \right)^2}{\sum_{j=1}^{n} \phi_a(i,j)^2 \sum_{j=1}^{n} \phi_x(i,j)^{*2}} \qquad (5.4\text{-}1)$$

where, n is the number of correlated mode pairs.

The COMAC has been developed to identify the region of the error and not which modes are responsible for the poor correlation. It was developed from the MAC but it relates to the degrees-of-freedom and not the mode numbers. It is a two-stage process. Firstly, the engineer should use the MAC to identify correlated mode-pairs

and then use the above equation to calculate the correlation at each coordinate of the mode-pairs.

The COMAC can take values between 0 and 1. However, it is difficult to interpret correctly the information provided by the COMAC. It is tempting to conclude that regions of low COMAC values are the regions where the errors occur. This is not always the case, because those regions could be the places where the consequences of any errors are most felt. It is good practice to prepare a plot of the COMAC, such as the one shown in Figure 5.4-1, where its value is plotted against the degree-of-freedom number. Lieven et al (1988) point out some applications of COMAC apart from localising errors in finite element models. Such applications include the indication of areas of scaled models, which do not correspond to their full size counterparts and detection of faults in hardware during tests.

Usually, large drops of COMAC are observed in regions of large amplitude such as the free ends of beams. These regions are most affected by erroneous flexibility data. It is advisable to use this method in cases where the structure is modelled and tested in free-free end conditions.

Another method for error localisation is the Dynamic Force Balance method, Silva et al (1999). In this method the experimental eigenvectors and eigenvalues do not satisfy the analytical eigendynamic equation, due to errors in the analytical model, causing a residual force term:

$$[[K_a] - (\omega_x)_r^2 [M_a]]\{\phi_x\}_r = \{f\} \qquad (5.4\text{-}2)$$

Large residuals indicate regions of error in mass or stiffness. The method requires co-ordinate completeness.

Waters (1995) uses the Force Balance method to develop a technique, which does not assume that regions of response error are necessarily an indication of modelling error. The technique identifies regions of spatial error and its success is demonstrated in a simulated case study.

5.5 Correlation techniques

The third stage in the updating process is the correlation of the analytical and experimental models. In this stage, properties, such as mass and/or stiffness, of the finite element model are varied so that its characteristics match the characteristics of the experimental model.

There are three groups of optimisation methods: Least squares updating, Direct optimisation and Neural Networks. The methods belonging to the first group are modal and FRF sensitivity techniques, which are described in detail in the following sections, whereas, Simulated Annealing and Genetic Algorithms belong to the second group.

5.5.1 Updating using Modal Sensitivity

Consider an undamped analytical model with the following equation of motion:

$$[K_a]\{\phi_a\}_r = (\lambda_a)_r [M_a]\{\phi_a\}_r \qquad (5.5.1\text{-}1)$$

where, $\{\phi_a\}_r$ and $(\lambda_a)_r$ are the eigenvectors and eigenvalues of the system.

In order to proceed and find the error matrices of the system, one must assume a form of the errors. The set of N_p design parameters, $\{p\}$, to be varied is selected. These parameters can be elemental parameters, such as the elemental mass and elemental stiffness matrices, or global parameters, such as material properties or thicknesses.

It is convenient to non-dimensionalise the updating parameters as:

$$p_i = \frac{\left(p_i - p_i^{FE}\right)}{p_i^{FE}} \qquad (5.5.1\text{-}2)$$

where $\{p^{FE}\}$ are the parameters of the original finite element model.

These non-dimensionalised parameters are also called *p-values* and represent the fractional changes in the design parameters. Therefore, $(\lambda_a)_r$ and $\{\phi_a\}_r$ are functions of $\{p\}$.

Suppose now that an experimental eigen-pair, $(\lambda_x)_r$, $\{\phi_x\}_r$ is available, which corresponds to the analytical pair, $(\lambda_a)_r$, $\{\phi_a\}_r$. Then the experimental eigensolution can be expressed as a Taylor's series in terms of the updating parameters:

$$(\lambda_x)_r = (\lambda_a)_r + \sum_{i=1}^{Np} \frac{\partial(\lambda_a)_r}{\partial p_i} p_i + O(p_i^2) \qquad (5.5.1\text{-}3)$$

$$\{\phi_x\}_r = \{\phi_a\}_r + \sum_{i=1}^{Np} \frac{\partial\{\phi_a\}_r}{\partial p_i} p_i + O(p_i^2) \qquad (5.5.1\text{-}4)$$

where, $O(p_i^2)$ are terms of second order and higher. However, one can assume that the changes in the modal parameters are small and, therefore, these higher order terms can be neglected. By retaining the first order terms in the above equations (5.5.1-3) and (5.5.1-4), the changes in the updating parameters become:

$$\Delta\lambda_r \approx \sum_{i=1}^{Np} \frac{\partial(\lambda_a)_r}{\partial p_i} p_i \quad \text{and} \quad \{\Delta\phi\}_r \approx \sum_{i=1}^{Np} \frac{\partial\{\phi_a\}_r}{\partial p_i} p_i \qquad (5.5.1\text{-}5)$$

The derivatives of the eigenvalues and eigenvectors, or *eigensensitivities*, can be expressed as follows:

$$\frac{\partial(\lambda)_r}{\partial p_i} = \{\phi_a\}_r^T \frac{\partial[K_a]}{\partial p_i}\{\phi_a\}_r - (\lambda_a)_r \{\phi_a\}_r^T \frac{\partial[M_a]}{\partial p_i}\{\phi_a\}_r \qquad (5.5.1\text{-}6)$$

$$\frac{\partial\{\phi\}_r}{\partial p_i} = \sum_{k=1;k\neq r}^{N} \frac{\{\phi_a\}_k \{\phi_a\}_k^T}{(\lambda_a)_r - (\lambda_a)_i}\left[\frac{\partial[K_a]}{\partial p_i} - (\lambda_a)_r \frac{\partial[M_a]}{\partial p_i}\right]\{\phi_a\}_r - \tfrac{1}{2}\{\phi_a\}_r^T \frac{\partial[M_a]}{\partial p_i}\{\phi_a\}_r \qquad (5.5.1\text{-}7)$$

The derivation of the above eigensensitivities can be found in Appendix 1.

The equations in (5.5.1-5) constitute (N+1) equations for the N_p unknown p-values, where N is the number of degrees-of-freedom. If m correlated mode-pairs are used, $m(N+1)$ equations can be obtained of the form:

$$[A]\{p\} = \{\Delta\xi\} \tag{5.5.1-8}$$

where

$$[A] = \begin{bmatrix} \frac{\partial\lambda_1}{\partial p_1} & \cdots & \frac{\partial\lambda_1}{\partial p_{Np}} \\ \frac{\partial\{\phi\}_1}{\partial p_1} & \cdots & \frac{\partial\{\phi\}_1}{\partial p_{Np}} \\ \vdots & & \vdots \\ \frac{\partial\lambda_m}{\partial p_1} & \cdots & \frac{\partial\lambda_m}{\partial p_{Np}} \\ \frac{\partial\{\phi\}_m}{\partial p_1} & \cdots & \frac{\partial\{\phi\}_m}{\partial p_{Np}} \end{bmatrix}_{m(N+1)\times Np} \qquad \{\Delta\xi\} = \begin{Bmatrix} \Delta\lambda_1 \\ \Delta\{\phi\}_1 \\ \vdots \\ \Delta\lambda_m \\ \Delta\{\phi\}_m \end{Bmatrix}_{m(N+1)} \tag{5.5.1-9}$$

The matrix $[A]$ is called the *Sensitivity* matrix of the system. Equation (5.5.1-8) can be solved using an iterative procedure called Singular Value Decomposition, described in section 5.5.2.

A number of researchers have used the modal sensitivity method to update analytical models. Fissette et al (1988) use the Force Balance method to locate errors in the analytical model and assume that the mass matrix is correct, concentrating to correct errors in the stiffness matrix. Maia et al (1996) use an Advanced Characteristic Response Function to determine the modal parameters to use for updating. This function is independent of the modal constants and the influence of neighbouring odes. Mayes et al (1996) present a technique that manipulates the analytical modeshapes to produce a modal filter, which is used to calculate enhanced FRFs from which the modal parameters of closely spaced modes can be easily identified. Friswell et al (1991) use system identification methods to update the modal

parameters in such a way that the results fit well to the corresponding measured data. Friswell et al (2000) use robust estimation techniques to determine the most robust parameter set so that the residuals are small for a range of uncertainties in the model and measurements. Ibrahim (2000) uses multiple analytical models to update a model in the modal domain. By using multiple models, the amount of information is increased and convergence ensured. Finally, Lin (1991) develops some criteria for the amount of data, needed to be measured, in order to update an analytical model so that the physical connectivity of the model is conserved.

5.5.1.1 Experimental Sensitivities

When the magnitudes of the finite element errors are quite large, the assumption that only the first order terms in the Taylor's series can be retained is not valid anymore. The iterative process may never converge. In order to overcome this problem, one can use both experimental and analytical eigen-data in the formulation of the eigensesitivities:

$$\frac{\partial(\lambda_a)_r}{\partial p_i} = \{\phi_a\}_r^T \frac{\partial[K_a]}{\partial p_i}\{\phi_x\}_r - (\lambda_x)_r \{\phi_a\}_r^T \frac{\partial[M_a]}{\partial p_i}\{\phi_x\}_r \qquad (5.5.1.1\text{-}1)$$

$$\frac{\partial\{\phi\}_r}{\partial p_i} = \sum_{k=1;k\neq r}^{N} \frac{\{\phi_a\}_k \{\phi_a\}_k^T}{(\lambda_x)_r - (\lambda_a)_i}\left[\frac{\partial[K_a]}{\partial p_i} - (\lambda_x)_r \frac{\partial[M_a]}{\partial p_i}\right]\{\phi_x\}_r - \tfrac{1}{2}\{\phi_a\}_r^T \frac{\partial[M_a]}{\partial p_i}\{\phi_x\}_r \qquad (5.5.1.1\text{-}2)$$

The above modifications enable convergence even when there is a large difference between the experimental and analytical results. The sensitivities are not calculated only in terms of the erroneous analytical data. Moreover, the calculation of the experimental sensitivities requires the inclusion of all the degrees-of-freedom of the analytical model, leading to co-ordinate incompleteness in all practical cases.

5.5.2 Singular value Decomposition

The equation (5.5.1-8) can be written in a dimensional form as:

$$[A]_{nr\times nC}\{p\}_{nC\times 1}=\{\Delta\xi\}_{nr\times 1} \tag{5.5.2-1}$$

where $n_r > n_c$. The rows of $[A]$ contain the coefficients for the unknown variables $\{p\}$. If the independent rows of $[A]$ are less than n_c, then $[A]$ is rank deficient. there are an infinite number of solutions and the problem is under-determined. If $[A]$ has more than n_c rows, n_c of which are independent (rank($[A]$)=n_c), then there are two possibilities:

1. if $[A]$ and $\{\Delta\xi\}$ are noise-free, then there is a true solution through which all the equations will pass; or
2. if $[A]$ and $\{\Delta\xi\}$ are contaminated with noise, then there is no exact solution.

However, in model updating an experimental data set is used which is contaminated with noise. Therefore, there is no exact solution, but a solution can be found that satisfies all the equations. A method used for finding such solutions is called the Singular Value Decomposition (SVD) technique, which finds optimal solutions in a least squares sense.

The SVD of a $n_r > n_c$ matrix is given by:

$$[A]_{nr\times nC}=[U]_{nr\times nr}[\Sigma]_{nr\times nC}[V]^T_{nC\times nC} \tag{5.5.2-2}$$

where $[U]$ and $[V]$ are orthogonal matrices:

$$[U]^T=[U]^{-1} \quad \text{and} \quad [V]^T=[V]^{-1} \tag{5.5.2-3}$$

and $[\Sigma]$ is a rectangular matrix of singular values of the form:

$$[\Sigma]=\underbrace{\left[\begin{array}{ccc}\sigma_1 & & 0\\ & \sigma_2 & \\ & \ddots & \\ & & \sigma_{nC}\\ \hdashline 0 & & \end{array}\right]}_{n_c}\begin{array}{l}\}\ n_c\\ \}\ n_r-n_c\end{array} \qquad (5.5.2\text{-}4)$$

Equation (5.5.2-2) can be written as:

$$[U]^T[A][V]=[\Sigma] \qquad (5.5.2\text{-}5)$$

The pseudo-inverse of $[\Sigma]$ is required so that:

$$[\Sigma]^+[\Sigma]=[I]_{n_C\times n_C} \qquad (5.5.2\text{-}6)$$

The above condition will be satisfied by any matrix of the form:

$$[\Sigma]^+=\left[\begin{array}{ccc:c}1/\sigma_1 & & 0 & \\ & 1/\sigma_2 & & ? \\ & \ddots & & \\ 0 & & 1/\sigma_{nC} & \end{array}\right]_{nC\times n_r} \qquad (5.5.2\text{-}7)$$

$\underbrace{\qquad\qquad}_{n_r-n_c}$

For a least squares solution, the norm of the pseudo-inverse of $[A]$ is minimised so that from equations (5.5.2-2) and (5.5.2-5) one gets:

$$[A]^+=[V][\Sigma]^+[U]^T \qquad (5.5.2\text{-}8)$$

$$\left\|[A]^+\right\|=\left\|[V][\Sigma]^+[U]^T\right\|=\left\|[\Sigma]^+\right\| \qquad (5.5.2\text{-}9)$$

This is minimised by choosing the right partition of $[\Sigma]^+$ to be zero:

$$[\Sigma]^+ = \begin{bmatrix} 1/\sigma_1 & & & 0 & \vdots & 0 \\ & 1/\sigma_2 & & & & \\ & & \ddots & & & \\ 0 & & & 1/\sigma_{nc} & \vdots & \end{bmatrix}_{nc \times n_r} \qquad (5.5.2\text{-}10)$$

$$n_r - n_c$$

If one pre-multiplies equation (5.5.2-1) by $[A]^+$ then one obtains the least squares solution by the following equation:

$$\{p\} = [A]^+ \{\Delta\xi\} = [V][\Sigma]^+ [U]^T \{\Delta\xi\} \qquad (5.5.2\text{-}11)$$

5.5.3 Updating using FRF sensitivity

Although this method of model updating is not used in this work, it is thought to be useful to give a brief description of the FRF sensitivities a derivation of which can be found in Appendix 2.

By making a direct comparison to the Modal sensitivities, the FRF sensitivity matrix is given by the following equation:

$$[S(\omega)]\{p\} = \{\Delta\alpha(\omega)\} \qquad (5.5.3\text{-}1)$$

where:

$$[S(\omega)] = [\alpha_a(\omega)]\left[\left[-\omega^2 \frac{\partial[M]}{\partial p_1} + \frac{\partial[K]}{\partial p_1}\right]\{\alpha_x(\omega)\} \cdots \left[-\omega^2 \frac{\partial[M]}{\partial p_{Np}} + \frac{\partial[K]}{\partial p_{Np}}\right]\{\alpha_x(\omega)\}\right] \qquad (5.5.3\text{-}2)$$

The sensitivity matrix $[S]$ gives the changes in the receptance due to unit changes in the updating parameters. The equation (5.5.3-1) provides N equations for N_p unknowns at a single excitation frequency, ω. If there are N_f measured frequency points, an equal set of equations can be formed as follows:

$$[A]\{p\} = \begin{bmatrix} [S(\omega_1)] \\ [S(\omega_2)] \\ \vdots \\ [S(\omega_{Nf})] \end{bmatrix} \{p\} = \begin{Bmatrix} \{\Delta\alpha(\omega_1)\} \\ \{\Delta\alpha(\omega_2)\} \\ \vdots \\ \{\Delta\alpha(\omega_{Nf})\} \end{Bmatrix} \qquad (5.5.3\text{-}3)$$

This equation is in a similar form to equation (5.5.2-1), a solution of which is obtained by applying Singular Value Decomposition to $[A]$.

The Frequency Response Function sensitivity method is not used very widely for optimisation. The reason may be that the FRFs are very sensitive to noise interference, Waters (1995), and therefore need to be smoothed out before they can be used with confidence. Normally the smoothing of the FRFs is done through curve fitting processes, which lead to the identification of the modal parameters, and therefore, it is those parameters that are used conveniently for updating. Two researchers that used FRF sensitivity updating are Fritzen (1990) and Waters (1995). The latter updated the analytical model of a cantilevered plate wing using as experimental results the data obtained from a simulated model, having +100% stiffness errors at two elements and investigated the susceptibility to noise of the FRF sensitivity approach.

5.5.4 Direct Optimisation

As already mentioned, the techniques belonging to this group of optimisation are Simulated Annealing and Genetic Algorithms. Levin et al (1997) present a comparison of these two techniques, which are capable of finding the global minimum amongst many local minima for a given objective function. The objective function quantifies the difference between the analytical and experimental models in

terms of the updating parameters. This function is minimised using the two techniques leading to an updated analytical model. A case study is presented. Zimmerman et al (1997) present a paper that deals with the Genetic Algorithm. The paper describes a model refinement approach based on this algorithm, which uses the frequency and modeshape information but avoids the problem of closely spaced modes. Ruotolo et al (1997) use Simulated Annealing to detect damage in structures. The authors apply the optimisation technique to two cases. In the first case, an objective function based on the residual forces concept is used to estimate the stiffness of the springs present in a Kabe's 8 dofs problem, as described in the same paper. In the second case, a cost function that measures the distance between measured and calculated natural frequencies is used to analyse experimental data and estimate the depth and position of cracks of three cantilevered steel beams.

5.5.5 Neural Networks

This is the third group of optimisation techniques and uses Neural Networks (NN). Qi et al (1992) present an approach for dynamic function mapping. The network is trained, tested and verified by using the responses recorded in a real structure during earthquakes. They conclude that the dynamic behaviour of the building can be well modelled by the trained network. Riva et al (1991) investigate the Neural Network behaviour when dealing with time domain data. They consider the possibility of extracting modal parameters from time series using Neural Networks. Their results are encouraging but further work involving MDOF systems is needed in order to consider NN a powerful tool for modal identification.

5.5.6 Updating parameters

The purpose of model updating is to correlate the analytical with the experimental model. In order to achieve that, the user should make parametric changes to the finite element model. The set of p-values, chosen by the user to vary, should contain the correct parameters that will give a solution to the problem that has a physical significance.

If one expresses the global mass and stiffness matrices in terms of the elemental matrices:

$$[M_a]=\sum_{i=1}^{Ne}[M_e]_i \quad \text{and} \quad [K_a]=\sum_{i=1}^{Ne}[K_e]_i \tag{5.5.6-1}$$

then, the updated matrices can be written as:

$$[M_u]=\sum_{i=1}^{Ne}(1+m_i)[M_e]_i \quad \text{and} \quad [K_u]=\sum_{i=1}^{Ne}(1+k_i)[K_e]_i \tag{5.5.6-2}$$

where m_i and k_i are constants.

Subtracting equations (5.5.6-2) from equations (A2-7) and (A2-8), the error matrices are given by:

$$[\Delta M]=\sum_{i=1}^{Ne}m_i[M_e]_i \quad \text{and} \quad [\Delta K]=\sum_{i=1}^{Ne}k_i[K_e]_i \tag{5.5.6-3}$$

The set of p-values consists of: $\{p\}=\{m_1,\cdots,m_{Ne},k_1,\cdots,k_{Ne}\}$ (5.5.4-4)

Another way of expressing the error matrices is by assuming that the errors occur at N_m and N_k groups of one or more elements. The advantage of this assumption is that it is not necessary to calculate the derivatives of the mass and stiffness matrices in equations (5.5.1.1-1) and (5.5.1.1-2), since they are given by:

$$\frac{\partial[M]}{\partial m_i}=[M_s]_i \quad \text{and} \quad \frac{\partial[K]}{\partial k_i}=[K_s]_i \tag{5.5.6-5}$$

Also, all the higher order derivatives in the Taylor's series are zero, so there are no errors in the equations (A2-7) and (A2-8).

5.6 Finite Element Modelling of a 2-D Beam

An updating exercise was undertaken involving the updating of a two-dimensional beam, clamped at both ends. Both the analytical and experimental models were prepared using ANSYS.

The experimental model had consistent material properties, which are given in Table 5.6-1

The model was one metre long and divided into 10 two-dimensional Euler-Bernoulli beam elements. A representation of the model can be seen in Figures 5.6-1 and 5.6-2. The elements have only three degrees-of-freedom at each node, two translations and a rotation.

Parameter	Value
Young's Modulus	200×10^{09} Nm^{-2}
Poisson's ratio	0.3
Density	7850 kgm^{-3}
Area	0.01 m^2

Table 5.6-1: Material properties of experimental 2-D beam

The analytical model had the same geometrical properties as the analytical one and the same material properties apart from one element, which had its Young's Modulus value increased by 30%. That was element 2 shown in Figure 5.6-3.

Thirteen modes were extracted from both models. The frequencies are given in the Table 5.6-2 below. Figure 5.6-4 shows a graphical comparison of the frequencies as described in section 5.3.1. As one can observe, there is very good correlation between the experimental and analytical frequencies, since all points lie close to the line of slope 1. Also, the modeshapes of the two models were compared and their correlation is shown as a MAC plot in Figure 5.6-5. The plot shows a perfect correlation between the modeshapes, since the leading diagonal terms have a MAC value of 1 and there are almost no off-diagonal terms appearing.

5.6.1 Updating of finite element model

The first stage in the updating process is to choose the updating parameters. In this case, it is known that the Young's Modulus of element 2 is different than the other elements. So one of the updating parameter for this exercise will be the stiffness of element 2.

Seven updating runs were performed. In the first four runs, the number of frequencies used varied and the only updating parameter was the stiffness of element 2. In order to chose which modes to use for the updating, the strain energy of element 2 for each mode was calculated.

Mode number	Analytical frequency (Hz)	Experimental frequency (Hz)
1	516.12	524.5
2	1403.6	1409.4
3	2534.2	2535.6
4	2697.1	2743.8
5	4345.7	4395.5
6	5130.9	5241.2
7	6302.5	6374.5
8	7853.7	7892.7
9	8524.1	8658.9
10	10765	10935
11	10973	11082
12	13595	13782
13	13914	14092

Table 5.6-2: Frequencies (f) of analytical and experimental 2-D beam

The modes, which give high strain energy in the element in question, were used. The number of frequencies varied from six to three, leading to an over-determined problem, since there is only one updating parameter used. In the last three runs, the updating parameters were the stiffnesses of elements 1, 2, 3. Again a different

number of frequencies were used. Table 5.6.1-1 summarises the differences between each run.

Run	Modes	Updating parameter
1	5,7,9,11,12,13	K2
2	7,9,11,12,13	K2
3	9,11,12,13	K2
4	11,12,13	K2
5	1:13	K1, K2, K3
6	7:13	K1, K2, K3
7	1:7	K1, K2, K3

Table 5.6.1-1: Summary of each updating run

The updating was carried out using the eigenvalue sensitivity method described in Chapter 5, Section 5.5.1. Convergence was achieved, in each case, after four or five iterations representing quite robust convergence. Convergence was assumed to have occurred when the largest change in the updating parameter dropped below 1% of the original value. Figures 5.6.1-1 and 5.6.1-2 show the value of the residual at each iteration for each updating run. Each line corresponds to an updating run. The residual is defined as:

$$R = \left\| \{\lambda\}_{ak} - \{\lambda\}_x \right\|_2 \qquad (5.6.1\text{-}1)$$

where $\{\lambda\}_{ak}$ are the analytical eigenvalues at k^{th} updating iteration.

The residual is an indication of how much the updated analytical model matches the experimental one. The least successful runs seem to be runs 1 to 4, whereas, the most successful are runs 5 to 7. The higher order modes are more useful in making changes to the finite element model than the lower order modes. This observation is entirely understandable, as higher order modes possess more localised strain energy. Figures 5.6.1-3 and 5.6.1-4 show the plot of p-values against the number of iterations for runs 1-4 and 5-7 respectively. As one can observe, updating runs 1-6 lead to a p-

value for the stiffness of element 2 of -0.25, which indicates that the stiffness of that element should be reduced by a factor of 0.25 in order to match the stiffness of the experimental model. However, run 7 leads to a higher p-value of –0.23, which is probably because, it uses only the lower frequencies to update the parameters. Figures 5.6.1-5 to 5.6.1-11 show the p-value plots against the element number for runs 1-7.

Table 5.6.1-2 shows the frequencies of the updated analytical and experimental models after updating runs 1-4. As one can observe from this table, the higher order updated analytical frequencies match the experimental frequencies. The frequencies enclosed in parentheses are frequencies not taken into account in the updating runs but are included here in order to observe whether they have improved or deteriorated as a result of updating. As one can see from this table, these frequencies seem to increase towards the corresponding experimental frequencies. This should be expected since the purpose of updating is to produce a closer match between an experimental and an analytical model.

Table 5.6.1-3 show the updated analytical frequencies after runs 5-7, including the frequencies not used in the updating runs. Again, as one can observe, the higher order updated analytical frequencies match closely the experimental frequencies, and the frequencies not included in the updating runs, seem to improve slightly.

Modes	Exper. frequencies	Initial analytical	Updated analytical – Run 1	Updated analytical – Run 2	Updated analytical – Run 3	Updated analytical – Run 4
5	7.63E+08	7.46E+08	7.60E+08	(7.47E+08)	(7.48E+08)	(7.48E+08)
7	1.60E+09	1.57E+09	1.60E+09	1.60E+09	(1.57E+09)	(1.58E+09)
9	2.96E+09	2.87E+09	2.94E+09	2.94E+09	2.95E+09	(2.89E+09)
11	4.85E+09	4.75E+09	4.82E+09	4.82E+09	4.83E+09	4.83E+09
12	7.50E+09	7.30E+09	7.45E+09	7.45E+09	7.48E+09	7.48E+09
13	7.84E+09	7.64E+09	7.79E+09	7.79E+09	7.81E+09	7.82E+09

Table 5.6.1-2: Comparison of frequencies (λ) of updated analytical and experimental models for runs 1-4

5.7 Concluding remarks

This chapter presented the theoretical background of the two model updating techniques, namely the modal sensitivity and FRF sensitivity methods, and included a description of all tools that the engineer may need to process data. These tools include model expansion and reduction techniques and frequency and/or modeshape comparison methods. Examples of the use of those methods were given using the analytical and experimental data of the plate tested in free-free conditions described in Chapter 4. The model updating of a 2-D beam was carried out using eigenvalue sensitivity updating. The model was prepared in ANSYS and the experimental model possessed a higher modulus of elasticity for element 2 than the analytical one. The updating results were presented in Tables 5.7.1-2 and 5.7.1-3 where one can observe that the updated frequencies correlate very closely with the experimental ones. These methods will be applied to a cable-stayed bridge cantilever described in the following chapter.

Modes	Exper frequencies	Initial analytical	Updated analytical – Run 5	Updated analytical – Run 6	Updated analytical – Run 7
1	1.09E+07	1.05E+07	1.08E+07	(1.05E+07)	1.06E+07
2	7.84E+07	7.78E+07	7.82E+07	(7.79E+07)	7.81E+07
3	2.54E+08	2.54E+08	2.54E+08	(2.54E+08)	2.55E+08
4	2.97E+08	2.87E+08	2.95E+08	(2.87E+08)	2.89E+08
5	7.63E+08	7.46E+08	7.60E+08	(7.47E+08)	7.55E+08
6	1.08E+09	1.04E+09	1.07E+09	(1.05E+09)	1.07E+09
7	1.60E+09	1.57E+09	1.59E+09	1.60E+09	1.58E+09
8	2.46E+09	2.44E+09	2.44E+09	2.45E+09	(2.44E+09)
9	2.96E+09	2.87E+09	2.92E+09	2.93E+09	(2.89E+09)
10	4.72E+09	4.57E+09	4.69E+09	4.70E+09	(4.60E+09)
11	4.85E+09	4.75E+09	4.82E+09	4.83E+09	(4.79E+09)
12	7.50E+09	7.30E+09	7.48E+09	7.48E+09	(7.33E+09)
13	7.84E+09	7.64E+09	7.79E+09	7.81E+09	(7.70E+09)

Table 5.6.1-3: Comparison of frequencies (λ) of updated analytical and experimental models for runs 5-7

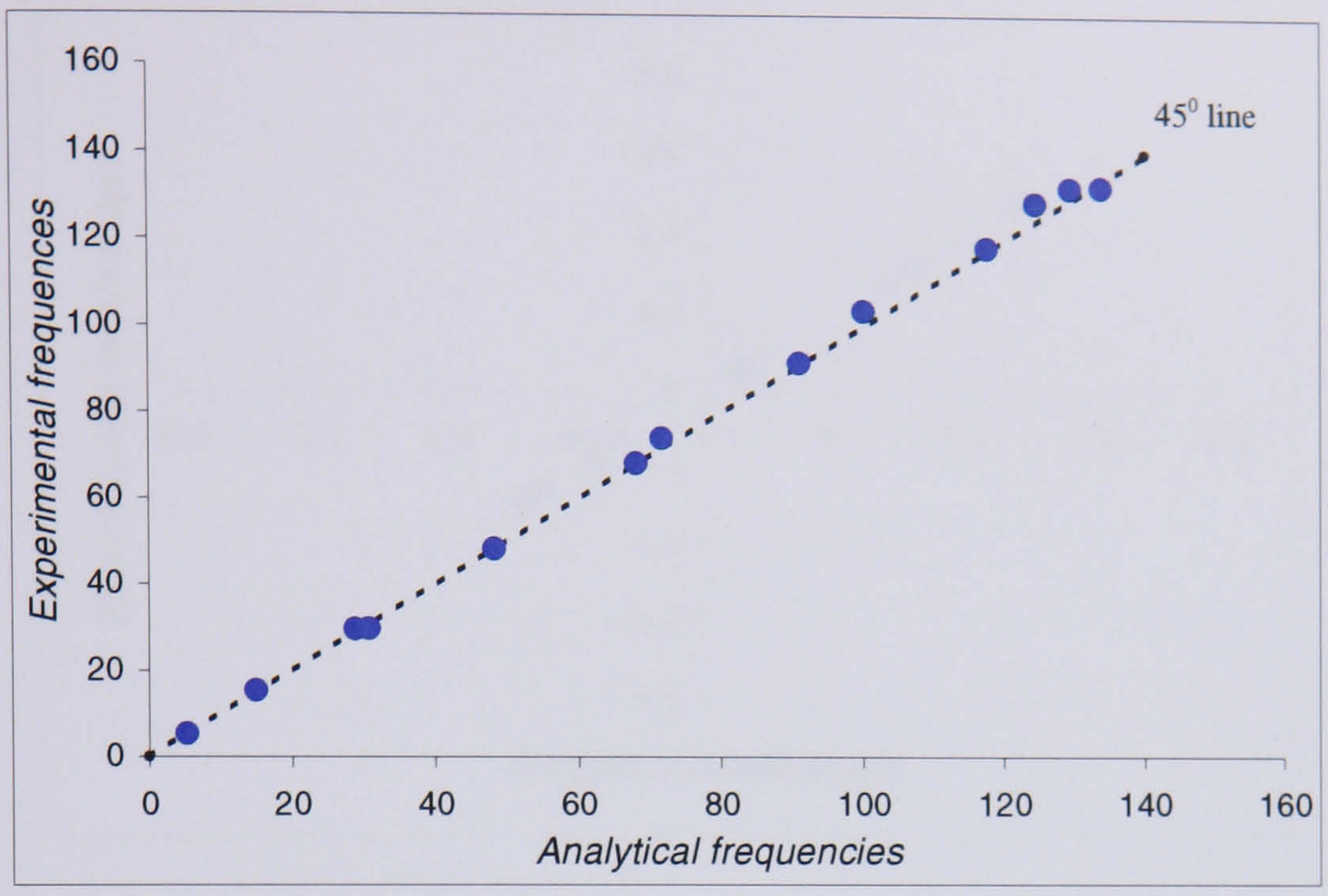

Figure 5.3.1-1: Plot of comparison of natural frequencies of free-free plate using the Effective Independence sensor location method

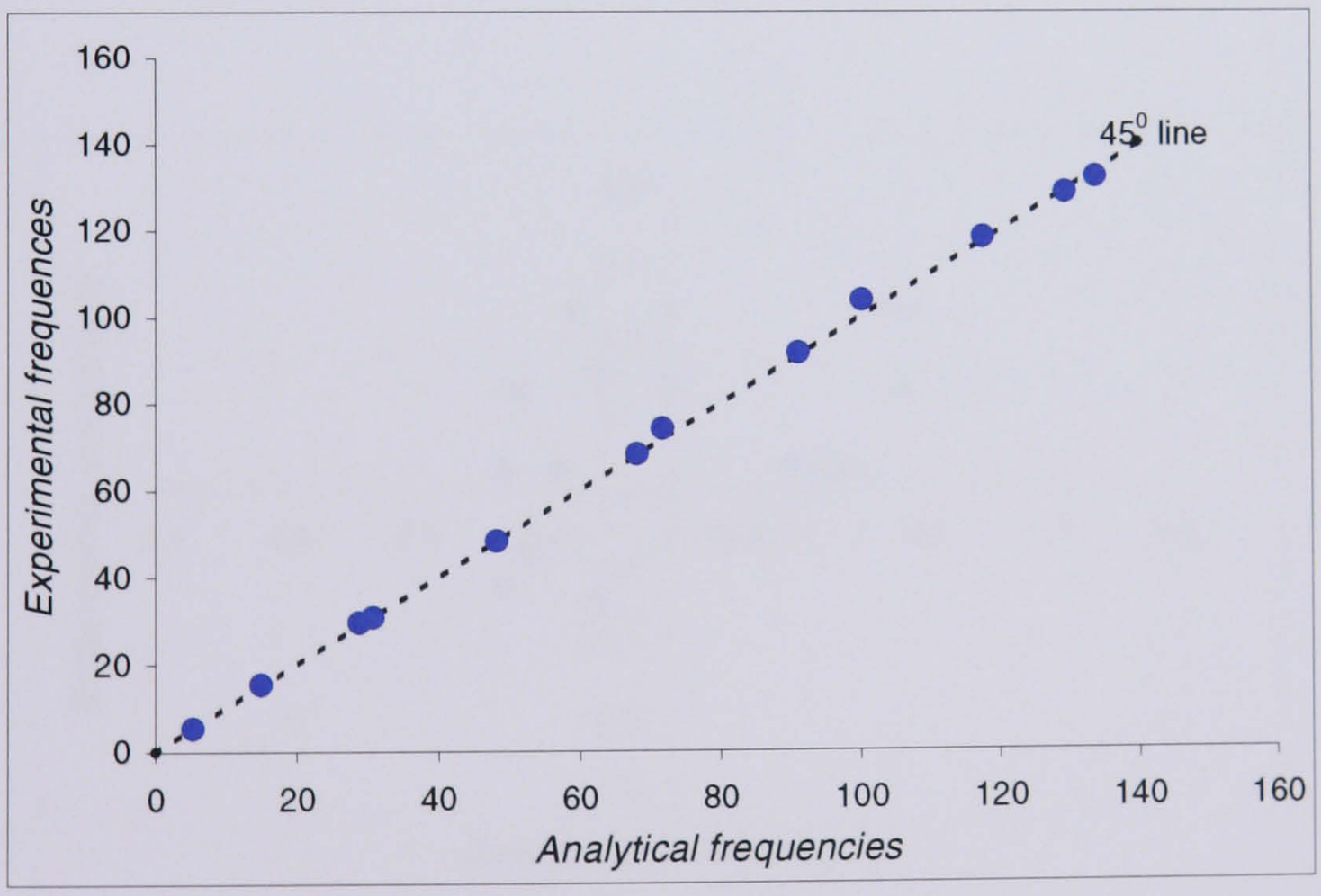

Figure 5.3.1-2: Plot of comparison of natural frequencies of free-free plate using the Energy Optimisation Technique for sensor placement

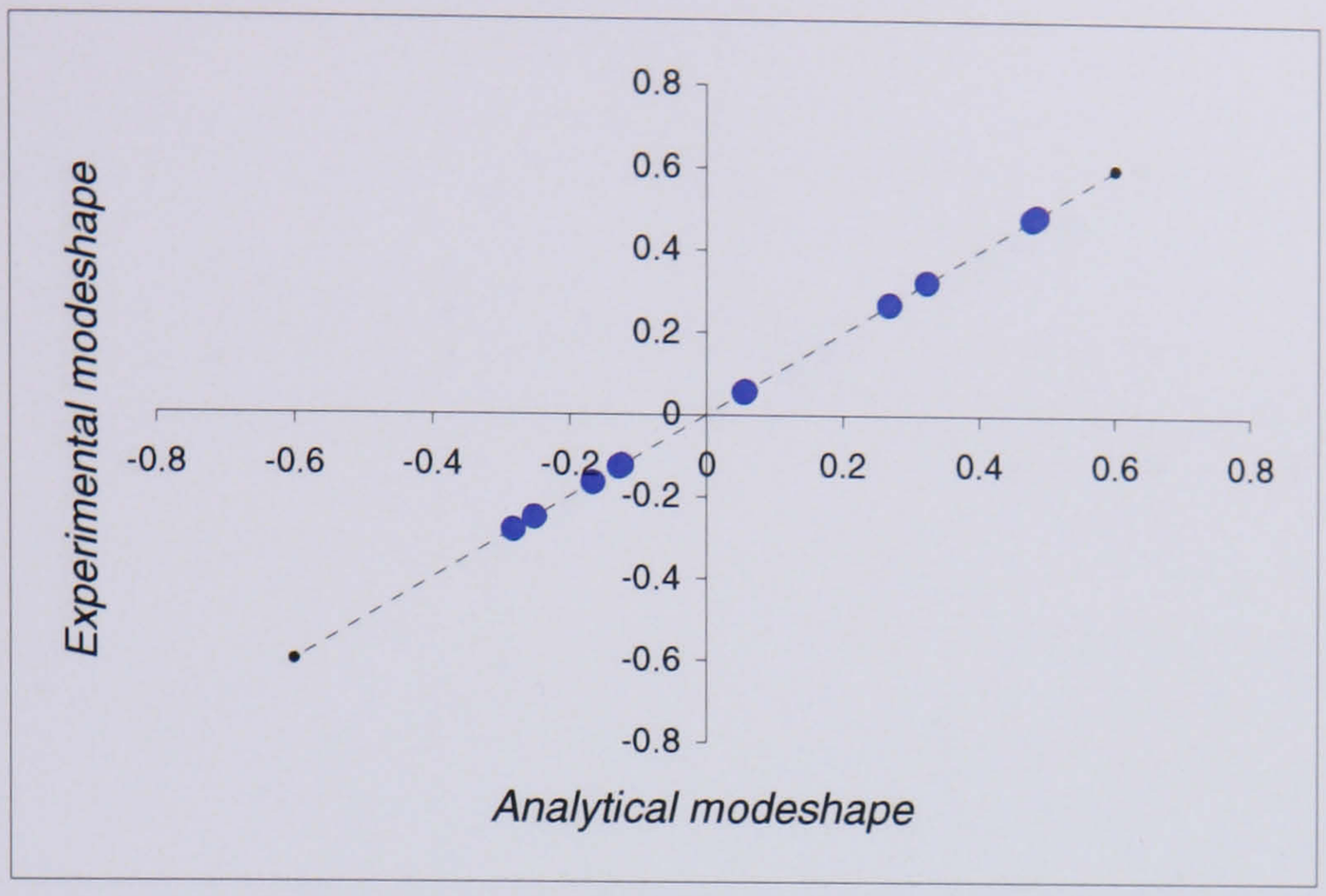

Figure 5.3.2-1: Comparison of correlated modeshapes of free-free plate using the EfI method of sensor placement

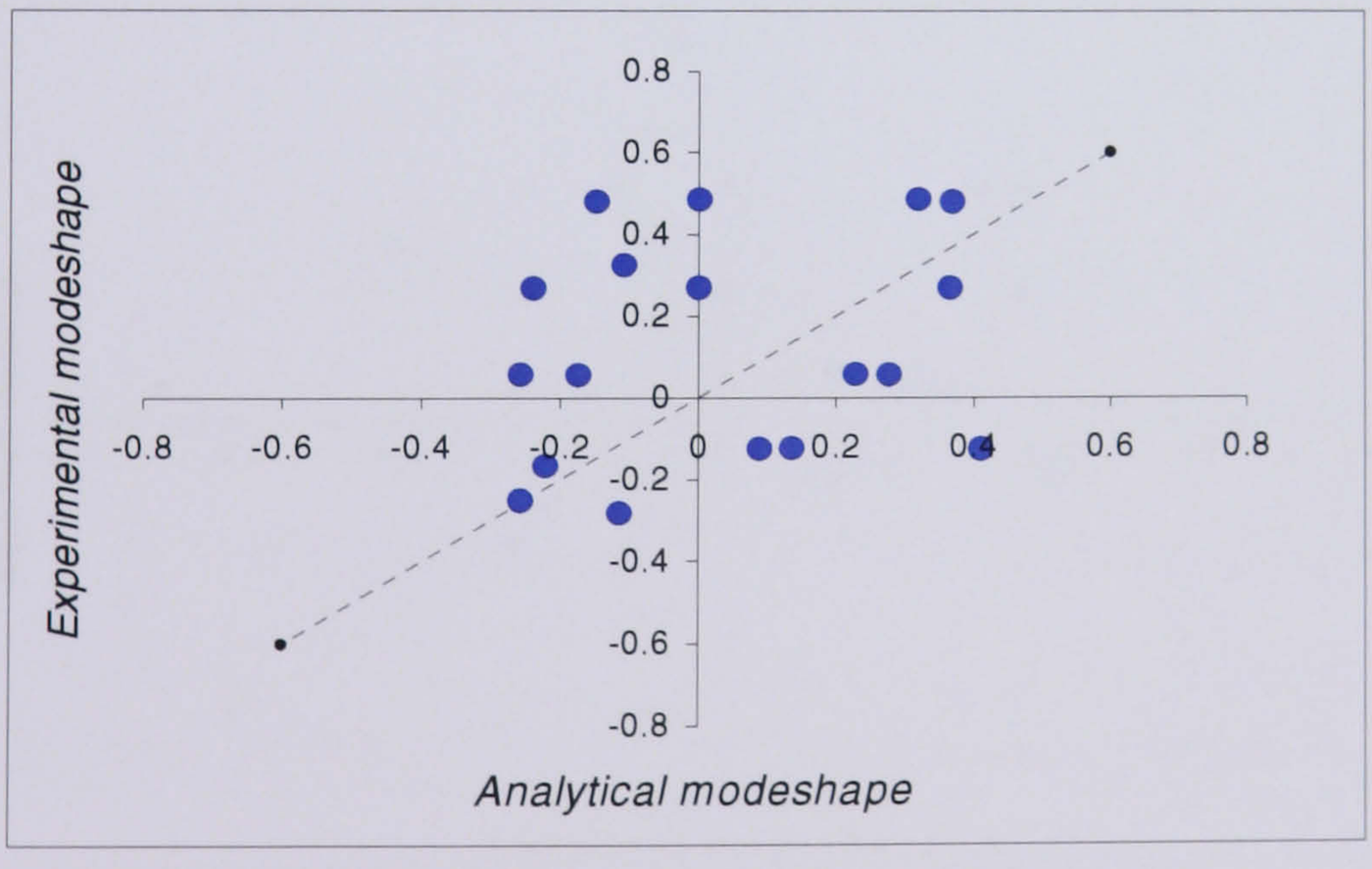

Figure 5.3.2-2: Comparison of uncorrelated modeshapes of free-free plate using the EfI method for sensor placement

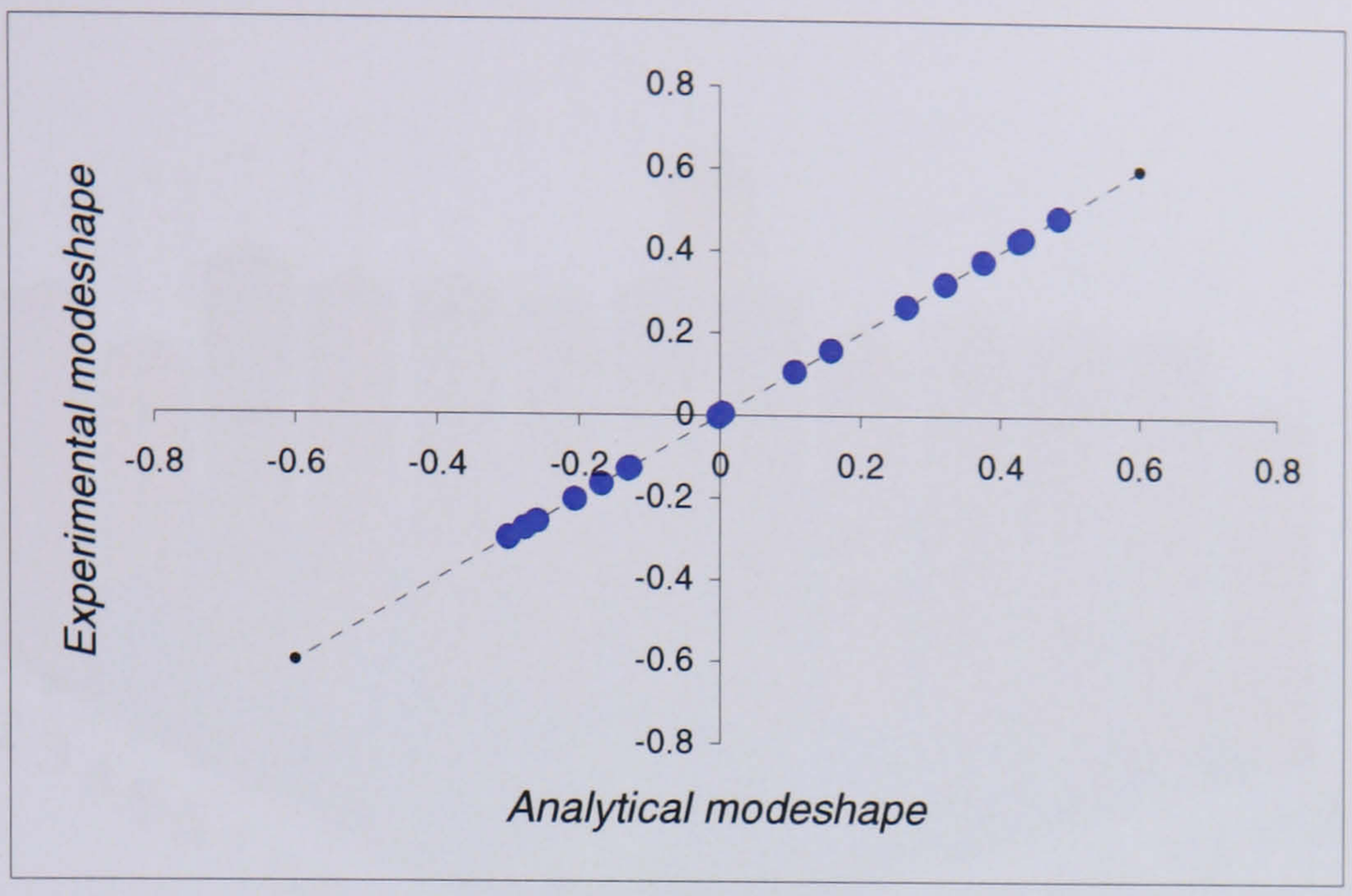

Figure 5.3.2-3: Comparison of correlated modeshapes of free-free plate using the EOT method for sensor placement

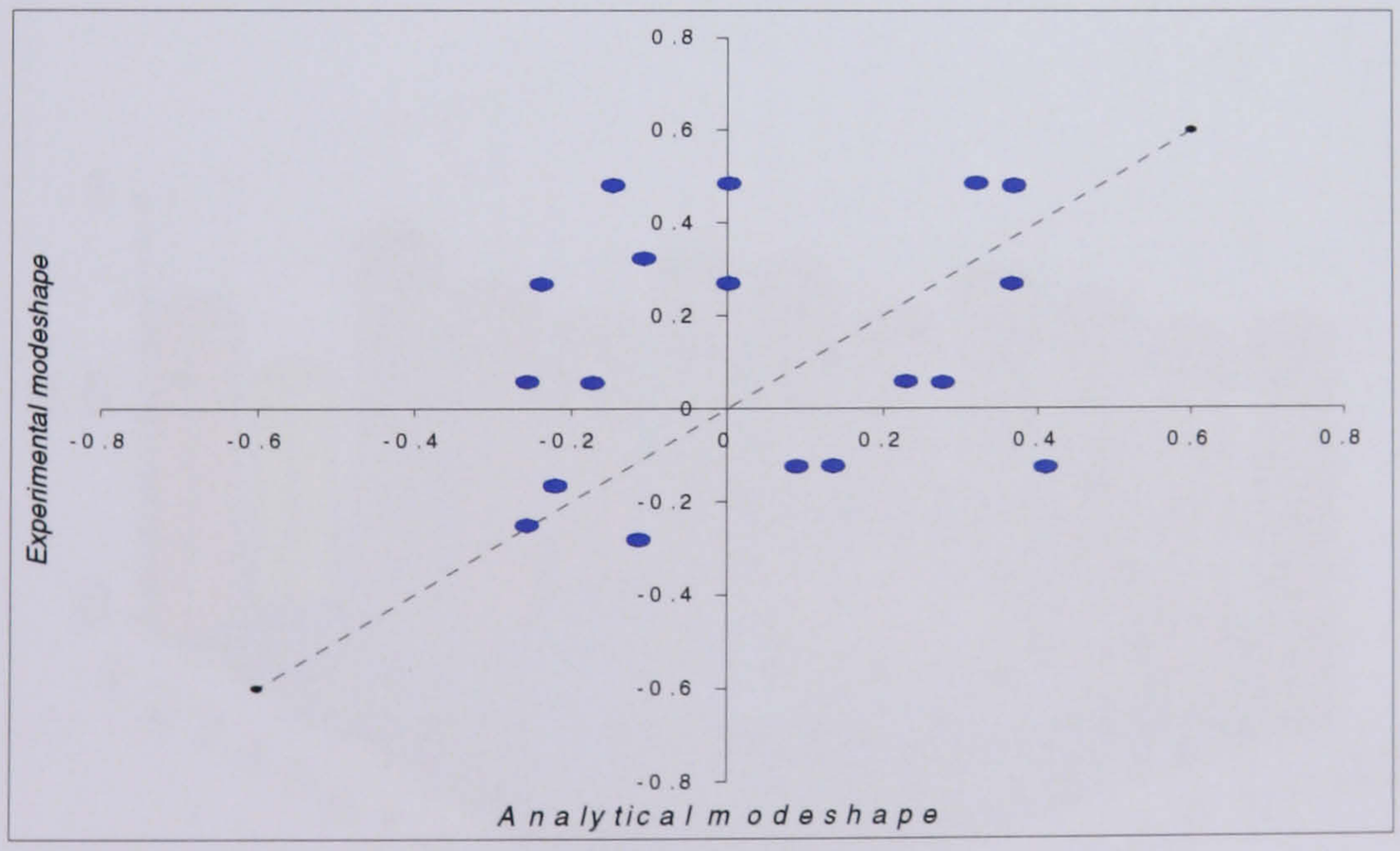

Figure 5.3.2-4: Comparison of uncorrelated modeshapes of free-free plate using the EOT method for sensor placement

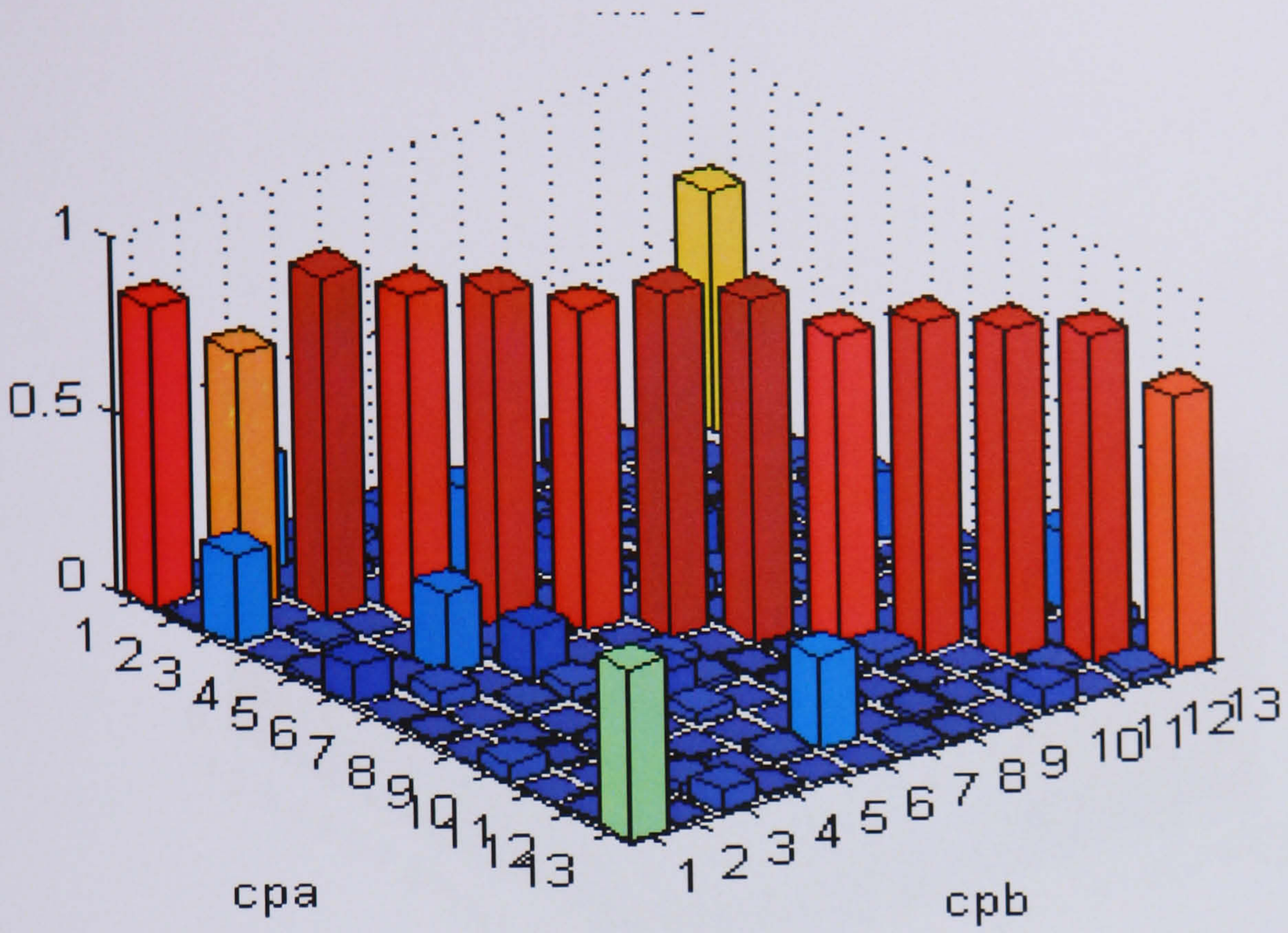

Figure 5.3.3.1: MAC plot of modes obtained using the EFI method

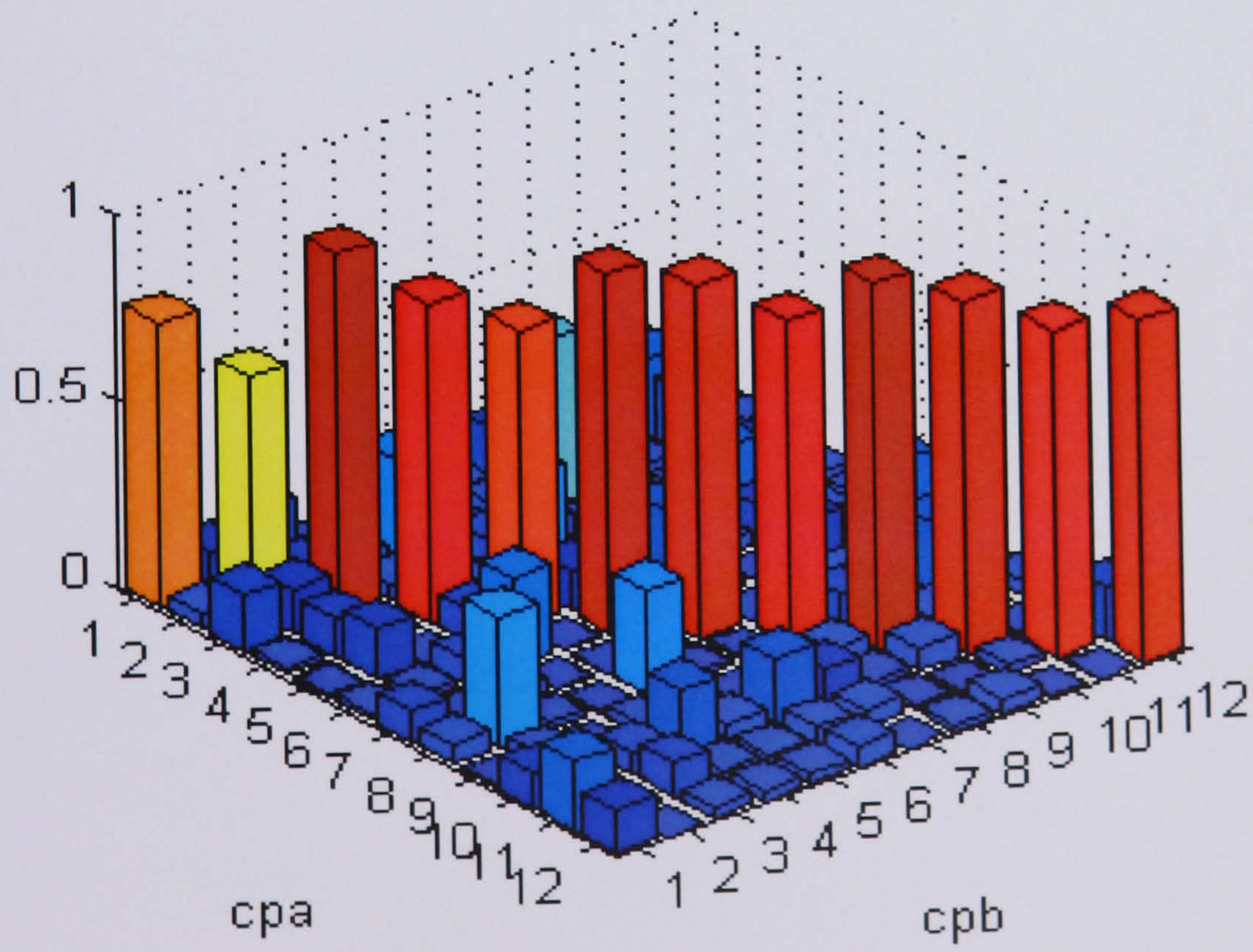

Figure 5.3.3.2: MAC plot of modes obtained using the EOT method

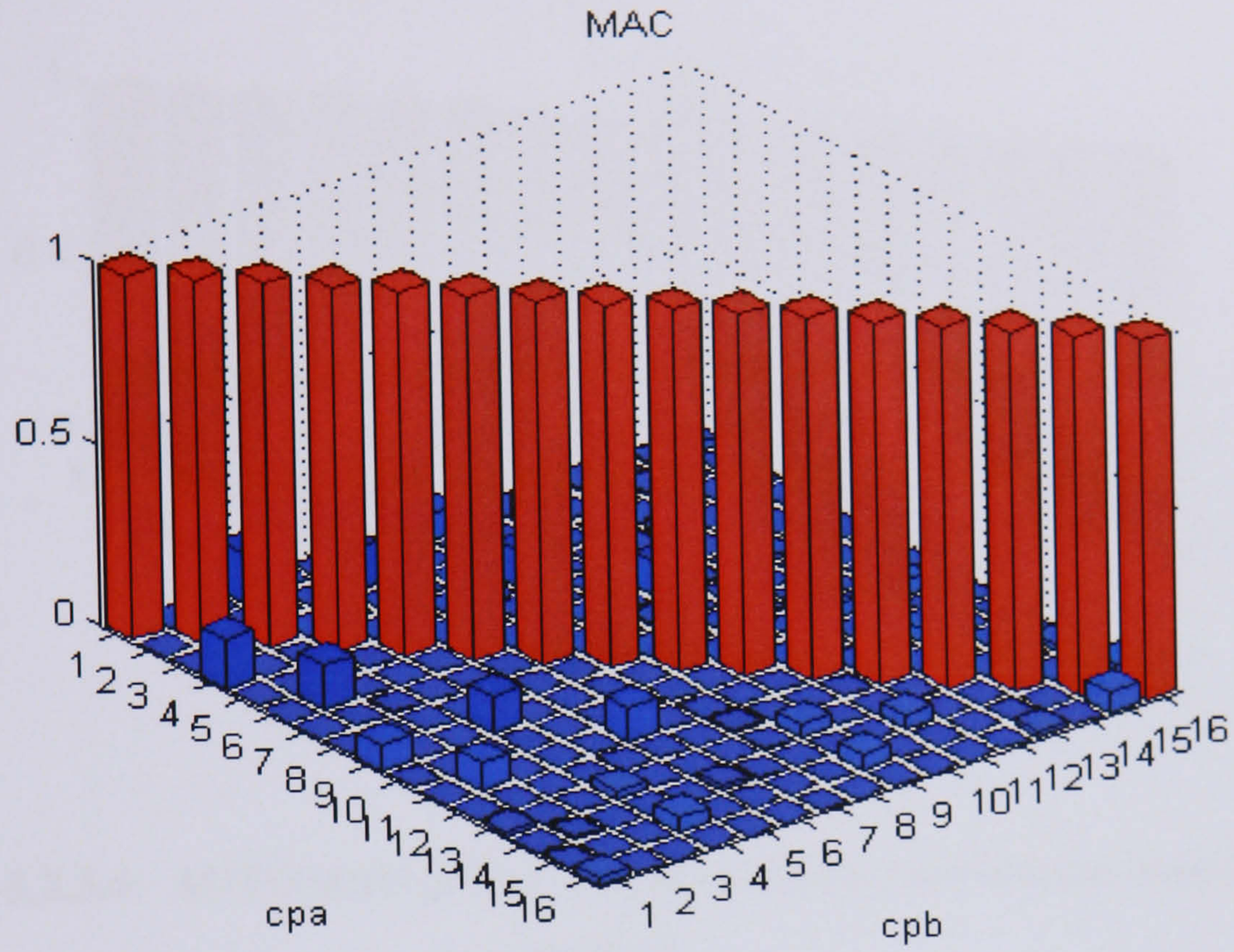

Figure 5.3.3-3: AUTOMAC of free-free plate using full set of co-ordinates

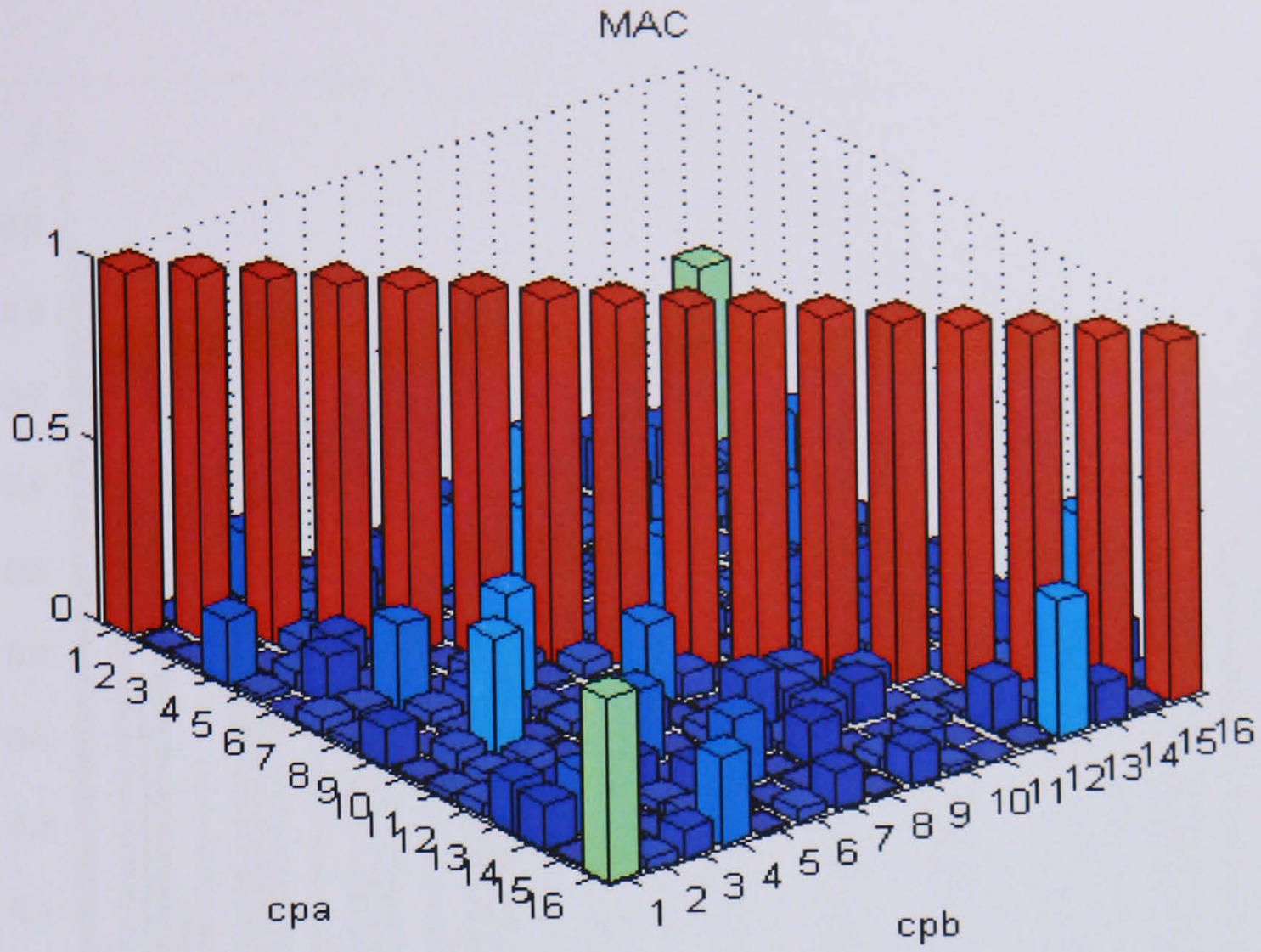

Figure 5.3.3.4: AUTOMAC of free-free plate using co-ordinates from EOT method

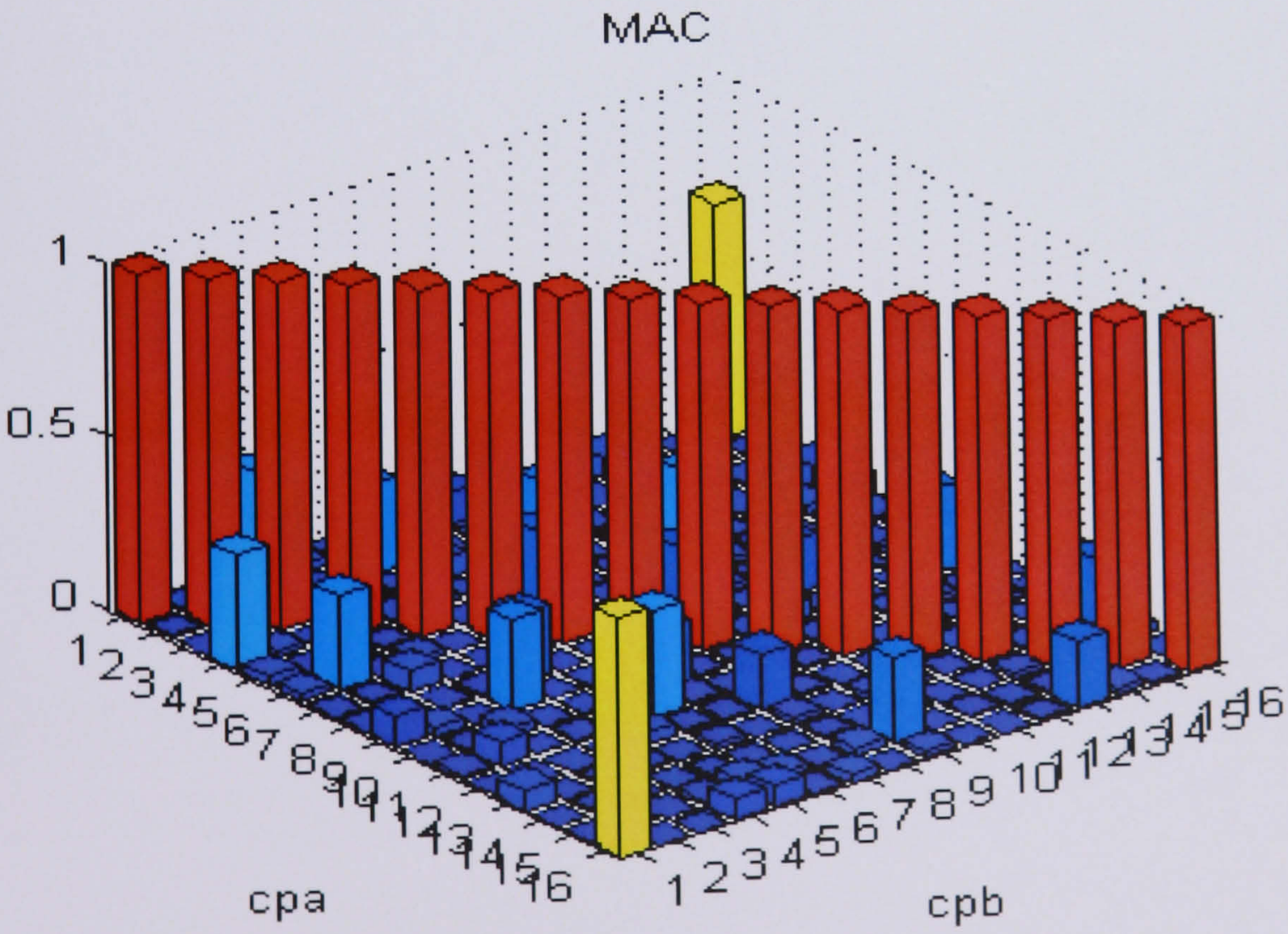

Figure 5.3.3-5: AUTOMAC plot for the EFI method

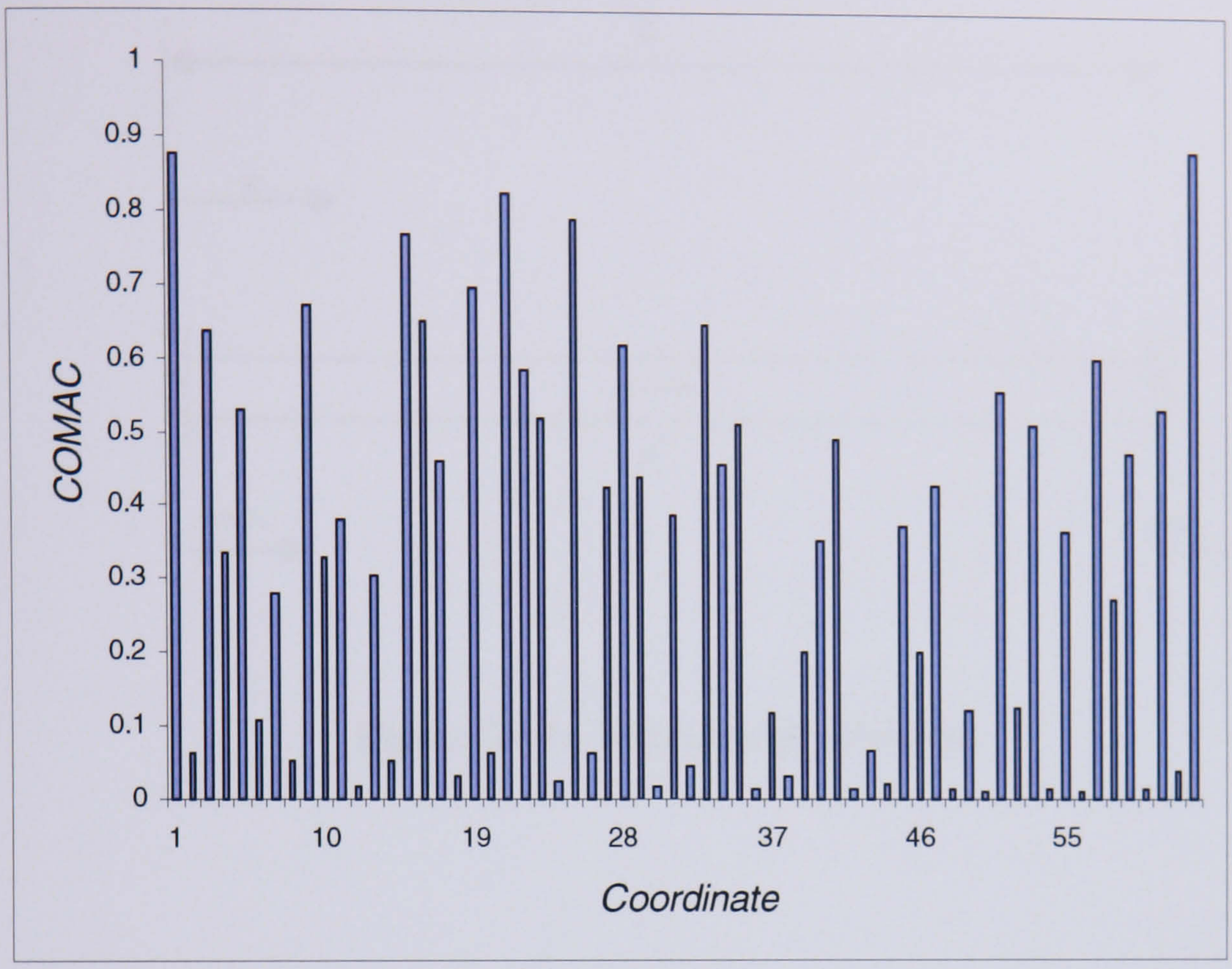

Figure 5.4-1: COMAC representation

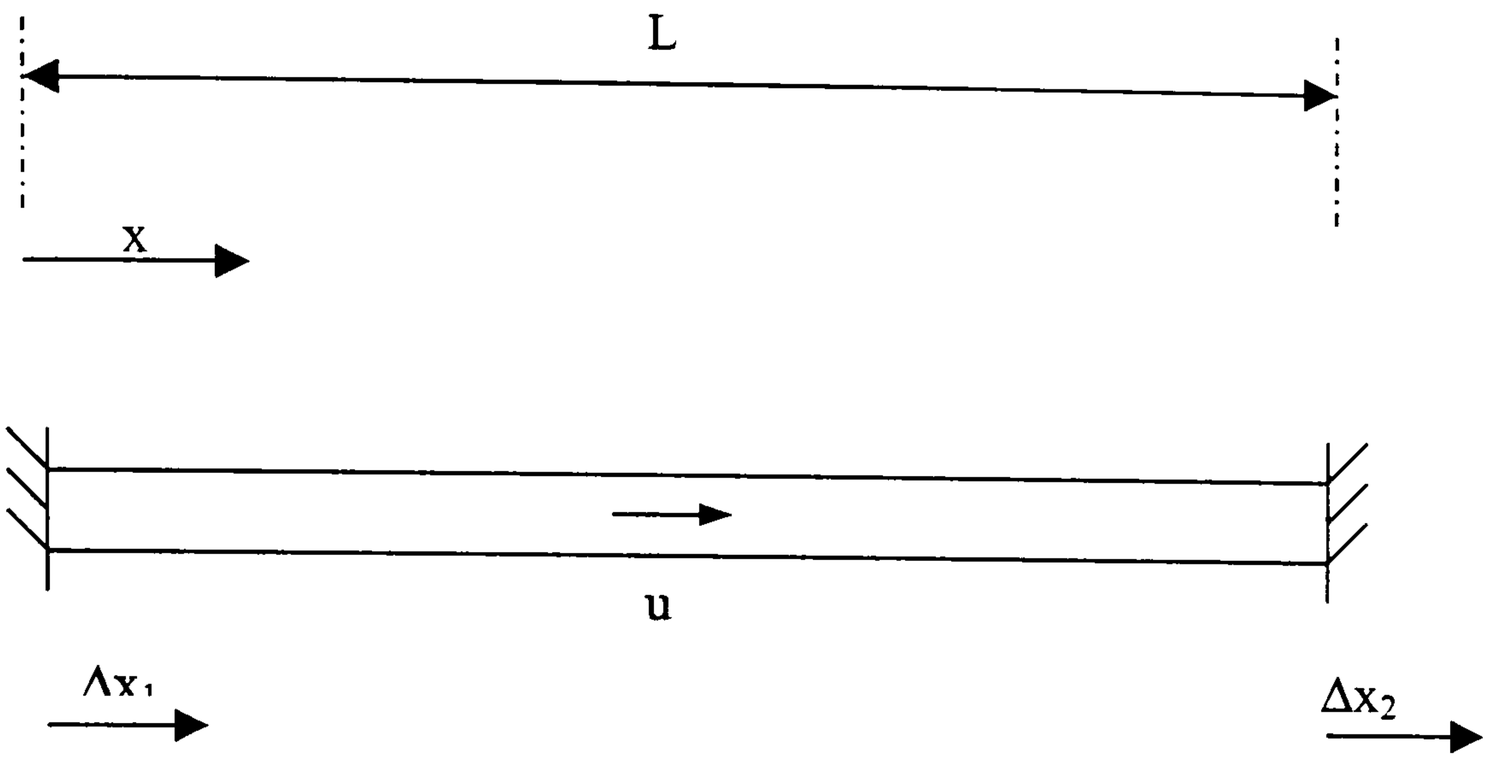

Figure 5.6-1: Beam under axial load

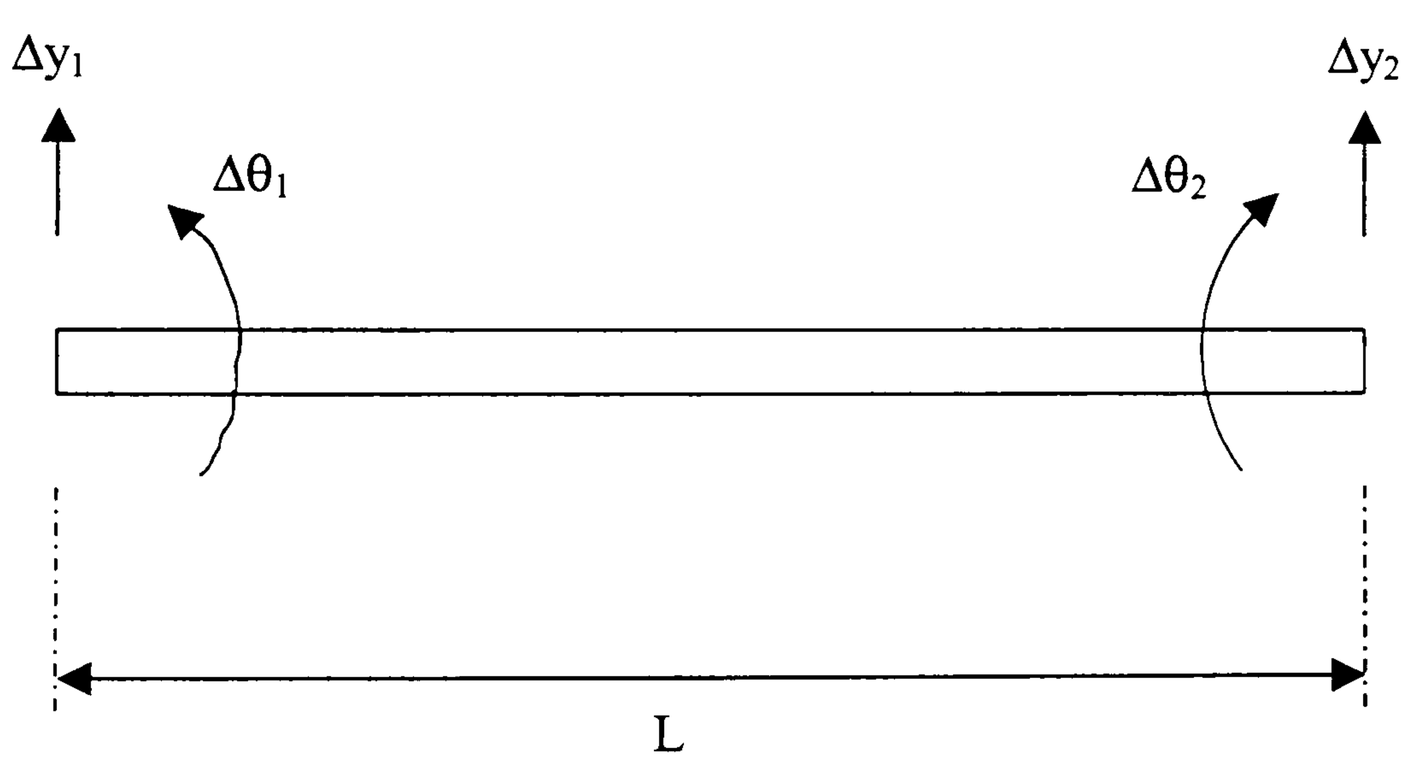

Figure 5.6-2: Beam under shear and rotational loads

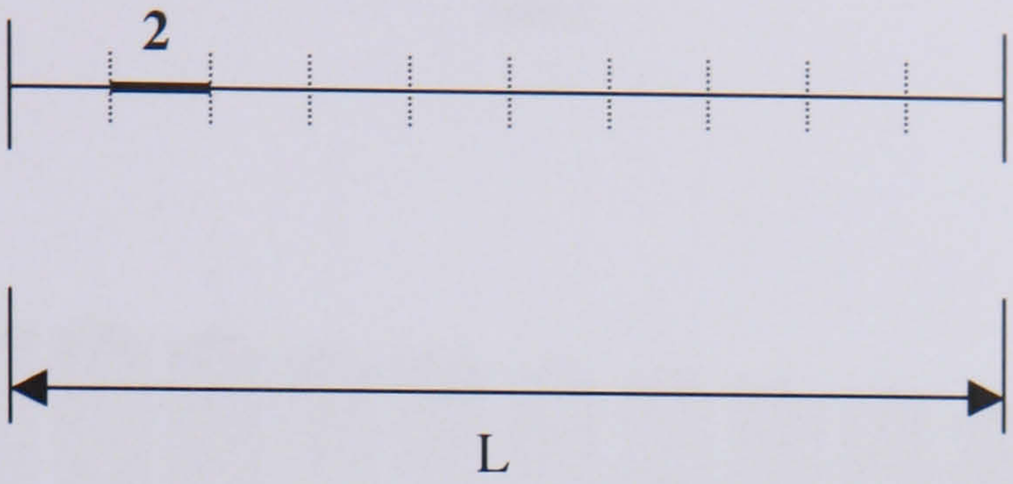

Figure 5.6-3: Finite element representation of 2-D experimental beam showing element 2

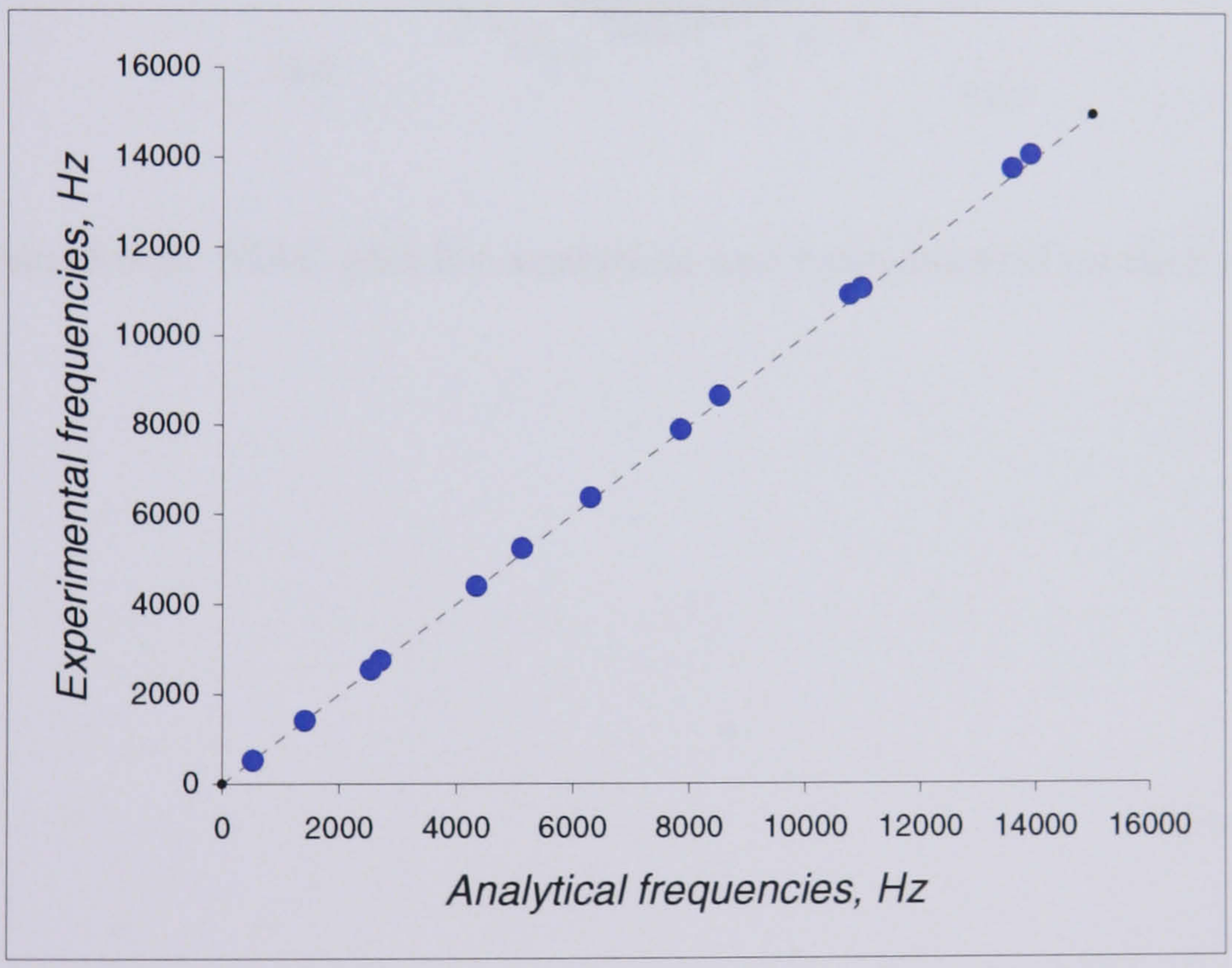

Figure 5.6-4: Comparison of analytical and experimental frequencies for 2-D beam

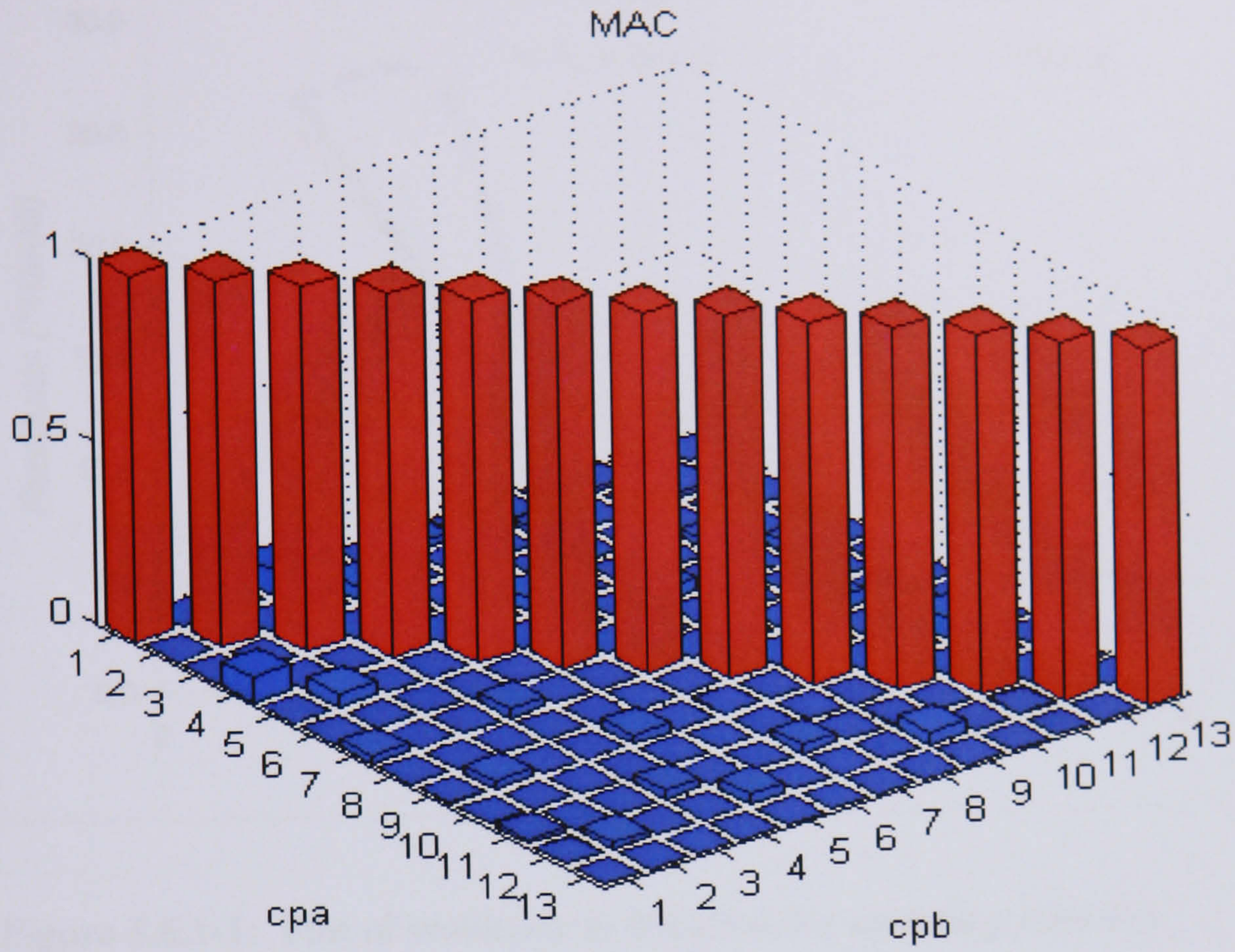

Figure 5.6-5: MAC plot for analytical and experimental modeshapes

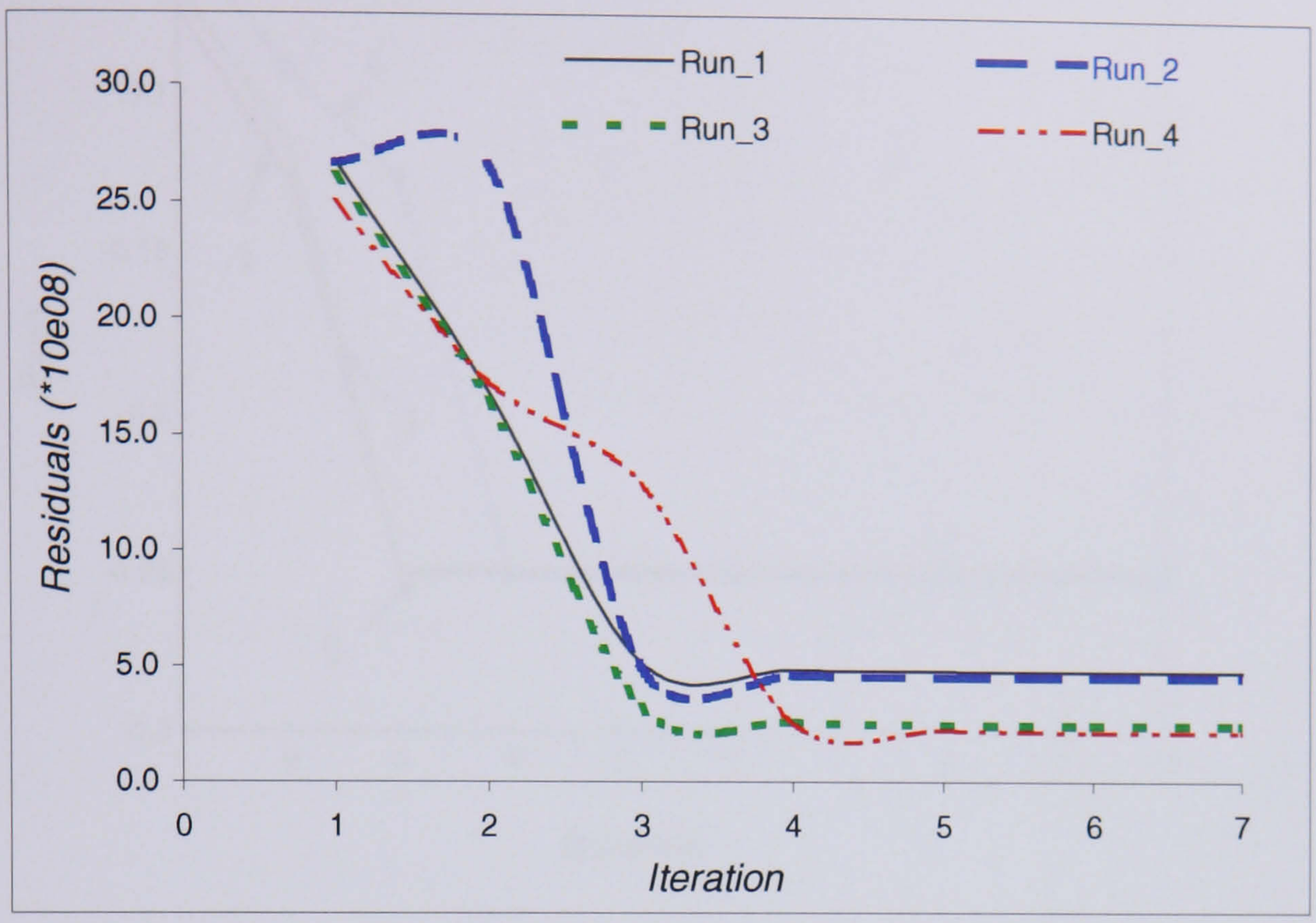

Figure 5.6.1-1: Plot of residuals vs iteration for updating runs 1-4

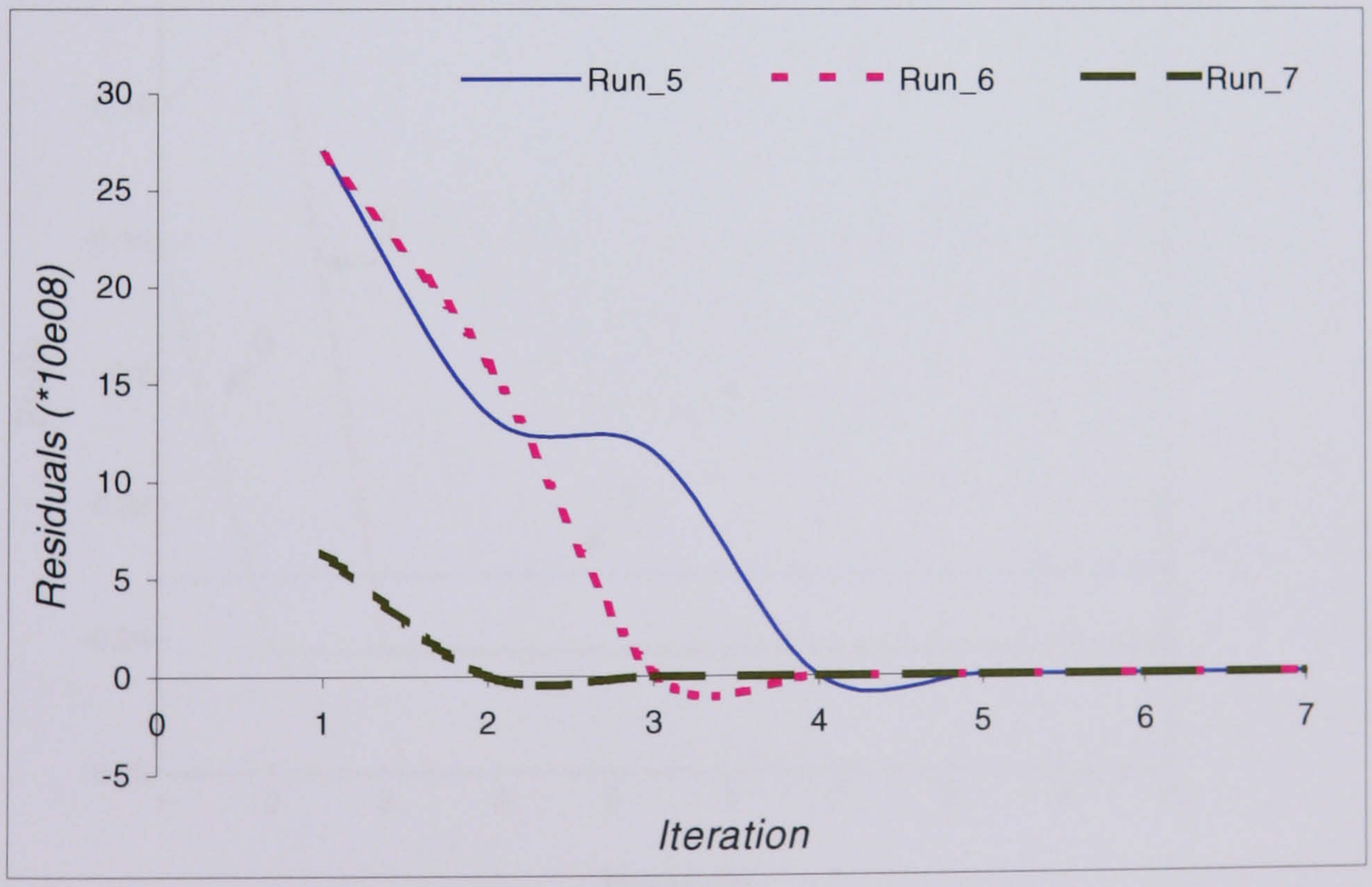

Figure 5.6.1-2: Plot of Residuals vs Iteration for updating runs 5-7

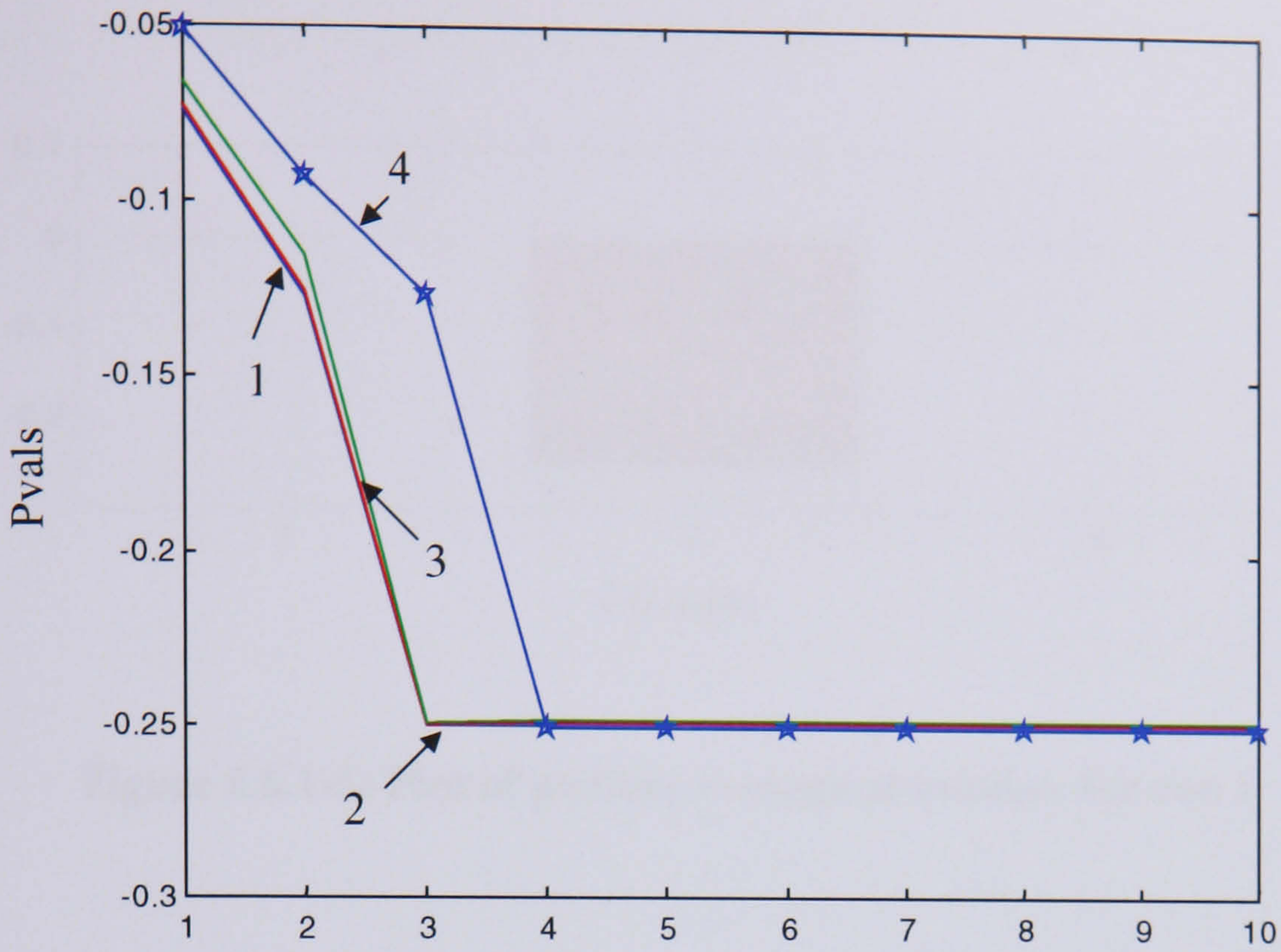

Figure 5.6.1-3: Plot of pvals vs iteration for the first four updating runs

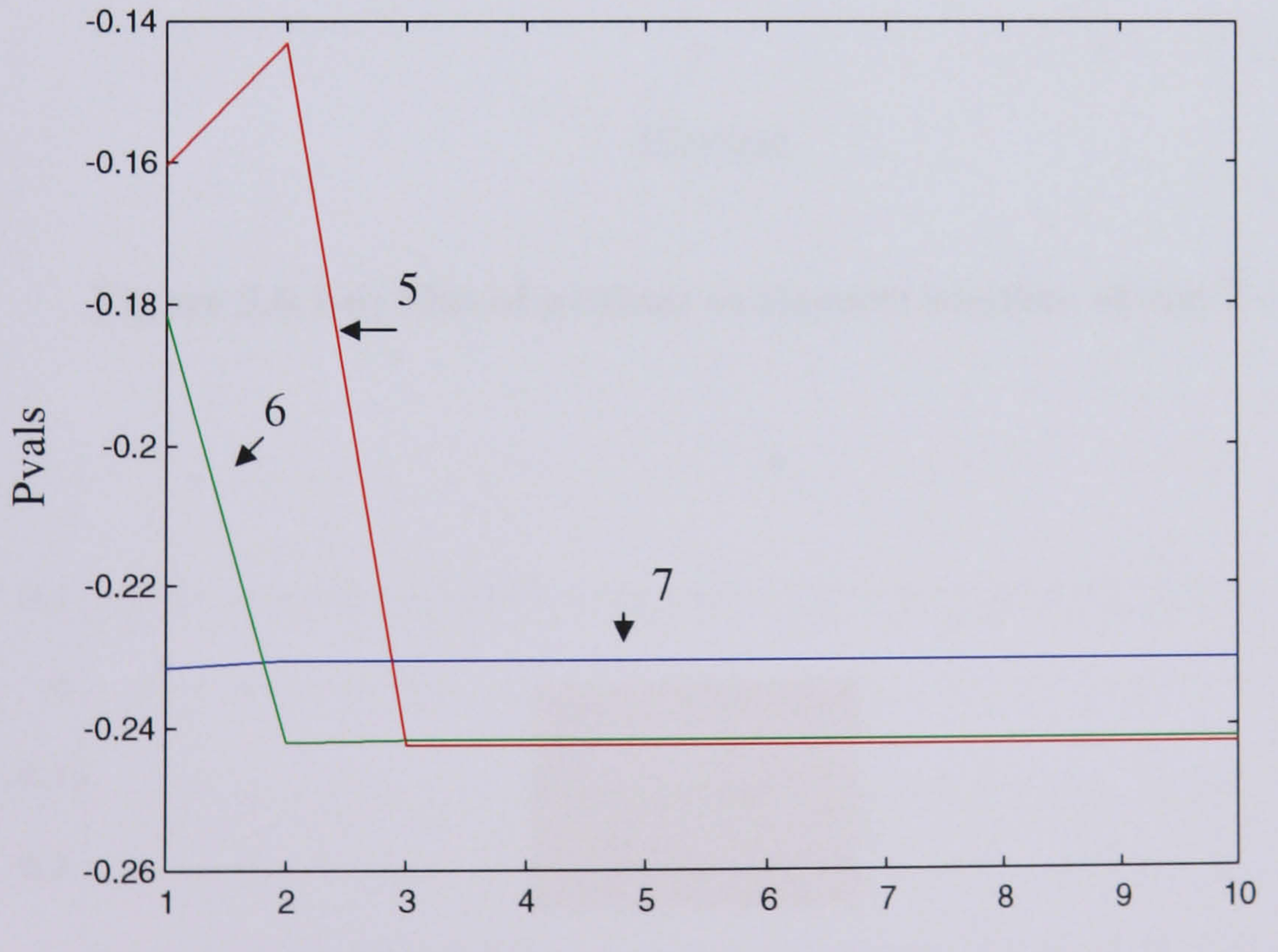

Figure 5.6.1-4: Plot of pvals vs iteration for the updating runs 5-7

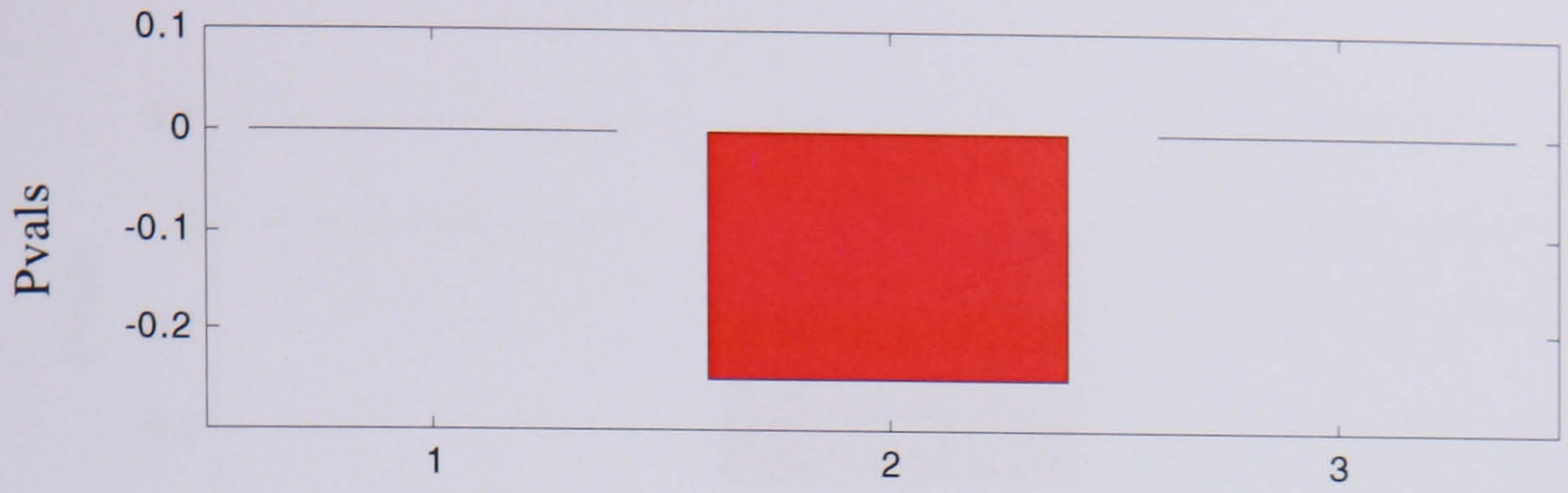

Figure 5.6.1-5: Plot of pvalues vs element number for run 1

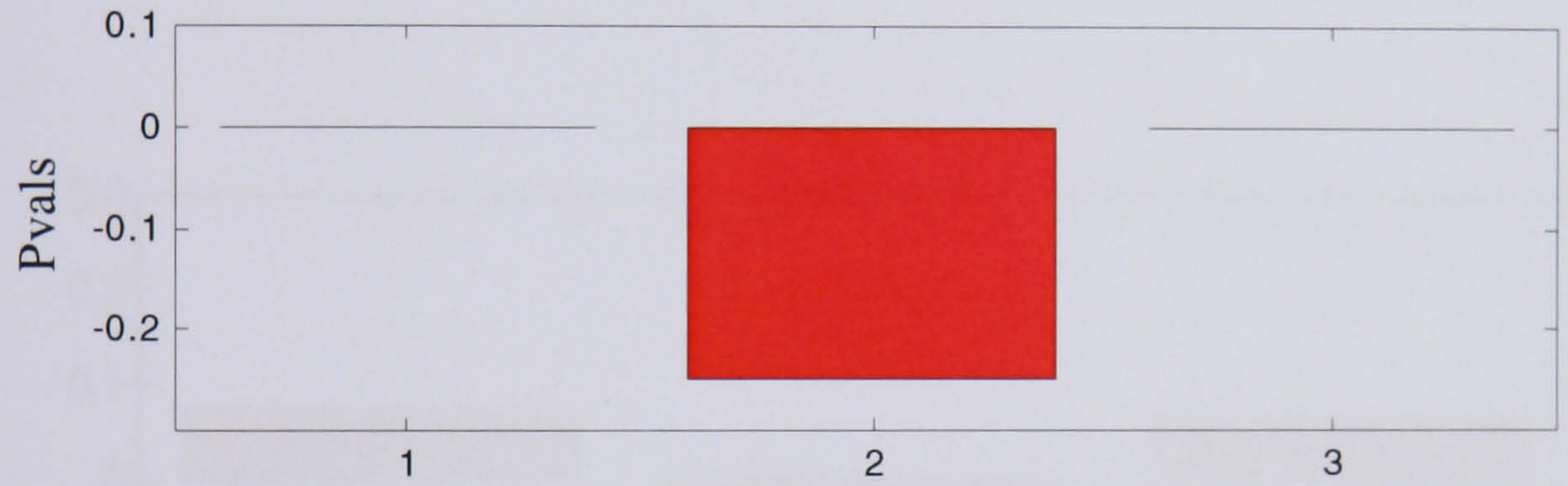

Figure 5.6.1-6: Plot of pvalues vs element number of run 2

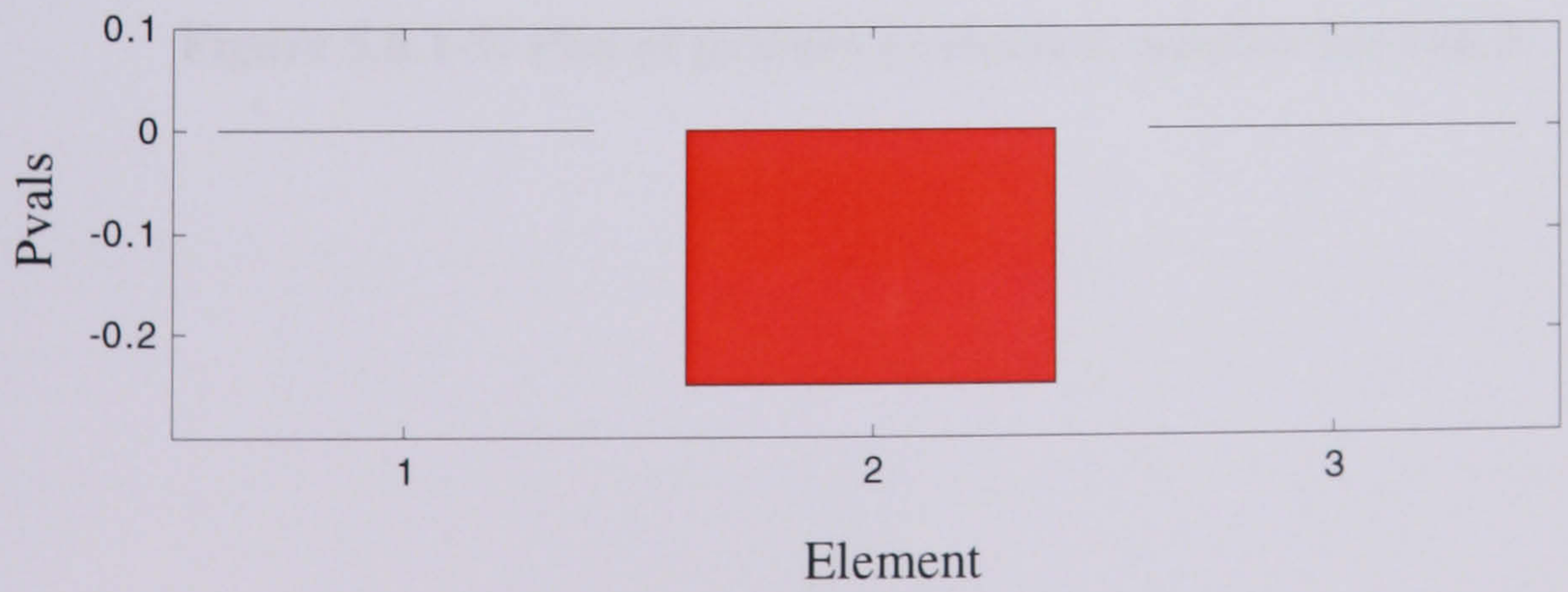

Figure 5.6.1-7: Plot of pvalues vs element number for run 3

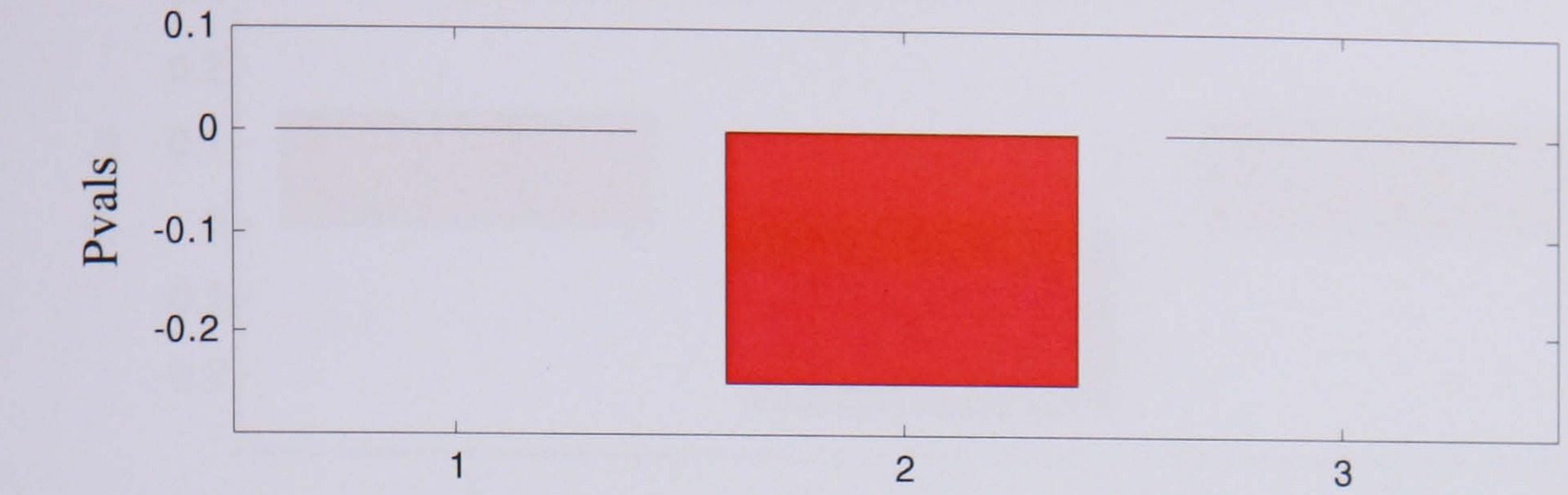

Figure 5.6.1-8: Plot of pvalues vs element number for run 4

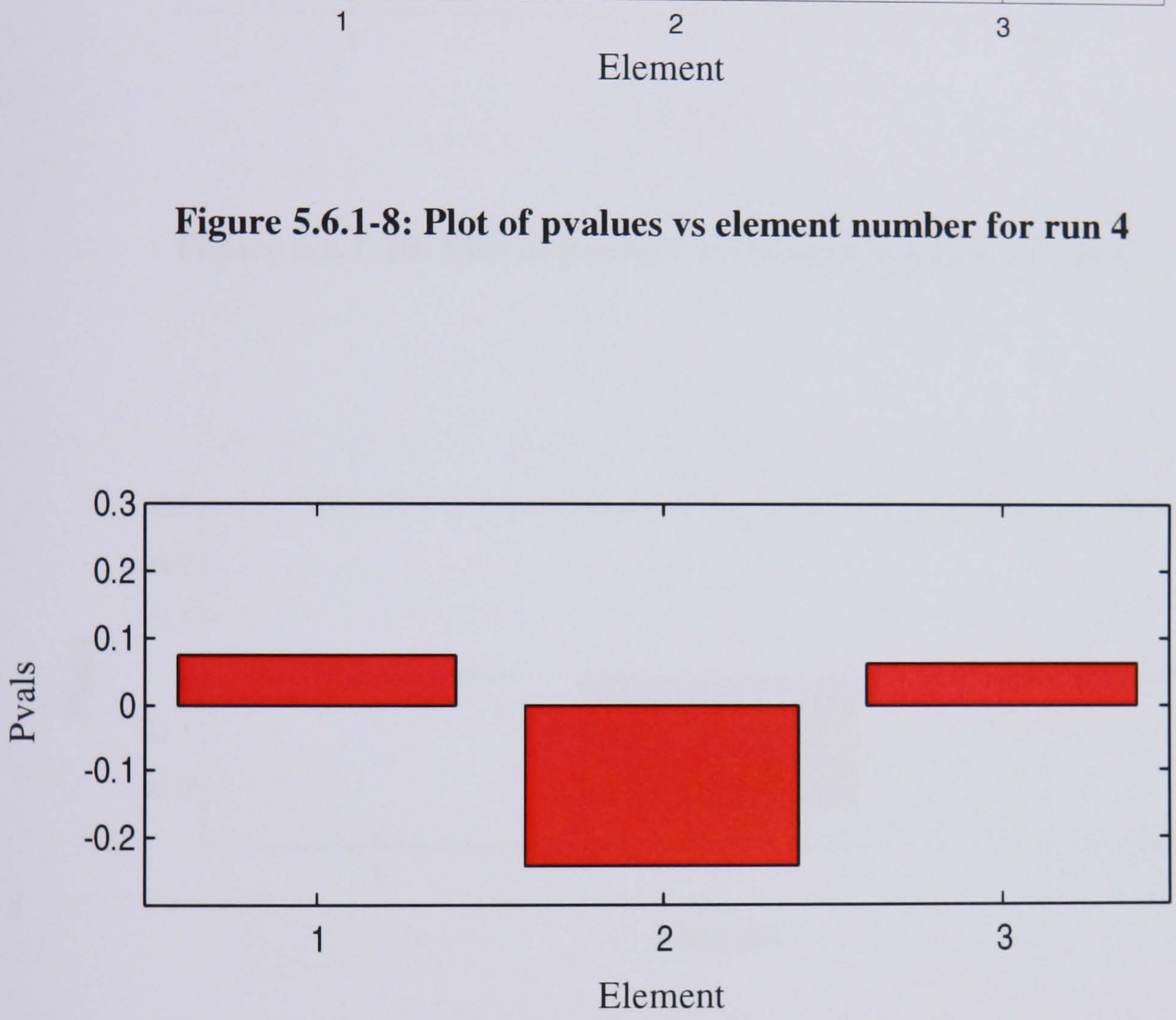

Figure 5.6.1-9: Plot of pvalues vs element number for run 5

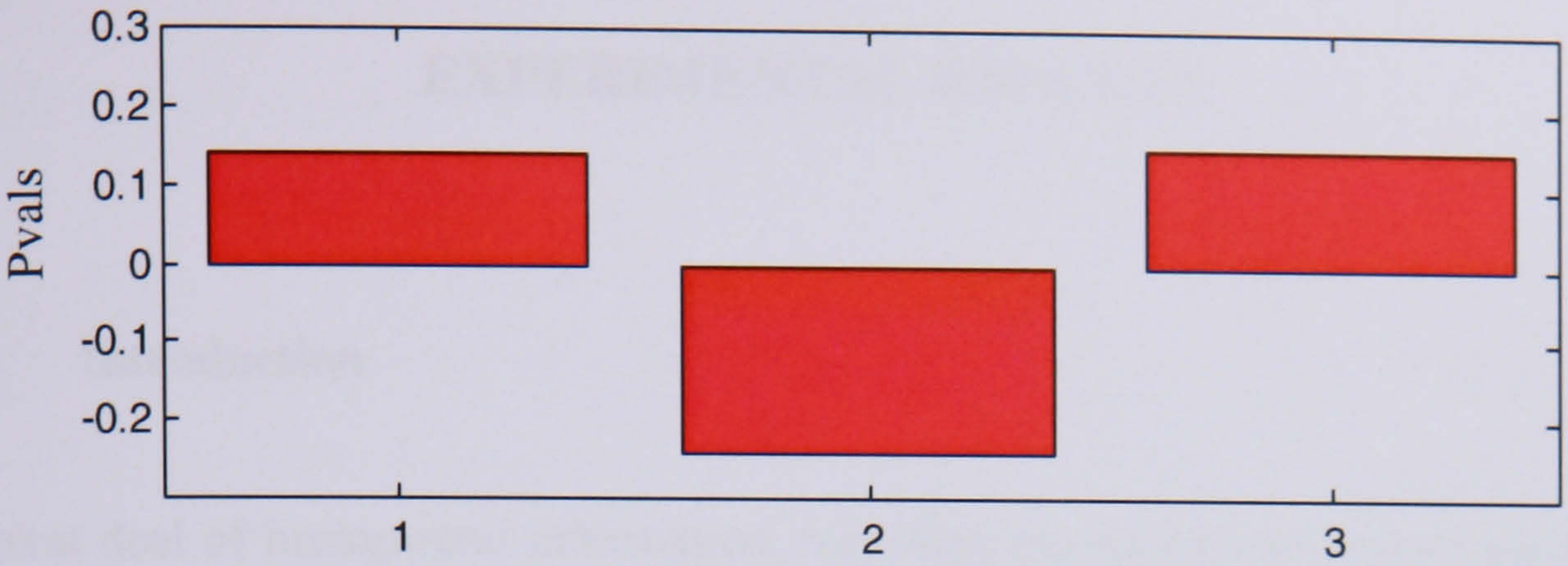

Figure 5.6.1-10: Plot of pvalues vs element number of run 6

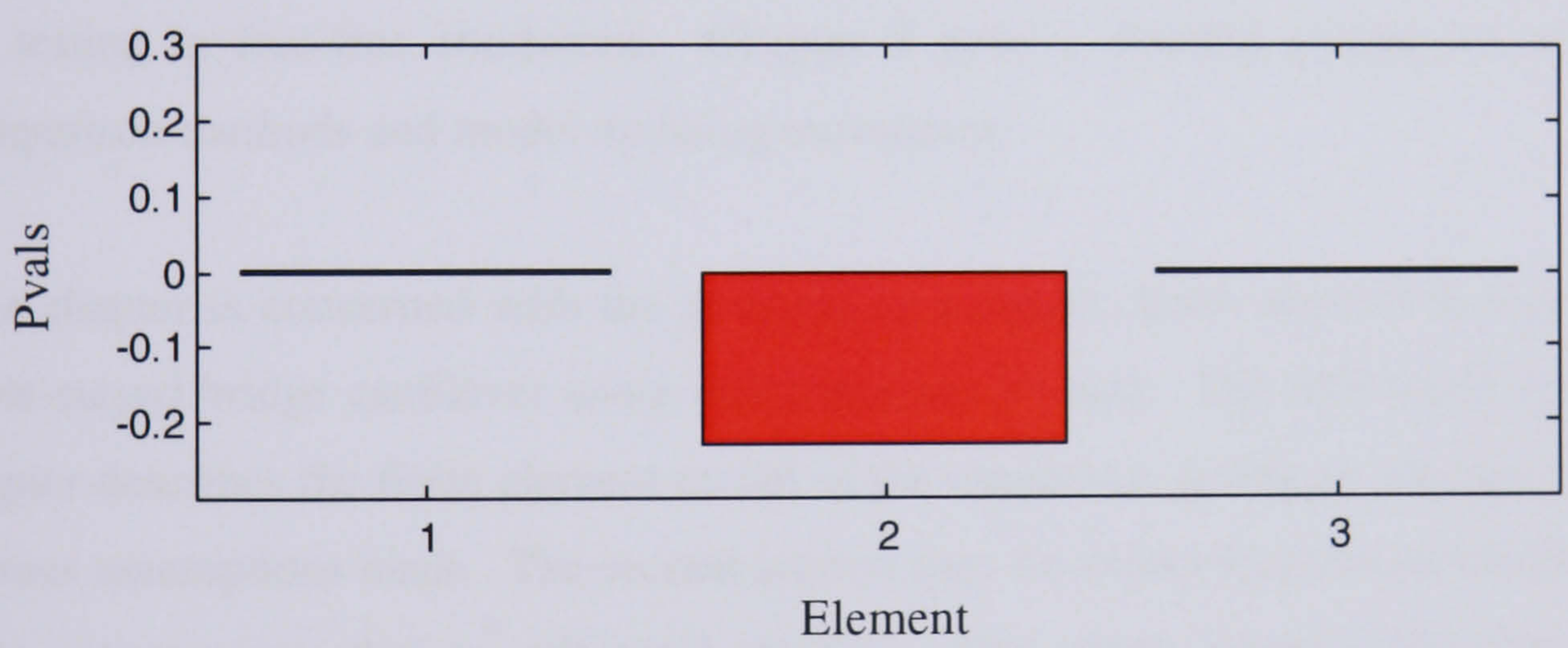

Figure 5.6.1-11: Plot of pvalues vs element number for run 7

CHAPTER 6

EXPERIMENTAL RESULTS

6.1 Introduction

A great deal of background information, regarding eigensolutions, sensor placement and model updating, has been presented in the previous chapters. Chapter 3 has dealt with the subject of nonlinearities, which are present in cable-stayed bridges, and gives an account of the effect of the application of an axial load in the natural frequencies and modeshapes of the loaded structure. Chapter 4 was concerned with pre-test planning, investigating the methods which can be used to place sensors on a structure, either to excite it or obtain the results, and mount the structure especially for testing in free-free conditions. Chapter 5 gave a detailed account on modal comparison methods and model updating techniques.

This chapter is concerned with the updating of a simple finite element model of a cable-stayed bridge cantilever using real experimental data. The first section of the chapter describes the finite element model of the cantilever, giving an account of the various assumptions made. The second section uses the sensor location techniques to place sensors on the experimental model. The third section describes the experimental model and testing procedure and provides MAC plots for the correlation of the experimental and analytical data, followed by a description of the model updating of the analytical model using the experimental results.

6.2 Finite element model of a cable-stayed bridge cantilever

The purpose of this exercise is to apply the sensor location methods and model updating techniques, used in the aerospace industry, to a civil structure and to identify any limitations that may exist. Civil structures and especially cable-stayed bridges are very complicated structures since they have to withstand a great variety of loading applied to them, such as wind, traffic, earthquakes. Model updating itself

is also a complicated task which requires the engineer to have control over the application of the techniques and which parameters to change. For these two reasons, it was decided to make a very simple finite element model of a cable-stayed bridge cantilever, and not a true replica, which will eliminate some of the complications in the application of the model updating methods.

It was decided to use the dynamic data from the Second Severn Crossing cable-stayed bridge, which connects England to Wales. Bristol University had undertaken the monitoring of the bridge during the construction process and dynamic information of one of the finished cantilevers was available. The first bending and torsion frequency of the real cantilever will be used to design the analytical model. In particular, the ratio of the first torsion frequency to the first bending frequency of the actual cantilever will be matched with the corresponding ratio of the analytical model. The reason for this is that both models will present similar dynamic behaviour. The torsion frequency should be separated sufficiently from the first bending frequency to prevent the structure from undergoing flutter, which may destroy it.

The real cable-stayed bridge cantilever consists of thirty sets of cable on either side of the portal frame pylons. It was decided that the analytical model would possess only three sets of cables, which will support the plate. The cables will be attached to a rigid frame, which will represent the pylons, and will be fixed at both ends. The plate will be pinned at the rigid frame end, to allow it to rotate but not permit any translational movements, corresponding to the way the true cantilever is built.

The next stage was to decide the dimensions of the various components of the model, such as the dimensions of the plate, the cable diameters, and the masses of the plate and cables, which should represent the real structure. It was decided to use the theory of scale factors to design the basic dimensions of the model. The real cantilever has a length of 228m, whereas, the model cantilever has a length of 2m, corresponding to a scale factor of $S_l = 1{:}114$. The plate was made of aluminium, corresponding to the steel deck of the cantilever, which gives a scale factor for the modulus of elasticity of the deck as $S_{Ed} = 70/210 = 0.33$.

The cables correspond to cables 10, 20 and 30 of the Second Severn Crossing cantilever, as given in the construction drawings. The dimensions of the real cables will be used to obtain the diameters of the model cables, which will be represented by piano wires. The reason for using piano wires is because they have similar yield strength as the real cables. Using the theory of scale factors, which gives a scale factor for the modulus of elasticity of the cables as $S_{Ec}=1$, the following areas are required for the cables:

$$A = A_{real} S_l^2 \frac{S_{Ed}}{S_{Ec}} \tag{6.1-1}$$

$$A_1 = 5400\times10^{-6}\times\frac{1}{114^2}\times\frac{0.33}{1} = 1.37\times10^{-7}\,mm^2$$

$$A_2 = 6750\times10^{-6}\times\frac{1}{114^2}\times\frac{0.33}{1} = 1.71\times10^{-7}\,mm^2$$

$$A_3 = 7950\times10^{-6}\times\frac{1}{114^2}\times\frac{0.33}{1} = 2.02\times10^{-7}\,mm^2$$

These areas correspond to the following diameters: 0.417mm, 0.467mm and 0.507mm. However, the piano wires used in the model corresponded to diameters of 0.405mm, 0.457mm and 0.508mm, which were available. The height of the attachment point of each cable to the rigid frame is also a scaled version of the real heights and corresponds to values of 0.74m, 0.65m and 0.52m.

Once the basic dimensions such as the length of the plate and the diameters of the cables and the height of the attachment points have been decided, the masses on the cables and plate and the thickness of the plate need to be modelled. However, this is not an easy task as just using the scale factors, since the model required in this work is not a true replica of the real cantilever but a simple homogeneous representation of it. Three finite element models were built. each corresponding to one of the real cables. The dimensions of the models were the true dimensions of the cables. The natural frequencies and the modeshapes for each one were obtained. The next stage

was to build three analytical models of the scaled cables, using the diameters extracted before. Their natural frequencies and modeshapes were obtained. The mass on the scaled cables was increased until their frequencies matched the corresponding scaled real frequencies. The scaling factor for the frequencies is given by $S_f = \frac{1}{\sqrt{S_L}}$. These masses were used to represent the point masses on the cables of the analytical model of the bridge cantilever. Table 6.2-1 gives the scaled natural frequencies of the finite element and the real models of the cables.

Cable	Scaled Freq of real cables Hz	Freq of scaled cables Hz
Short	8.201	8.177
	8.375	8.352
	16.087	16.275
	16.088	16.276
	23.360	24.174
Middle	4.773	4.738
	5.136	5.111
	9.361	9.426
	9.363	9.429
	13.595	13.998
Long	3.345	3.403
	3.893	3.901
	6.559	6.771
	6.562	6.775
	9.529	10.070

Table 6.2-1: Natural frequencies of model and real cables

The final stage of the modelling process was to decide the width and thickness of the plate and the discrete masses on it. Many trials had been carried out to find an

arrangement that would give the required ratio of the first torsion to the first bending frequency of the model. In the end it was decided to fix the dimensions of the plate and change the masses on it in order to obtain the correct frequency ratio. The width of the plate was decided to be 0.42m and the thickness of the plate 4mm. Discrete masses were placed on either side of the plate and their values varied until the frequency ratio matched the ratio of the real cantilever. Figure 6.2-1 shows the model arrangement and Figure 6.2-2 shows the mass arrangement on the plate. As one can see, at the front corners of the plate, two large masses are required. That is probably because at the time of monitoring construction machinery was present at these points, thus increasing the mass requirements.

The modelling of the cantilever was carried out using the commercial finite element program ANSYS. The plate as modelled using 240 SHELL elements, each having four nodes and six degrees-of-freedom at each node. The properties of the plate elements were that of aluminium except the outside elements along the length of the plate that had different density that represented the applied masses. The cables were modelled using LINK10 elements that are tension and/or compression only. A full representation of the model with all the element numbers shown is not included here since the large number of elements would render the figure incomprehensible. The density of the cables represented the applied masses on them. Table 6.2-2 gives the section properties of the cables and Table 6.2-3 the properties of the plate.

Cable	**Area** m^2	**Length** m	**Density** kg/m^3
Small	$1.29x10^{-7}$	0.832	2015000
Middle	$1.64x10^{-7}$	1.453	2060000
Long	$2.03x10^{-7}$	2.080	2000000

Table 6.2-2: Section properties of the cables

In Chapter 3, a detailed account of the two important properties that characterise cable-stayed bridges, namely Stress stiffening and Large deformations, was given. As mentioned at the same chapter, the engineer should take into account those

Dimension, m	2.0 x 0.42 x 0.004
Density 1, kg/m^3	2700
Density 2, kg/m^3	13000
Density 3, kg/m^3	9725
Density 4, kg/m^3	13000
Density 5, kg/m^3	100100

Table 6.2-3: Properties of the plate

properties when preparing an analytical model of a cable-stayed bridge, in order to obtain the correct stiffness matrix of the system. However, Stress stiffening and Large deformations are not applied by default by any finite element program and the engineer should ensure that these properties are selected before a modal analysis of the structure is undertaken. Therefore, these properties need to be selected for the cable-stayed bridge cantilever before the modal analysis is carried out. In Ansys, a non-linear static analysis is carried out before the modal analysis, in order to obtain the mass and stiffness matrices of the system, and the option of large deflections is selected. This option enables both large deformations and stress stiffening effects to be taken into account. During the static analysis, the load applied is broken into a series of load increments, which are applied over several load steps. At the end of each incremental solution, the programme adjusts the stiffness matrix to reflect the non-linear changes in the stiffness before proceeding to the next step. With this option, the user is able to define the number of load steps and the convergence criteria that will be used in each load step. After the static analysis, a modal analysis is carried out using the derived mass and stiffness matrices in order to obtain the natural frequencies and modeshapes of the model. The method of modal analysis used is the Subspace iteration and 100 modes were obtained. The natural frequencies of the model cantilever are given below in Table 6.2-4.

The real ratio of first torsion to first bending frequency of the Second Severn Crossing cantilever is 1.62, whereas, the corresponding ratio of the analytical model

is 1.66. This ratio thought to be quite satisfactory and the final model configuration, which gave this ratio, was adopted.

Mode	Frequency, Hz
B1	4.756
B2	7.309
T1	7.909
B3	10.394
B4	14.922
T2	15.152
T3	20.801
B5	27.503
T4	28.373
T5	39.615
B6	40.333
T6	55.026

Table 6.2-4: Natural frequencies of analytical cantilever

6.3 Sensor placement

Once the analytical model is prepared and the eigen solution is obtained, the engineer can start to prepare the test model in the laboratory. The most important step in this stage is to follow the pre-test planning procedure described in Chapter 4. The methods described in the aforementioned chapter, regarding the placement of sensors on the structure, are used in this section to provide information on where the excitation source can be positioned, how many sensors can be used to extract the information and where they can be placed on the structure. Of course, at this stage the engineer should take into account the fact that only a limited number of transducers can be used when testing the structure.

6.3.1 Mounting of the test structure

As already mentioned in section 6.2, the structure is a cantilevered plate, supported at a third and two thirds of its length and at the two free ends by the three sets of cables. At the end close to the rigid frame, the plate is pinned, allowing it to rotate but not to translate in any direction. The cables are fixed at both ends. The arrangement can be seen in Figure 6.2-1.

6.3.2 Excitation Locations

The analytical natural frequencies and modeshapes of the bridge cantilever are used to calculate the average displacement, velocity and acceleration parameters that were described in Chapter 4. As mentioned in the same chapter, these parameters can be used to find the best positions to support a structure, to excite it using a hammer or a shaker, respectively. The contour plots for the three parameters can be seen in Figures 6.3.2-1 to 6.3.2-3. All three diagrams indicate that the two corners at the free edge of the plate have higher average response levels that anywhere else, whereas, the middle area of the plate has low levels. There is also a difference in the area of low parameter values between the three plots. As one can see from the figures, the displacement plot has the smallest area of low values, whereas, the acceleration plot has the greatest. The average displacement parameter is used to find positions to support a structure, which in this case, are dictated by the way the bridge cantilever is usually constructed. Therefore, this parameter is not used in this exercise. The average velocity plot can be used to find the regions where the possibility of double-hit effects - when the structure is excited by a hammer - is high and should be avoided. The acceleration plot can be used to find the best possible location to place a shaker to excite the structure. The plot indicates this position by a high average value.

In this exercise it was decided to use a hammer to excite the structure. Therefore, the plot of the average velocity parameter is used to indicate the best positions to hit the structure. As already mentioned, the positions of high average response should be avoided in order to prevent any double-hit effects. For this reason, the two free

corners of the plate should be avoided since the response at those positions is the greatest. The best positions are indicated to be in the two outer thirds of the plate. along the centre-line of its length.

6.3.3 Sensor placement

The next stage, in the pre-test planning procedure, is to find the best possible locations to place the accelerometers. The three methods described in Chapter 4, the Effective Independence Method (EfI), the Energy Optimisation Technique (EOT) and the Energy Matrix Rank Optimisation (EMRO) are used, together with 12 calculated modeshapes, to find the transducer locations. Since it is not possible to measure rotational degrees-of-freedom conveniently, the analytical model is reduced to the three translational degrees-of-freedom. Also, it was decided to place accelerometers onto the plate only, so the model was reduced further to the plate degrees-of-freedom. The full mass and stiffness matrices had to be reduced also to the corresponding coordinates.

Each method was used in turn and a final set of sensor locations was derived. However, the Energy Matrix Optimisation Technique could not be used since the stiffness matrix of the model was positive definite. The reason for this is because there are some very stiff elements, the plate elements, and some very flexible elements, the cable elements, which comprise the stiffness matrix of the system resulting in zero values at the diagonal. The results from the other two methods are presented herein. Figure 6.3.3-1 shows the sensor locations given by the Effective Independence Method, whereas Figure 6.3.3-2 shows the sensor arrangement obtained by the Energy Optimisation Technique. The first method requires 24 sensors to be placed on the structure, whereas, the second method requires 19 sensors.

Once the sensor arrangements are obtained, the Modal Assurance Criterion or MAC should be used to check the independence of the modes. The MAC was described in Chapter 5 and is a way of checking the correlation of the modes. The full eigenvectors of the bridge model, twelve in number, are reduced to the sensor

locations given by the two methods using Guyan reduction. The reduced modes are correlated with themselves using the MAC in order to check their independence. This check is undertaken in order to ensure that the dynamic data obtained from the limited sensor locations can actually be of good quality so as to identify each mode clearly. Figure 6.3.3-3 shows the MAC plot using the sensor set from the Effective Independence method, whereas, Figure 6.3.3-4 shows the MAC plot obtained from the Energy Optimisation Technique. Observing the first figure, one can see that the MAC values of the diagonal are 1, which is what one should expect since each mode corresponds perfectly with itself. There are some off diagonal terms, which are of quite low value, indicating that this sensor arrangement can identify the modes quite well. Observing the second figure, one can see that again the MAC values of the diagonal are 1 and that there are some off-diagonal terms, more than in the previous figure, but of low value. This method can also identify the modes. In order to distinguish between them and draw a conclusion about which method gives the best results, one should take into account the number of sensors needed to identify the modes in each case. The EfI method requires more sensors than the EOT method, which makes the latter a better method to use. However, in the experimental testing, both methods will be used to extract the experimental modes, and a further conclusion can be drawn then as to which method actually gives the best results.

6.4 Experimental Testing

Once the pre-test planning has been completed, the experimental testing can be carried out. The first stage is to build the model in the laboratory. The aluminium plate was ordered together with the piano wires. The plate was measured in order to check that the dimensions are the correct ones. The piano wires have the diameters already mentioned the section 6.2. The masses on the cables and plate were made of lead, which has a greater density than steel or aluminium, thus reducing the cross-section area of the mass components. Cylindrical masses of the right weight were prepared for the cables, through which the piano wires were threaded, and the masses were placed in their pre-determined positions easily using tape. The masses on the plate were of small rectangular sections that corresponded to the required mass. At the two free corners of the plate larger masses were positioned. All masses were positioned in place using double-sided tape so it was easy to mount them and change

their position if required. Figures 6.4-1 to 6.4-4 show the experimental model in the laboratory.

Two supports were prepared for the plate in order to be mounted, under pinned boundary conditions, on the rigid frame. The supports allowed the plate to rotate at these two positions but restricted it from moving longitudinally or sideways. The cables were attached to the plate through holes drilled in the sides of the plate and held in place by screws. The cables were attached to the rigid frame in the same way as to the plate. In order to check that the tension in the wires is correct, an acoustic vibrometer was used to measure the frequency of vibration of each wire. The vibrometer was placed very close to the wire, which was plucked and left to vibrate. With the help of a spectrum analyser, the fundamental frequency of vibration of the wire was recorded and compared with the corresponding frequency obtained from the analyses. If the frequencies were close enough, the cables were tightened in place. Figure 6.4.5 shows the vibrometer in place and Table 6.4-1 shows the frequencies of the cables as given by the real and the analytical model and the vibrometer.

Once the model is in place, the engineer needs to position the accelerometers in place. However, as mentioned in the previous section, this exercise requires 19 and 24 accelerometers in order to obtain the dynamic data of the model. For economic reasons, it is impossible to have so many accelerometers available. Therefore, a way to overcome this problem was devised. Since one hammer and one accelerometer were available, it was thought a good idea to reverse the roles of the two transducers.

Cable	**True freq, Hz**	**Analytical freq, Hz**	**Experimental freq, Hz**
Short	8.20	8.70	8.90
Middle	5.11	5.10	5.00
Middle	9.43	10.00	9.80
Long	3.40	3.60	3.50
Long	6.80	7.10	7.30

Table 6.4-1: Frequencies of the cables

The accelerometer would be positioned at a fixed location and the hammer would move around the plate at the positions dictated by the two sensor location techniques. These positions were marked clearly on the plate. The accelerometer would be placed at the position, which is indicated by high average velocity response, shown in Figure 6.3.2-2 as the two free corners of the plate enclosed in a circle. The accelerometer was fixed at the left hand front corner of the plate using wax.

As one can see from Figures 6.3.3-1 and 6.3.3-2, the Effective Independence method places sensors mainly at the edges of the plate, whereas, the Energy Optimisation technique places sensors more at the inside of the plate. In Chapter 4, it was mentioned that in order to avoid double-hit effects, when using a hammer as the excitation source, the hammer should hit positions on the structure where the ADDOFV parameter has low values. By observing Figures 6.3.2-2. 6.3.3-1 and 6.3.3-2, one can see that the Energy Optimisation technique places sensors at locations where the ADDFOV parameter has lower values, whereas, the Effective Independence method places the transducers at locations of higher ADDOFV values. Since the hammer will hit the structure at the sensor locations, it is evident that the Energy Optimisation technique may yield better results than the Effective Independence method. This observation will be shown later in this chapter.

The data were then acquired using a spectrum analyser and a personal computer with ICATS modal analysis software loaded on it in order to process and save the dynamic data. Figure 6.4-6 shows the arrangement. The spectrum analyser receives signals from both the accelerometer, as amplitude response, and hammer. as force response, and by dividing the force with the amplitude it creates Frequency Response Functions, FRFs. These are represented by plots of response amplitude versus frequency and are used to find the natural frequencies of the system. Large peaks of response represent the natural modes of the model. However, when many Frequency Response Functions are available, ICATS possess the option for multiple-curve fitting. where all FRFs can be used simultaneously to obtain the natural modes of the system.

It is worth mentioning at this point the subject of variability. which was included in the literature review. section 1.2.5. Variability in the results can be attributed to

temperature changes that cause parts of a model to expand or contract, structural changes due to ageing or loading conditions. Variability can also be caused by the effect of the extra mass of a transducer or change in stiffness due to the presence of a shaker. Usually, the means to test the effects of variability is to extract results in different periods of time and compare them. However, in this work its effects on the test results was not taken into account, mainly because the structure was tested in a very short period of time, thus not allowing it to change structurally under the application of its weight. Moreover, only an accelerometer was used, positioned at one corner of the model, the mass of which was thought not to affect significantly the total mass of the system.

Once the two sets of results were extracted and processed using the program ICATS, the natural frequencies were compared with the analytical ones and the results are given in Table 6.4-1. Figures 6.4-7 and 6.4-8 show a graphical comparison of the frequencies. The Energy Optimisation Technique gives a closer frequency correlation than the Effective Independence method, which was expected since the method placed sensors at positions of lower ADDOFV values and the hammer excited the structure at those positions, thus reducing any double-hit effects. This observation emphasises the fact, also observed in Chapter 5, section 5.3.1, that the quality of modal identification depends on the set of sensor locations used in the experiment. Moreover, it is noticeable that the two methods failed to identify all the modes and this could be attributed to the post-processing method used to extract these results from the raw data obtained. Some of the positions may have been at node locations and, therefore, the curve fitting method used to process the data failed to identify some modes.

Furthermore, the experimental modeshapes were expanded to the analytical degrees-of-freedom and compared with the analytical ones using the Modal Assurance Criterion (MAC). Figures 6.4-9 and 6.4-10 show the MAC plots for the Effective Independence Method and Energy Optimisation Technique, respectively. As one can observe from the first plot, there is a very good correlation (MAC>0.8) for the correlated modepairs 3, 6 and 8, whereas, the other modepairs do not match very closely. Also there is some degree of cross-correlation between the modes, indicated by the off-diagonal MAC values, which should have been very low. The second

MAC plot for the Energy Optimisation Technique shows that there is a high degree of correlation between four modepairs, 4, 5, 7 and 8 and there is a smaller level of correlation between modepairs 1 and 3 and even less for 2 and 6.

Mode	Analytical freq Hz	Exp freq – EOT Hz	Exp freq – EFI Hz
B1	4.756	4.854	3.189
B2	7.309	7.533	8.034
T1	7.909	8.090	-
B3	10.394	10.753	10.791
B4	14.922	15.267	15.096
T2	15.152	15.643	-
T3	20.801	-	21.054
B5	27.503	29.125	27.936
T4	28.373	-	29.178
B6	40.330	41.317	41.355

Table 6.4-1: Analytical and Experimental frequency comparison

It is evident from the above that the sensors seem to pick up better the bending modes of the plate and not being so successful in identifying the torsion modes apart from mode T4 identified by the Effective Independence method. Although twelve analytical modes were used to obtain the sensor arrangements, only eight modes were identified by each method and not all modeshapes were clearly correlated. This can be attributed to many factors such as poor modal testing technique, noise in the measurements or poor processing of the dynamic data. On the other hand, it is very difficult to control the response of such a flexible structure, even in the laboratory, and certainly difficult to test it under very controlled conditions. In any case it is a simplified model, used to demonstrate the application of model updating techniques.

6.5 Model Updating

Chapter 5 gave a detailed account of the various methods used for updating. such as modal sensitivity methods and FRF updating. The method of updating chosen for this work is the eigenvalues sensitivity method, which tries to match the natural frequencies of the experimental and analytical models.

Once, the experimental testing is concluded and the correlated modepairs are obtained, the engineer needs to select the best-correlated modes in order to use them in the updating exercise. Model updating requires experimental modes that compared best with the corresponding analytical ones. Therefore. modepairs that possess a MAC value of greater than 0.8 are considered to be sufficiently correlated. and are chosen for this updating exercise. Since only a few modes compare so well with each other, the best correlated modepairs from both sensor location methods and their frequencies are used to form the set of eigenvectors and eigenvalues, which will be used for the updating. Four modes were selected from the Energy Optimisation Technique, named B3, B4, B5 and B6, and one mode from the Effective Independence method, named T4. These five modes and their correlation with the experimental ones are shown in Figure 6.5-1.

6.5.1 Selection of updating parameters

A strenuous exercise was carried out in order to find the most important elements for updating, which must be less than the experimental data available consisting of five modes only. It was decided that the stiffness and mass update would be carried out separately since different elements may be important for each type. All elements were selected, both plate and cable, and a method was devised in order to select the most suitable elements for both types of update. This method was repeated twice. once for selecting elements for stiffness update and once for mass update. What follows is a description of the steps taken to select the elements, which were carried out with the commercial program MATLAB. The number of updating runs undertaken was a total of 120 with 440 updating iterations carried out.

For stiffness update

Since the strain energy of an element is directly proportional to its stiffness.

$$SE = \frac{1}{2}\{\phi\}_j^T [K]\{\phi\}_j \qquad (6.5.1\text{-}1)$$

elements that possess high strain energy for each of the experimental modes are selected. Figure 6.5.1-1 shows the strain energy distribution for each mode. Elements of high strain energy are the ones shown in red colour. Using the modal sensitivity updating routine, which was described in Chapter 5, section 5.5.1. written by the author of this thesis in MATLAB, each element is updated for each available mode, checking whether this element changes the frequency of that particular mode and ensuring that all the other modes converge to their constant values. The elements that provide the above requirements are selected. The number of elements that satisfied the above criteria was larger than the number of available modes, five. Therefore, the elements that resulted in the greatest changes in the required frequencies were the ones selected. Table 6.5.1-1 shows some of the elements together with their initial experimental and the updated frequencies as obtained after a few iterations. As one can observe from the above, the cable elements are the most influential and this is expected since the stiffness of the structure is dominated by the cable system. Table 6.5.1-2 shows some of the most important elements that can be used for updating and how they influence the updating of the five experimental frequencies. As one can see from this table, elements 248 and 256 are the ones producing the more pronounced changes in the frequencies and these elements are selected for the stiffness updating exercise.

For Mass update

The procedure for selecting the most important elements for mass updating is very similar to the one described previously. However, in this case we select the elements that possess the greatest kinetic energy, since the kinetic energy of an element is directly proportional to its mass:

$$KE = \frac{1}{2}\{\phi\}_j^T [M]\{\phi\}_j \qquad (6.5.1\text{-}2)$$

Figure 6.5-3 shows the kinetic energy distribution for each required mode.

By trying to update each frequency separately, a large number of elements were selected.

Mode	Element	Experimental frequency, λ^2	Updated frequency, λ^2
1	261	4564	4261
1	264	4564	4281
2	277	9202	8794
2	279	9202	8787
2	281	9202	8771
2	285	9202	8756
3	241	30811	30005
3	248	30811	29962
3	253	30811	29995
3	256	30811	30054
3	258	30811	29970
4	242	33610	31147
4	248	33610	31288
4	251	33610	31233
4	254	33610	31702
4	256	33610	30986
5	241	67395	65944
5	247	67395	66203
5	248	67395	69495
5	253	67395	65943

Table 6.5.1-1: Elements for stiffness update together with initial and updated experimental frequencies

		Element No					
		241	246	247	248	251	252
Experimental frequency, λ^2	**Initial analytical frequency, λ^2**	**Updated frequency, λ^2**					
4565	4265	4266	4266	4265	4267	4266	4266
9202	8790	8790	8790	8790	8790	8790	8790
30811	29968	29970	29976	29968	29976	29975	29970
33611	31163	31181	31177	31163	31185	31177	31166
67395	65944	65944	65943	65941	65944	65942	65942

		Element No					
		253	254	255	256	264	277
Experimental frequency, λ^2	**Initial analytical frequency, λ^2**	**Updated frequency, λ^2**					
4565	4265	4267	4263	4265	4273	4266	4266
9202	8790	8790	8790	8790	8795	8790	8792
30811	29968	29972	29939	29968	30013	29968	29968
33611	31163	31172	31128	31163	31336	31163	31163
67395	65944	65943	65935	65941	65961	65942	65941

Table 6.5.1-2: Table showing elements that influence the updating frequencies

The elements that influence most the updated frequencies were the ones selected for the final updating exercise.

It was found that the plate elements influence more the mass of the system and this is reasonable since the plate has greater kinetic energy than the cables. Table 6.5.1-3 shows elements and how they influence the updating of each of the five frequencies

Mode	Element	Experimental frequency, λ^2	Updated Frequency, λ^2
1	39	4564	4266
1	40	4564	4268
2	239	9202	8792
2	240	9202	8793
3	39	30811	29969
3	40	30811	29999
3	240	30811	29971
4	19	33610	31179
4	40	33610	31184
4	240	33610	31165
4	239	33610	31164
5	39	67395	65951
5	40	67395	66022
5	239	67395	65958
5	240	67395	65949

Table 6.5.1-3: Elements for mass update showing the initial and the updated experimental frequencies

		Element No						
		19	20	21	39	40	239	240
Experimental frequency, λ^2	Initial analytical frequency, λ^2	Updated frequency, λ^2						
4565	4265	4280	4267	4267	4266	4289	4266	4286
9202	8790	8814	8828	8841	8793	8885	8795	8843
30811	29968	30007	29967	29976	29969	29999	29969	30174
33611	31163	31197	31164	31166	31164	31198	31164	31165
67395	65944	66891	66203	66329	65951	66922	65958	66475

Table 6.5.1-4: Elements used to update all five frequencies

separately. Table 6.5.1-4 shows some selected elements that most influence the updating of all the five experimental frequencies. As one can observe from this table, elements 40 and 240, which are the two front corner elements with the two greatest masses attached to them, are the most important for mass update and they are chosen for this exercise.

As one can observe from the above conclusions, only two elements were selected for the stiffness or mass update, which are less than the number of available experimental modes. This is a requirement in model updating, since a number of updating parameters greater than the number of available modes will lead to an underdetermined problem.

Once the elements are selected, the updating exercise can be undertaken. The updating routines, based on the eigen-sensitivity updating methods described in Chapter 5, were written by the author of this thesis and carried out in MATLAB, using the Standard Dynamic Toolbox. Since the analytical model was built in ANSYS, a special routine was written in MATLAB and used to extract the elemental mass and stiffness matrices from one of ANSYS output files, with the extension "emat", in order to be in the desired format and used in the updating exercise.

6.5.2 Stiffness Update

Firstly, the stiffness matrix update was carried out using elements 248 and 256 as already mentioned previously. The position of the two elements on the structure is shown in Figure 6.5.2-1. The updating of the stiffness matrix proved to be quite a strenuous exercise, since over thirty-five iterations were required in order for the updated experimental frequencies to reach convergence. Convergence was assumed to have occurred when the largest change in the stiffness matrix was below 1% of the original value.

Table 6.5.2-1 shows the original analytical and the updated analytical frequencies as obtained at the end of the updating process. The experimental frequencies are also shown. It can be seen from this table that the values of the updated frequencies are very close, almost similar, to the corresponding experimental values, which suggests

that the updating exercise was carried out successfully, despite the limited data available.

Figure 6.5.2-2 shows the comparison between the initial and updated analytical and the experimental frequencies. As one can see, there is a very close match between the updated analytical and the experimental frequencies, which is indicated by the fact that that the points lie on a line drawn at 45 degrees to the x axis. The frequencies seem to be perfectly correlated and one can assume that the updating exercise was very successful.

Figure 6.5.2-3 shows a plot of the residual versus the iteration number. The residual is given by the following formula:

$$R = \left\| \{\lambda\}_{FEk} - \{\lambda\}_{Exp} \right\|_2 \qquad (6.5.2\text{-}1)$$

Mode	Experimental frequencies, Hz	Initial analytical frequencies, Hz	Updated analytical frequencies, Hz
1	10.753	10.394	10.525
2	15.267	14.922	15.258
3	29.125	27.503	28.010
4	29.178	28.373	29.245
5	41.318	40.330	41.646

Table 6.5.2-1: Updated analytical frequencies obtained from stiffness update

where, $\{\lambda\}_{FEk}$ are the five analytical eigenvalues at the k^{th} updating iteration. As a reminder, the eigenvalues are related to the resonant frequencies by the following expression:

$$\lambda_j = (2\pi f_j)^2 \qquad (6.5.2\text{-}2)$$

The residual plot, Figure 6.5.2-3, shows that at each updating iteration the corrected analytical model becomes a closer match of the experimental model, since the updated frequencies converge to the experimental values.

The convergence of the two updating parameters, the stiffness of the cable elements 248 and 256, against the number of iterations can be seen in Figure 6.5.2-4. As already described previously those elements were chosen because they possessed the highest strain energy for the number of modes used in the updating, since the strain energy of an element is directly proportional to its stiffness.

The converged values of the updating parameters should be multiplied by the corresponding elemental stiffnesses and added to the total stiffness matrix in order to obtain the updated stiffness matrix of the system. This is expressed as follows:

$$[K]_u = [K] + \sum_{j=1}^{n_p} p_j [K]_{ej} \qquad (6.5.2\text{-}3)$$

where,

$[K]_u$ is the updated global stiffness matrix,

$[K]$ is the original global stiffness matrix,

$[K]_{ej}$ is the elemental stiffness matrix of element j,

p_j is the updating parameter for element j, and finally

n_p is the number of updating parameters.

The converged values of the two updating parameters indicate that the stiffness of element 248 should be increased by 4.80% since the pvalue is 0.048, whereas, the stiffness of element 256 should be increased by 68.5%, denoted by pvalue of 0.685. It should be noted here that a p-value of 1.0 indicates that the stiffness of that element should be increased by 100%, which is feasible. However, a p-value greater than 1.0 does not produce physically realisable results and it can be an indicator that there is a serious error in our initial assumptions. On the other hand, it can be considered acceptable since the application of such a value produces an analytical model whose dynamic behaviour matches closely the behaviour of the real structure.

It would be interested at this point to draw attention again to non-linearity and investigate its influence on the updating process. As already mentioned in this chapter, non-linear static and dynamic analyses were carried out in order to obtain the natural frequencies and modeshapes of the cantilever model. In order to investigate the influence of large deflections and stress stiffening in the updating of the analytical model, linear modal analysis was carried out and the new modes of the model was obtained. The frequencies are given below in Table 6.5.2-2.

Mode	Frequencies With non-linearities Hz	Frequencies Without non-linearities Hz
B1	4.756	3.125
B2	7.309	5.678
T1	7.909	6.037
B3	10.394	9.214
B4	14.922	12.845
T2	15.152	13.623
T3	20.801	19.442
B5	27.503	25.763
T4	28.373	27.215
B6	40.330	37.438

Table 6.5.2-2: Analytical frequencies of cantilever model with and without considering non-linearities

As one can observe from the above table, if the non-linearities are not considered in the analyses, the natural frequencies of the model are less than when they are taken into account. This agrees with the theoretical observations presented in Chapter 3, which was dedicated to the influence of an axial force on the dynamic behaviour of a structure. The next step was to carry out the eigenvalue model updating exercise for the linear model. The same elements were selected for the analysis (248 and 256)

and the exercise followed the same steps as before. The updating was continued for over thirty-five iterations and it was observed that the updating parameters could not converge to particular values but they followed a random route and each alternated between positive and negative values. This can be seen in Figure 6.5.2-5. which shows the plot of pvalues against the number of iterations. This can be attributed to the unstable nature of the linear model, which is the result of not considering the non-linearities that provide stiffness to the system. Therefore. the updating exercise is not successful in this case and it can be concluded that the stiffness update of the cantilever model can be carried out successfully only when stress stiffening and large deformations are considered in the analyses.

6.5.3 Mass Update

The next step was to carry out the mass updating exercise. The elements chosen for this exercise were the plate elements 40 and 240, shown in Figure 6.5.3-1, which were the two front corner elements that required two large masses to be applied to these points. As already mentioned, the reason for this requirement can be attributed to the fact that during the construction phase of the Second-Severn cantilever, the presence of machinery at these points is inevitable, which will increase the total mass of the system.

More than thirty-five iterations were required to update the two elemental masses and convergence was assumed when the changes in the mass matrices were below 1% of the original values. The updated analytical frequencies together with the original analytical and the extracted experimental frequencies are shown in Table 6.5.3-2. As one can observe from the above table, there is a close match between the experimental and the updated analytical frequencies, which can also be seen in Figure 6.5.3-2. This figure shows a plot of the initial analytical against the experimental frequencies and a plot of the updated analytical against experimental frequencies. The points corresponding to the updated data lie on the straight line drawn with a slope of 1. indicating that there is a perfect correlation between the data compared.

Figure 6.5.3-3 shows the plot of the residual function against the number of iterations. This plot indicates the extent to which the updated analytical data matches the experimental data.

Figure 6.5.3-4 shows the convergence plot of the two updating parameters, the mass matrices of the plate elements 40 and 240. Those elements were chosen because they possessed the greatest kinetic energy for the selected modes, since the kinetic energy of the elements are directly proportional to their mass matrix.

The converged values of the updating parameters should be multiplied by the corresponding elemental mass matrices and added to the global mass matrix of the system. The resulting matrix can be considered to be the corrected mass matrix of the system. This process can be described by the following formula:

$$[M]_u = [M] + \sum_{j=1}^{n_p} p_j [M]_{ej} \qquad (6.5.3\text{-}1)$$

where,

$[M]_u$ is the updated global mass matrix,

$[M]$ is the initial global mass matrix

$[M]_{ej}$ is the elemental mass matrix of element j,

p_j is the updating parameter corresponding to element j, and finally

n_p is the number of updating parameters.

The converged values of the two updating parameters indicate that the mass matrix of element 40 should be increased by 81%. indicated by the pvalue of 0.81, whereas. the mass matrix of element 240 should be decreased by 33% indicated by the pvalue of –0.33. As already noted before, p-values of greater than 1.0 are not physically realisable and indicate that there is an error in our initial assumptions. However, they can be acceptable since the dynamic properties of the updated analytical model match closely the corresponding ones of the real structure.

The following table, Table 6.5.3-2. contains the experimental, initial analytical and the updated frequencies obtained from both runs. The table includes the frequencies

that were not used in the updating of the model and are presented here to observe whether they are a closer match to the experimental. As one can observe from the above table, the updated analytical frequencies seem to increase and become a closer match to the experimental data.

Mode	Experimental frequencies, Hz	Initial analytical frequencies, Hz	Updated analytical frequencies, Hz
1	10.753	10.394	10.532
2	15.267	14.922	15.520
3	29.125	27.503	27.878
4	29.178	28.373	28.884
5	41.318	40.330	41.900

Table 6.5.3-1: Updated analytical frequencies obtained from mass update

Mode	Analytical freq Hz	Stiffness Update Hz	Mass Update Hz	Exp freq – EOT Hz	Exp freq – EFI Hz
B1	4.756	5.182	5.182	4.854	3.189
B2	7.309	7.460	7.460	7.533	8.034
T1	7.909	8.889	8.840	8.090	-
B3	10.394	10.525	10.532	10.753	10.791
B4	14.922	15.258	15.520	15.267	15.096
T2	15.152	15.280	16.040	15.643	-
T3	20.801	20.977	20.977	-	21.054
B5	27.503	28.010	27.878	29.125	27.936
T4	28.373	29.245	28.884	-	29.178
B6	40.330	41.646	41.900	41.317	41.355

Table 6.5.3-2: Table of updated frequencies including those not used in the updates

6.6 Conclusions

A very simple finite element model of one of the Second Severn Crossing cantilevers was prepared with the commercial program ANSYS. The model consisted of only an aluminium plate representing the deck of the real cantilever and three sets of cables representing some of the cables of the structure. The model was not intended to be a true replica of the real structure but only to possess the dynamic characteristics of it. Therefore, scaling factors were used and various assumptions were made in order to prepare a model, which gives the same torsion over first bending frequency ratio as the real cantilever. This ratio is an indication of the resistance of the structure to flutter, since the higher the ratio the greater the torsion frequency of the structure is and the further away from its first bending frequency.
Once the analytical model was prepared, pre-test planning techniques were followed to obtain the best possible sensor locations for the experimental testing of the model. The experimental model was prepared in the laboratory and the testing took place to obtain the experimental data required to update the analytical model. Once the results are extracted, the experimental model is expanded to the analytical degrees-of-freedom, since as already explained in Chapter 4, the experimental data is incomplete. Then, the experimental modeshapes are compared with the analytical ones, using the Modal Assurance Criterion, (MAC), and the corresponding frequencies are compared, in order to obtain the correlated mode pairs that were used for the updating exercises. However, only a few modes correlated perfectly and therefore, a limited number of updating parameters could be used for the updating. Only five modes correlated and after a strenuous exercise, two cable elements were chosen for the stiffness update and two plate elements for mass update.

The updating exercises were carried out and the corrected analytical models were obtained. It is well-worth noted from the above updating exercise, that although the number of available experimental data was limited and the number of updating parameters had to be restricted to only a few, two in this case, the updating process was successful in both cases. This can be attributed to the fact that only higher order modes were used in the exercise, which seem to provide useful information in updating the elemental mass and stiffness matrices. This is in accordance with the findings of other researchers. However, the updating exercises proved to be quite

strenuous, since more than fourty-five iterations had to be undertaken in order to achieve convergence in both cases. The fact that convergence was achieved makes updating in such a narrow range of parameters acceptable, but the author feels that it could be advisable to have a wider range of parameters or use FRFs for updating.

Moreover, the effects of the inclusion of non-linearities in the updating process were investigated. The updating exercise for the stiffness matrix was repeated for a linear model and failed to correct the two updating parameters. This observation leads to the conclusion that the stiffness updating exercise was successful because stress stiffening and large deformations were included in the model analyses.

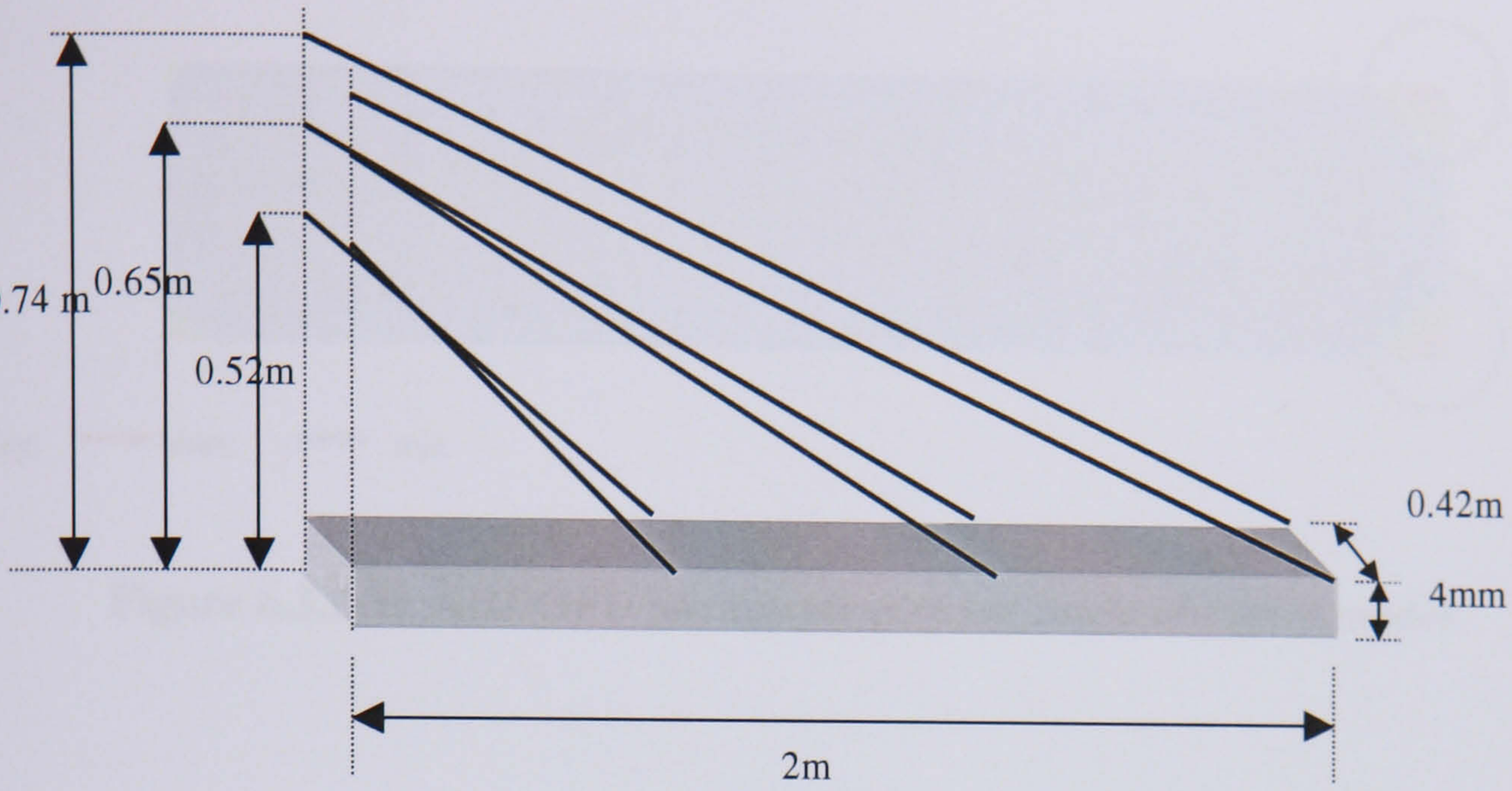

Figure 6.2-1: Representation of model bridge cantilever

Figure 6.2-2: Mass arrangement on the plate

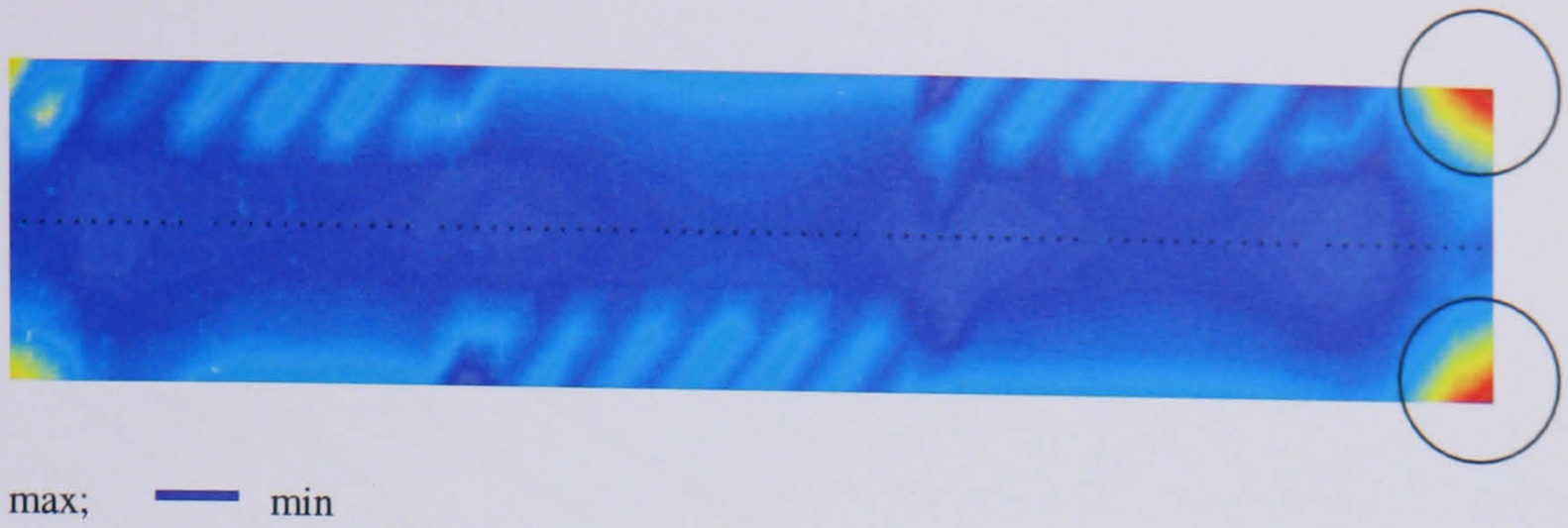

Key: max; min

Figure 6.3.2-1: ADDOFD parameter plot for 3 sets of cables model

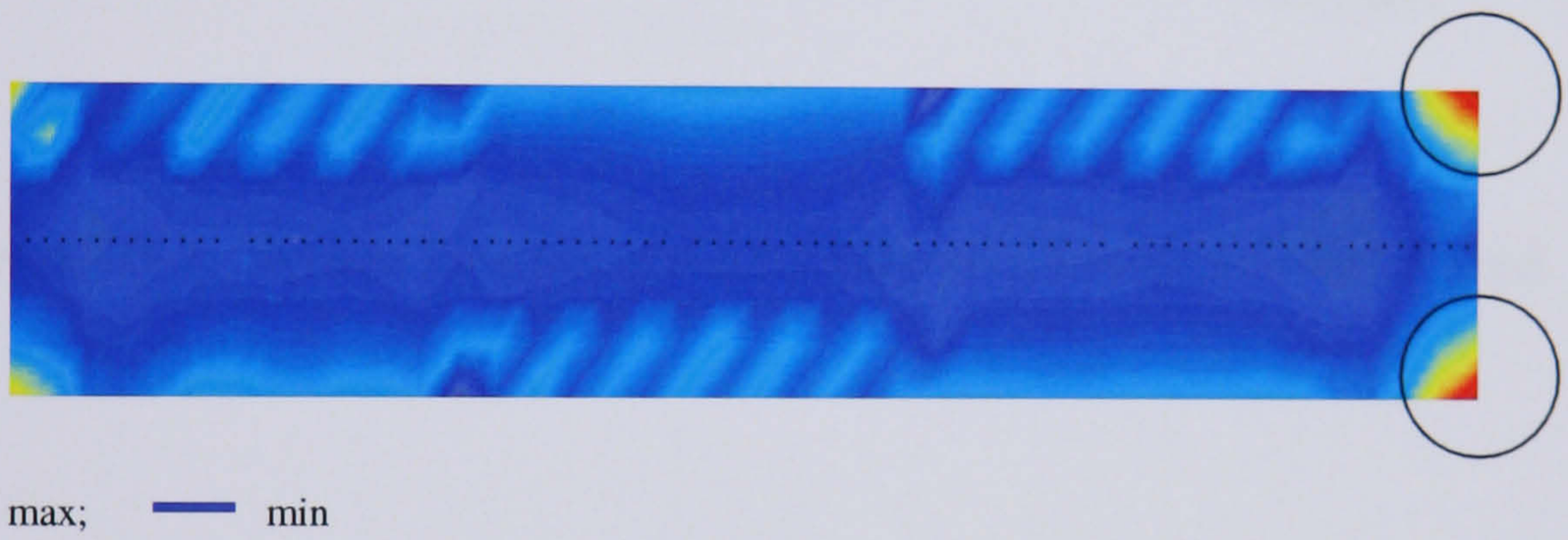

Key: max; min

Figure 6.3.2-2: ADDOFV parameter plot for 3 sets of cables model

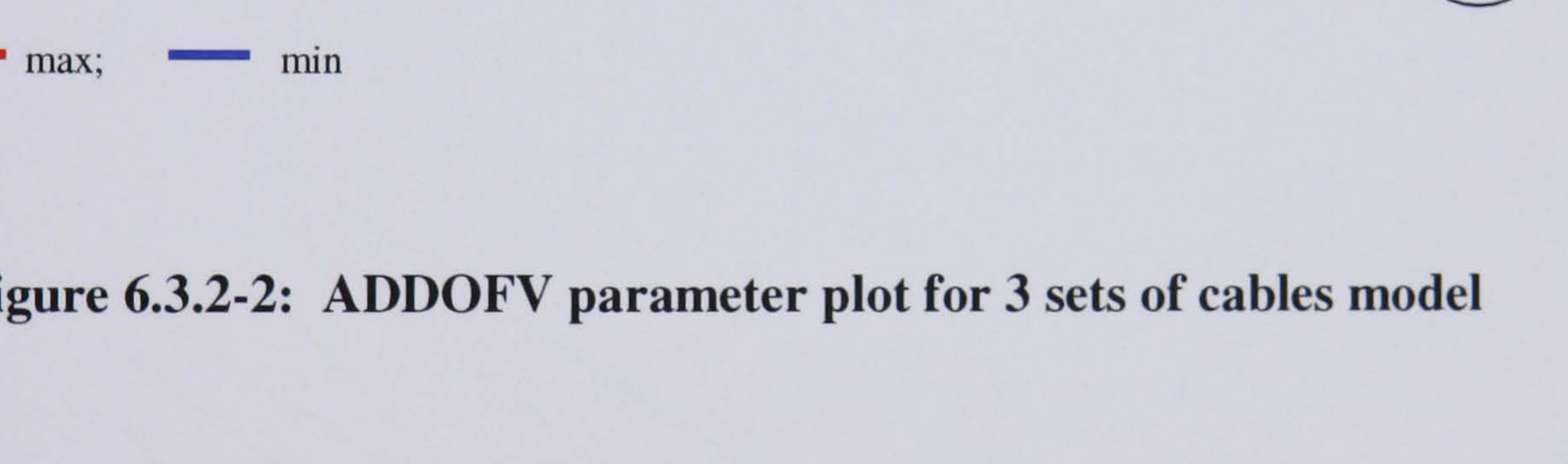

Key: max; min

Figure 6.3.2-3: ADDOFA parameter plot for 3 sets of cables model

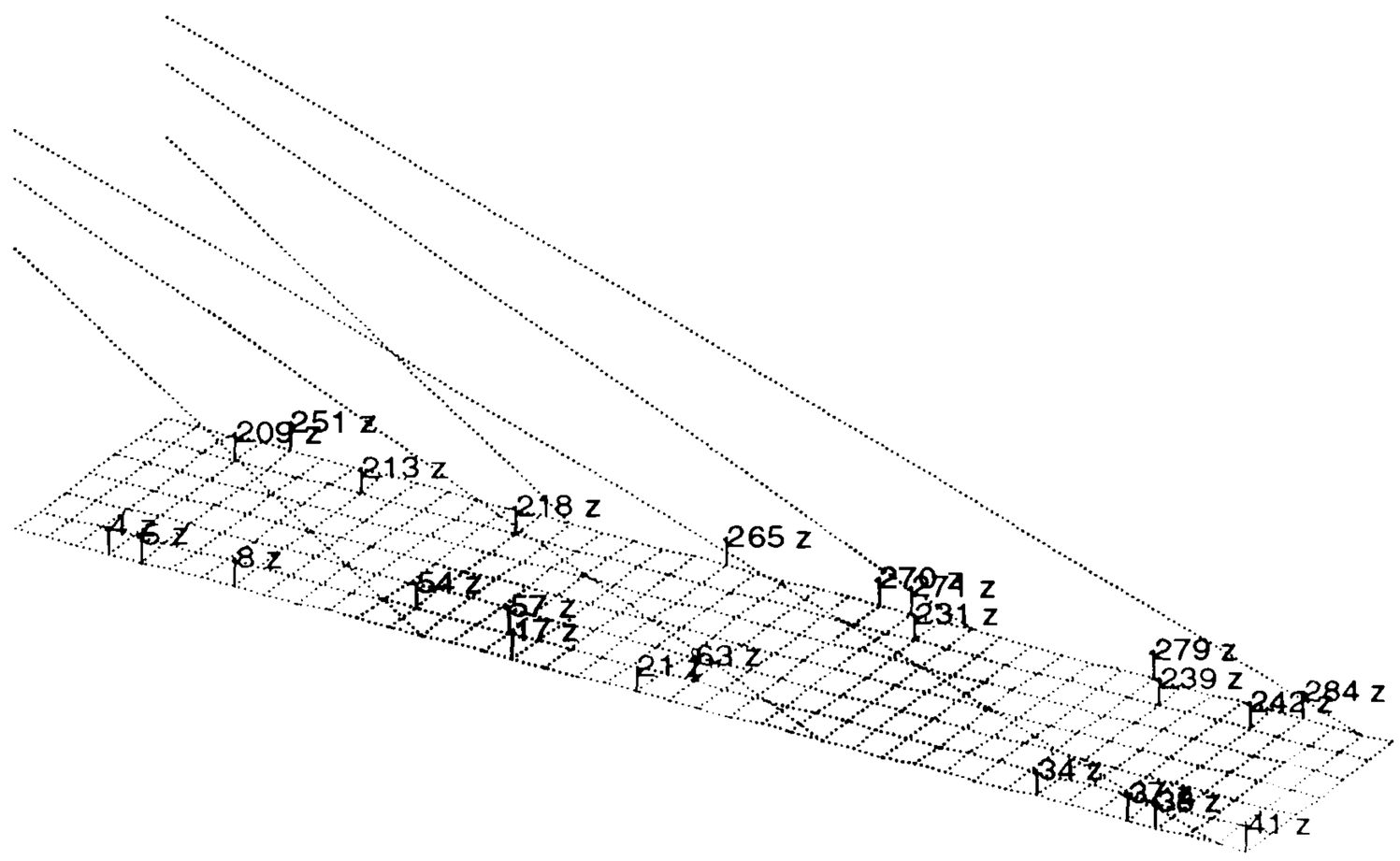

Figure 6.3.3-1: Sensor location given by Effective Independence Method

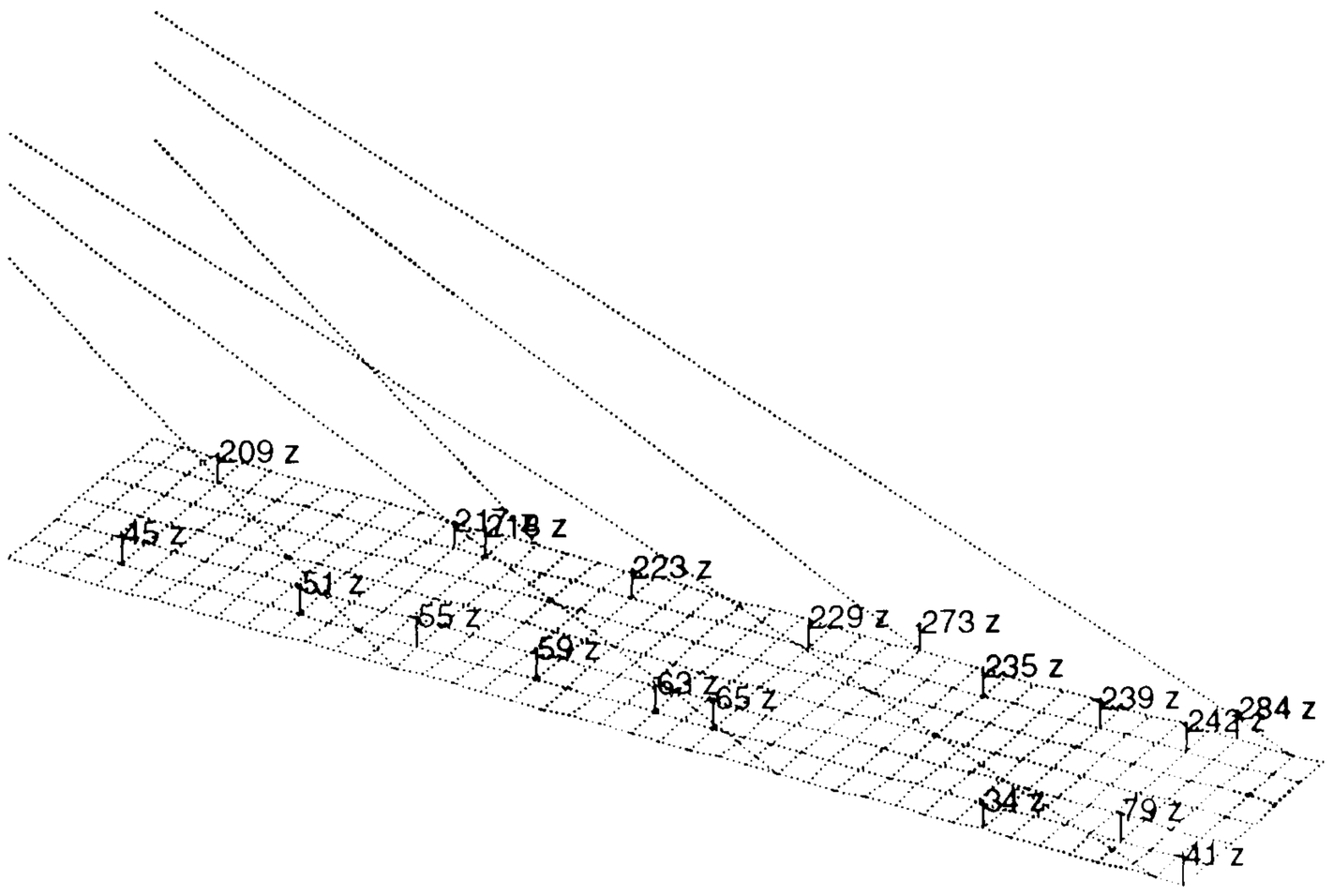

Figure 6.3.3-2: Sensor locations given by Energy Optimisation Technique

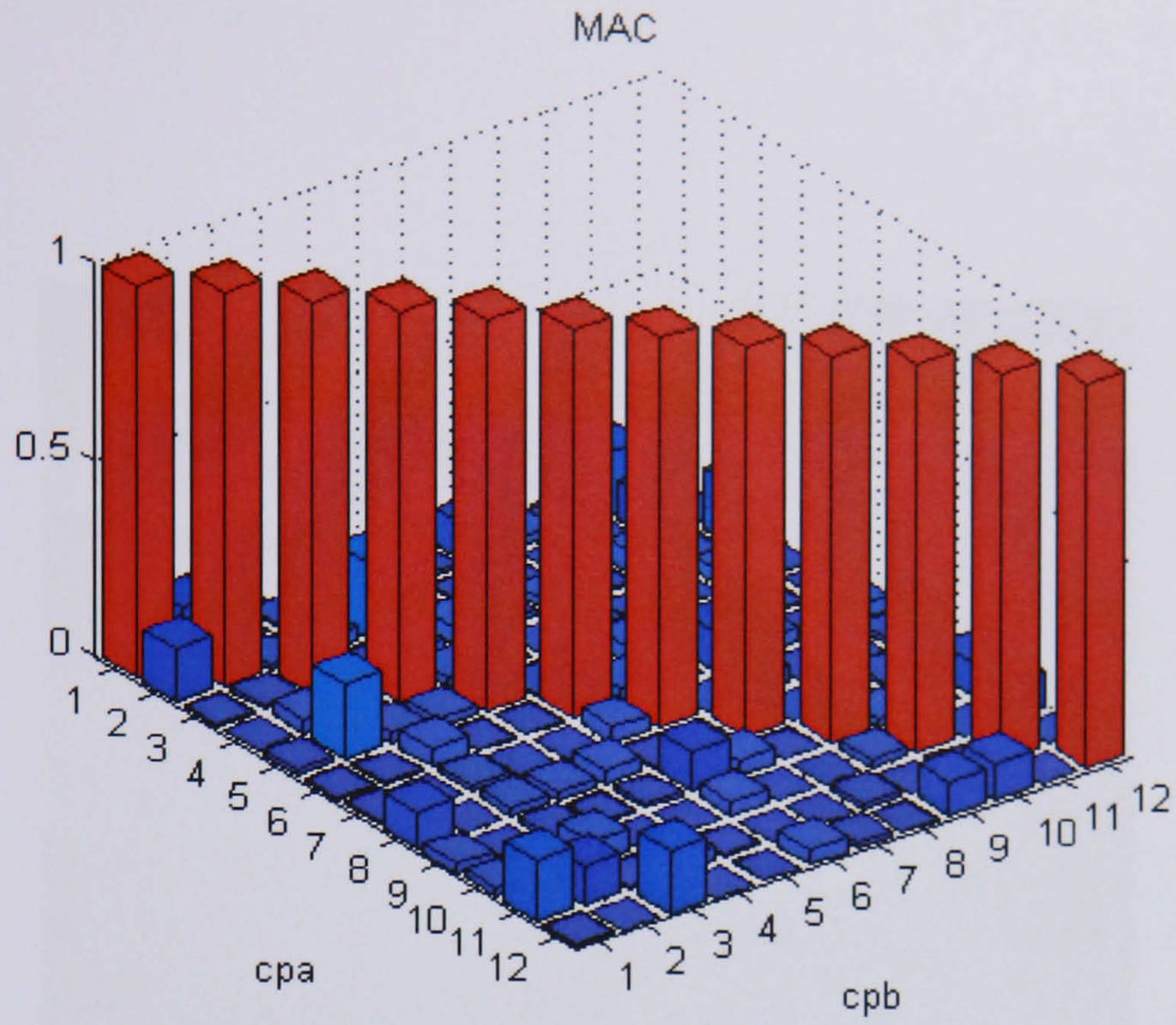

Figure 6.3.3-3: MAC for 24 sensor locations given by the Effective Independence Method

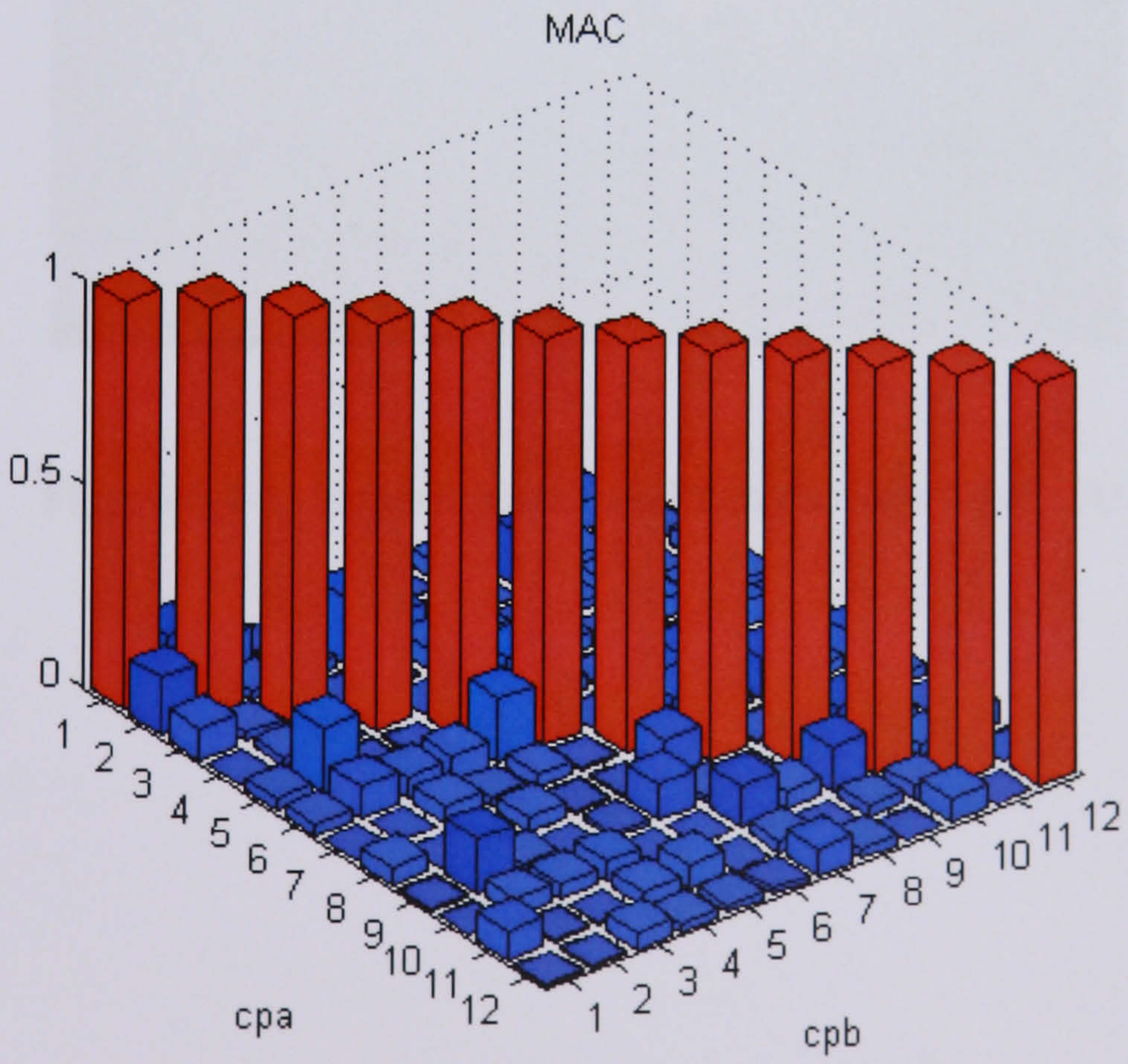

Figure 6.3.3-4: MAC plot for 19 sensor locations given by the Energy Optimisation Technique

Figure 6.4-1: Experimental model in the laboratory (1)

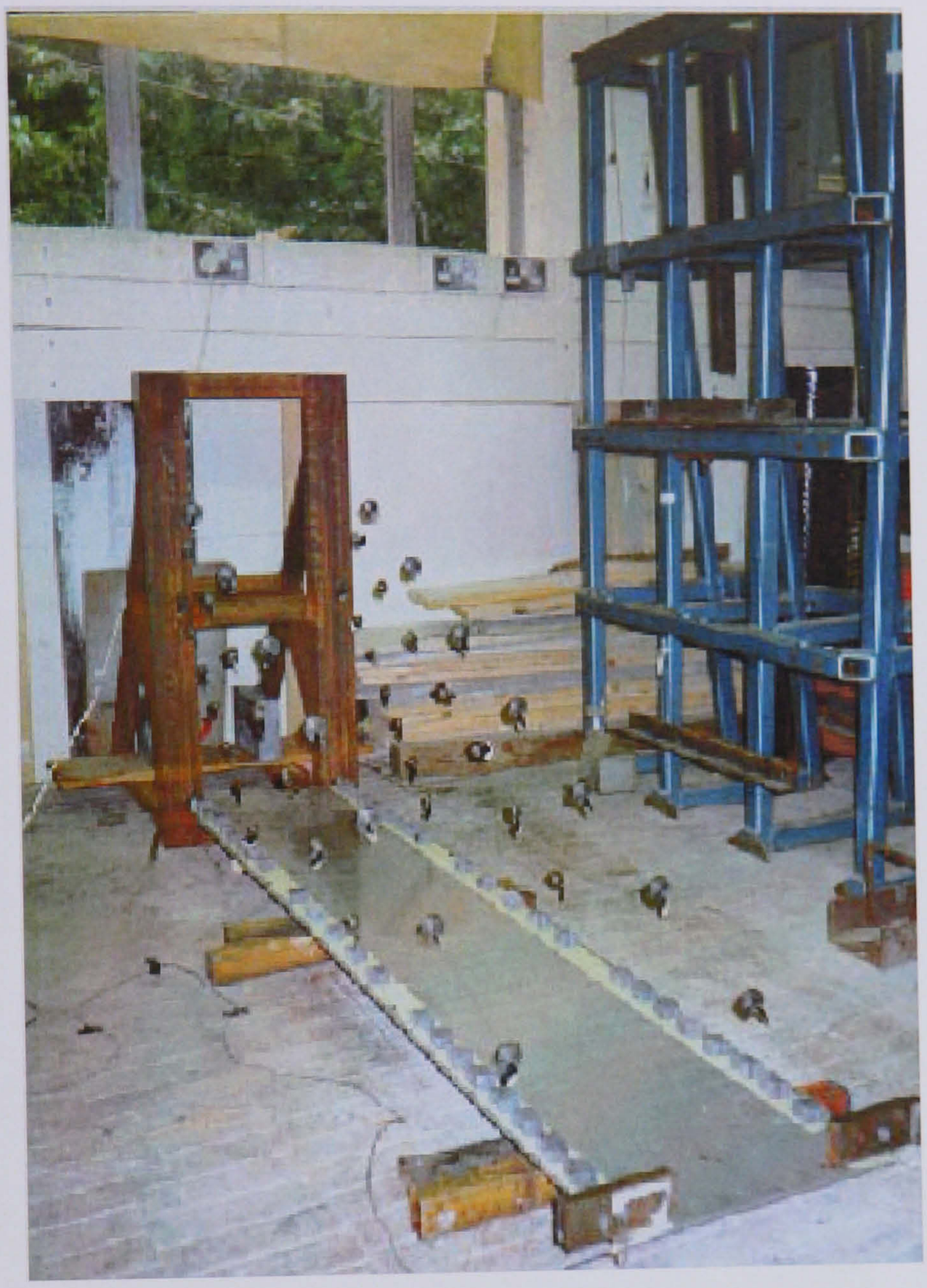

Figure 6.4-2: Experimental model in the laboratory (2)

Figure 6.4-3: Experimental model in the laboratory (3)

Figure 6.4-4: Experimental model in the laboratory (4)

Figure 6.4-5: Figure shows the vibrometer in place

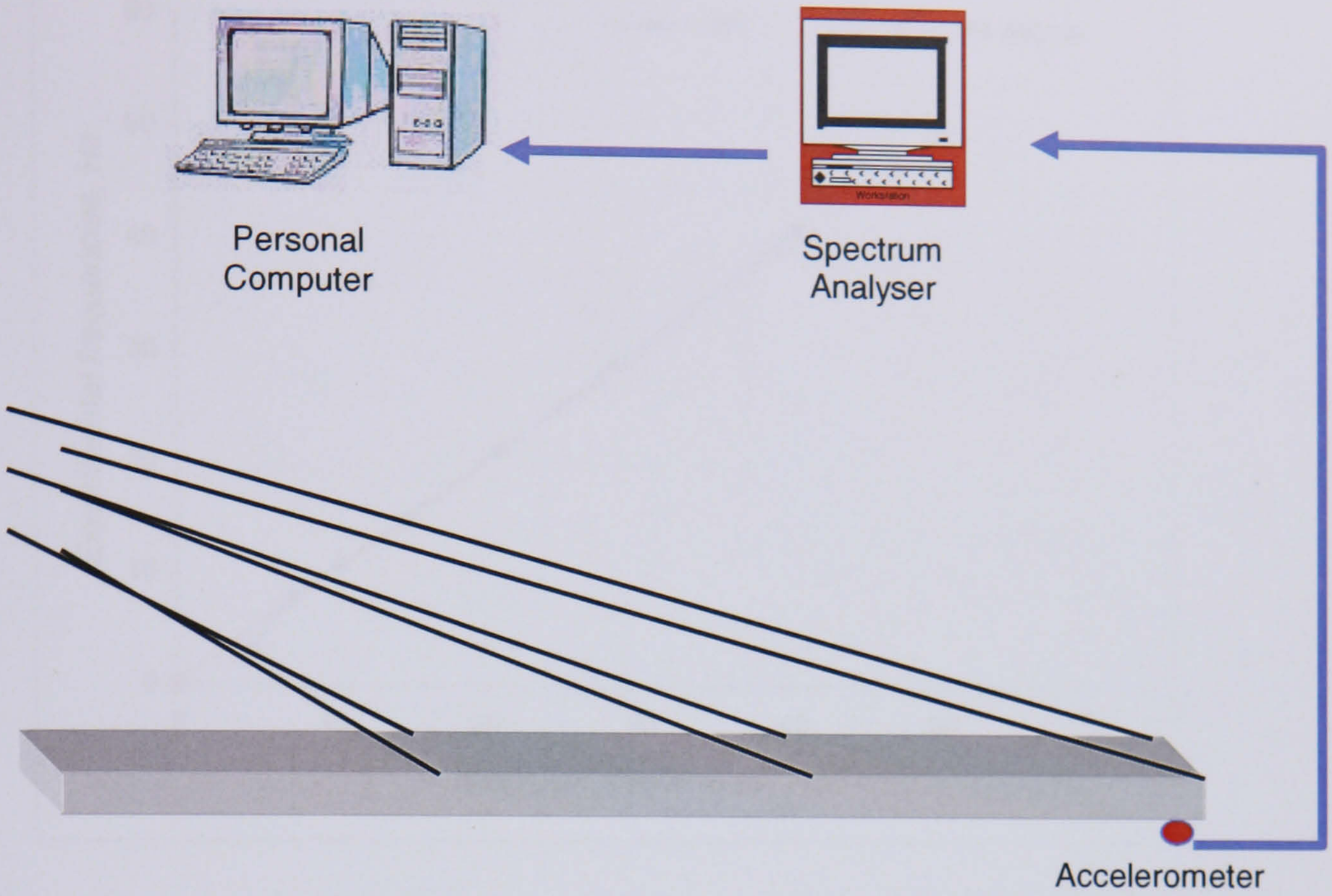

Figure 6.4-6: Experimental arrangement

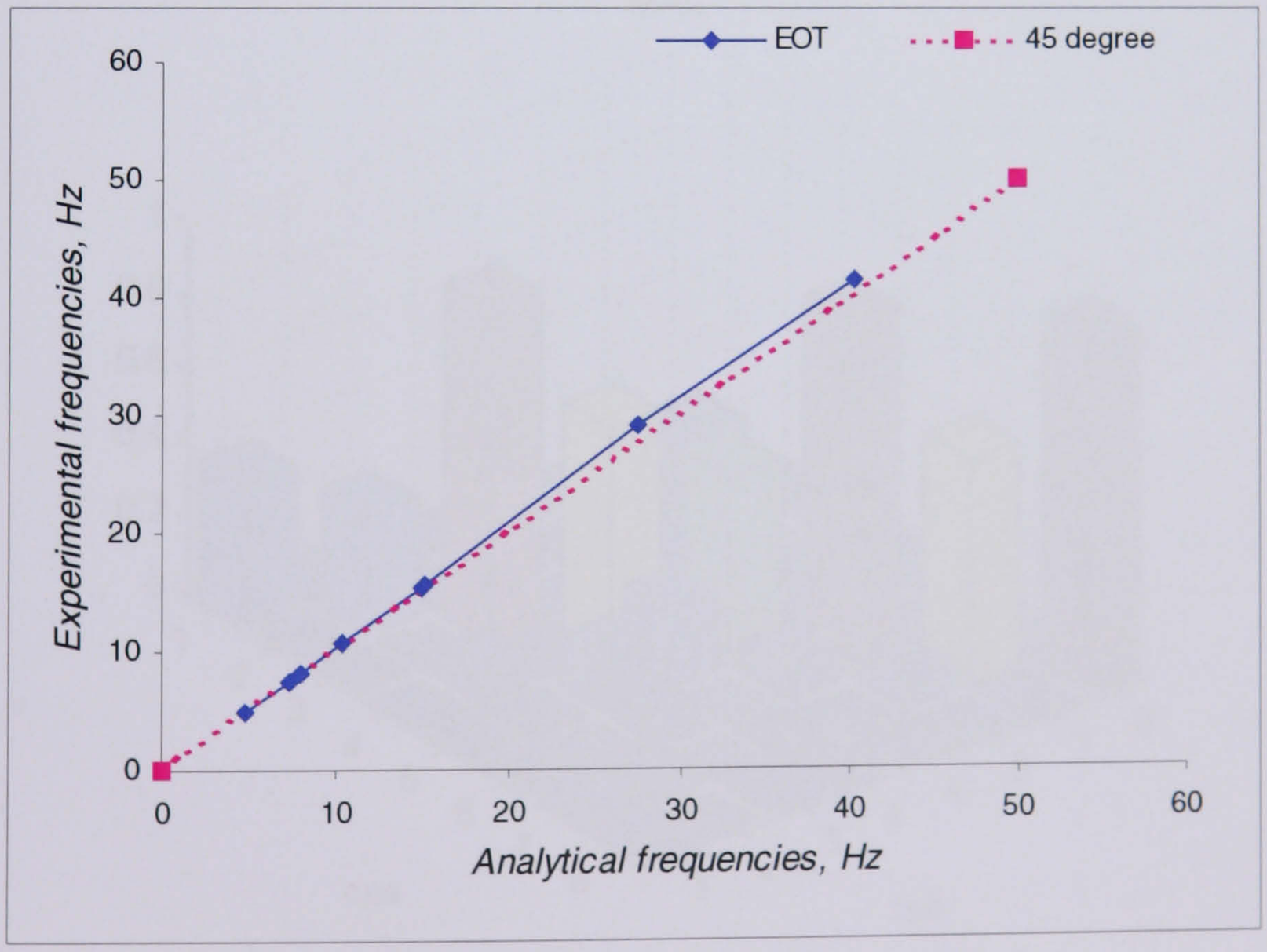

Figure 6.4-7: Graphical frequency comparison for the EOT method

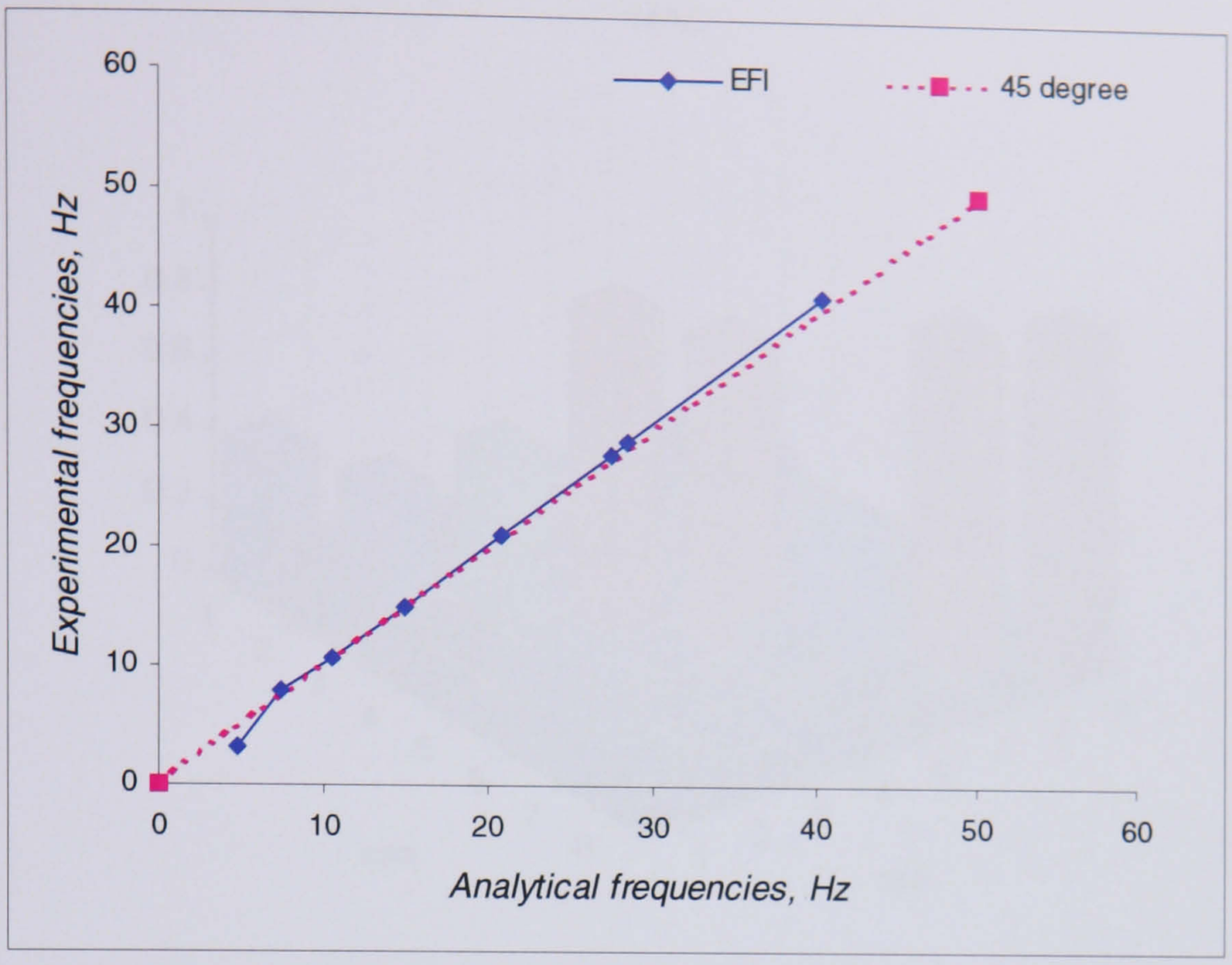

FIgure 6.4-8: Graphical frequency comparison for the EfI method

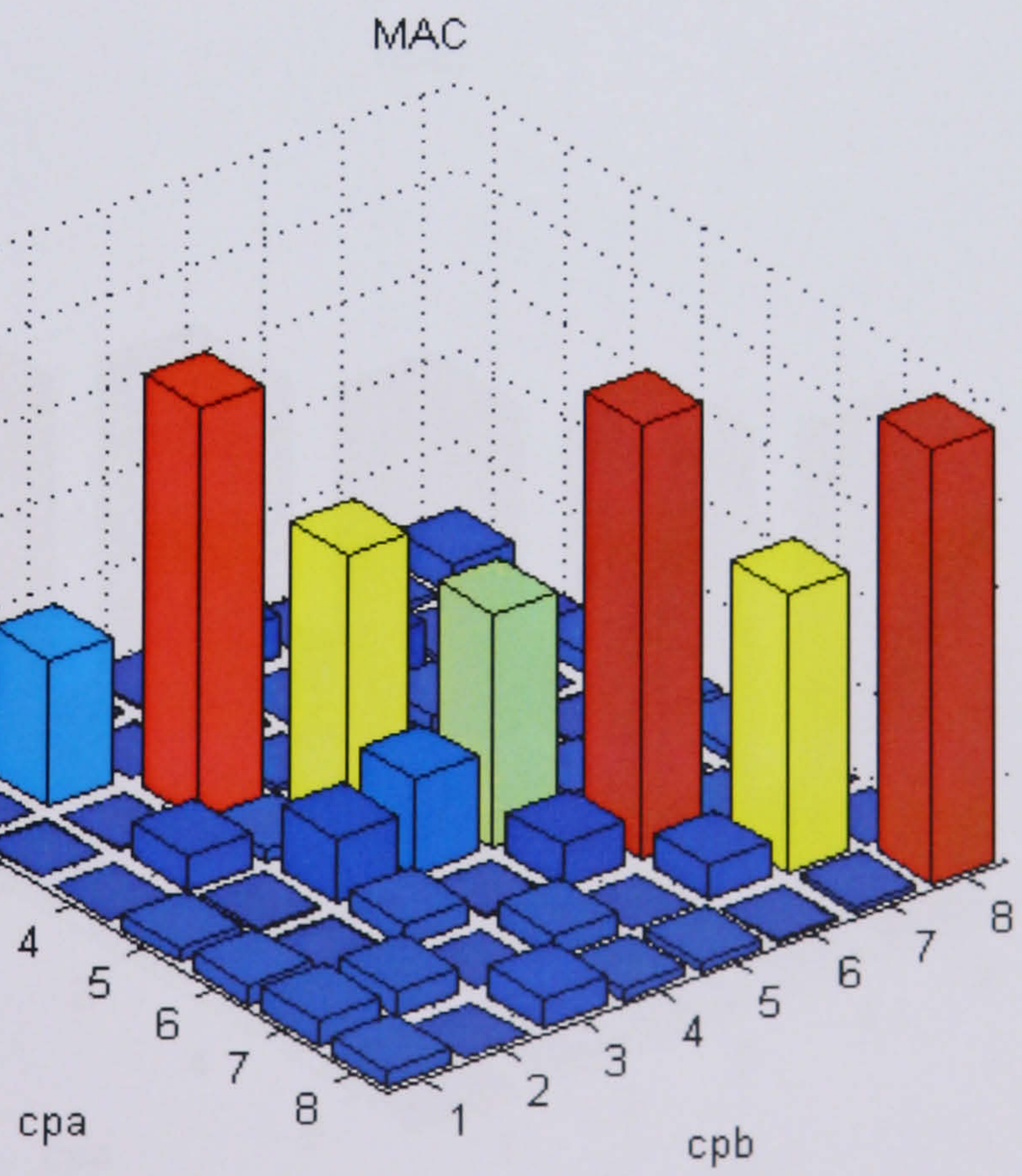

Figure 6.4-9: MAC plot for Experimental vs analytical modeshapes derived using the Effnective Independence method

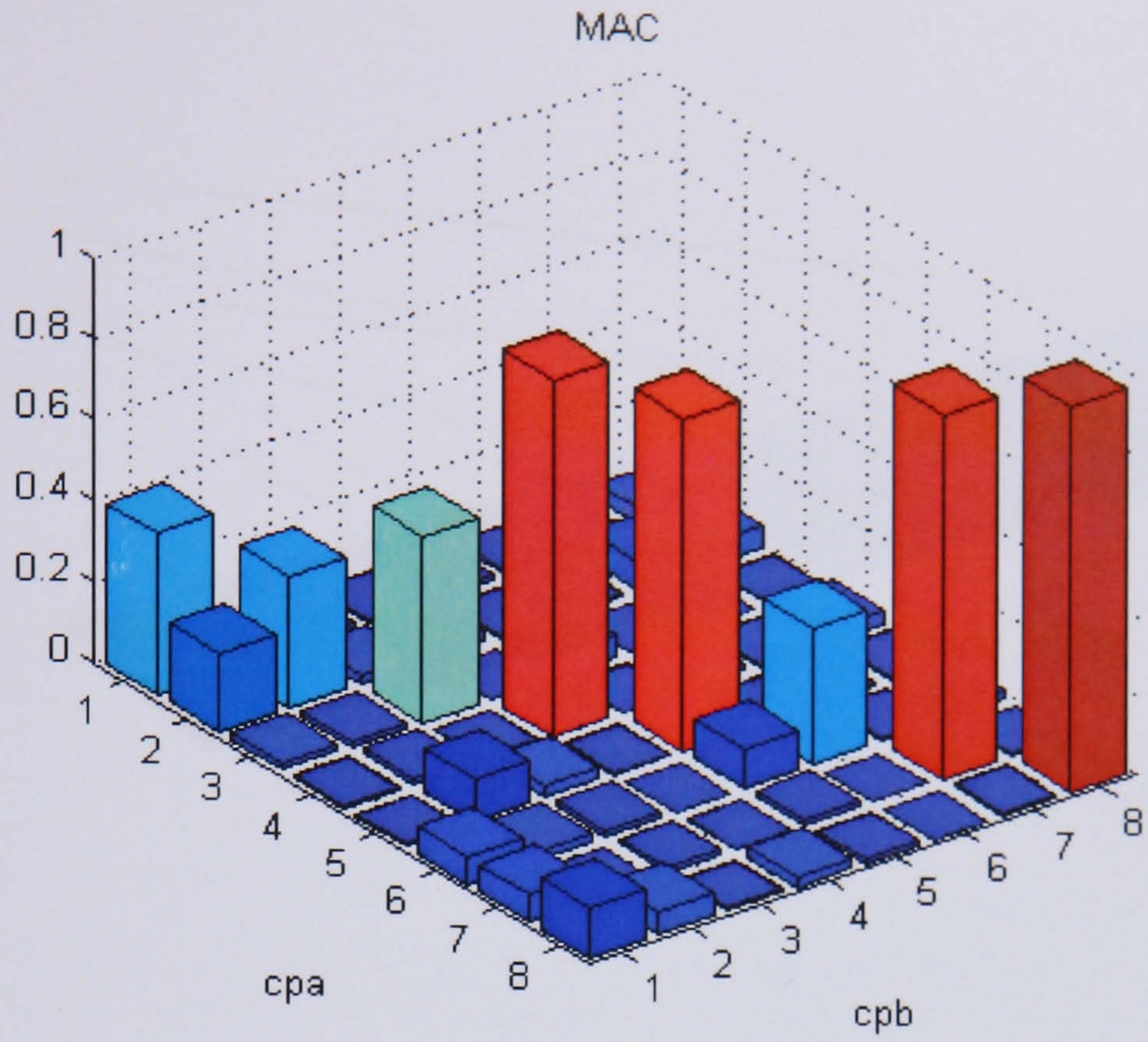

Figure 6.4-10: MAC plot for Experimental vs analytical modeshapes derived using the Energy Optimisation Technique

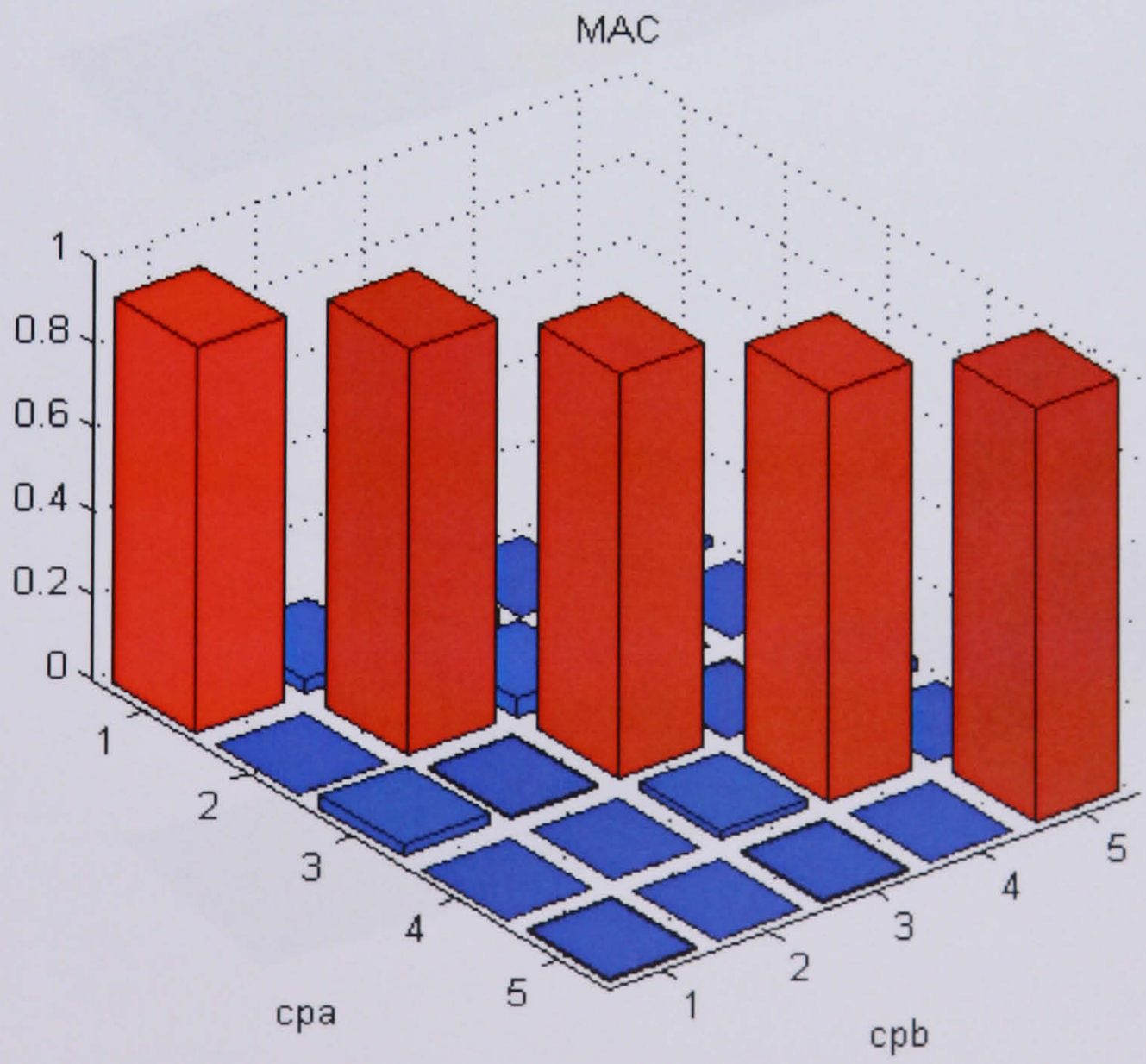

Figure 6.5-1: MAC plot for experimental vs analytical modeshapes used for model updating

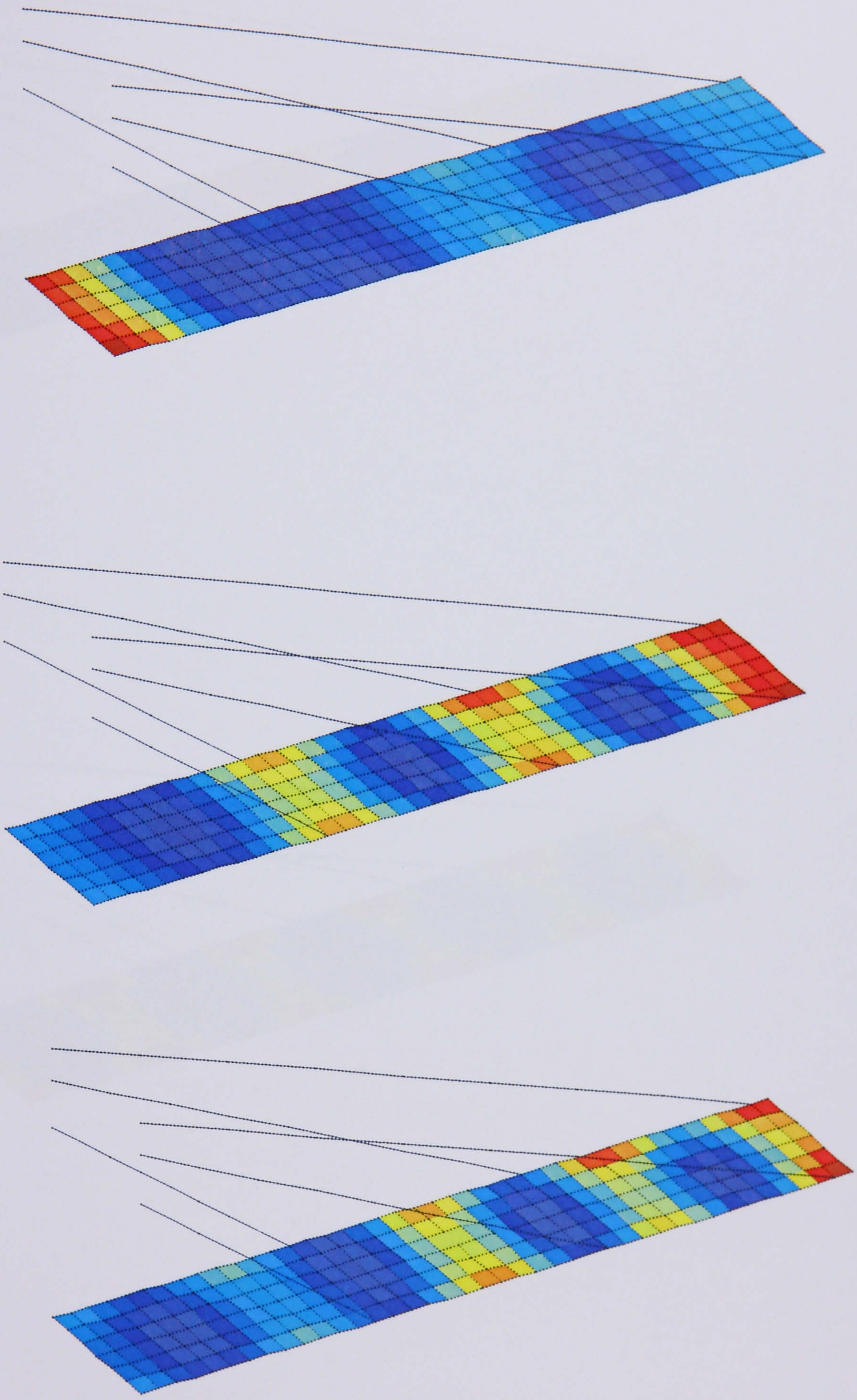

Figure 6.5.1-1(a): Strain energy distribution

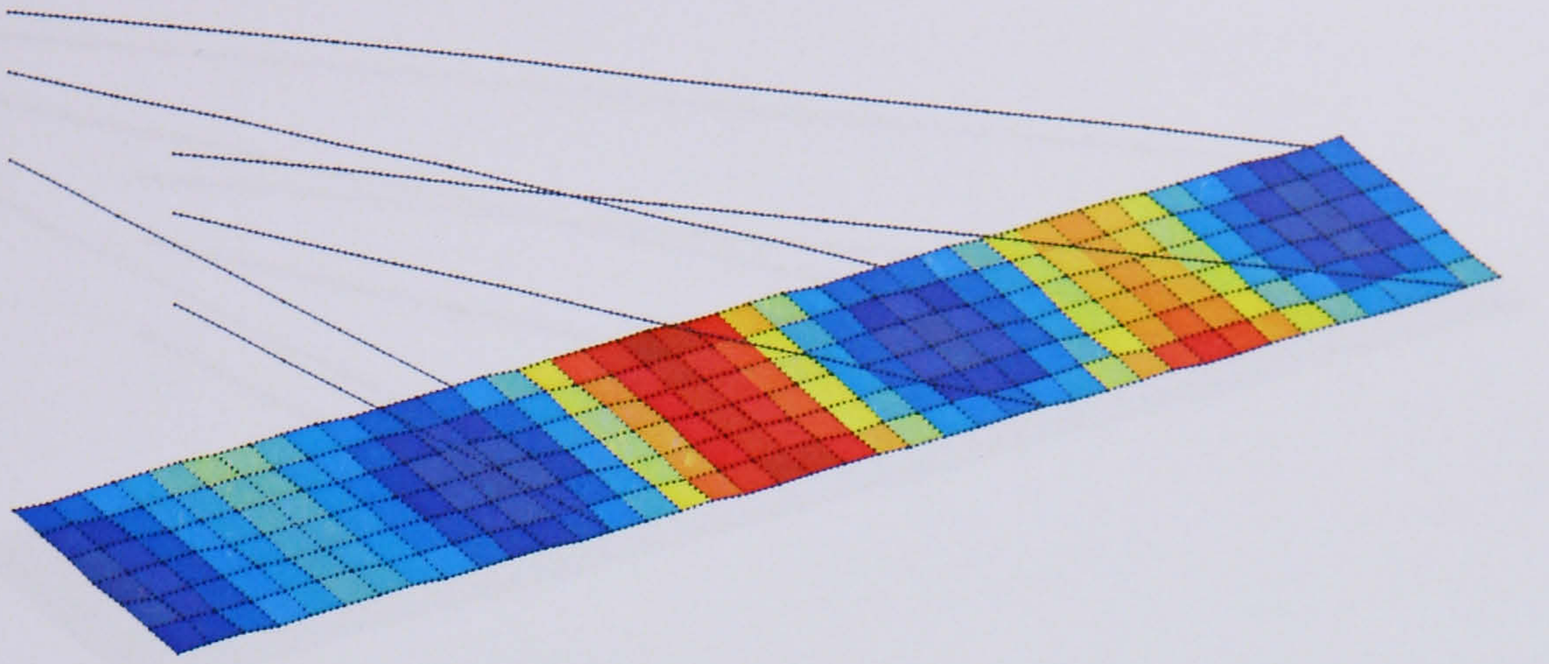

Figure 6.5.1-1(b): Strain energy distribution

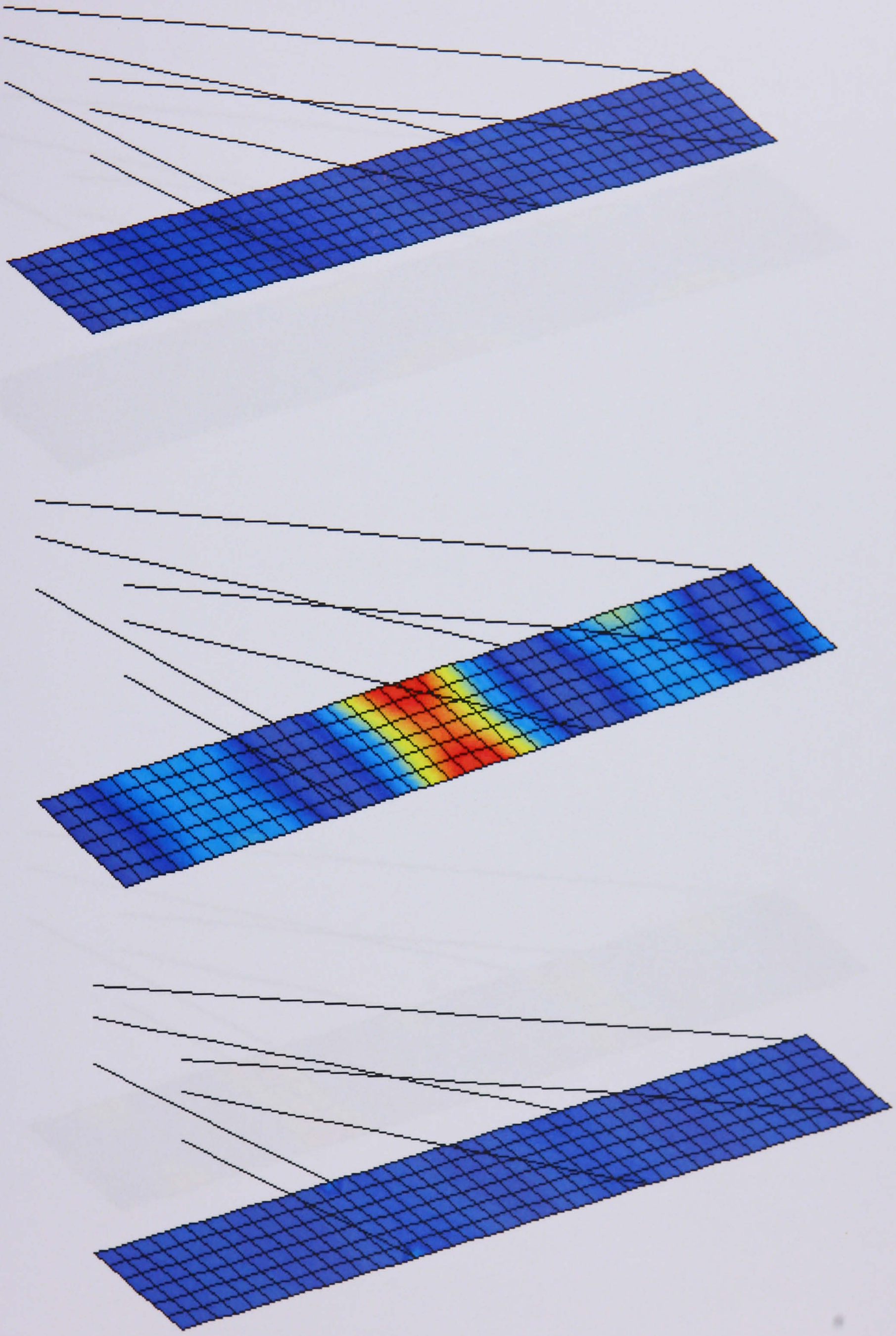

Figure 6.5.1-2(a): Kinetic energy distribution

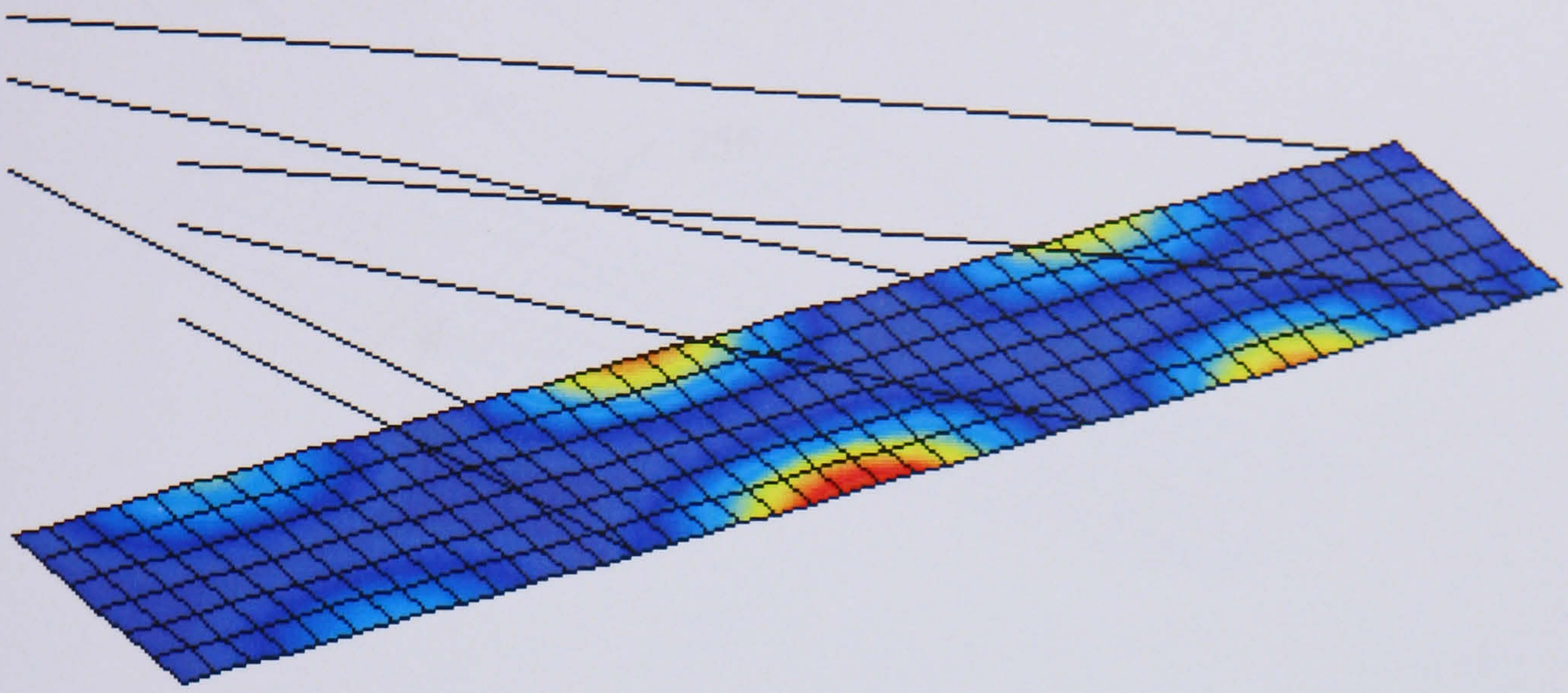

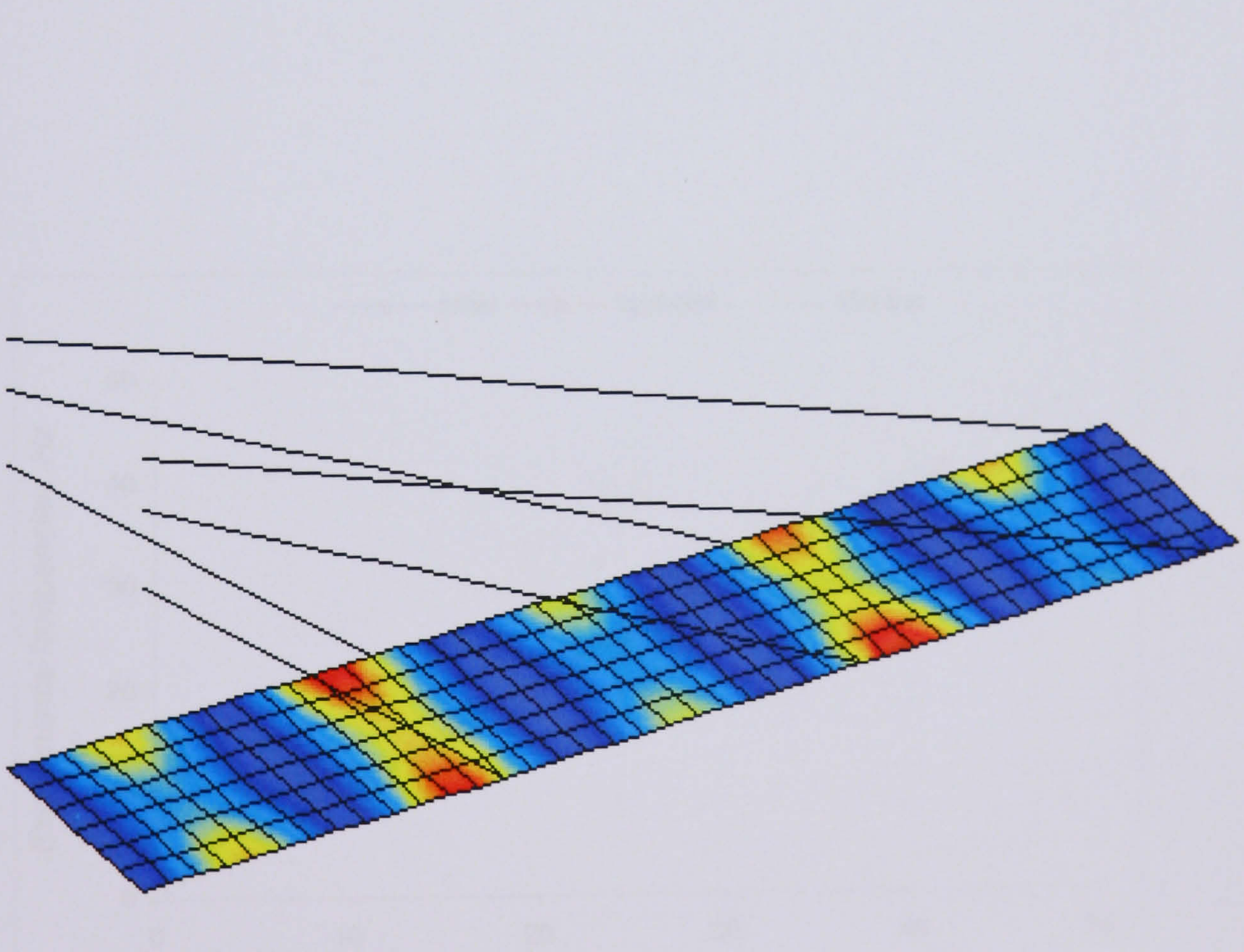

Figure 6.5.1-2(b): Kinetic energy distribution

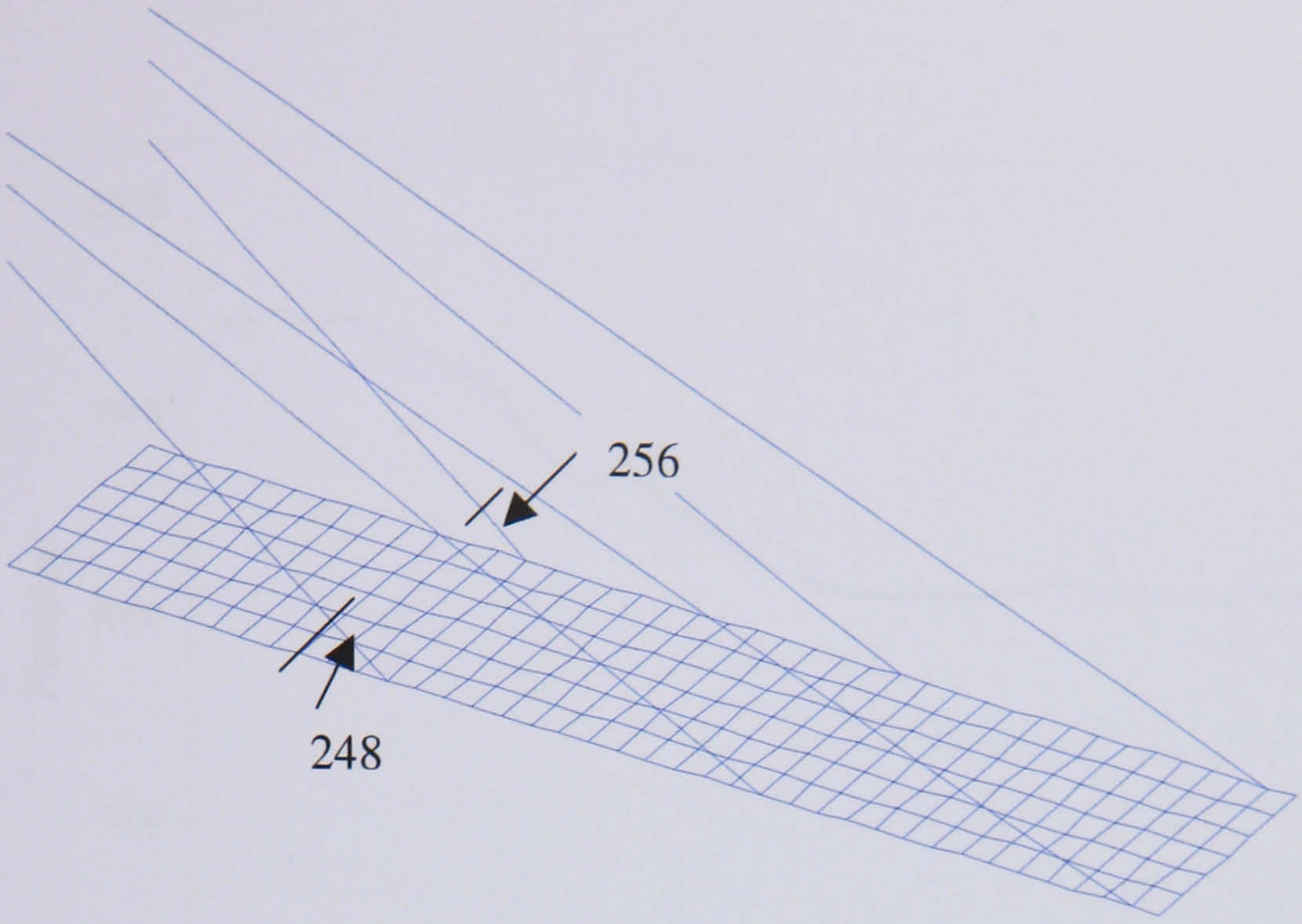

Figure 6.5.2-1: Positions of the two updating elements (248, 256) used for stiffness update

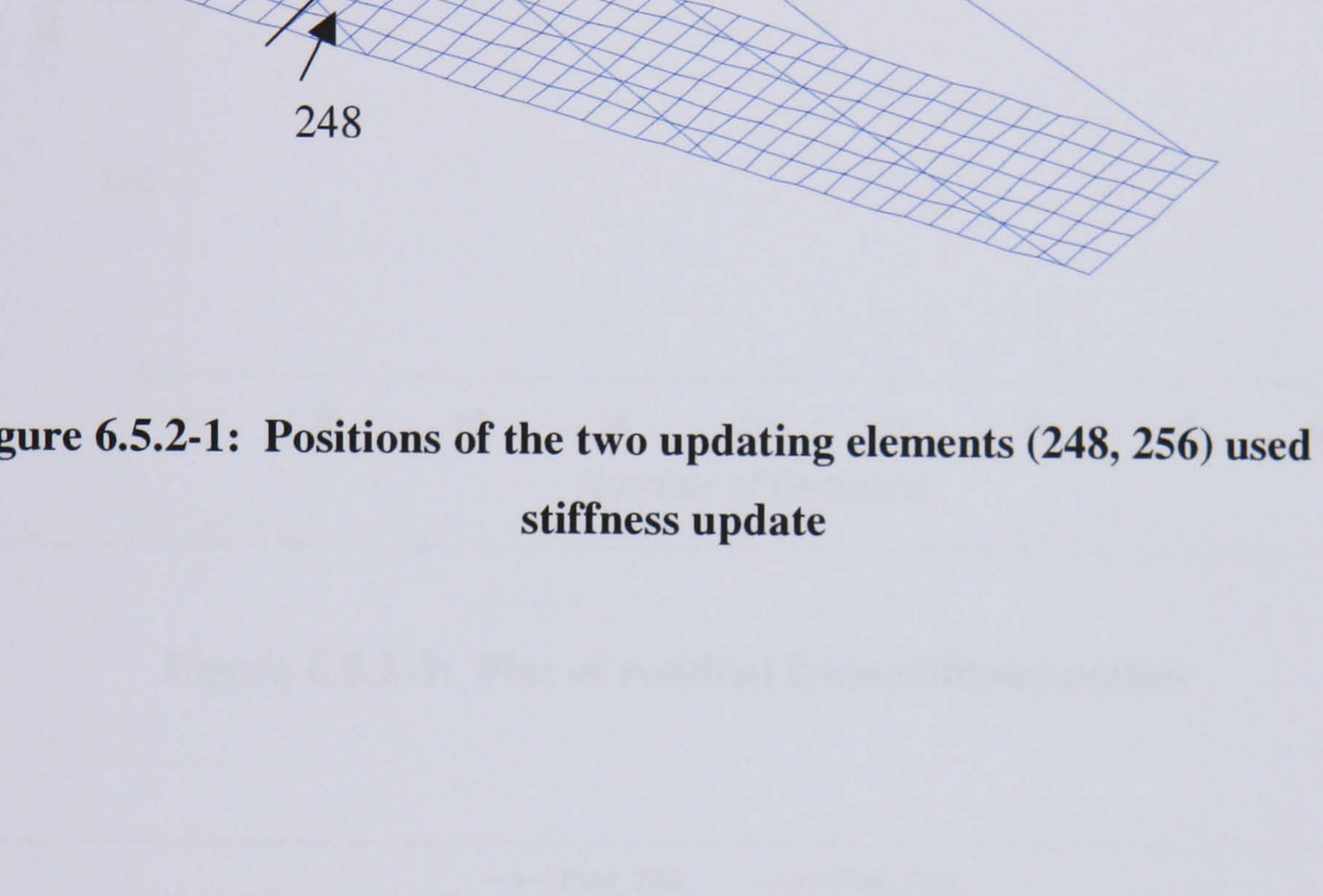

Figure 6.5.2-2: Plot of initial and updated analytical frequencies against experimental frequencies from stiffness update

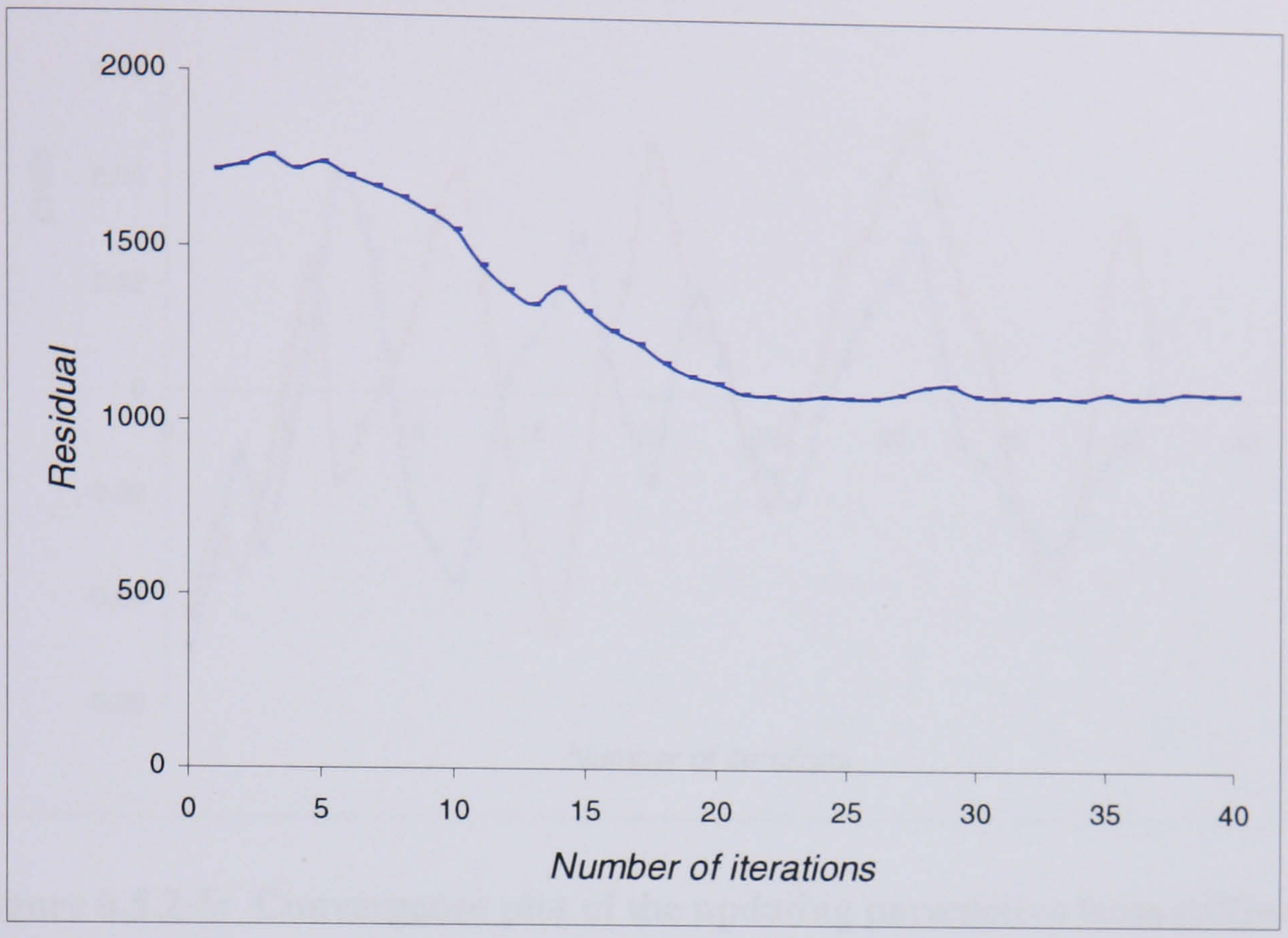

Figure 6.5.2-3: Plot of residual from stiffness update

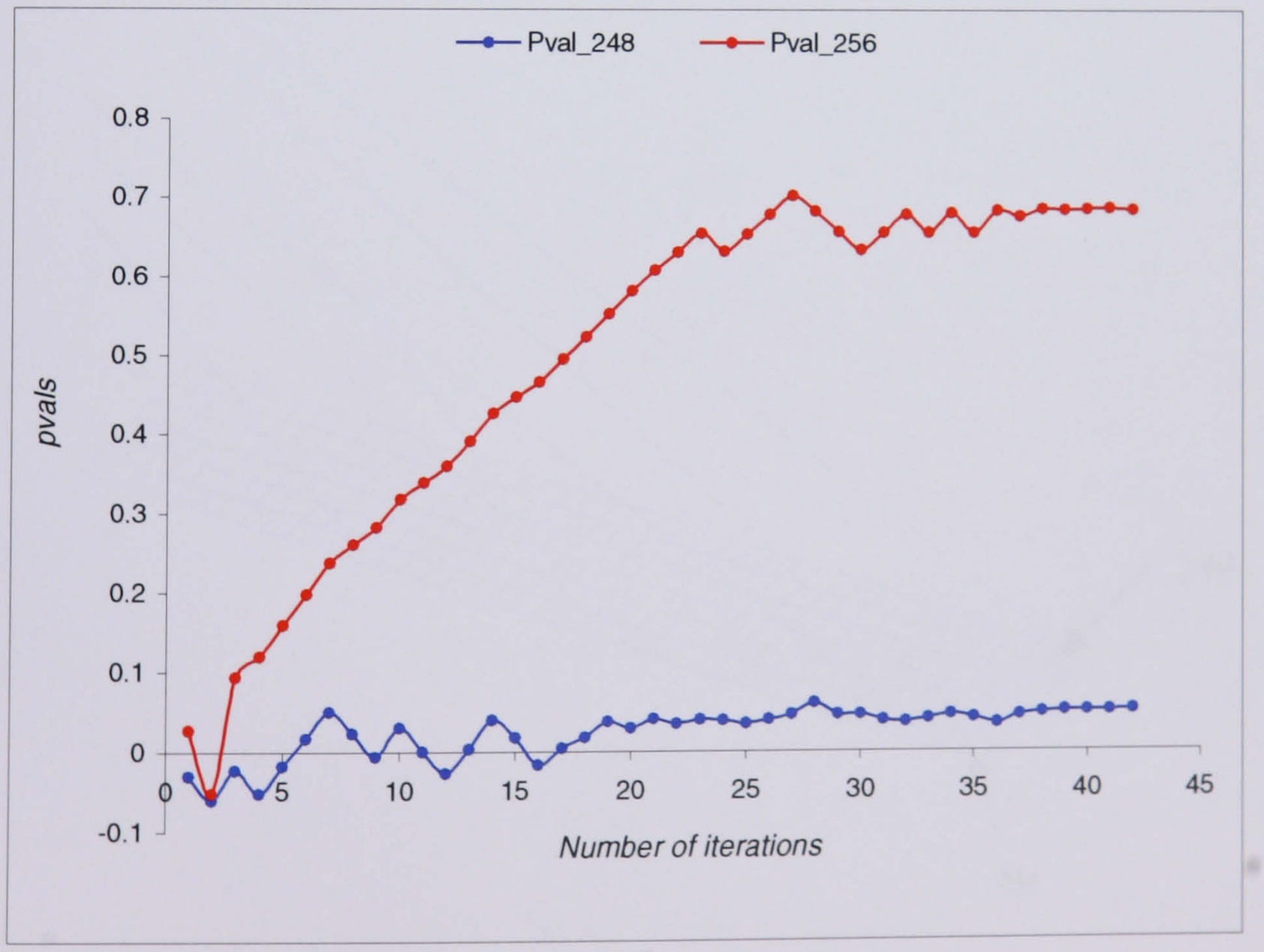

Figure 6.5.2-4: Convergence plot of the updating parameters from stiffness update

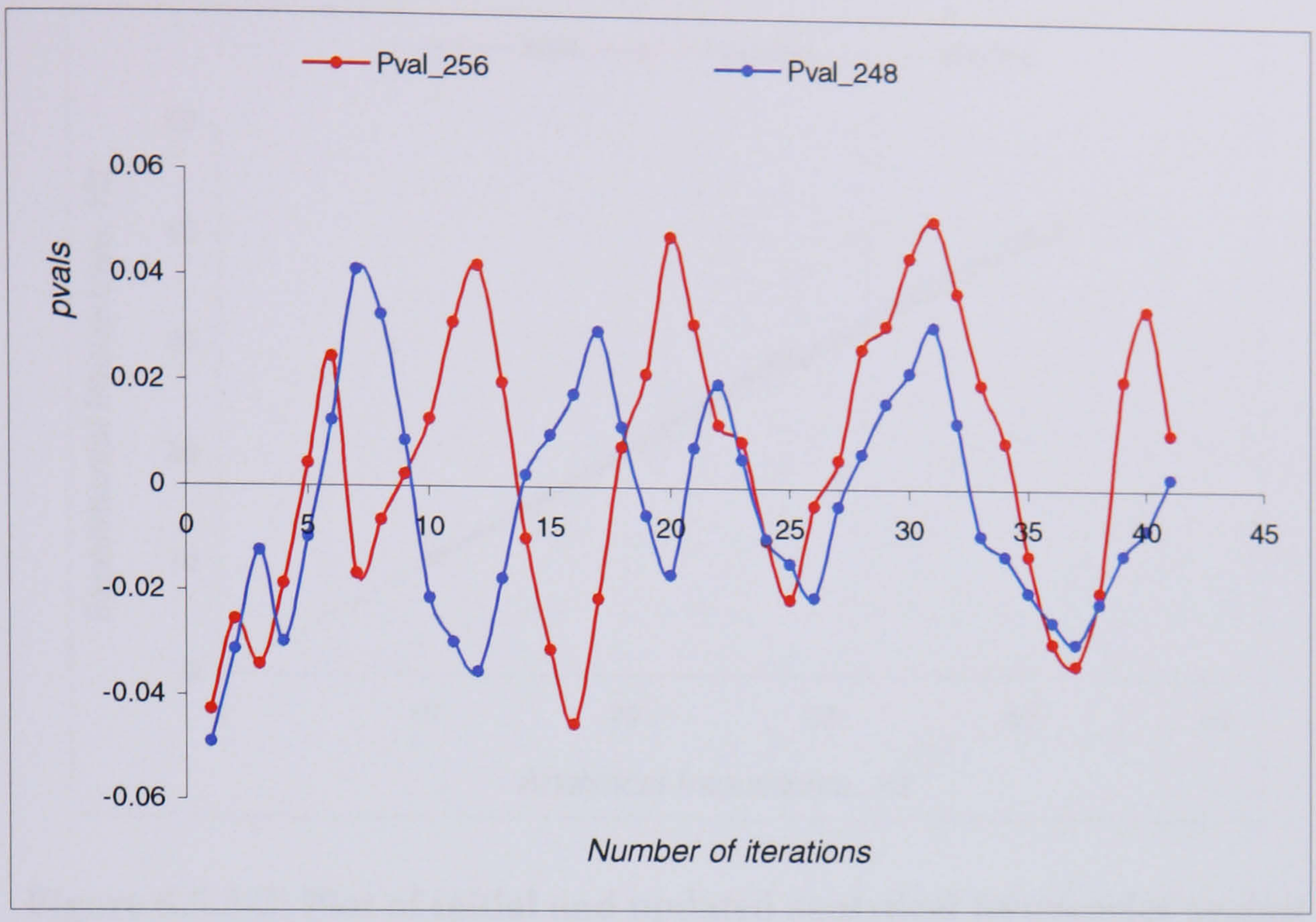

Figure 6.5.2-5: Convergence plot of the updating parameters from stiffness update (linear analysis)

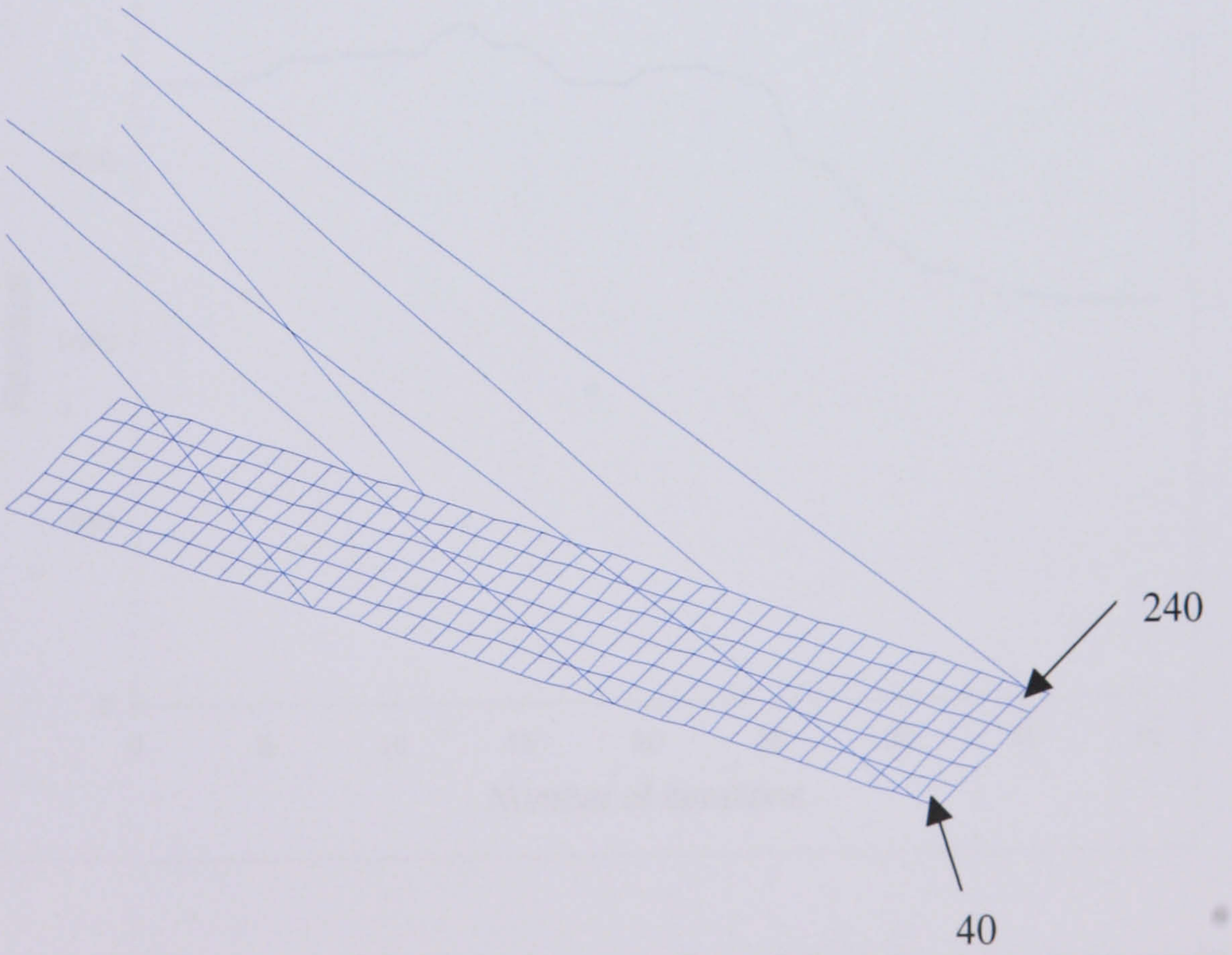

Figure 6.5.3-1: Positions of the two updating elements (40 and 240) used for mass updating

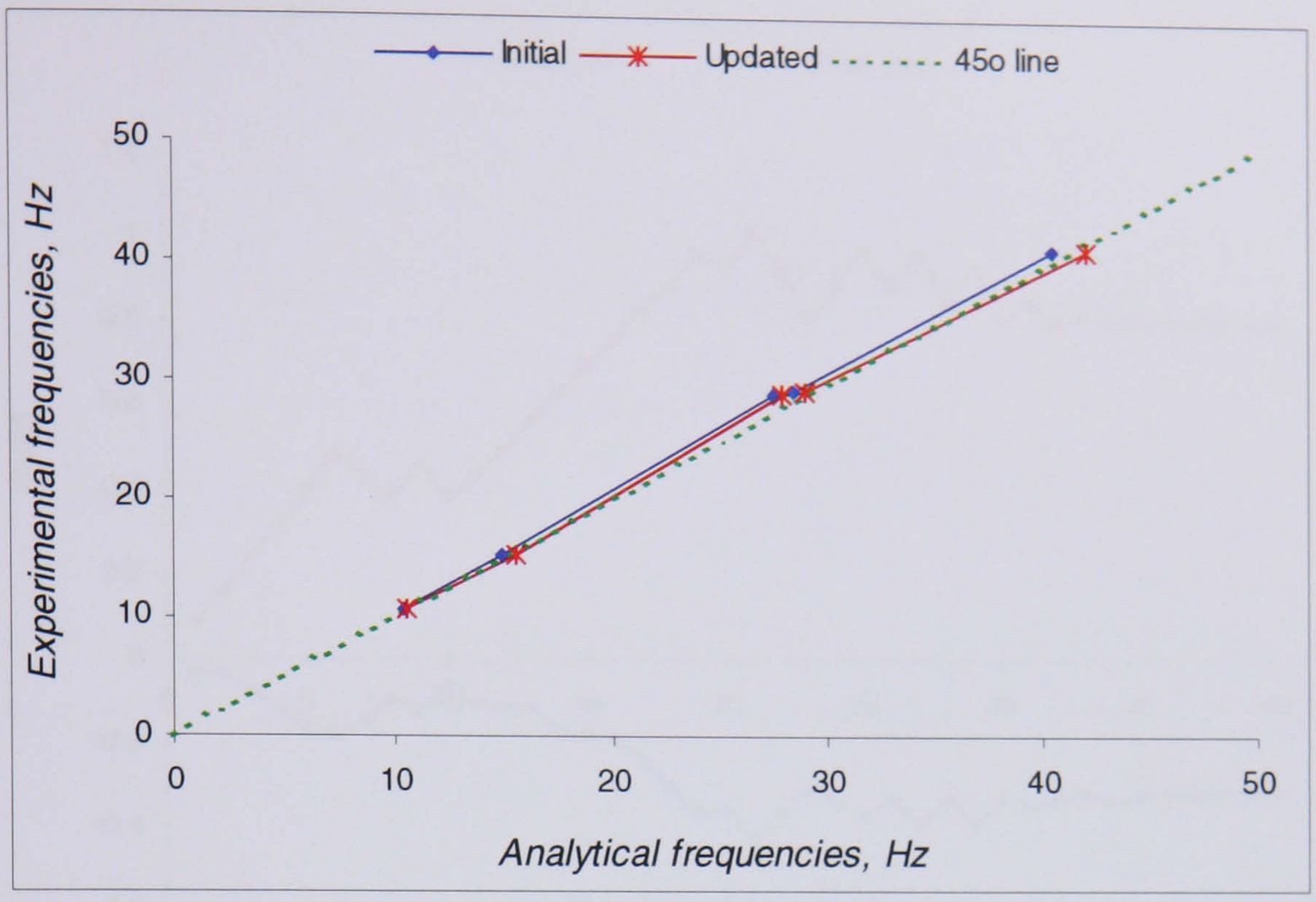

Figure 6.5.3-2: Plot of initial and updated analytical frequencies against experimental frequencies from mass update

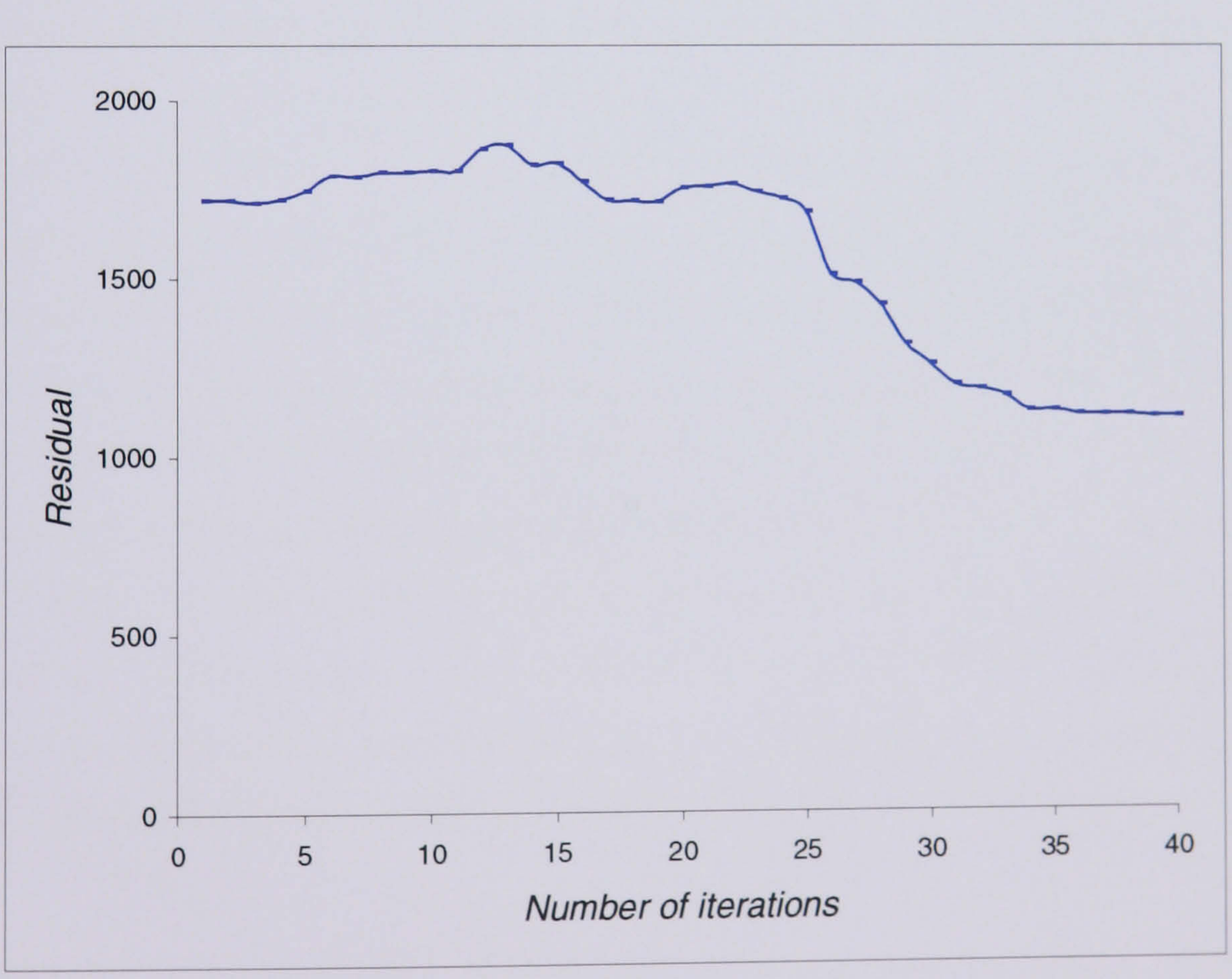

Figure 6.5.3-3: Plot of residual against number of iterations for mass update

Figure 6.5.3-4: Convergence plot for pvalues from mass update

CHAPTER 7

CONCLUSIONS AND FUTURE WORK

7.1 Introduction

This chapter presents an account of the various conclusions that can be drawn from the present work including some general observations about cable-stayed bridges and the use of model updating techniques. Also, the contributions of this work and some recommendations for future studies are presented.

7.2 Conclusions

The main objective of this research was to investigate the applicability of model updating techniques to a civil structure, and in particular, to a cable-stayed bridge cantilever. Model validation techniques have been used to optimise aerospace structures but without success for many years, but they have never been applied to complicated civil engineering structures. One of the reasons that this may be is because civil engineering structures, and especially cable-stayed bridges, are very complicated systems, constructed using non-homogeneous materials and are usually expressed by a large number of degrees-of-freedom. Model updating requires simplicity in the modelling, good quality data and to be carried out under controlled conditions. However, none of these criteria can be met with a cable-stayed bridge cantilever, which requires a large model. Also, the very fact that experimental data rather than analytically simulated data are used for optimisation renders the problem even more difficult and challenging.

Chapter 1

This chapter presents an introduction to the scope of the thesis and sets out its main objectives. Brief summaries on the sensor placement techniques and model updating, including the work done up to date on model optimisation are presented.

Chapter 2

Chapter 2 presented a description of the various parts that comprise a cable-stayed bridge. An account into a very important characteristic of cable-stayed bridges was given here, which is called *Geometric nonlinearity*. It is divided into *stress-stiffening* and *large deformations* effects, and influences the dynamic behaviour not only of this type of structure but also of any structure subjected to axial forces. Also, an extensive literature review on cable-stayed bridge modelling and analyses, dynamic. and earthquake testing presented an insight into the extensive work that has been carried out for many years into this fairly new type of structure.

Chapter 3

This chapter gave the theoretical background of geometrical nonlinearities and was illustrated with the example of a simply-supported beam subjected to an axial force. The effect on the frequencies of the beam of the presence of an axial force was presented.

Chapter 4

Chapter 4 presented the importance of pre-test planning before an experimental test. The various considerations that the experimentalist has to take into account before commencing an experiment in the laboratory were presented, together with the methods that can be used to fulfill each requirement. The first stage in the pre-test process is to decide how the structure can be mounted. Imamovic (1998) gives a detailed account of the various methods that can be used for finding the best locations to support a structure, especially for testing in free-free conditions and they are also presented in this work. The next stage is to decide where to place the excitation source and the measurement sensors. Imamovic (1998) presents various methods for finding the best locations to excite a structure. These methods were given also in this presentation and used for placing the accelerometer on a plate tested in free-free conditions and on the cable-stayed cantilever experimental model, presented in Chapter 6. Moreover, three different methods were presented for placing measurement sensors on a structure. These methods were described in detail and were applied in the testing of the plate and cantilever. The methods were compared with each other and the most successful method was the one that gave the best information with the least number of sensors. In the case of the plate and

cantilever models, only the Effective Independence method and the Energy Optimization technique were used for placing sensors on the models. since the stiffness matrix of the systems were not positive definite. For the plate model, both methods gave a set of 19 sensors each, whereas, for the cantilever the first method required 24 sensors, whereas, the second required 19 transducers. Both methods used to extract the experimental results, and it was concluded that the Energy Optimization technique was the most preferred method, since it gave slightly better results than the Effective Independence method using a smaller number of sensors. An observation regarding the values of the extracted frequencies led to the conclusion that the quality of the experimental data depends on the set of sensor locations used in the experiment. In the case of the both the plate tested in free-free conditions and the cantilever model, it was shown that the Energy Optimisation technique was more successful in identifying the frequencies of the models than the Effective Independence method. By observing the position of the sensors on the models, one can see that the Energy Optimisation technique placed sensors on positions of low ADDOFV values. This parameter, as mentioned in Chapter 4, shows the best positions to hit a structure with a hammer. Positions of low ADDOFV values are preferred as double-hit effects are avoided. Since the hammer hit both structures at those sensor positions, double-hit effects were avoided, leading to better frequency estimation. Although twelve analytical modes were used to find the sensor locations for the cantilever model only five were identified perfectly, four bending modes and one torsion, all of which were higher order modes. These modes were used later in Chapter 6 for model updating.

Chapter 5

Chapter 5 gave a detailed account of the methods used for modal expansion or reduction, comparison and model updating. Usually, the experimental model possesses a smaller number of degrees-of-freedom than the analytical model. Therefore, in order to compare the experimental with the analytical data, it is customary either to expand the experimental data to the analytical degrees-of-freedom, or to reduce the analytical data to the experimental coordinates. In any case, both models should possess the same number of coordinates in order to be compared and correlated. The methods for modal expansion or reduction were presented in this chapter.

There are many ways to compare modal data, such as the graphical way, where the two sets of data compared are plotted against each other in a x-y plot or the tabular presentation of the results, where one can actually compare the values. However, the most commonly used method for comparing modeshapes is the Modal Assurance Criterion or MAC, which is based on the orthogonality properties of the modeshapes and is a scalar quantity. The MAC was used in this work to compare the analytical with the experimental modeshapes, and the MAC values for the five modes used for updating are above 0.9, indicating good correlation.

The chapter continues by presenting the available model updating techniques, which are sensitivity based methods. They are divided into modal sensitivity and FRF sensitivity updating and a description of both was included. The first method uses the experimental and analytical natural frequencies and/or the modeshapes of the structure to correct the analytical model, whereas, the second method uses the Frequency Response Functions. In this work the modal sensitivity method was used. The first stage before commencing the updating procedure is to decide which parameters to choose for optimization. These parameters are called p-values and usually are the elemental stiffness or mass matrices. The selection of those parameters is a very important stage in the updating process and they must represent the site of errors in the model. In number, they should be less than the number of available modes, which otherwise will lead to an under-determined system of equations that have an infinite number of solutions.

Chapter 6

Chapter 6 presented descriptions of the analytical and experimental models. The techniques for sensor and excitation placement developed in Chapter 4 were applied to the model and used to carry out the experimental test. The eigenvalue sensitivity method, presented in Chapter 5, was used to update the analytical mass and stiffness matrices. Because only five modes were available, the number of updating parameters should have been less than five, rendering the problem very difficult since the total number of available elements was large. Therefore, two methods were employed to find the best possible elements to update. For stiffness update, the strain energy of the elements was calculated and elements that possess the highest energy were selected. The number of elements needed to be further reduced. By following the updating procedure using the five modes available, elements that

significantly changed the analytical frequencies within two or three iterations were selected. Finally, elements 248 and 256 were selected for the stiffness update exercise. The same procedure was followed to select elements for mass update. However, in this case, elements that possessed the greatest kinetic energy were selected. The elements chosen were 40 and 240. As one can observe from the above, only two elements were selected for either the stiffness or mass update, rendering the optimisation problem as over-determined. The optimisation procedures were carried out. Over thirty-five iterations were necessary to update the stiffness and the mass matrix of the system. The corrected frequency values were very close to the experimental values, indicating the successful optimisation of the analytical model. Also, the non-included in the updating frequencies seem to increase slightly and be closer to the experimental frequencies. This emphasizes more the success of the updating of the finite element model of the cable-stayed bridge cantilever.

The effect of the inclusion of the non-linearities in the updating process was investigated. The natural frequencies and modeshapes of the cantilever model were obtained without considering stress stiffening and large deformations in the analyses. The stiffness updating exercise was repeated for the new linear model using the same elements, and it was seen that the updating exercise was unsuccessful since the updating parameters could not converge to any particular values. This lead to the conclusion that the stiffness updating exercise was successful because the non-linear characteristics of the cable-stayed bridge cantilever were taken into account in the analyses.

The updating attempts made in this work are by no means unique. It is possible to have many analytical models that give a similar degree of correlation with the experimental model. It should be noted here that the purpose of model updating is not to create a physically realizable model but a structure that presents similar dynamic behaviour as the real structure.

The fact that only a limited amount of data was available to update the model, led to a strenuous exercise of finding the best possible elements to choose for the updating. However, these elements are certainly not the only elements that can be used for the

optimisation and a different selection of parameters may have led to a more robust convergence. The use of such a restricted range of parameters made the updating exercise acceptable, since it was successful. However, a larger number of updating parameters or the use of FRFs may be advisable. On the whole. this exercise demonstrates that model updating can be successful when applied to civil engineering structures using test data.

7.3 Contributions

There are two main contributions that this work has made to civil engineering. One is the sensor placement techniques that have been applied to place sensors on both the plate, tested in free-free conditions, and on the cable-stayed bridge cantilever. The techniques were very successful in finding the best positions to place the sensors, indicated by the MAC values between the analytical and the derived experimental results of both models.

Moreover, the observation that the quality of the experimental data identification depends on the set of sensor locations used in the experiment is an important one, since it emphasizes the need for careful test planning. The engineer should ensure that, if the test involves exciting a structure using a hammer, the hammer should hit the model at positions of low ADDFOV values, Chapter 4. In particular, if the hammer hits at the sensor positions, then these locations should lie at an area of low ADDFOV parameter values.

The fact that only five modes were obtained for the cantilever model does not indicate that the methods were not very successful, since the modes were perfectly correlated with the corresponding analytical ones. The accelerometer might have been placed at node position for some of the modes, thus not being able to read the data. However, more sensors may be needed to increase the chances of obtaining more information.

The second contribution is the actual application of model updating to a civil structure. As already mentioned, civil structures are complex systems, difficult to model accurately, both analytically and experimentally. The use of such systems for model updating is challenging and interesting. Up to now, optimisation techniques were used in the aerospace industry, to correct fairly simple models using test or real

data. However, these techniques have not been applied to civil engineering especially for updating large analytical models with test or real measurements. This work demonstrates that model updating can be used for large models, and can be very successful. However, care must be taken to use a substantial amount of experimental information, since this information should be greater then the number of updating parameters in order to obtain physically realisable parameter values.

7.4 Future work

Model optimisation is widely applied to the aerospace industry. However, civil engineering currently recognises the need for such applications to its own products. The structures and the surrounding environment become increasingly complicated and the need for accurate analytical models is developing rapidly. These models are usually used for further dynamic or even earthquake studies and an accurate representation of the real structure's dynamic behaviour is vital.

Some recommendations for future work follow that are derived based on the experiences of the author of this thesis.

1. Since the analytical model of the cable-stayed bridge cantilever was based on the Second Severn bridge cantilever, it would be interested to use the real data to update the mass and stiffness matrices of the analytical model.

2. It was felt that the use of limited modal data, such as natural frequencies and modeshapes, was not the best way to update the model. The model itself possessed a large number of elements, and the selection of just a few of them for updating was a very difficult exercise. The best solution was to use Frequency Response Function updating, which includes more information, especially in the higher frequency range where modal density is large, than the modal data. This way the engineer has to work on a wider frequency range, which could make the selection of a number of updating parameters easier.

3. Grouping elements together and using super-elements could be another way to optimise such a model as a cable-stayed bridge cantilever. The engineer will have to optimise whole parts of the structure and not to select just a few single elements located at various positions on the model. That could lead to more physically realisable corrections in the model.

4. The use of test data for updating seems to lead to a successful optimisation, which could be extended to the use of real data. This is a task that should be carried out, which the author has never come across at the literature review. It is a very interesting and challenging recommendation that should be followed. The applicability of the optimisation techniques would be challenged and any limitations can be addressed.

5. Apart from the sensitivities methods, modal or FRF, there are other more sophisticated methods for optimisation, such as Genetic Algorithms and Simulated Annealing. These methods have been mentioned in the literature review and should be explored for civil engineering structures.

6. Concerning future work in general, the author believes that the optimisation techniques can be further developed to optimize not only the stiffness or mass matrices of cable-stayed bridges, but also other parameters of it. As already mentioned in Chapter 3, cable-stayed bridges possess a very distinctive characteristic: geometric nonlinearities and stress stiffening in particular. It is described in the same chapter, that the stiffness matrix of the system comprises of the usual stiffness matrix of the elements plus the stress stiffness matrix, which is updated at each load increment. It would be very interesting to develop the updating algorithms to update the stress stiffness matrix of the bridge system.

7.5 Final thoughts

The aims of this work were to demonstrate the applicability of sensor location methods and model updating techniques to a cable-stayed bridge cantilever. It was a

challenging and enjoyable experience, involving analytical and experimental work and the use of advanced methods of analyses.

The sensor location methods were very successful in finding the best positions to place the transducers and can be recommended for use in the civil engineering industry.

The updating procedure itself was interesting and brought about many difficulties and limitations which should be taken into account in future work. However, the results obtained were very encouraging and further developments are recommended so that the methods can be used with confidence in all fields of engineering.

APPENDIX 1

DERIVATION OF EIGENSENSITIVITIES

Consider the eigendynamic equation:

$$[[K]-\lambda_r[M]]\{\phi\}_r=\{0\} \tag{A1-1}$$

where,

$[K]$, $[M]$ are the stiffness and mass matrices and λ_r, $\{\phi\}_r$ are the eigenvalues and eigenvectors of the system. All these quantities are functions of the p-values, $\{p\}$.

The eigenvectors are assumed to be mass-normalised so that:

$$\{\phi\}_r^T[M]\{\phi\}_r=1 \tag{A1-2}$$

If one differentiates equation (A1-1) with respect to p_i:

$$\left[\frac{\partial[K]}{\partial p_i}\{\phi\}_r+[K]\frac{\partial\{\phi\}_r}{\partial p_i}\right]=\left[\frac{\partial\lambda_r}{\partial p_i}[M]\{\phi\}_r+\lambda_r\frac{\partial[M]}{\partial p_i}\{\phi\}_r+\lambda_r[M]\frac{\partial\{\phi\}_r}{\partial p_i}\right] \tag{A1-3}$$

which gives:

$$\frac{\partial\lambda_r}{\partial p_i}[M]\{\phi\}_r=\frac{\partial[K]}{\partial p_i}\{\phi\}_r-\lambda_r\frac{\partial[M]}{\partial p_i}\{\phi\}_r+[[K]-\lambda_r[M]]\frac{\partial\{\phi\}_r}{\partial p_i} \tag{A1-4}$$

But:
$$[[K]-\lambda_r[M]]=\{0\} \tag{A1-5}$$

Pre-multiplying equation (A1-4) by $\{\phi\}_r^T$ and using equation (A1-5), one gets the expression for the eigenvalue sensitivity:

$$\frac{\partial \lambda_r}{\partial p_i} = \{\phi\}_r^T \frac{\partial [K]}{\partial p_i} \{\phi\}_r - \lambda_r \{\phi\}_r^T \frac{\partial [M]}{\partial p_i} \{\phi\}_r \qquad \text{(A1-6)}$$

The eigenvector derivatives are assumed to be linear combinations of the eigenvectors $\{\phi\}_r$:

$$\frac{\partial \{\phi\}_r}{\partial p_i} = \sum_{j=1}^{n} {}_r c_{ij} \{\phi\}_j \qquad \text{(A1-7)}$$

This equation is exactly true if all eigenvectors are used, n=N.

If equation (A1-7) is substituted in equation (A1-4) and pre-multiply (A1-4) by $\{\phi\}_k^T$ and re-arrange, one gets:

$$\{\phi\}_k^T \left[\frac{\partial [K]}{\partial p_i} - \frac{\partial \lambda_r}{\partial p_i} [M] - \lambda_r \frac{\partial [M]}{\partial p_i} \right] \{\phi\}_r + \{\phi\}_k^T [[K] - \lambda_r [M]] \sum_{j=1}^{N} {}_r c_{ij} \{\phi\}_j = 0 \qquad \text{(A1-8)}$$

From equations (A1-1) and (A1-2)

$$\{\phi\}_k^T [K] \{\phi\}_j = \begin{cases} \lambda_k & j = k \\ 0 & j \neq k \end{cases} \qquad \{\phi\}_k^T [M] \{\phi\}_j = \begin{cases} 1 & j = k \\ 0 & j \neq k \end{cases} \qquad \text{(A1-9)}$$

Using the information of equations (A1-9), equation (A1-8) becomes:

$$\{\phi\}_k^T \left[\frac{\partial [K]}{\partial p_i} - \frac{\partial \lambda_r}{\partial p_i} [M] - \lambda_r \frac{\partial [M]}{\partial p_i} \right] \{\phi\}_r + {}_r c_{ik} (\lambda_k - \lambda_r) = 0 \qquad \text{(A1-10)}$$

When $k \neq r$ $\dfrac{\partial \lambda_r}{\partial p_i}$ is zero and equation (A1-10) can be re-arranged to give ${}_rc_{ik}$ as follows:

$$ {}_rc_{ik} = \frac{\{\phi\}_k^T \left[\dfrac{\partial [K]}{\partial p_i} - \lambda_r \dfrac{\partial [M]}{\partial p_i} \right] \{\phi\}_r}{(\lambda_r - \lambda_k)} \qquad k \neq r \tag{A1-11} $$

When $k = r$, one can obtain ${}_rc_{ir}$ by differentiating equation (A1-2) with respect to p_i, as follows:

$$ 2\{\phi\}_r^T [M] \frac{\partial \{\phi\}_r}{\partial p_i} + \{\phi\}_r^T \frac{\partial [M]}{\partial p_i} \{\phi\}_r = 0 \tag{A1-12} $$

Substituting equation (A1-7) into (A1-12):

$$ {}_rc_{ir} = -\tfrac{1}{2} \{\phi\}_r^T \frac{\partial [M]}{\partial p_i} \{\phi\}_r \tag{A1-13} $$

Substituting equations (A1-11) and (A1-13) into equation (A1-7), one gets the eigenvector sensitivity:

$$ \frac{\partial \{\phi\}_r}{\partial p_i} = \sum_{k=1;k\neq r}^{N} \frac{\{\phi_a\}_k \{\phi_a\}_k^T}{(\lambda_a)_r - (\lambda_a)_i} \left[\frac{\partial [K_a]}{\partial p_i} - (\lambda_a)_r \frac{\partial [M_a]}{\partial p_i} \right] \{\phi_a\}_r - \tfrac{1}{2} \{\phi_a\}_r^T \frac{\partial [M_a]}{\partial p_i} \{\phi_a\}_r \tag{A1-14} $$

APPENDIX 2

DERIVATION OF FRF SENSITIVITIES

Consider a finite element and an experimental model of an undamped system. If a single input force is applied to both models, the equation of motion becomes:

$$[-\omega^2[M]+[K]]\{\alpha_x(\omega)\}=\{f\}=[-\omega^2[M_a]+[K_a]]\{\alpha_a(\omega)\}_j \qquad \text{(A2-1)}$$

The excitation $\{f\}$ is unity at the j^{th} degree-of-freedom and zero elsewhere.

The mass and stiffness matrices can be expressed in terms of the errors in the analytical matrices:

$$[M]=[M_a]+[\Delta M] \quad \text{and} \quad [K]=[K_a]+[\Delta K] \qquad \text{(A2-2)}$$

Substituting equations (A2-2) into equation (A2-1)

$$[-\omega^2[\Delta M]+[\Delta K]]\{\alpha_x(\omega)\}=[-\omega^2[M_a]+[K_a]]\{\{\alpha_a(\omega)\}_j-\{\alpha_x(\omega)\}\} \qquad \text{(A2-3)}$$

The analytical dynamic stiffness matrix is given by:

$$[\alpha_a(\omega)]=[-\omega^2[M\ ]+[K_a]]^{-1} \qquad \text{(A2-4)}$$

Assuming that the matrix $[\alpha_a(\omega)]$ is non-singular, then equation (A2-3) can be written as:

$$[\alpha_a(\omega)][-\omega^2[\Delta M]+[\Delta K]]\{\alpha_x(\omega)\}=\{\Delta\alpha(\omega)\} \qquad \text{(A2-5)}$$

where:

$$\{\Delta\alpha(\omega)\} = \{\alpha_a(\omega)\}_j - \{\alpha_x(\omega)\} \tag{A2-6}$$

The updated matrices are a function of the p-values. They can be expressed as a Taylor expansion series about the original finite element model:

$$[M_u] = [M_a] + [\Delta M] = [M_a] + \sum_i \frac{\partial [M]}{\partial p_i} p_i + O(p_i^2) \tag{A2-7}$$

$$[K_u] = [K_a] + [\Delta K] = [K_a] + \sum_i \frac{\partial [K]}{\partial p_i} p_i + O(p_i^2) \tag{A2-8}$$

where $O(p_i^2)$ represents terms of order p_i^2 and higher. If these higher order terms are not considered, and only the first order terms on the above two equations are retained, one can get the error matrices:

$$[\Delta M] = \sum_i \frac{\partial [M]}{\partial p_i} p_i \quad \text{and} \quad [\Delta K] = \sum_i \frac{\partial [K]}{\partial p_i} p_i \tag{A2-9}$$

Substituting these error matrices into equation (A2-5) one gets:

$$[\alpha_a(\omega)]\left[\left[-\omega^2 \frac{\partial [M]}{\partial p_1} + \frac{\partial [K]}{\partial p_1}\right] p_1 + \cdots + \left[-\omega^2 \frac{\partial [M]}{\partial p_{Np}} + \frac{\partial [K]}{\partial p_{Np}}\right] p_{Np}\right]\{\alpha_x(\omega)\} = \{\Delta\alpha(\omega)\} \tag{A2-10}$$

The above equation can be written as follows:

$$[\alpha_a(\omega)]\left[\left[-\omega^2 \frac{\partial [M]}{\partial p_1} + \frac{\partial [K]}{\partial p_1}\right]\{\alpha_x(\omega)\} \cdots \left[-\omega^2 \frac{\partial [M]}{\partial p_{Np}} + \frac{\partial [K]}{\partial p_{Np}}\right]\{\alpha_x(\omega)\}\right]\begin{Bmatrix} p_1 \\ \cdots \\ p_{Np} \end{Bmatrix} = \{\Delta\alpha(\omega)\} \tag{A2-11}$$

and, in a more compact form: $[S(\omega)]\{p\} = \{\Delta\alpha(\omega)\}$ (A2-12)

where:

$$[S(\omega)] = [\alpha_a(\omega)]\left[\left[-\omega^2\frac{\partial[M]}{\partial p_1} + \frac{\partial[K]}{\partial p_1}\right]\{\alpha_x(\omega)\} \cdots \left[-\omega^2\frac{\partial[M]}{\partial p_{Np}} + \frac{\partial[K]}{\partial p_{Np}}\right]\{\alpha_x(\omega)\}\right] \quad \text{(A2-13)}$$

This matrix $[S]$ is called the Sensitivity matrix.

REFERENCES

Abdel-Ghaffar A.M., *"Cable-stayed bridges under seismic action"*, Cable-stayed bridges: Recent developments and their future, Proc. of the Seminar, Yokohama, Japan, 10-11 December 1991, pp 171-192.

Abdel-Ghaffar A.M., Khalifa M.A., *"Importance of cable vibration in dynamics of cable-stayed bridges"*, J.Engrg.Mech., ASCE, 1991, Vol. 117, No.11. pp 2571-2589.

Abdel-Ghaffar A.M., Nazmy A.S., *"Nonlinear seismic response of cable-stayed bridges subjected to nonsynchronous support motions"*. Proc 9th W.Conf.Earthq.Engrg., 1988, Vol.VI, pp 483-488.

Achkire Y., Preumont A., *"Active tendon control of cable-stayed bridges"*, Earthq.Engrg.Struc.Dyn., 1996, Vol. 25, pp 585-597.

Ahmadi-Kashani K., *"Vibration of hanging cables"*, Computers and Structures, 1989, Vol. 31, No 5, pp 699-715.

Al-Noury S.I., Ali S.A., *'Large-amplitude vibrations of parabolic cables'*, J.Sound and Vibration, 1985, 101(4), pp 451-462.

Ali S.A., *"Dynamic response of sagged cables"*, Computers and Structures, 1986, Vol. 23, No 1, pp 51-57.

Allemang R.J., Brown D.L., *"A Correlation Coefficient for Modal Vector Analysis"*, IMAC I, 1982, pp 110-116.

Anderson J.R., Ferri A.A., *Behaviour of a single-degree-of-freedom system with a generalised friction law'*, J.Sound and Vibration, 1990, Vol. 140(2). pp 287-304.

ANSYS, Version 5.4, Swanson Analysis Systems Inc., 1997.

Azevedo J.J., Branco F.A., Virtuoso F., *"The seismic study of the cable-stayed international Guadiana bridge"*, Earthq.Engrg.Struc.Dyn , 1989, pp 8.3.17-8.3.24.

Baruh H., Choe K., *"Sensor placement in structural control"*, J.Guidance,Control and Dynamics, 1990, Vol. 13, No. 3, pp 524-533.

Baruh H., Khatri H.P., *'Identification of modal parameters in vibrating structures'*. J.Sound and Vibration, 1988, 125(3), pp 413-427.

Beards C.F., *"Structural vibration: Analysis and damping"*, 1996, Arnold.

Beards C.F., Williams J.L., *'The damping of structural vibration by rotational slip in joints'*, J.Sound and Vibration, 1977, Vol. 53(3), pp 333-340.

Benedettini F., Rega G., *"Non-linear dynamics of an elastic cable under planar excitation"*, Int.J.Non-linear Mechanics, 1987, Vol. 22, No 6, pp 497-509.

Benedettini F., Rega G., *"Planar non-linear oscillations of elastic cables under superharmonic resonance conditions"*, J.Sound and Vibration, 1989, 132(3), pp 353-366.

Blakeborough A., Severn R.T., Taylor C.A., *"The new UK National six-axis earthquake shaking table"*, Proc. 8th E.C.E.E. Lisbon, Vol. 4, pp 97-100.

Blaschke P.G., Ewins D.J., "*The MAC Revisited and Updated*", IMAC XV, 1997, pp 147-154.

Brandon J.A., *"Strategies for Structural Dynamic Modification"*, 1990, Research Studies Press LTD.

Brillhart R.D., Kammer D.C., *"Evaluation of optimal modal sensor placement using a system realisation method"*, Proc. 12th IMAC, 1994, Vol. 2, pp 1401-1407.

Brincker R., DeStefano A., Piombo B., *'Ambient data to analyse the dynamic behaviour of bridges: a first comparison between different techniques'*. Proc. 14the IMAC, 1996, Vol. 1, pp 477-482.

Bucher C.G., Wall F.J., *"Stochastic response of bridges in turbulent wind"*. J.W.E.I.A., 1992, Vol. 41-44, pp 1347-1358.

Burgess J.J., Triantafyllou M.S., *"The elastic frequencies of cables"*, J.Sound and Vibration, 1988, 120(1), pp 153-165.

Caetano E., Cunha A., Taylor C., "*Dynamic Cable-Deck Interaction In Cable-Stayed Bridges*", IMAC XV, 1997, pp 301-307.

Casas J.R., *"Full-scale dynamic testing of the Alamillo cable-stayed bridge in Sevilla (Spain)"*, Earthq.Engrg.Str.Dyn., 1995, Vol. 24, pp 35-51.

Clough R.W., Penzien J., *'Dynamics of structures'*, McGraw-Hill publication, 1975.

Crowley S.M., Brown D.L., Allemang R.J., *'The extraction of valid residue terms using the Polyreference technique'*, 3rd IMAC, 1985, Vol. 1, pp 80-87.

Darbre G.R., *"In-plane free vibration of supported/free parabolic cables"*, Earthq.Engrg.Str.Dyn., 1989, Vol. 18, pp 435-443.

DeLorenzo M.L., *"Sensor and actuator selection for large space structure control"*, J.Guidance, Control and Dynamics, 1990, Vol. 13, No. 2, pp 249-257.

Ewins D.J., Gleeson P.T., *'A method for modal identification of lightly damped structures'*, J.Sound and Vibration, 1982, 84(1), pp 57-79.

Fissette E., Stavrinidis C., Ibrahim S., "*Error location and updating of analytical dynamic models using a Force Balance Method*", IMAC VI, 1988. pp 1063-1070.

Fleming J.F., Egeseli E.A., *"Dynamic Behaviour of a Cable-Stayed Bridge"*. Earthq.Engrg.Str.Dyn., 1980, Vol.8, pp 1-16.

Fritzen C.P., Kiefer T., *"Localization and Correction of errors in Finite Element Models based on experimental data"*, 17th Int.Sem.Mod.Anal., KULeuven, 1990, pp1581-1596.

Fritzen C.P., Zhu S., *"Updating of Finite Element models by means of measured information"*, Computers and Structures, 1991, Vol. 40, no. 2, pp 475-486.

Garevski M.A., *'Dynamic analysis of cable-stayed bridges by means of analytical and physical modelling'*, PhD Thesis, University of Bristol, Department of Civil Engineering, 1990.

Garevski M.A., Brownjohn J.M.W., Blakeborough A., Severn R.T., *"Resonance-search tests on a small-scale model of a cable-stayed bridge"*, Eng.Struct., 1991, Vol. 13, pp 59-66.

Gentile C., Martinez y Cabrera F., *"Dynamic investigation of a repaired cable-stayed bridge"*, Earthq.Engrg.Struc.Dyn., 1997, Vol. 26, pp 41-59.

Gersch W., Nielsen N.N., Akaike H., *'Maximum likelihood estimation of structural parameters from random vibration data'*, J.Sound and Vibration, 1973, 31(3), pp 295-308.

Gimsing N.J., *'Cable supported bridges: concept and design'*, John Wiley & Sons publication, 1983.

Gupta S.P., Kumar A., *"A study on dynamics of cable-stayed bridge including foundation interaction"*, pp 8.3/9-8.3/16.

Gupta S.P., Kumar A., *"Dynamic response of cable-stayed bridge including foundation interaction effect"*, Proc. 9th W.Conf.Earthq.Engrg., 1988, Vol. VI, pp 501-506.

Guyan R.J., *"Reduction of Stiffness and Mass Matrices"*, AIAA J..1965, Vol.3, pp 380.

Hablowetz T., Lieven N., *'Provision of damping models for use in Neural Networks'*, Report No. 702, Department of Aerospace Engineering, University of Bristol, Aug. 1994.

Hemez F.M., Farhat C., *"An energy based optimum sensor placement criterion and its application to structural damage detection"*, Proc 12th IMAC, 1994, Vol. 2, pp 1568-1575.

Heo G., Wang M.L., Satpathi D., *'Optimal transducer placement for health monitoring of long span bridge'*, Soil.Dyn.Earthq.Engrg., 1997, 16, pp 495-502.

Huang D., Wang T.L., *"Impact analysis of cable-stayed bridges"*, Computers and Structures, 1992, Vol. 43, No. 5, pp 897-908.

Hunter N.F., Barney P., Ferregut C., Perez L., Paez T.L., "*Statistical Validation Of Stochastic Models*", IMAC XV, 1997, pp 605-611.

Imregun M., *"Three Case Studies in Finite Element Model Updating"*, Shock and Vibration, 1995, Vol. 2, No. 2, pp 119-131.

Irvine H.M., *"Free vibrations of inclined cables"*, Proc.of the ASCE, 1978, Vol. 104, ST2, pp 343-347.

Ito M., Fujino Y., Miyata T., Narita N., *"Cable-stayed bridges: Recent developments and their future"*, Proc. of the Seminar, Yokohama, Japan, December 1991.

Iyengar R.N., Rao G.V., *"Free vibrations and parametric instability of a laterally loaded cable"*, J.Sound and Vibration, 1988, 127(2), pp 231-243.

Jung H., Ewins D.J., *"On the use of simulated 'experimental' data for evaluation of Modal Analysis Methods"*, IMAC X, 1993, pp 421-429.

Kahan M., Gibert R.J., Bard P.Y., *"Influence of seismic waves spatial variability on bridges: A sensitivity analysis"*, Earthq.Engrg.Str.Dyn., 1996, Vol. 25. pp 795-814.

Kammar D.C., *"Sensor placement for On-Orbit modal identification and correlation of Large Space Structures"*, J.Guidance, Control and Dynamics, 1991, Vol. 14, No. 2, pp 251-259.

Kammar D.C., *"Effect of Model Error on Sensor Placement for On-Orbit Modal Identification of Large Space Structures"*, J.Guidance,Control and Dynamics, 1992, Vol. 15, No. 2, pp 334-341.

Kawano K., Furukawa K., *"Random seismic response analysis of soil cable-stayed bridge interaction"*, Proc. 9th W.Conf.Earthq.Engrg., 1988, Vol. VI, pp 495-500.

Kawashima K., Unjoh S., Azuta Y., *"Damping characteristics of cable-stayed bridges"*, Proc. 9th.W.Conf.Earthq.Engrg., 1988, Vol. VI, pp 471-476.

Kim H.B., Park Y.S., *"Sensor placement guide for structural joint stiffness model improvement"*, Prepared to be submitted to J.Mech.Syst.Sign.Proc., 1996.

Larsen A., *"Advances in aeroelastic analyses of suspension and cable-stayed bridges"*, J. Wind Engrg and Industrial Aerodynamics, 1998, pp 73-90.

Larson C.B., Zimmerman D.C., Marek E.L., *"A comparison of modal test planning techniques: Excitation and sensor placement using the NASA 8-bay truss"*, Proc. 12th IMAC, 1994, Vol. 1, pp 205-211.

Leung K.N., Wong J., *"Non-linear behaviour of inclined cable"*, Report submitted for the degree of Beng in Civil Engineering, University of Bristol, 1993.

Levin R.I., Lieven N.A.J., "*Dynamic Finite Element Model Updating Using Simulated Annealing and Genetic Algorithms*", IMAC XV, 1997, pp 1195-1201.

Lieven N.A.J., Ewins D.J., "*Spatial Correlation Of Mode Shapes, The Coordinate Modal Assurance Criterion (COMAC)*", IMAC VI, 1988. pp 690-695.

Lieven N.A.J., Ewins D.J., *"Call for comments: A proposal for standard notation and terminology in modal analysis"*, IJAEMA, 1992, Vol. 7, No. 2. pp 151-156.

Lieven N.A.J., *"Finite Element Updating using Measured data"*, Ch. 7.

Lin R.M., *"On measured data required to update an analytical model"*, IMAC XI, 1991, pp 462-468.

Luongo A., Rega G., Vestroni F., *'Monofrequent oscillations of a non-linear model of a suspended cable'*, J.Sound and Vibration, 1982, 82(2), pp 247-259.

Maia N.M.M., Silva J.M.M., He J., Lieven N.A.J., Lin R.M., Skingle G.W., To W., Urgueira A.P.V., *"Theoretical and Experimental Modal Analysis"*, Research Studies Press LTD., John Wiley & Sons INC, 1997.

Maia N.M.M., Silva J.M.M., Ribeiro A.M.R., *"A new modal identification method using an Advanced Characteristic Response Function(ACRF)"*, pp 1069-1075.

Mayes R.L., Carne T.G., *"Extraction of Modal Parameters with the aid of Predicted Analytical Mode Shapes"*, IMAC XIV, 1996, pp 267-271.

McConnell K.G., Han S.B., *"A theoretical basis for Cross-Axis Corrections in Tri-axial Accelerometers"*, IMAC IX, 1992, pp 171-175.

McConnell K.G., Varoto P.S., *"An FE study of the exciter-structure interaction in vibration testing"*, IMAC XII, 1994, pp 1018-1025.

Menq C.H., Bielak J., Griffin J.H., *'The influence of microslip on vibratory response. Part I: A new microslip model'*, J Sound and Vibration, 1986, Vol. 107(2), pp 279-293.

Menq C.H., Chidamparam P., *'Friction damping of two-dimensional motion and its application in vibration control'*, J.Sound and Vibration, 1991, Vol. 144(3), pp 427-447.

Morris N.F., *"Dynamic analysis of cable-stiffened structures"*, ASCE, May 1974, Vol. ST5, pp 971-981.

Mottershead J.E., Friswell M.I., *"Model updating in structural dynamics: A survey"*, J.Sound and Vibration, 1993, Vol. 167, No. 2, pp 347-375.

Muria-Vila D., Gomez R., King C., *"Dynamic structural properties of cable-stayed Tampico Bridge"*, J.Str.Engrg., 1991, Vol. 117, No. 11, pp 3396-3416.

Narendra K.S., Parthasarathy K., *"Identification and control of dynamical systems using Neural Networks"*, IEEE Transactions on Neural Networks,1990, Vol.1, No.1, pp 4-27.

Nazmy A.S., Abdel-Ghaffar A.M., *"Effects of ground motion spatial variability on the response of cable-stayed bridges"*, Eartq.Engrg.Struc.Dyn., 1992, vol. 21, pp 1-20.

Norton A., Perry M., *"The effects of damping on closed modes of vibration"*, Report submitted for the degree of Beng in Aeronautical Engineering, University of Bristol, 1996.

O'Callahan J., "*A procedure for an Improved Reduced System (IRS) Model*", IMAC VII, 1989, pp 17-21.

O'Callahan J., Avitabile P., Riemer R., "*System Equivalent Reduction Expansion Process (SEREP)*", IMAC VII, 1989, pp 29-37.

Ogawa K., Shimodoi H., Ishizaki H., *"Aerodynamic stability of a cable-stayed bridge with girder, tower and cables"*, J.W.E.I.A., 1992, Vol. 41-44, pp 1227-1238.

Pandey A.D., Krishna P., Sethia M.R., *"Seismic response analysis of cable-stayed bridges"*, Earthq.Engrg.Struc.Dyn, 1989, pp 343-350.

Park Y., Kim H., *"Sensor placement guide for model comparison and improvement"*, Proc. 14th IMAC, 1996, Vol. 1, pp 404-409.

Parvez S.M., Wieland M., *"Earthquake behaviour of continuous multi-span cable-stayed bridge"*, Proc. 9th W.Conf.Earthq.Engrg., 1988, Vol. VI, pp 477-482.

Pascual R., Golinval J.C., Razeto M., "*A Frequency Domain Correlation Technique for Model Correlation and Updating*", IMAC XV, 1997, pp 587-592.

Phillips A.W., Allemang R.J., *"Single Degree-of-Freedom Modal Parameter Estimation Methods"*, IMAC XIV, 1996, pp 253-260.

Qi G.Z., Chen H.M., Tsai K.H., Yang J.C.S., *"Structural Dynamic Model Identification Through Neural Network"*, IMAC XII, 1992, pp 1167-1172.

Rega G., Benedettini F., *"Planar non-linear oscillations of elastic cables under subharmionic resonance conditions"*, J.Sound and Vibration, 1989, 132(3), pp 367-381.

Riva A., Giorcelli E., Garibaldi L., Fasana A., *"Dynamic System Identification by means of Neural Networks"*, IMAC XI, 1991, pp 928-933.

Ruotolo R., Mares C., "*Damage Identification Using Simulated Annealing*". IMAC XV, 1997, pp 954-959.

Ruotolo R., Surace C., Mares C., *"Damage identification using Simulated Annealing"*, IMAC XV, 1997, pp 954-959.

Sabnis G.M., Harris H.G., White R.N., Mirza M.S., *"Structural modelling and experimental techniques"*, 1983, Prentice-Hall, Inc., Englewood Cliffs, N.J. 07632.

Sarkar P.P., Jones N.P., Scanlan R.H., *"System identification for estimation of flutter derivatives"*, J.W.E.I.A., 1992, Vol. 41-44, pp 1243-1254.

Shah P.C., Udwadia F.E., *"A methodology for optimal sensor locations for identification of dynamic systems"*, J.Appl.Mech., 1978, Vol. 45, pp 188-196.

Shaw S.W., *'On the dynamic response of a system with Dry Friction'*, J.Sound and Vibration, 1986, Vol. 108(2), pp 305-325.

Silva and Maia, *Modal Analysis and Testing"*, Kluwer Accademic Publicaitions, 1999.

Sophianopoulos D.S., Ioannidis S.S., Ermopoulos I.Ch., *"Dynamic analysis of horizontally stayed bridges under wind loading"*, Computers and Structures, 1993, Vol. 49, No. 4, pp 693-703.

Stewart G.W., *"Computer Science and Applied Mathematics"*, Academic Press, 1973.

Takahashi K., Konishi Y., *"Non-linear vibrations of cables in three dimensions, Part I: Non-linear free vibrations"*, J.Sound and Vibration, 1987, 118(1), pp 69-84.

Takahashi K., Konishi Y., *"Non-linear vibrations of cables in three dimensions, Part II: Out-of-plane vibrations under in-plane sinusoidally time-varying load"*, J.Sound and Vibration, 1987, 118(1), pp 85-97.

Triantafyllou M.S., *"The dynamics of translating cables"*, J.Sound and Vibration, 1985, 103(2), pp 171-182.

Triantafyllou M.S., Grinfogel L., *"Natural frequencies and modes of inclined cables"*, J.Str.Engrg, 1986, Vol. 112, No 1, pp 139-148.

van Nunen J.W.G., Persoon A.J., *"Investigation of the vibrational behaviour of a cable-stayed bridge under wind loads"*, Eng.Struct., 1982, Vol. 4, pp 99-105.

Vaz C.T., Rito A., Duarte R.T., *"Seismic studies of the Arade river cable-stayed bridge"*, Proc. 9th.W.Conf.Earthq.Engrg., 1988, Vol. VI, pp 507-512.

Veletsos A.S., Darbre G.R., *"Dynamic stiffness of parabolic cables"*. Earthq.Engrg.Str.Dyn., 1983, Vol. 11, pp 367-401.

Vold H., Geisler D., Crowley S., Wolfer A., *'Maximum Entropy Frequency Response Function'*, 3rd IMAC, 1985, Vol. 2, pp 876-881.

Wang M.L., Heo G., Satpathi D., *'Dynamic characterisation of a long span bridge: a finite element based approach'*, Soil Dyn.Earthq.Engrg., 1997, 16, pp 503-512.

Waters T.P., *"Finite Element Model Updating using Frequency Response Functions"*, PhD Thesis, Department of Aerospace Engineering, University of Bristol, 1995.

Waters T.P., *"A Modified Force Balance Method for locating errors in Dynamic Finite Element Models"*, Internal report, University of Bristol, Department of Aerospace Engineering, 1995.

Wilson J.C., Gravelle W., *"Modelling of a cable-stayed bridge for dynamic analysis"*, Earthq.Engrg.Str.Dyn., 1991, Vol. 20, pp 707-721.

Wilson J.C., Liu T., *"Ambient vibration measurements on a cable-stayed bridge"*, Earthq.Engrg.Str.Dyn., 1991, Vol. 20, pp 723-747.

Worden K., Burrows A.P., Tomlison G.R., *"A combined neural and generic approach to sensor placement"*, Proc. 13th IMAC, 1995, Vol. 2, pp 1727-1731.

Ying R., *'The analysis and identification of friction joint parameters in the dynamic response of structures'*, PhD Thesis, Department of Mechanical Engineering, Imperial College, 1992.

Yokoyama M., Tanaka S., Iwano M., *"Analytical study on seismic behaviour of cable-stayed bridge"*, Proc. 9th W.Conf.Earthq.Engrg., 1988, Vol. VI, pp 489-494.

Yoshimura T., *"Aerodynamic stability of four medium span bridges in Kyushu district"*, J.W.E.I.A., 1992, Vol. 41-44, pp 1203-1214.

Yu T.K., Seinfeld J.H., *"Observability and optimal measurement location in linear distributed parameter systems"*, Int.J.Control, 1973, Vol. 18, No. 4, pp 785-799.

Zaghlool S.A., *'Single-station time-domain (SSTD) vibration testing technique: Theory and application'*, J.Sound and Vibration, 1980, 72(2), pp 205-234.

Zienkiewicz O.C., Taylor R.L., *'The Finite Element Method'*, McGraw-Hill, 1986, ISBN 0-07-084072-5.

Zimmerman D.C., Yap K.C., Hasselman T., "*Evolutionary Approach for Model Refinement*", IMAC XV, 1997, pp 551-557.